Dissecting the role of hepatic Nfκb1 in inflammation and ageing

Letizia Marchetti

Doctor of Philosophy

Submitted May 2022

Abstract

The NF-κB family is a group of 5 subunits functioning as transcription factors in a variety of important cellular pathways, including inflammation, cell proliferation and cancer. They work as hetero and homodimers to regulate the gene expression. In particular, Nfκb1 can form homodimers and recruit epigenetic modifiers at gene promoters, modulating their expression in both directions, depending on the coupling co-factor. Previous studies have shown that *Nfκb1*$^{-/-}$ cells presented higher expression of inflammatory genes compared to normal cells (wt). Also, mice globally lacking *Nfκb1* aged faster compared to their wt littermates and with particular attention to the liver, they develop more tumours.

I wanted to dissect the contribution of *Nfκb1* to inflammation and ageing in a specific cell type, namely hepatocytes. To do so, I used a Cre-LoxP system in a mouse model to selectively knock out *Nfκb1* in hepatocytes.

RNA sequencing in primary murine hepatocytes suggested that upon acute treatment with LPS, *Nfκb1*$^{-/-}$ hepatocytes failed to repress the expression of a subset of inflammatory genes at the resolution stage. In a more complex model such as Precision Cut Liver Slices, *Nfκb1*$^{-/-}$ slices did not show the same trend observed in primary cells, probably due to the compensatory mechanisms ongoing in other cell types. Lastly, aged *Nfκb1*$^{-/-}$ mice presented more steatosis and a greater number of immune cells aggregates resembling ectopic lymphoid structures. Interestingly, the same mice presented extensive damage in the kidneys, despite expressing *Nfκb1.*

I hypothesise that because of their more inflamed phenotype, hepatocytes lacking *Nfκb1* secrete more inflammatory mediators that damage the cells and the whole organ as the mice age. This damage is spread through soluble factors in the blood stream, causing the loss of architecture and function in organs expressing *Nfκb1*, such as the kidneys.

These results support the idea that *Nfκb1* might be dispensable to induce an inflammatory response, but it is necessary to limit inflammation in hepatocytes in order to prevent the onset of chronic inflammation with accelerated ageing.

Acknowledgments

I would like to acknowledge and thank the people who supported me and helped me during this important and stimulating experience. First of all, I would like to thank my supervisors, Derek Mann, Jelena Mann and Caroline Wilson, for the incredible chance they gave me when they offered me the PhD position. Thank you for the knowledge and for the guidance that you provided me, your contribution had been essential to allow me to become a better scientist and I will always be grateful for this. Also, I would like to thank the Dame Barbour Foundation for funding my PhD and for supporting so many other doctorate students across the North – East.

I would also like to thank Dr Paula Salgado and Prof Matthias Trost for their insights and help as members of my progression panel, they always had my best interests at heart, and they showed genuine curiosity and enthusiasm for my project.

I would like to acknowledge Prof Fiona Oakley for adopting me as a PhD student and for the amazing support that she was able to provide, despite being busy with other millions of things, including her official PhD students.

I would like to thank the whole Newcastle Fibrosis Research Group, for the lovely days in the lab and the office fun. I will miss you deeply.

Lastly, I would like to thank my family, and my mum in particular, for the unconditional support that she always showed me, no matter how painful it was for her. If I have come this far, if I have managed to become the person I am today, part of the merit is hers, for all the sacrifices and the deep love for knowledge that she had been able to pass on since I was a child. Thank you.

Table of contents

List of Tables and Figures

All the figures presented in the introduction are original and created with Biorender.

Chapter 1. Introduction

Inflammation is an evolutionarily conserved response to harmful stimuli, both external, e.g., infection, and internal, e.g., tissue stress and malfunction (Medzhitov, 2008). This defensive mechanism aims to bring about the elimination of the initial source of damage, recruiting cells from the innate immune system to the site involved in the process. Tissue – resident macrophages and neutrophils are the first cell types to respond: macrophages recognise the infection and produce inflammatory mediators that will induce a change into the vessels permeability and attract other immune cells; neutrophils are some of the immune cells recruited to the damaged area and they release the toxic content of their granules to neutralise the infecting pathogen. These mediators are very efficient, but they do not discriminate between the host and the noxious stimulus that must be removed. For this reason, to avoid any further damage once the infection has been cleared, the inflammatory response needs to be limited and resolved, hence it requires a tight and controlled regulation. A dysfunction of this negative feedback can lead to chronic inflammation and long - term diseases (Hunter, 2012).

In the context of the liver, unresolved inflammation and persistent tissue damage can cause the induction of early fibrosis, characterized by excessive scar deposition and eventually loss of tissue functionality. If the process is not resolved at this stage, fibrosis becomes chronic, establishing a condition of sterile inflammation that will eventually progress to cirrhosis, in which the disease becomes clinically significant (Bataller and Brenner, 2005). In some cases, cirrhosis can evolve to Hepatocellular Carcinoma, in which repeated damage to hepatocytes leads to a cycle of cell death and regeneration, which causes genomic instability and predisposition to cancer development. Even if HCC can occur under other circumstances, such as hepatitis B infection and haemochromatosis, the 80-90% of HCC cases are developed from liver cirrhosis and the incidence of this type of malignancy is drastically increasing, making it the sixth most common cancer worldwide (Dhanasekaran, Bandoh and Roberts, 2016).

At the early stage of fibrosis, the organ is usually able to revert to a physiological state but depending on the burden of the damage and the duration of the inflammatory event, some functionality might be lost, as the scar tissue does not possess the same characteristics and functions of the damaged tissue that had been replaced (Figure 1).

The key to limit inflammation and for preventing the onset of a chronic and deleterious illness lies in a better understanding of the intricate network of pathways that the inflammatory response is composed of, aiming to the investigation of new targets for therapies and drug discovery.

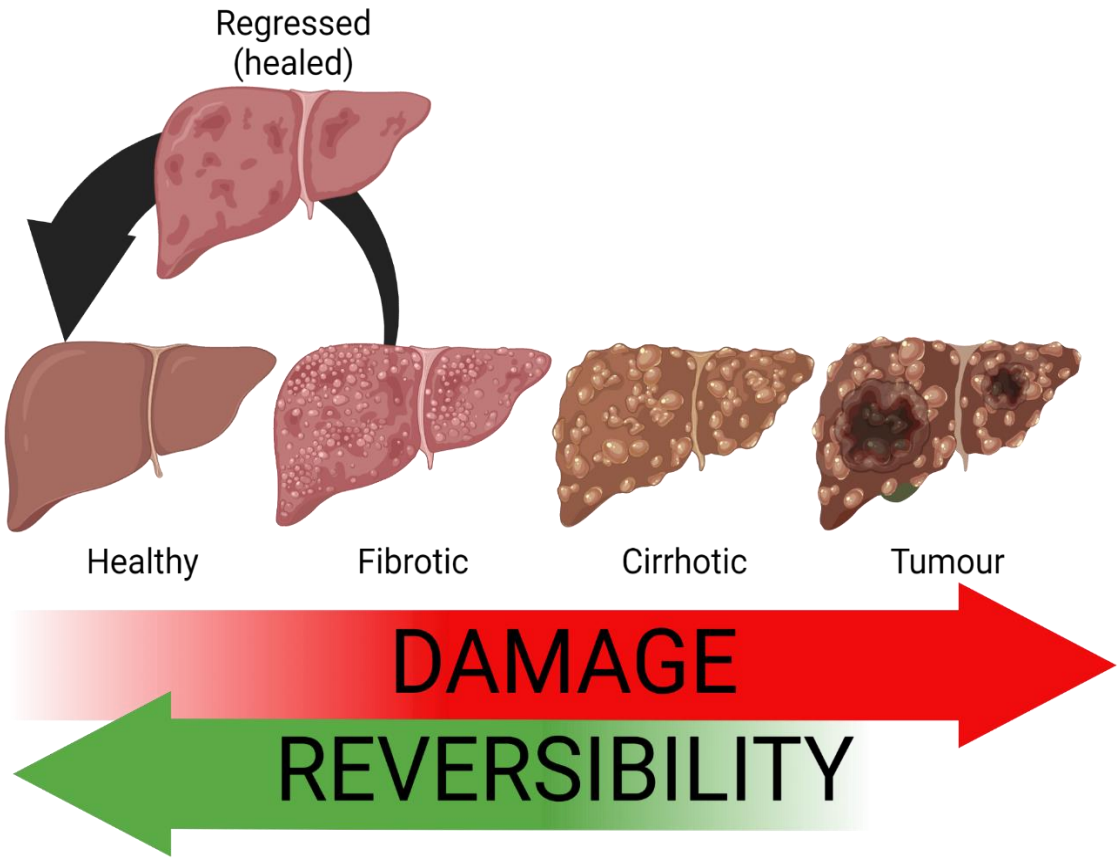

Figure 1. Schematic representation of the possible progression from a healthy liver to hepatocellular carcinoma caused by chronic inflammation and increasing liver damage. Once the scar tissue becomes predominant, the possibility to heal completely and regress to a normal state is lost and the consistent inflammatory stimuli create the perfect microenvironment for carcinogenesis.

As aforementioned, inflammation is a complex network of pathways involving different mediators and signalling cascades; tumour necrosis factor receptors (TNFR), interleukin 1 receptor (IL1R) and toll like receptors (TLRs) are just some examples of the numerous proteins playing an important role in the inflammatory process (Lawrence and Fong, 2010).

Inflammatory responses are triggered by specific molecules or external stimuli, and they lead to the activation of distinct signalling cascades, based on signal specificity. The same pathways include downregulation and self-limiting steps, which are put in place to dampen the inflammation and facilitate the transition back to a normal state;

thus, components from the same families previously named are pivotal for the negative regulative action as well, involving gene expression inhibition and apoptosis.

A well-known group of proteins involved in inflammation is the Nuclear Factor (NF)- κB family. The five members RelA, RelB, c-Rel, p100/p52 and p105/p50 can associate as hetero – and homo – dimers and depending on the activated dimer different effects on gene regulation can be achieved (Lawrence and Fong, 2010). Because of its vast regulation on gene expression, the NF-κB family has been broadly investigated, uncovering its role in long-term diseases and cancer, and rendering it an interesting target for further studies and new therapies (Zhang, Lenardo and Baltimore, 2017).

1.1. The NF-κB family

Nuclear factor kappa-light-chain-enhancer of activated B cells, commonly referred as NF-κB, is a family of transcription factors involved in the regulation of different cellular processes including immune responses, cell proliferation and cancer. As the name suggests, NF-κB was firstly discovered in immune B cells and identified as a nuclear factor able to bind a site in the immunoglobulin κ enhancer (Sen and Baltimore, 1986). Subsequently, the same team showed that NF-κB was inducible in other cell types as well, such as Jurkat (T cells line) and HeLa (nonlymphoid cell line) (Sen and Baltimore, 1966). The targeted binding sites, called κB sites, were characterised and they were found to be variations of the sequence with a consensus of 5'-GGGRNWYYCC-3' (N, any base; R, purine; W, adenine or thymine; Y, pyrimidine). Lastly, later investigations highlighted that κB binding sites were present in enhancers and promoters of genes involved in the inflammatory response and cell survival, such as IL-2, IL-6, GM-CSF, ICAM-1, and class I MHC, pointing out the role of NF-κB as transcription factor after immunological stimulation *via* TNF, IL-1, and T cell activators (Baldwin, 1996).

The mammalian family of NF-κB consists of five members, RelA (p65), RelB, c-Rel, p100/p52 and p105/p50. They share N-terminal homology with the v-Rel oncogene and within the same region the Rel homology domain (RHD) is found, a 300-long amino acids region that enables DNA interactions, dimerization, and interactions with IκB forms. The RHD is followed by the nuclear localization sequence (NLS), which allows translocation into the nucleus. Lastly, the C-terminal is characterized by hydrophobic residues that form an interface involved in dimerization and interaction with inhibitory proteins.

Based on their structure, the NF-κB subunits are divided in two classes: class I subunits, p100/p52 and p105/p50, are firstly synthesised as longer precursors and to be functionally active they must undergo a proteolytic cleavage, which eliminates the several IκB-like ankyrin-repeats at the C-terminal. The remaining three members RelA (p65), RelB and c-Rel belong to the class II subunits; unlike the other class, these proteins are synthetised in their active form, and they include a transcriptional activation domain (TAD) at the C-terminal end of the protein (Figure 2), which is necessary for the positive regulation of gene transcription (Hayden and Ghosh, 2008). Multiple combinations of the five subunits can be formed and dimer formation is not restricted to members of the same class; this heterogeneity of dimers represents the broad range of effects that NF-κB has on transcription, differentially modulating gene expression based on the activated dimer (Smale, 2012).

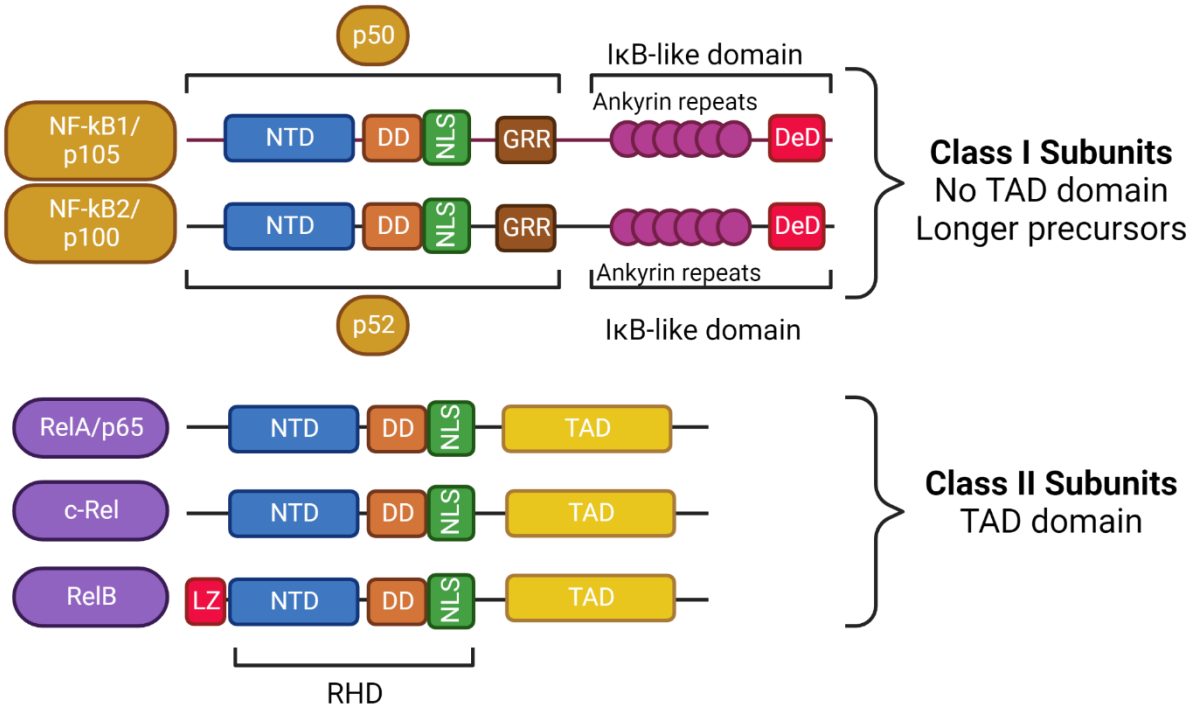

Figure 2. Graphic representation of NF-κB subunits structure. They all present a Rel Homology domain (RHD), which includes the N terminal domain (NTD) and the Dimerization Domain (DD), important for interactions with other subunits; next to it, the Nuclear Localisation Sequence (NLS) is found, important for dimers nuclear translocation. Class I subunits are synthetised as longer precursors and the IκB-like domain at the C terminal includes several ankyrin repeats and a Death Domain (DeD). Class II subunits on the other hand possess a Trans Activation Domain (TAD) at the C terminus that allows them to induce the expression of target genes. RelB is the only subunit with a Leucine Zipper (LZ) domain at the N terminal.

1.2. NF-κB activation mechanisms

Under resting conditions, NF-κB proteins are retained in the cytoplasm, due to the association with inhibitory proteins called IκB (IκBα, IκBβ and IκBε); these proteins, similarly to non-canonical NF-κB inhibitors such as BCL-3 and IκBζ (Oeckinghaus and Ghosh, 2009), contain five to seven tandem ankyrin-repeats (AnkR); AnkRs are 33 amino acid ankyrin-like protein-protein association domains that are able to bind and mask the NF-κB NLS, thus preventing migration into the nucleus. The C-terminus of class I subunits p100/p52 and p105/p50, also known as IκBδ and IκBγ respectively, include the same AnkRs repeats, (Figure 3); the presence of this motif renders these two proteins intrinsically inactivated and unable to migrate into the nucleus until they are processed, and the C-terminus is removed (Zhang, Lenardo and Baltimore, 2017).

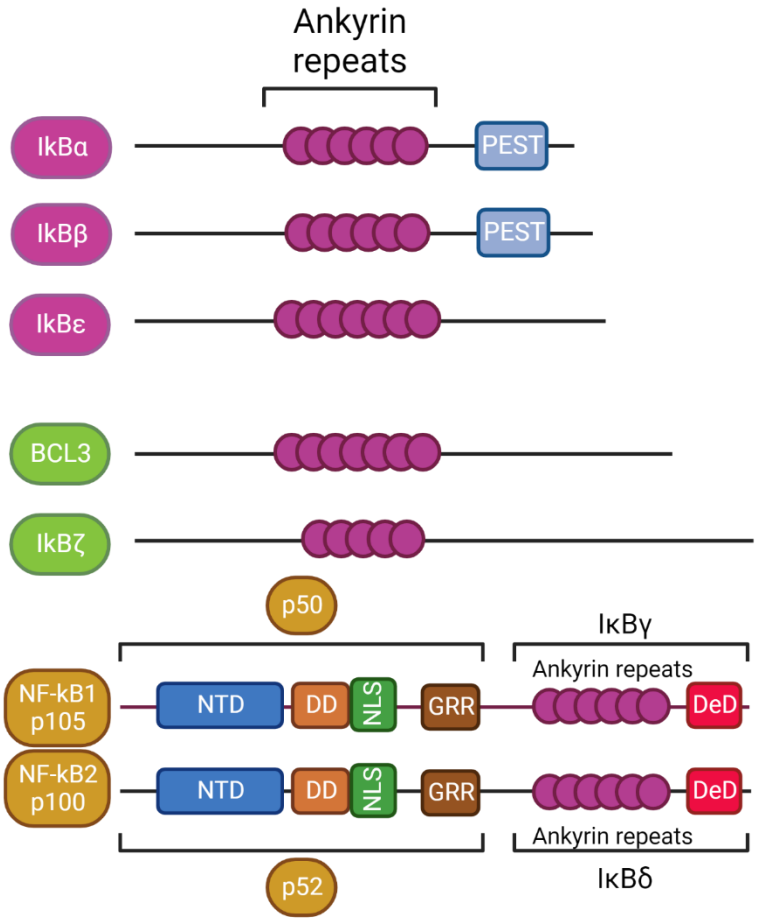

Figure 3. Inhibitors of NF-κB. They all contain Ankyrin repeats which are essential for binding and masking the NLS on NF-κB subunits, preventing their translocation and activity in the nucleus. The first three IκBs are known as classical inhibitors. IκBα and IκBβ present a PEST sequence rich in proline, glutamic acid, serine and threonine that works as a degradation signal. BCL3 and IκBζ are considered less canonical NF-κB inhibitors, even if they present a similar structure of the previous group. Lastly, the C terminus of p105 and p100 acts as an IκB protein, also known as IκBγ and IκBδ respectively, limiting the activation of NF-κB dimers.

The first proposed mechanism for NF-κB inhibition suggested that IκB proteins were able to hide the NLS, preventing the nuclear translocation of NF-κB dimers until stimulation. However, further investigations contributed to the improvement of this model, showing that the balance between cytoplasmic and nuclear NF-κB is more dynamic, and that the strategy to retain inactivated NF-κB in the cytoplasm depends on the inhibitor protein involved (Figure 4). For example, IκBβ presents a high affinity toward NF-κB complexes because of its ability to bind the NLS in both subunits of the dimer, thus retaining NF-κB in the cytoplasm until activation. On the other hand, IκBα recognises and hides the NLS in one subunit only, so under basal conditions the dimers can still migrate into the nucleus, where NF-κB-IκBα complexes are constitutively found, even if at a low concentration (Malek *et al.*, 2001); IκBα is then able to force the export via Chromosomal Maintenance 1 (CRM1) exportin of the inactivated nuclear NF-κB-IκBα complexes back into the cytoplasm through a Leucin-rich nuclear export sequence (NES) at the N terminal (Huang *et al.*, 2000), thus resulting in a dynamic regulation of the rates of import/export of the dimers associated with the inhibitory protein. However, recent studies showed that IκB proteins can be dispensable for cytoplasmic retention of NF-κB dimers, but they are essential to prevent DNA binding activity under resting conditions and to guarantee the responsiveness of the dimers upon stimulation (Tergaonkar *et al.*, 2005). Lastly, a recent paper contested the ability of NF-κB-IκBα complexes to migrate in the nucleus without stimulation (Florio *et al.*, 2022). In vitro assays showed that importin α3, the main importin responsible for NF-κB nuclear translocation (Fagerlund *et al.*, 2005), was unable to bind to NF-κB dimers when coupled to IκBα, thus the import of the dimers would be possible only after the inhibitor protein degradation, which is a consequence to cells stimulation (Florio *et al.*, 2022).

Another level of NF-κB activation regulation is provided by ubiquitination and enzymes adding and removing these groups are important for the modulation of NF-κB activity. A20, also known as TNFAIP3, is one of the most prominent and best studied deubiquitinating enzymes involved in the negative control of NF-κB activity (Shembade and Harhaj, 2012). So far, the ubiquitin – editing activity of A20 has been reported in the TNFR pathway only, where A20 downregulated the activity of NF-κB through the cooperative actions of its two ubiquitin – editing domains (Wertz *et al.*, 2004). The amino terminal of A20 acts as a de – ubiquitinase by removing the lysine 63 (K63) polyubiquitin chains from Receptor Interacting Protein (RIP), which is an essential upstream activator in the TNFR pathway (Kelliher *et al.*, 1998). The carboxy terminal

of A20 is then able to act as a ubiquitin ligase, transferring the polyubiquitin chains to K68 on the same RIP, targeting it for proteasomal degradation; by missing a key upstream regulator, NF-κB fails to be activated and hence its activity is downregulated. These results are supported by *in vivo* studies, showing that $A20^{-/-}$ mice developed severe inflammation and hypersensitivity to both LPS and TNFα, as they fail to limit immune responses (Lee *et al.*, 2000).

Many pathways lead to the downstream activation of NF-κB, and they are distinguished as canonical, non-canonical and atypical. The first step shared by all three activation processes is the degradation of IκB proteins via ubiquitin – proteasome system.

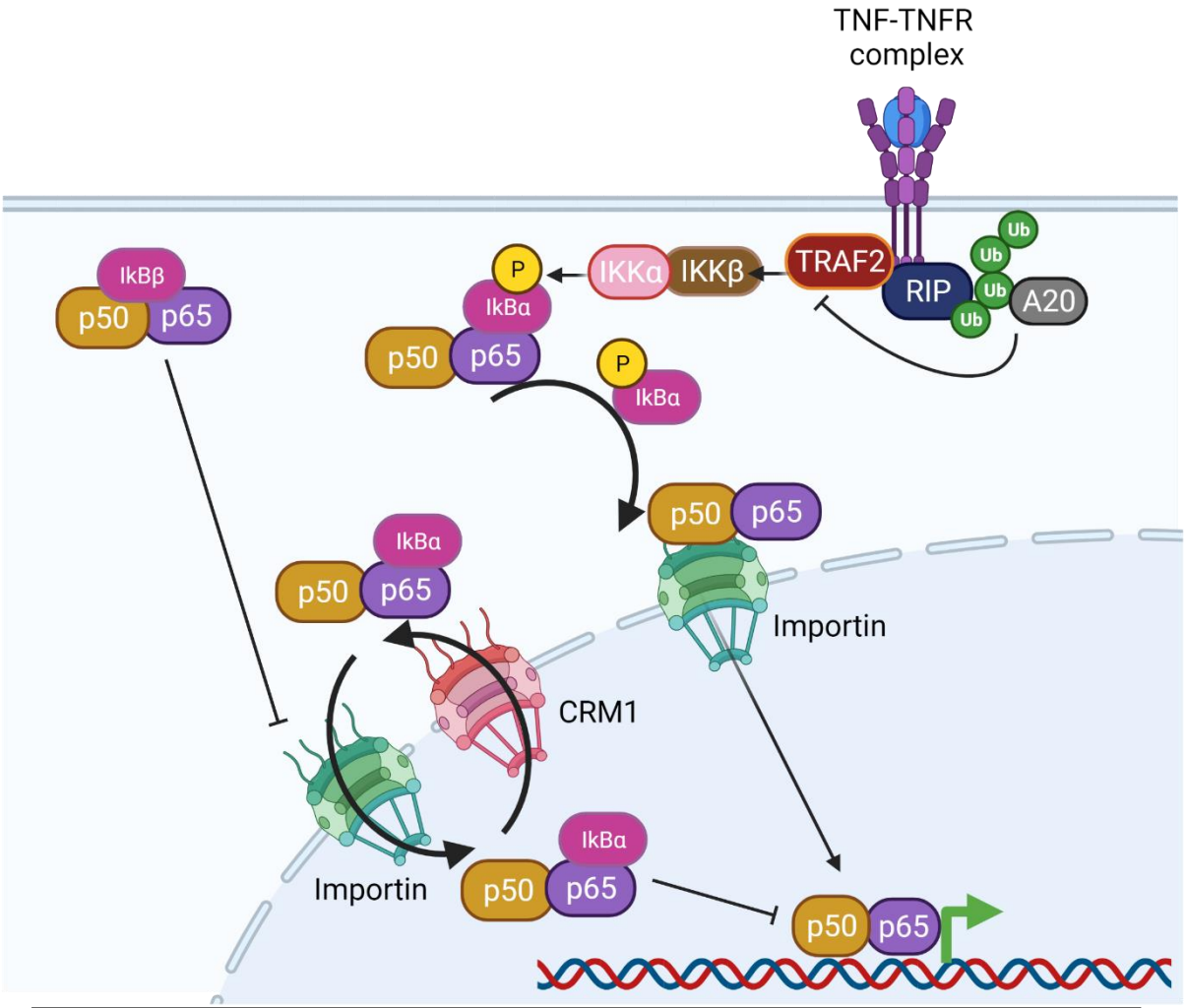

Figure 4. Different mechanisms to negatively regulate NF-κB. Conventionally, IκB proteins were thought to prevent the translocation in the nucleus, and that is still the proposed mechanism for IκBβ, which masks both NLS in the dimer, retaining them in the cytoplasm until stimulation. However, IκBα mechanism is debated, as some works suggested that under basal conditions, NF-κB-IκBα could still be found in the nucleus, even if inactive. More recent papers showed that the interaction with the importin responsible for NF-κB translocation cannot happen if the dimers are bound to IκBα, suggesting that a stimulus is needed. Lastly, A20 negatively regulates NF-κB activity acting as a ubiquitin editing protein and targeting an important upstream activator, namely RIP, for proteasomal degradation.

In the canonical pathway, the extracellular stimulation activates TGFβ-activated kinase 1 (TAK1) which in turn activates the cytosolic holoenzyme IκB kinases (IKK) (Sun, 2017). The IKK complex is formed by a regulatory subunit IKKγ, also known as NEMO (NF-κB essential modifier) and two kinase subunits, IKKα and IKKβ. NEMO has no catalytical activity but functions as a scaffold that assembles IKKα and IKKβ into a holoenzyme. Moreover, NEMO is required for the ubiquitination activity that leads to the elimination of IκBs *via* proteasomal degradation (Cartwright, Perkins and L Wilson, 2016). After IKK phosphorylates IκBα on either Ser^{32} or Ser^{36}, the $E3^{IκB}$ ubiquitin ligase complex β-TrCP-SCF recognises these sites and attaches ubiquitin motifs as a signal for degradation (Ben-Neriah, 2002). In this pathway, the signalling is triggered by a variety of stimuli, including TNF receptor family members, patter-recognition receptors (PPRs) and B- and T-cell receptors (Liu et al., 2017). IKK itself responds to different factors, including growth factors, mitogens and agents causing stress (Zhang and Sun, 2015).

The non-canonical pathway is triggered by other members of the TNF family, including CD40 and BAFF ligands recognising their receptors on cell surface (Sun, 2012). This results in the activation of the NF-κB inducing kinase (NIK) that can phosphorylate and activate IKKα dimers; IKKα uses its kinase activity to induce the maturation of p100 into p52, through the phosphorylation of the protein, especially when coupled with RelB (Hayden and Ghosh, 2008).

Lastly, the atypical pathway is initiated by UV, ROS or Hypoxia stresses. IKKs are not involved in this case, but they are substituted by other kinases (Janssens and Tschopp, 2006). Similar to the canonical mechanism, IκBα is phosphorylated by specific activated kinases, such as Casein Kinase II in response to UV (Kato *et al.*, 2003) and Tyrosine Kinase in response to ROS (Takada *et al.*, 2003), and it is sent to the proteasome to be degraded. Once the dimers are free from IκBs inhibition, they translocate into the nucleus, recognise their target sequence and stimulate gene transcription (Figure 5).

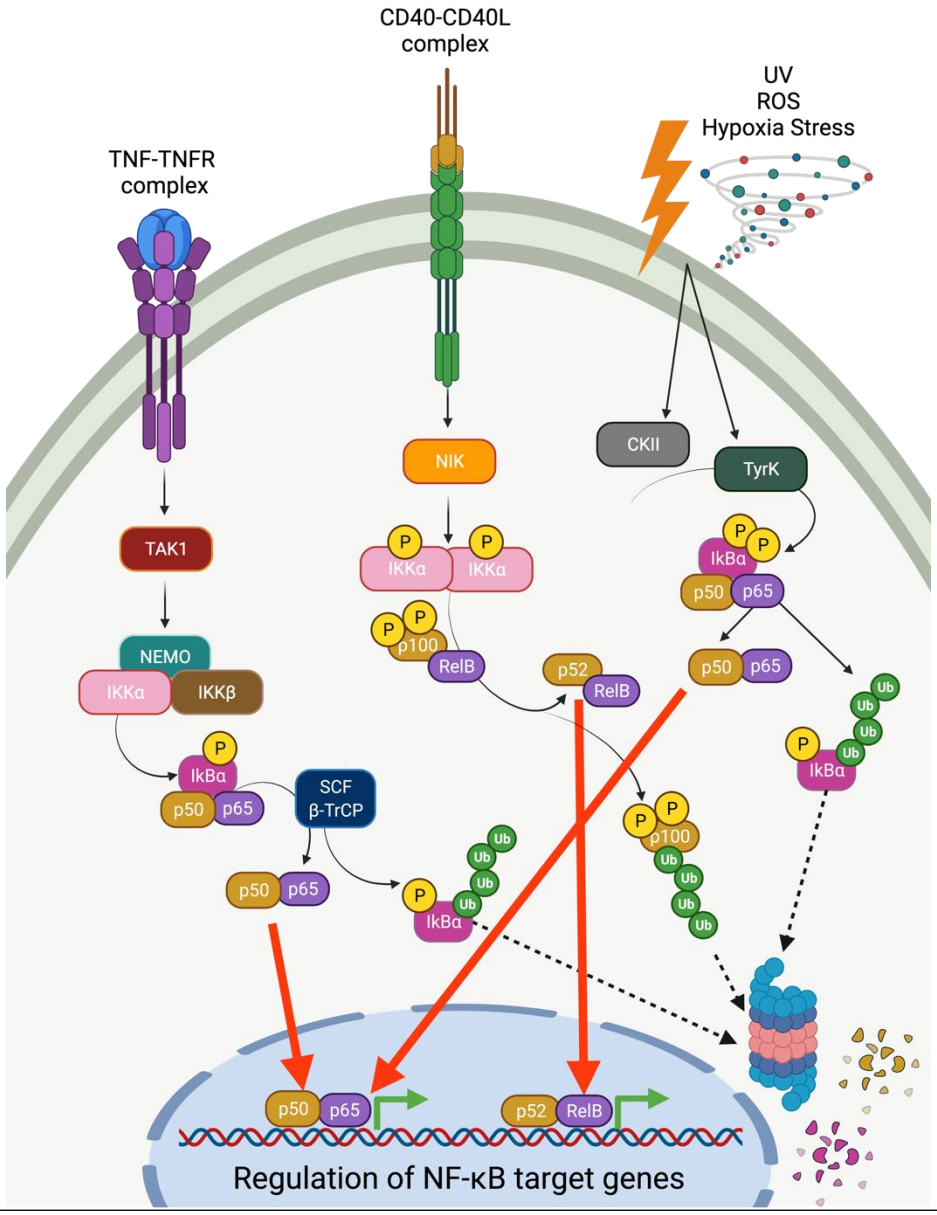

Figure 5. Different mechanisms of NF-κB activation. The canonical pathways can be activated by TNFα, IL1 and LPS. TGFβ-activated kinase 1 (TAK1) recruits the IKK complex (NEMO, IKKα, IKKβ) that phosphorylates IκBα, which is ubiquitinated and degraded by the proteasome; p65:p50 dimers migrate in the nucleus and stimulate gene expression. The non-canonical pathway is activated by CD40L; NF-κB inducing kinase (NIK) phosphorylates and activates IKKα, which mediates the maturation of p100 to p52 when bound to RelB. The atypical pathway is activated by external stresses, and it leads to the phosphorylation of IκBα by other kinases, such as Casein Kinase II (CKII) and Tyrosine kinases (TyrK). Adapted from Cartwright, Perkins and L Wilson, 2016.

1.3. NF-κB role in inflammation and beyond

The majority of NF-κB targets are pro – inflammatory genes and in particular NF-κB is rapidly activated to support the innate immune response. Several triggers lead to NF-κB activity, such as the inflammatory cytokines TNFα and IL-1 in the canonical pathway, and CD40 ligand in the non-canonical. NF-κB subunits can combine in up to

15 known dimers, but the best – studied and characterised is p65:p50, also called the "canonical" dimer because of the important role played in the inflammatory process.

Historically, p65 had been widely investigated because of the observation that $RelA^{-/-}$ leaded to embryonic lethality and liver degeneration in mice (Beg *et al.*, 1995). Also, loss of RelA affects cell proliferation and exacerbates immune responses (Steinbrecher *et al.*, 2008); on the other hand, $nfκb1^{-/-}$ mice had normal development, but they displayed defects in immune responses, with abnormal B cell activity (Sha *et al.*, 1995a) and age – related neural degeneration (Lu *et al.*, 2006).

Upon stimulation, the degradation of IκBα occurs in minutes (Karin, Ben-Neriah and Ben-Neriah, 2000) and the lack of inhibition allows the translocation of the dimers in the nucleus. p65:p50 are activated and they bind the κB sites located at enhancers and promoters of pro-inflammatory and anti-apoptotic genes, stimulating their transcription. The dimers efficiently control the expression of cytokines and chemokines, amplifying the inflammatory signal, but p65:p50 also upregulate the production of adhesion molecules such as ICAM-1, VCAM-1 and ELAM, essential for the recruitment of other immune cells in locus. P65:p50 regulates genes involved in apoptosis and cell-survival.

In a similar manner, RelB:p52 dimers are able to induce the activation of the non-canonical pathway, even if the signalling is more tightly controlled than the canonical pathway and its rate limiting step is the maturation of p100 into p52 (Xiao, Harhaj and Sun, 2001). Upon activation, RelB:p52 dimers stimulate the production of chemokines, such as B-lymphocyte chemoattractant (BLC or CXCL13), and cytokines as B-cell activating factor belonging to the TNF family (BAFF); unlike p65:p50, RelB:p52 is involved in adaptive immunity, rather than innate. This was supported by studies involving B cells lacking nfkb2 or other activators of the pathway, such as NIK and IKKα, providing evidence which highlighted the importance of this pathway for maturation and survival *in vivo* of B cells (Gardam *et al.*, 2008). Interestingly, the non-canonical pathway is also fundamental for the development of lymphoid organs, both primary and secondary; in the thymus, the non-canonical pathway regulates the development of thymic epithelial cells (TECs), important mediators of immune tolerance, as they are required for the negative selection of thymocyte and generation of immunosuppressive regulatory T_{reg} cells (Abramson and Anderson, 2017). The NF-κB pathway also mediates the development and the structural organisation of

secondary lymphoid organs, such as the spleen, lymph nodes and mucosal lymphoid tissues (Weih *et al.*, 2003). Lastly, *nfκb2*$^{-/-}$ (p100/p52) and *relb*$^{-/-}$ mice showed impairment in T-cell maturation (Burkly *et al.*, 1995; Franzoso *et al.*, 1998) with impaired antigen – presenting functions and excessive production of granulocytes and macrophages for *relb*$^{-/-}$ mouse models. Milder effects to these processes were observed in case of lacking *nfκb1*$^{-/-}$ (p105/p50) (Bonizzi and Karin, 2004).

Lastly, with regards to the fifth NF-κB subunit, c-rel, knockout mice present impairment in lymphocyte proliferation and activity (Kontgen *et al.*, 1995), and recent findings suggested that c-rel is essential for the cytotoxic activity of Natural Killer (NK) cells (Vicioso *et al.*, 2021).

Although the triggers and the downstream effects are different, the two types of dimers just discussed stimulate gene expression through the TAD domain in RelA and RelB, enabling the activation of transcription. This event would not occur with p50 and p52 homodimers, as they lack the transactivation domain. Because of this, p50 and p52 homodimers are normally associated with repression. To induce gene expression, p50 and p52 homodimers need to be associated with transcriptional co-regulators, such as B-cell lymphoma 3 (Bcl3) or CREB binding protein (CBP). For example, p50:p50:Bcl3 was found to attenuate the inflammatory response in macrophage after LPS activation, including the expression of anti-inflammatory genes, such as IL-10 (Wessells *et al.*, 2004).

It is evident that different dimers play separate and sometimes opposite roles within the same pathway; this is one of the layers of control associated with the NF-κB system, in order to keep a balance between the two possible directions of gene regulation. Excessive activation of canonical p65:p50 leads to autoimmune and inflammatory diseases, such as Rheumatoid arthritis, inflammatory bowel disease and multiple sclerosis (Liu *et al.*, 2017b). Also, its continual activation can stimulate tumour initiation by promoting a microenvironment rich in reactive oxygen species (ROS) and reactive nitrogen intermediates (RIN) (Yu *et al.*, 2020). Canonical NF-κB promotes cell survival by triggering the expression of anti-apoptotic genes, such as *BCLX*, *X-IAP*, *BIRC2* and *TNFAIP3*, reducing the effectiveness of many anti-cancer therapies; P65:p50 can also facilitate tumour cell proliferation with the production of c-Myc; the dimers induce tumour invasion and metastasis *via* the stimulation of cellular adhesion molecules and factors involved in angiogenesis, like vascular epithelial growth factor

(VEGF). Lastly p65:p50 stimulates cell immortalisation due to the activation of telomerase (Perkins and Gilmore, 2006)(Figure 6).

Over the past years different NF-κB targeted therapies have been employed in order to limit the excessive activity of P65:p50 in the background of persistent inflammation or illness (Liu *et al.*, 2017b), including the use of antibodies against ligands involved in the cascade, e.g. anti TNFα approaches (Yu *et al.*, 2020). Another option may employ the action of p50 homodimers to balance the activity of the canonical dimer, due to their anti p65:p50 function. For this reason, p50 has been widely investigated.

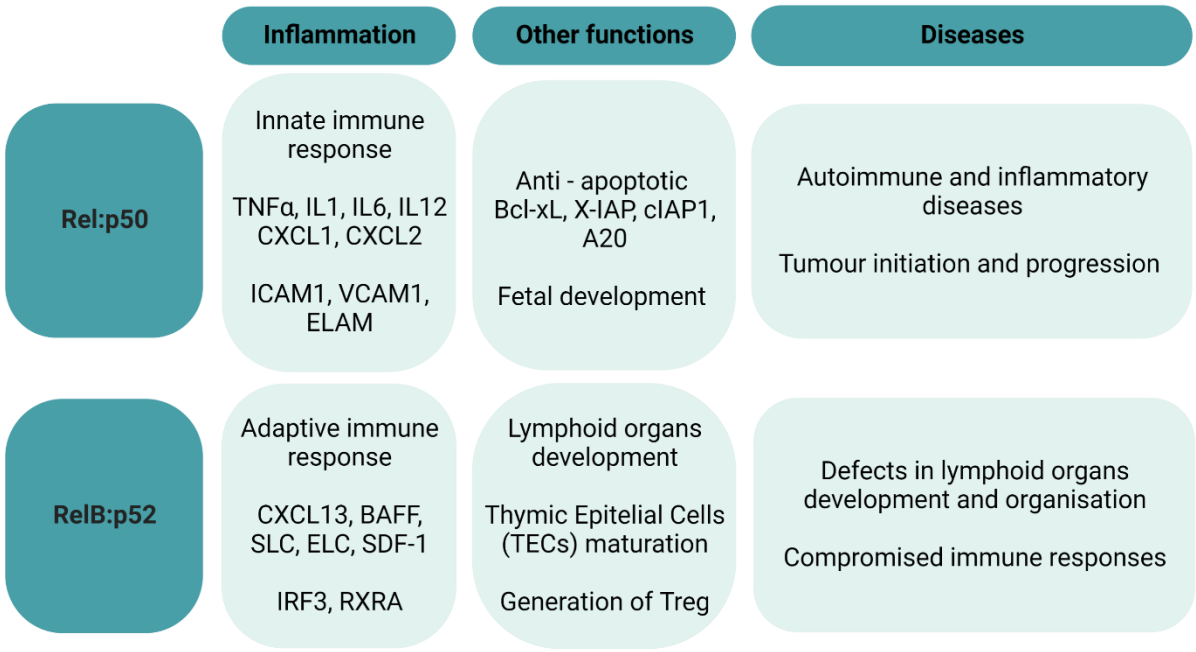

Figure 6. Summary of the different effects and functions of the canonical RelA:p50 and the non-canonical RelB:p52. Both dimers are essential to successfully trigger the immune response, native and adaptive respectively. RelA:p50 controls the expression of anti – apoptotic and cell survival genes as well, so it is not surprising that dysregulation of the dimer activity leads to autoimmune and inflammatory disease, easily progressing to tumorigenesis. RelB:p52 is important for lymphoid organs development and immune cells maturation, so changes to its functions can compromise immune responses and lymphoid organs organisation.

1.4. NF-κB1

1.4.1. p105 and p50

Nκb1 is the gene that encodes for the precursor p105 or NFκB1, composed of the active form p50 at the N-terminus and the inhibitory IκBγ at the C-terminus, rich in ankyrin-repeats; this motif serves to maintain the dimers inactive, under resting conditions (Figure 7).

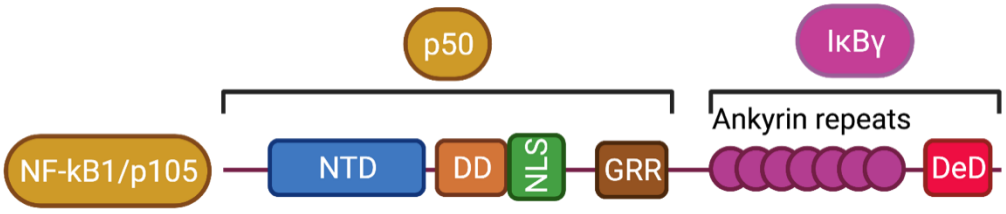

Figure 7. Graphic representation of NF-κB1 structure. p105 is the longer precursor, composed of the active form p50 at N terminal and the inhibitory IκBγ at the C terminal. The latter aims to keep the dimers inactive prior to stimulation. Once processed, the C terminal is degraded via proteasome processing and the dimers can translocate in the nucleus to exert their activity.

Despite the greatest importance given to the mature p50, several studies have shown that its precursor p105 has independent functions, before being processed to the mature protein. In fact, p105 has been found to be part of high-molecular-weight inhibitory complexes with the other NF-κB precursor p100 and together they regulate various NF-κB subunits (Savinova, Hoffmann and Ghosh, 2009). Also, p105 is involved in the downstream negative regulation of the extracellular regulated kinase (ERK) signalling. p105 interacts with the tumour progression locus 2 (Tpl-2), involved in inflammation and in carcinogenesis. Two different interactions occur: the Tpl-2 C – terminus recognises a region encompassing residues 497 to 534 in the p105 sequence; on the other hand, the Tpl-2 kinase domain interacts with the p105 death domain, which stabilizes Tpl-2 and blocks its kinase activity, inhibiting the ERK pathway (Beinke *et al.*, 2003). Tpl-2 is also responsible for the proteolysis of p105 to generate p50, but in vitro experiments suggested it does not phosphorylate p105 directly, as kinase – inactive Tpl-2 does not affect NF-κB activity (Belich *et al.*, 1999). Interestingly, Bcl3 can also interact with Tpl2, promoting its nuclear translocation and degradation, acting as a negative regulator of the Mitogen – Activated Protein Kinase (MAPK) pathway (Collins *et al.*, 2019); in the absence of MAPK activity, NF-κB activation does not result in inflammation (Guma *et al.*, 2011), highlighting Bcl3 as an important factor linking MAPK and NF-κB pathways in the nucleus.

p105 phosphorylation is essential for its processing. Two phosphorylatable residues specifically, serine 927 and 932, at the C terminal are essential for maturation to p50 and these sites are targeted by different kinases, depending on the context (Heissmeyer *et al.*, 2001).

Upon TNFα stimulation, p105 is phosphorylated by the IKK complex and this modification creates a recognition site for the β-TrCP E3 complex, very similarly to the IκBα degradation process. In the same manner, the ubiquitin ligase targets the phosphorylated p105, resulting in the complete elimination of the molecule and the

release of NF-κB dimers anchored to the p105 ankyrin-repeats (Heissmeyer *et al.*, 2001). This controlled p105 degradation is important in the regulation of p50 homodimers, because once activated they migrate into the nucleus and, based on the availability of Bcl3, they then act as inhibitors of P65:p50 dimers activity. As previously mentioned, Bcl3 can interact with p50 homodimers, and in particular it stabilises them by preventing their ubiquitination and following degradation (Carmody *et al.*, 2007). In turn, Bcl3 – stabilized p50 homodimers form a repressive complex that competes with other transcriptionally active NF-κB dimers, downregulating the expression of cytokines and limiting inflammation. For this reason, exploiting Bcl3 activity has been considered as an effective approach to limit detrimental consequences of uncontrolled inflammatory responses (Collins *et al.*, 2015).

Under basal conditions, the presence of a long Gly-Ala repeat (GRR) adjacent to the RHD in p105 sequence seems to be important as a “stop signal” for the proteasome, that leads to p105 processing rather than degradation, resulting in the generation of the shorter and mature p50 (Li and Ghosh, 1996). Similarly to stimulated conditions, ubiquitin ligases are also involved in the basal maturation of p105 to p50, but they were initially unknown. A recent study identified the KIP ubiquitination-promoting complex (KPC) as the Ub ligase (E3) required for the processing of p105 under both stimulated and unstimulated conditions. The KPC complex is composed of KPC1, a RING-finger protein acting as the ligase, and KPC2, a shuttle protein that is able to interacts with ubiquitinated proteins and the proteasome; also, KPC2 stabilizes KPC1, promoting its activity (Figure 8).

The “decision-making” between complete degradation or processing is still unclear, but it was proposed to be dependent on the length of the ubiquitin chain and anchoring sites, affecting the recognition and the action of the 26S proteasome (Kravtsova-Ivantsiv *et al.*, 2015). Although the similar mechanism is shared by the two Ub ligases, β-TrCP E3 and KPC, the latter seems to be also relevant as a tumour suppressor. By regulating the processing of p105, KPC is able to increase the concentration of p50 protein, supporting the formation of p50:p50 dimers, rather than the canonical P65:p50, promoting their anti-tumour activity (Kravtsova-Ivantsiv *et al.*, 2015).

Certain domains within the p105 sequence have also been proved to be important for p50 survival to the proteasomal process, at least under basal conditions. The stability of RHD is a peculiar example of this, as mutations occurring in its sequence destabilise the domain and the processing fails to generate p50 (Lin and Kobayashi, 2003).

Lastly, the generation of p105 can be translation- and ubiquitination- independent when involving the 20S proteasome subunit. In this case, the GRR is again essential as a stop signal and the 20S subunit is able to cleave the precursor and selectively degrade the C terminal of p105, resulting in mature p50 (Moorthy *et al.*, 2006).

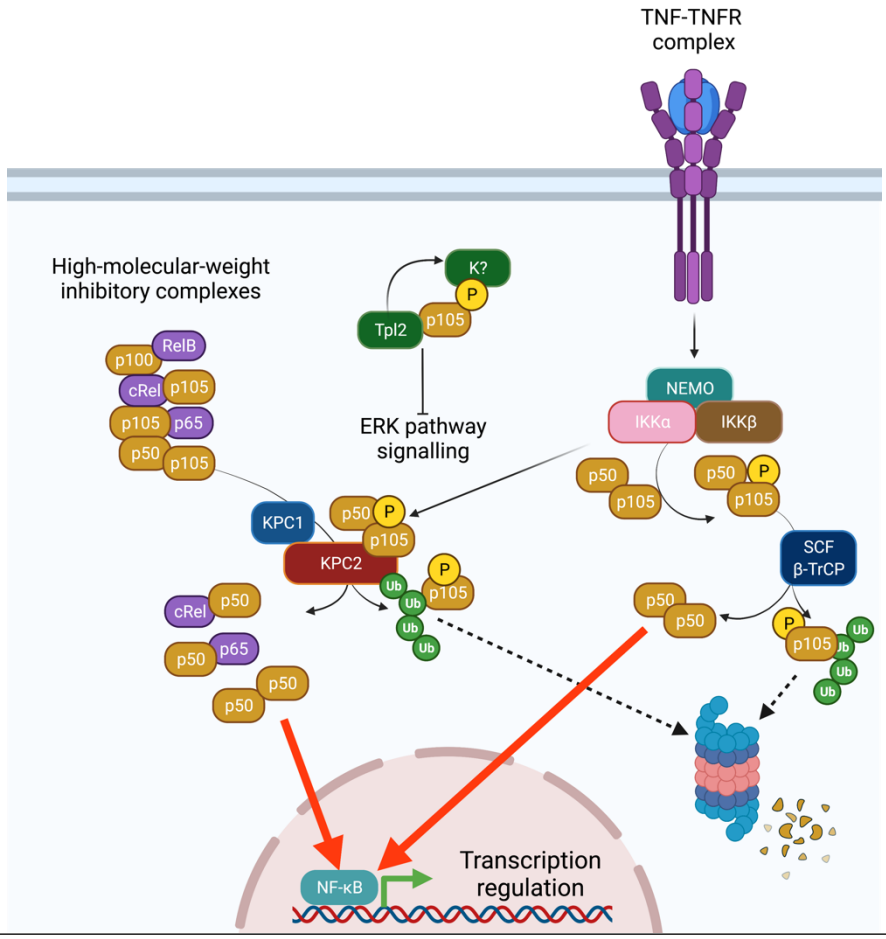

Figure 8. Mechanisms to p105 processing and degradation. p105 can form high molecular weight inhibitory complexes with other NF-κB subunits and regulate their activation. p105 can also inhibit the kinase activity of tumour progression locus 2 (Tpl2), blocking the ERK pathway cascade. Tpl2 in turn modulates the processing of p105 by activating another kinase to phosphorylate p105, as degradation signal. TNFα signalling activates IKK complex, which phosphorylates p105, recognised by the SCF-β-TrCP E3 ligase complex; the ubiquinated protein is sent to the proteasome. KPC complex (KPC1:KPC2) is the ubiquitin ligase complex that contributes to p50 maturation under both basal and stimulated conditions.

1.4.2. Nfκb1 in inflammation

It has been previously reported that p65:p50 can play a fundamental role in the onset of chronic diseases, such as cancer and ageing (García-García *et al.*, 2021), and that p50 homodimers are able to contrast this action. These opposite effects are the result of the structural difference existing between RelA and p50, as the latter does not possess the TAD. For this reason, p50 is able to stimulate gene expression only when

forming a dimer with RelA and other subunits possessing a TAD, or if the p50 homodimers are associated with co-factors; under normal conditions, p50 homodimers bind the same sites of p65:p50, but they exert the opposite effect on the expression of those genes. The global effect on inflammation and other pathways depends on the stoichiometry of the two types of dimers, but also on the competition and the affinity for the same κB sites at gene promoters, targeted by both p65:p50 and p50:p50 (Cartwright *et al.*, 2018).

Consequences of NFKBI knockout on other subunits and dimers formation have been assessed in different models. In B cells, lack of NFκB1 does not seem to affect p52 levels in the cytoplasm, but c-rel, RelB and p65 expression was substantially lower in *nfκb1*$^{-/-}$ cells (Sha *et al.*, 1995b); another *nfκb1*$^{-/-}$ model was used to assess the composition of active NF-κB dimers in ko cells, which presented p52:p65 heterodimers and no p65:p50 and p50:p50 (as expected), but also p65 homodimers were found, similarly to wt cells (Hoffmann, Leung and Baltimore, 2003), suggesting that the knock out of a single subunit impacts not only expression levels of the other subunits, but it can also result in partial compensatory effects in dimer formations and NF-κB activity (Perkins, 2012).

Under physiological conditions, regulation of dimer formation is controlled on many levels, and in particular co- and post-translational modifications on p50 protein can greatly affect its ability to either bind the DNA or to form homodimer with itself. Serine 65 and 343 are essential for the homodimerization but not required for the heterodimer formation (Cartwright *et al.*, 2018); if mutated, the possibility to form p50:p50 is disrupted, while the heterodimer formation remains unaffected. Furthermore, serine 903 and 907 are involved in p50 maturation as they are essential phosphorylation sites involved in p105 cleavage and p50 release. S903/7A mutation prevents the degradation of p105 upon TNFα. Other residues, such as K431, K440 and K441, can be acetylated, thus enhancing the DNA binding activity (Cartwright, Perkins and L Wilson, 2016).

The precise mechanism by which one dimer can displace another dimer is still unclear, but it seems that different dimers directly compete for the κB sites and regulate gene expression accordingly. Further studies highlighted that an epigenetic component might be involved too, as p50 is able to remodel the state of chromatin, promoting a repressive state (Elsharkawy *et al.*, 2010).

Because of its ability to modulate gene expression in both directions and its opposite role to RelA activity, p50 has been broadly investigated in the context of inflammation and in particular great attention has been given to its role in liver inflammation.

Several studies have shown that total *nfκb1*$^{-/-}$ mice present enhanced inflammation in different organs, such as liver, kidney and lung. With particular attention to the liver, *nfκb1*$^{-/-}$ hepatic stellate cells (HSCs) were investigated and compared to wt HSCs upon unstimulated conditions, in order to understand which genes are regulated by p50 activity at basal levels. The choice of this cell type was justified by the importance of HSCs in the context of liver inflammation; in absence of damage, HSCs mainly store vitamin A, and they sense damage. Also, according to some studies, they act as antigen presenting cells (APCs) but this concept has been debated over the last decade (Viñas *et al.*, 2003; Bomble *et al.*, 2010; Benitez *et al.*, 2020). However, when activated, they transdifferentiate in myofibroblasts, which are essential for wound healing and scar tissue deposition (Mann *et al.*, 2007). When lacking p50, HSCs express upregulated levels of TNFα and other 107 genes belonging to a wide number of processes, including inflammation and immunity. Four of the most up-regulated genes in *nfκb1*$^{-/-}$ cells, Mmp-13, GM-CSF, CCL2 and CXCL10 were further investigated, and they were found to be upregulated in a model of CCl_4 liver injury as well. Altogether these results suggested that the lack of p50 induces an upregulation of a panel of inflammatory genes, without the need of a stimulus. Also, the absence of p50 makes the cells more prone to damage after CCl_4 treatment (Elsharkawy *et al.*, 2010).

The mechanism by which p50 was able to regulate the expression of those genes was unclear, as p50 homodimers can exert their role on their own, but they can also recruit co-factors which influence the dimers activity (Wessells *et al.*, 2004; Paz-Priel *et al.*, 2011; Ea *et al.*, 2012) . In this case, they suggested that p50 homodimers were able to form a repressive complex with the histone deacetylase 1 (HDAC1) and the complex was then recruited to the targeted genes, promoting the condensation of chromatin into a repressive state (Figure 9). Chromatin Immunoprecipitation (ChIP) against HDAC1 elucidated that in normal conditions the enzyme is enriched at specific κB sites, but in *nfκb1*$^{-/-}$ HSCs the amount of HDAC1 at the same promoters was drastically reduced, comparable to the low levels detected in the control IgG sample (Elsharkawy *et al.*, 2010). This result supported the hypothesis that HDAC1 is recruited at genes

promoters in a p50-dependent fashion, as the recruitment is abolished when the cells lack p50. Moreover, these findings opened the hypothesis that p50 homodimers are able to modify the structure of chromatin when recruiting and coupling with epigenetic modifiers, such as HDAC1 (Elsharkawy *et al.*, 2010).

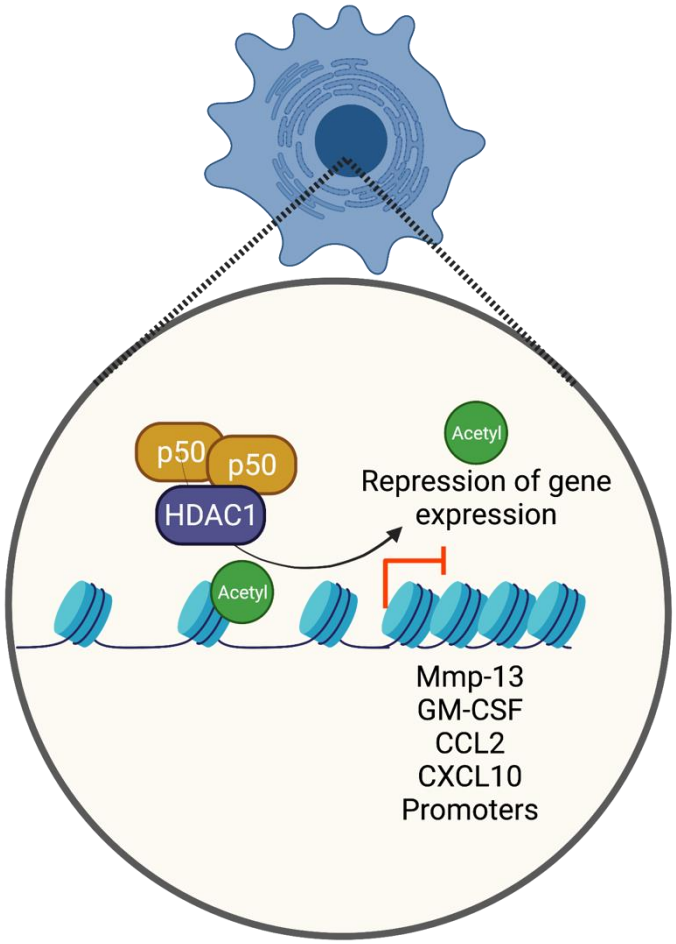

Figure 9. Repressive activity of p50 homodimers through the recruitment of the epigenetic modifier HDAC1, according to the results obtained in an in vitro model in HSCs. Under basal conditions, cell lacking p50 expressed more inflammatory genes, the top four (Mmp-13, GM-CSF, CCL2 and CXCL10) being found upregulated in other models of liver damage. ChIP assays resulted in decreased enrichment of HDAC1 at the same gene promoters when p50 was missing, indicating that the gene transcription of those genes is regulated in a p50-dependent fashion.

1.4.3. Nfκb1 in chronic diseases

When inflammation becomes chronic, the excessive scar deposition and the consistent release of cytokines and chemokines alter the tissue integrity and functionality. The damage to the cells results in genomic instability and persistent DNA damage can trigger different responses, including cell senescence and the associated senescence – associated secretory phenotype (Rodier *et al.*, 2009).

Because NFκB1 is responsible for essential inhibition of acute inflammation and repression of p65:p50 – dependent expression of pro-inflammatory genes, its contribution to chronic liver diseases and ageing has been explored using mouse models.

nfκb1$^{-/-}$ mice were used to investigate p50 effects on inflammation *in vivo* (Jurk *et al.*, 2014). *Nfκb1*$^{-/-}$ cohort was found to be more prone to inflammation compared to control mice, even without external stimuli. High levels of the pro-inflammatory IL-6 were detected in their serum and CD3+ cells infiltration in the liver and other organs occurred. The phenotype could be ameliorated with the anti-inflammatory drug Ibuprofen (COX inhibitor).

It is known that sterile low-grade chronic inflammation and accumulation of cell damage are events associated with the ageing process. The time-dependant loss of functionality decreases the fitness of the system, and this generates a feed – forward loop where inflammation exacerbates the ageing process and vice versa (Salmien, Kaarniranta and Kauppinen, 2012; López-Otín *et al.*, 2013). The same *nfκb1*$^{-/-}$ mouse model was interrogated for biomarkers linked to ageing. *Nfκb1*$^{-/-}$ mice displayed a more aged phenotype compared to age-matching control mice. As a symptom of premature tissue ageing, lack of p50 caused senescence, leading to impairment of liver regeneration, which was restored when suppressing inflammation with an anti – inflammatory drug (ibuprofen). *Nfκb1*$^{-/-}$ mice presented more ATM-ATR foci, indicating DNA damage, and enhanced telomere dysfunction. As a conclusion, they confirmed that chronic inflammation in *nfκb1*$^{-/-}$ mice is responsible for accelerated senescence and accumulation of mutations and errors in the DNA predisposes to the progression from a chronic inflammatory disease to tumour development (Jurk *et al.*, 2014).

Due to the pleiotropic effects of p50 on different cellular processes, including inflammation and regeneration, the possible link between Nf-κB1 and ageing has been investigated. *Nfκb1*$^{-/-}$ mouse models were used to assess the influence of the gene in the ageing process. 12 months old *nfκb1*$^{-/-}$ mice, corresponding to middle aged humans (Flurkey, Currer and Harrison, 2007), presented visible indications of premature ageing compared to their control littermates, including rough fur coat, alopecia and rectal prolapses. Loss of *nfκb1*$^{-/-}$ also led to more tissue inflammation and cell senescence (Bernal *et al.*, 2014). These results were confirmed in 19-month-old *nfκb1*$^{-/-}$ mice, corresponding to 56-69 years old humans. With particular attention to the liver, mice

lacking p50 presented more steatosis and inflammation; a greater number of infiltrating immune cells (B cells and T cells) was also found in the hepatic tissue of *ko* mice, and the aggregates seemed to be organised in ectopic lymphoid structures (ELSs) (Bianchi *et al.*, 2021).

Briefly, ELSs, also known as tertiary lymphoid tissues, were first associated with localised and extended inflammatory response due to persistent pathogens (Mazzucchelli *et al.*, 1999). Chronic inflammation and repeated insults lead to the recruitment of T cells and B cells that would automatically organise themselves in structures resembling secondary lymphoid organs (SLOs), with distinct T regions and B cells follicles (Neyt *et al.*, 2012). This event has been named Tertiary Lymphoid Organs (TLOs) formation. Several chronic diseases have been associated with TLOs neogenesis, including autoimmune diseases (Aloisi and Pujol-Borrell, 2006; Corsiero *et al.*, 2016).

Following studies suggested that ELSs might have a more physiological function too, working with the SLOs to control and respond to local infections and damages. In particular, ELSs have been investigated in relation to cancer. Their development surrounding the tumour appears to be beneficial for the recognition of cancer antigens and tumour regression (Carragher, Rangel-Moreno and Randall, 2008). This hypothesis was confirmed in a mouse model of pulmonary metastasis and subcutaneous tumours. Certain cancers are particular immunogenic, and their markers are recognised by T cells. By stimulating the development of tertiary lymphoid organs at the cancer sites, the tumour growth was greatly inhibited in the lung and the cancer was completely eradicated in the case of melanoma (Schrama *et al.*, 2001). These results confirmed that the presence of ELSs in specific tumours and at specific stages of development can affect and help towards tumour suppression and elimination.

Although ELSs are associated with good prognosis in some types of malignancies, their presence in HCC was shown to correlate with poor prognosis (Jia *et al.*, 2022). A study involving HCC human tissues screening reported the presence of a 12-gene signature related to ELSs generation and development (Finkin *et al.*, 2015). The same samples were analysed for gene enrichment and NF-κB was found in the list on enriched genes, suggesting a possible role of NF-κB in tertiary lymphoid organs genesis in the liver. They confirmed this by using a mouse model in which IKKβ (involved in NF-κB activation) was constitutively active in hepatocytes only, resulting

in persistent activity of inflammatory NF-κB. The number of ELSs in these mice was greater than in the control group and as the mice aged, the ELSs increased in number. Moreover, the same mice presented aggressive HCC, in terms of tumour number and burden. These findings suggested that the ELSs can function as microniches for tumour development in the liver, because of excessive NF-κB activation that leads to atypical hepatocytes being generated at this site, which promote the progression to cancer (Figure 10) (Finkin *et al.*, 2015).

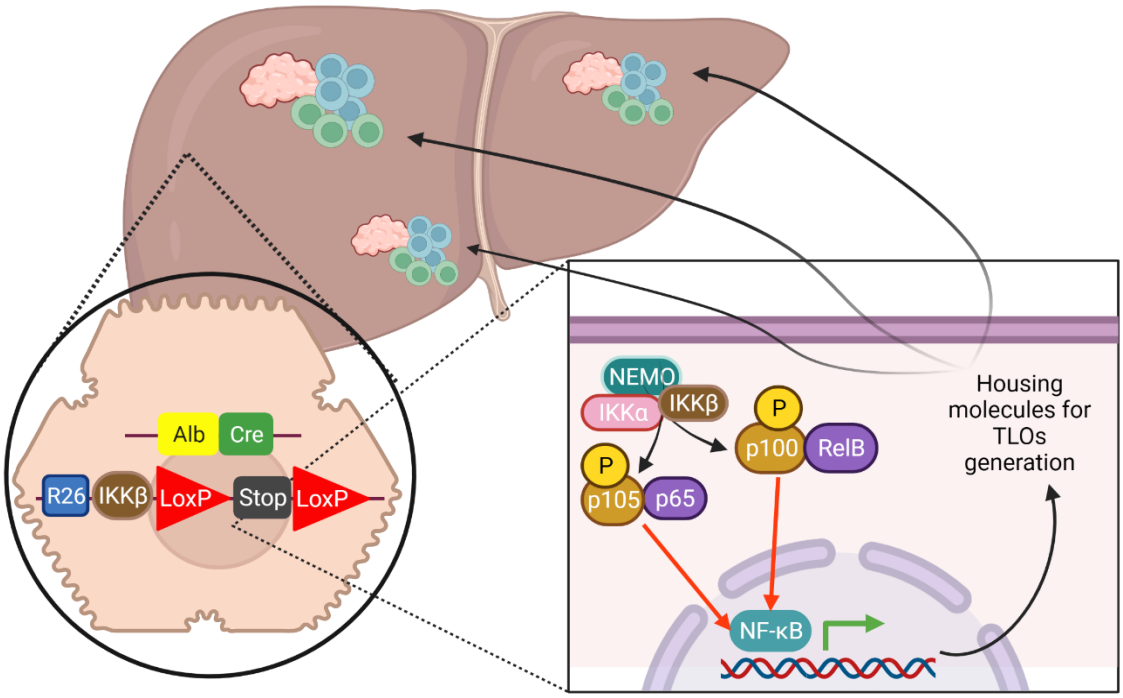

Figure 10. Graphic representation of the mechanism proposed by Finkin et al. (Finkin *et al.,* 2015) regarding NF-κB contribution to Tertiary Lymphoid Organs (TLO) or Ectopic Lymphoid Structures (ELSs) generation in the liver, associated with cancer. A mouse model carrying a constitutively active form of IKKβ in hepatocyte only was found to be more prone to ELSs and HCC development, compared to their control littermates. This phenotype was found to become worst as the mice were ageing. Consistent activation of NF-κB induces the secretion of housing molecules for B cells and T cells, which get recruited in the liver, forming ELSs. The environment rich in inflammatory mediators and immune cells promotes the transformation of hepatocytes towards malignant, resulting in tumorigenesis.

In recent years, next generation sequencing has been employed to characterise NFκB1 in the human population, in particular its mutations and the diseases correlating to them. Whole genome and exome sequencing highlighted mutations in both intronic and exonic regions in the *nfκb1* gene of subjects who suffered from Common Variable Immunodeficiency (CVID) (Fliegauf *et al.*, 2015), a heterogenous disorder affecting B and T cells function and characterised by recurrent infections and lymphoproliferative conditions (Cunningham-Rundles, 2012). Single Nucleotide Polymorphisms (SNPs) occurring at the *nfκb1* gene have also been correlated to cancers developing in

different organs, including liver (Cheng *et al.*, 2013; Gao *et al.*, 2014), stomach (Arisawa *et al.*, 2013; Chen *et al.*, 2015) and bladder (Li *et al.*, 2013).

1.4.4. Nfκb1 in HCC

Hepatocellular carcinoma (HCC) is the most common form of liver cancer and 90% of the cases are thought to arise on the background of chronic liver disease (CLD), with very poor prognosis when developing from cirrhosis. The immune system can have different effects on HCC, as some studies reported a better outcome when immune infiltrates were present, while others underlined the contribution of the immune system to create the perfect microenvironment for tumour progression (Llovet *et al.*, 2021).

An example of the latter has been demonstrated in a Diethylnitrosamine (DEN) cancer model in *nfκb1*$^{-/-}$ mice. DEN is a compound that acts as a liver carcinogen in mice 15 days after birth with a single injection. DEN-treated *nfκb1*$^{-/-}$ mice presented a greater number of neutrophils infiltrating the hepatic tissue, compared to the control group, accompanied by the presence of large tumours, liver enlargement and increased PCNA-positive hepatocytes. The recruitment of neutrophils on site was showed to be essential for tumorigenesis, as treatment with anti - Ly6G (neutrophils antigen) antibody ameliorated the phenotype of DEN-treated *nfκb1*$^{-/-}$ mice, reducing immune cell infiltration and tumour burden. The same mice also showed increased levels of pro-inflammatory CXCL2, TNFα and S100A9, which are necessary for the neutrophil migration to the injured liver, as investigated elsewhere (Moles *et al.*, 2013), and their expression is under the control of NF-κB. Following experiments confirmed that the negative regulation of those genes was p50 homodimers – dependent, as ChIP assays in control mice showed accumulation of p50 at the gene promoters. Moreover, the repression of gene expression was achieved by p50 homodimers through the recruitment of HDAC1 at the same gene promoters, as high levels of the protein were found at CXCL2, CXCL1 and S100A9 promoters in control mice, but HDAC1 levels were drastically reduced in *nfκb1*$^{-/-}$ mice. This result suggested that NF-κB1 represses the expression of chemokines involved in a neutrophil inflammation network, thus acting as tumour suppressor. The anti-tumour activity of the homodimers was confirmed by the use of another mouse model carrying a mutation to a residue essential for p50 homodimerization (S340A), while the ability to form heterodimers was conserved. Although the transcript levels were similar, *nfκb1*$^{S340A/S340A}$ mice presented reduced expression of both p105 and p50, indicating that the lack of the serine residue might affect p105/50 translation and/or stability. When the model was challenged with

DEN, *nfκb1*$^{S340A/S340A}$ presented enlarged livers and more tumours; the same inflammatory molecules previously analysed were found to elevated in *nfκb1*$^{S340A/S340A}$ compared to the control and because of this, a greater number of infiltrated neutrophils was found. The mechanism by which the neutrophils' induced HCC was unclear, but further analyses indicated that after being recruited *in situ*, neutrophil activity led to the accumulation of ROS, which in turn induced DNA damage and telomere dysfunction in hepatocytes, facilitating the progression to cancer (Figure 11) (Wilson *et al.*, 2015a).

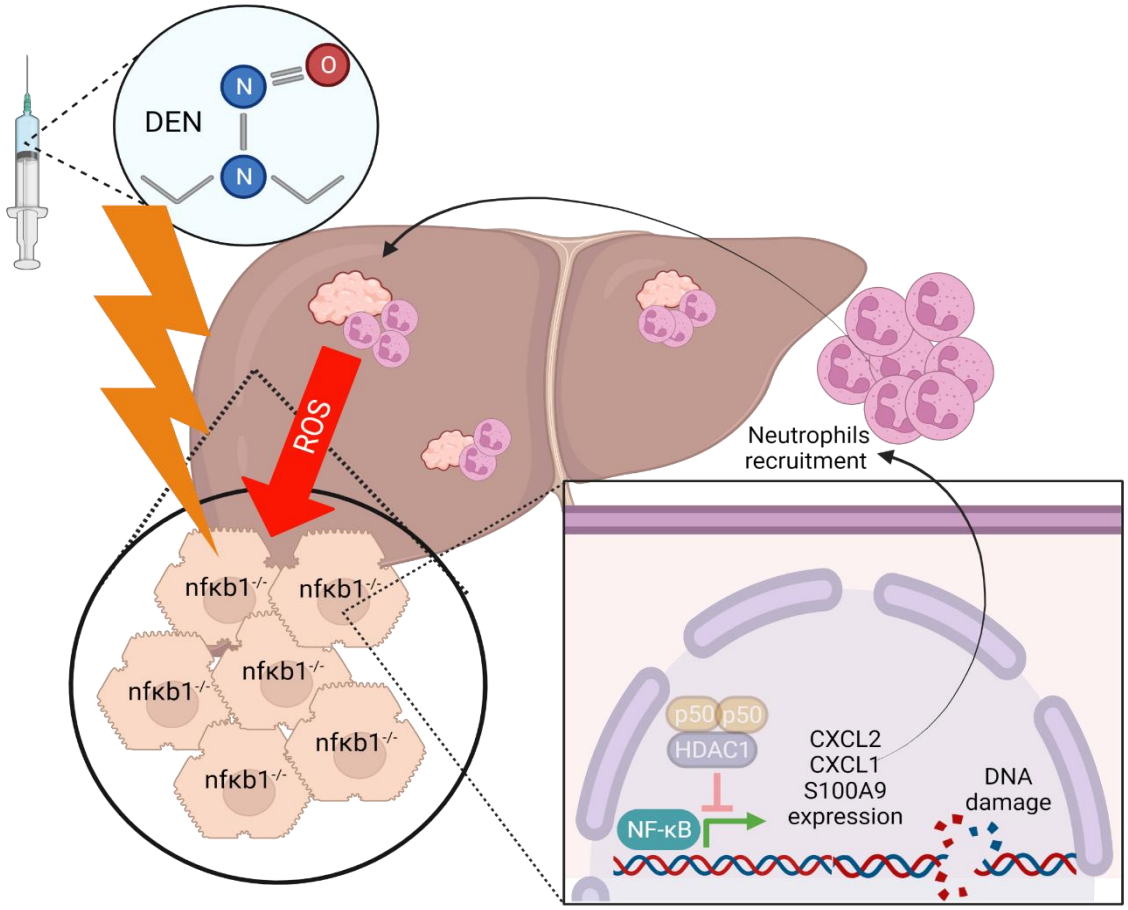

Figure 11. Diethylnitrosamine (DEN) model in *nfκb1*$^{-/-}$ mice as shown in Wilson et al. (Wilson *et al.,* 2015a). The damage caused to the hepatocytes lacking p50 resulted in more expression of chemokines involved in neutrophils networking, such as CXCL2, CXCL1 and S100A9. These genes are normally under the negative regulation of p50 homodimers couples with HDAC1, which were found at those gene promoters in ChIP assays in control mice. The lack of inhibition caused by the loss of *nfκb1* promoted the recruitment of neutrophils to the liver, which in turn perpetuated the loop of inflammation by producing ROS; the consistent exposure to inflammatory stimuli and ROS induced DNA damage and telomere dysfunction in the hepatocytes, leading to a more aggressive HCC, compared to the control group.

Similar effects were seen in a 19-month-old *nfκb1*$^{-/-}$ mouse ageing model previously described (Bianchi *et al.*, 2021). Without the need of any stimulus, *nfκb1*$^{-/-}$ mice developed severe hepatic and gastric inflammation, which spontaneously progressed to cancer. ELSs were observed in different organs, including liver and lung, and

NanoString analyses on them confirmed the same signature found in human ELS samples. These structures were thought to be the trigger for HCC development, and this was confirmed as cancer stem cell marker CD44v6-positive cells were found within larger ELSs. By lacking *nfκb1*, these mice miss an important control on inflammatory and regeneration processes; as a result, the genetic and epigenetic landscape in the cells of those mice will certainly be different compared to a control.

These changes associated with HCC were investigated in human tumour samples through the use of Next Generation Sequencing (NGS), in order to identify the pathways which are most affected in the process, in particular at the different stages of cancer progression (Li, Chang and Chen, 2016). NFκB1 was found to be one of the transcription factors belonging to genetic and epigenetic networks (GENs) involved in stage II HCC. Together with DNA Damage Inducible Transcript 3 (DDIT3) and Jun Proto – Oncogene (JUN), NF-κB1 was identified in the Mitogen – Activated Protein Kinase (MAPK) pathway, which has been implicated in the development of different types of cancers. Also, the miRNA let – 7a molecule seemed to work as a NF-κB1 inhibitor (downward red arrowhead in figure 12, indicating miRNA downregulation) and changes to its activity might result in aberrant functions of its target genes, including p50 (Li, Chang and Chen, 2016) . The downstream target of NF-κB1 in this context was CYLD, a tumour suppressor involved in cell proliferation and apoptotic processes. In the progression from stage II to stage III NF-κB1 was identified again in the MAPK pathway, but this time NF-κB2 was also present (Li, Chang and Chen, 2016); NF-κB1 was found to control the activity of CYLD, as previously reported, and GATA4, coordinator of cell maturation involved in proliferation and cell survival. The same miRNA let – 7a regulated p50 activity in the transition and was detected at lower levels compared to the previous, together with differential levels of p50 methylation. It is possible that miRNA deregulation induces changes in the progression from II HCC to III HCC, promoting a different methylation pattern that in turn affects pathways involved in cell survival and proliferation. The differential methylation landscape also provokes a shift from MAPK to TGFβ pathway, which promotes the progression to stage III. Lastly, both NF-κB1 and NF-κB2 were found in the transition from III to IV stage HCC and NF-κB2 protein was differentially methylated when compared to stage III levels. Once again, NF-κB1 was found in the MAPK pathway, where let – 7a regulated its activity. One of the downstream targets of NF-κB1 in this case was Growth Arrest And DNA Damage inducible Beta (GADD45B), involved in cell cycle and arrest. It is clear

how different methylation and epigenetic modifiers are able to regulate p50 activity, especially considering that NF-κB1 can influence epigenetic changes on its own too, by recruiting co – factors (Figure 12).

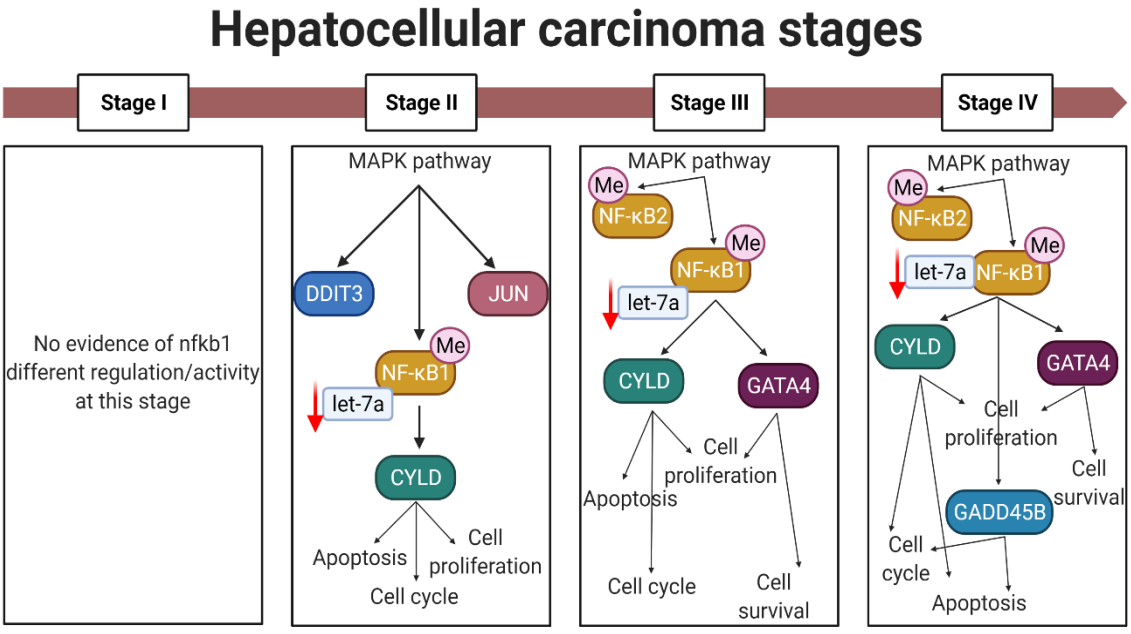

Figure 12. Summary of genetic and epigenetic networks (GENs) analyses provided in Li et al. (Li, Chang and Chen, 2016). NfκB1 was found differentially modified and activated in the last three stages of HCC, while no significant results were found for stage I. In all three stages, p50 was found diversely expressed in the MAPK pathways when compared to the control, with a different methylation state, which might affect nfκb1 activity; also, miRNA let-7a was downregulated, likely to affect p50 action too. The downstream target is CYLD, which is involved in apoptotic processes, cell proliferation and cell cycle. Stage III presented different levels of methylation for both NfκB1 and NfκB2 proteins; p50 was found able to control the activity of GATA4, involved in cell survival. Lastly, another protein involved in cell cycle processes and apoptosis, GADD4B, was found to be regulated by NfκB1 in the last stage of HCC.

1.4.5. Nfκb1 and its co-factors

In the last three decades, p50 has been mainly studied as part of the pro-inflammatory and heterodimer p65:p50, or more recently as homodimers able to limit inflammation. Great interest has been given to the ability of p50 to form complexes with a variety of cofactors, which allow the control of gene expression in both directions, depending on the recruited enzyme. The domains and the residues responsible for p50 interaction with its cofactors have been widely investigated.

For example, the mechanism by which p50 homodimers and HDAC1 interact with each other at the molecular level required elucidation. A recent paper dissected p50

sequence and structure, using *in silico* approaches to determine the putative interaction sites of p50 with HDAC1 (Cartwright *et al.*, 2018). Through an Alanine scanning assay, they found a 7 amino acid long motif in the NF-κB1 NLS in which single point mutations were used to determine the residues essential to HDAC1 binding. The same mutations were also applied to study p50 protein – protein interactions with other factors, such as IκBα and p65. The results confirmed that the motif was necessary to interact with HDAC1, but it did not seem to affect the interaction with other proteins or p50 activity. Surprisingly, the NLS was not strictly necessary for the nuclear translocation of p50 homodimers, as mutant forms of the protein were still found in the nucleus and at comparably similar levels found in control samples. As observed in previous studies, this model confirmed the recruitment of p50:p50:HDAC1 at the promoters of inflammatory genes, such as CXCL1, CXCL2, CXCL10, MMP13 and IL-6, in order to inhibit their expression under normal conditions.

As aforementioned, p50 homodimers are able to induce gene expression as well as repress it, depending on the cofactor involved. Bcl3 is an example of this alternative control on gene expression, as the complex p50 homodimers:Bcl3 stimulates the expression of pro-inflammatory cytokines, such as IL-10, during LPS-induced macrophages activation in order to limit the inflammatory response. However, Bcl3 is also able to suppress the expression of TNFα-related genes, such as IL-1α and IL-1β, and TNFα itself when coupled with p50 homodimers, through the recruitment of HDAC1 (Wessells *et al.*, 2004). Once at the targeted gene promoters, HDAC1 uses its deacetylase activity to induce a repressive state of the surrounding chromatin, similarly to what is seen for p50 homodimers:HDAC1. Since the importance of HDAC1 in helping NF-κB1 at repressing canonical inflammatory NF-κB targets, it is likely that dysregulation and modifications to this mechanism result in the onset of diseases.

It has been reported that in a subgroup of acute myeloid leukaemia the mutated form of the transcription factor CCAAT/Enhancer Binding Protein α (C/EBPα) influences the activity of p50 by influencing the stoichiometry of p65:p50 and p50 homodimers towards the formation of the latter; in addition to this, C/EBPα is able to remove HDAC1 or HDCA3 from the homodimers, resulting in the p50-dependent expression of anti-apoptotic genes, such as Bcl2 and Flip, whose expression ultimately leads to the survival of malignant cells. Lastly, p50 homodimers induce the expression of C/EBPα itself, creating a positive feedback loop that favours the progression of leukaemia.

These findings highlight the possible therapeutic intervention against this type of leukaemia by targeting C/EBPα:p50 (Paz-Priel *et al.*, 2011).

Other enzymes have been investigated for their ability to bind p50 homodimers in order to regulate gene expression. Euchromatic H3K9 methyltransferase EHMT1 was found to work with p50:p50 to repress the expression of IFN-regulated genes, but also IFNβ itself. Similarly to HDAC1, EHMT1 is recruited by p50 homodimers to repress their expression. By adding methyl groups to the target gene promoters, EHMT1 influences the structure of the chromatin, inducing a condensed state, which is associated with gene expression inhibition as the promoters are made unavailable to transcription factors binding (Ea *et al.*, 2012).

Lastly, a paper from 2016 reported that another epigenetic modifier, Lysine Demethylase 5A (KDM5A), is involved in inflammation *via* p50 homodimer-dependent recruitment. KDM5A-mediated repression of suppressor of cytokine signalling 1 (SOCS1) is essential for priming the activation of Natural Killer (NK) cells and initiation of innate immunity. *Kdm5a*$^{-/-}$ mice are more susceptible to infections and the loss of KDM5A leads to impairments in JAK-STAT signalling, which would normally result in NK cells activation (Zhao *et al.*, 2016).

Collectively, these observations support the importance of p50 homodimers as transcription regulators, either alone or and with the collaboration of other enzymes, the majority of which are epigenetic modifiers; by modifying the structure of chromatin, these enzymes control the accessibility of transcription factors to the target genes promoters, influencing their gene expression (Figure 13).

Epigenetics is a broad field that aims to the investigation of how different states of chromatin and modifications occurring on it affect the global gene expression in the cell.

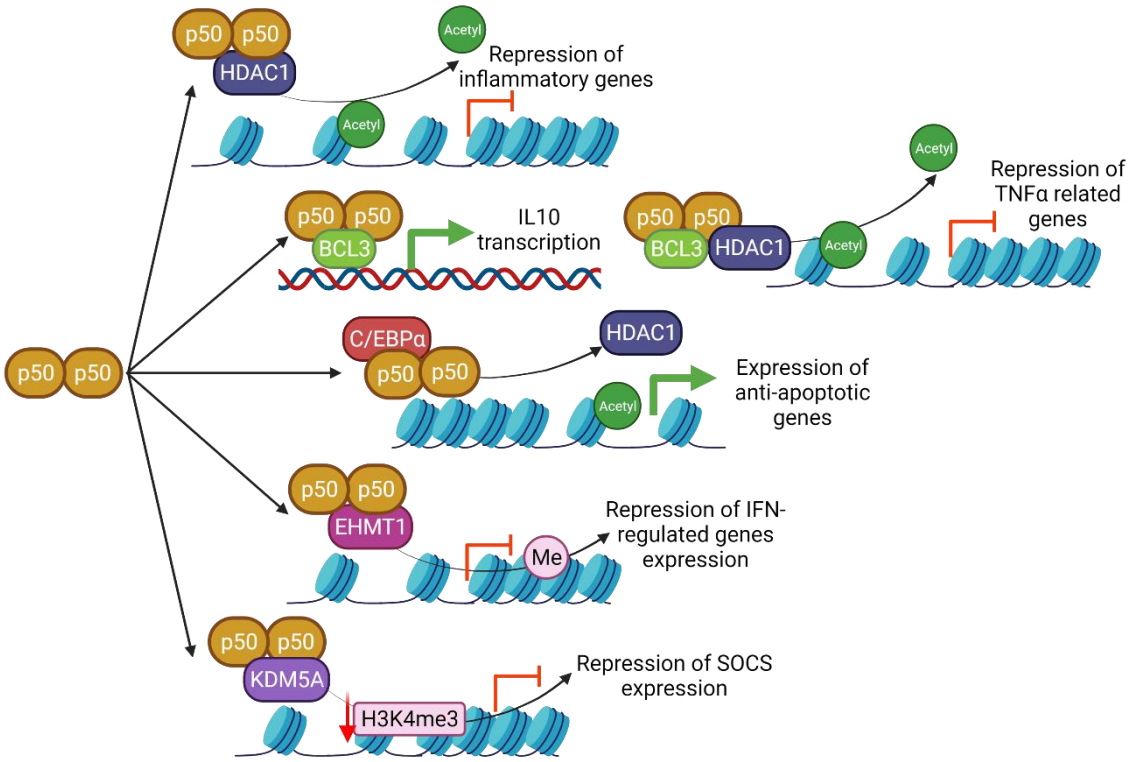

Figure 13. Examples of p50 regulation on gene expression through the interaction with other co – factors. p50 homodimers repress the expression of inflammatory genes by recruiting HDAC1 at the gene promoters and inducing a repressive state of the chromatin. BCL3 cooperates with p50 homodimers to stimulate the expression of the anti – inflammatory IL10, but it also recruits HDAC1 to repress the expression of TNFα related genes. In a particular type of leukaemia, the mutated C/EBPα is able to remove HDAC1 from the homodimers and stimulate the p50-dependent expression of anti – apoptotic genes. Upon recruitment, EHMT1 catalyses the methylation of IFN-related genes which need to be inhibited. Lastly, KDM5A works with p50 homodimers in order to decrease H3K4me3 at the SOCS gene, keeping it repressed to allow the priming activation in Natural Killer (NK) cells.

1.5. Epigenetics and liver fibrosis

Epigenetics is a relatively recent field, and its focus is on how gene expression is influenced by reversible changes that do not involve alteration in the DNA sequence, but that can be heritable during cell division.

In the nucleus, the DNA is organized in a structure called chromatin, in which the nucleic acid is wrapped around structural proteins called histones. The functional unit of chromatin is the nucleosome, where 146 bp are wrapped around eight histones, consisting of two copies of each monomer, also referred as core histones: H2A, H2B, H3 and H4 (Tessarz and Kouzarides, 2014). These proteins promote the condensation of the DNA, that would otherwise not package into the nucleus. Also, post-translational modifications (PTMs) can occur at the N-terminal tails of the histones, creating specific

binding sites for protein complexes, known as “readers”, which recognise the signal and regulate gene expression accordingly.

The epigenome is defined by all the modifications present in the genome of a single cell at a specific moment; different patterns of epigenetic signals will generate different signatures of gene expression, resulting in the generation of multiple cell types from a single shared genome. Three mechanisms regulate and influence the epigenome: non – coding RNA gene silencing, DNA methylation and histone modifications (Figure 14) (Moran-Salvador and Mann, 2017).

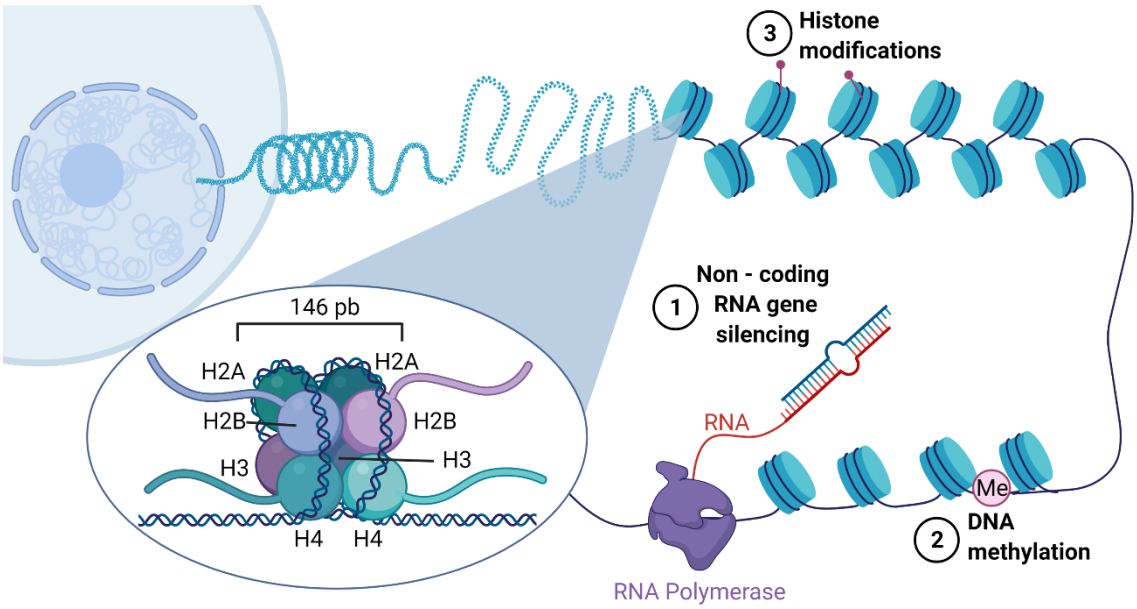

Figure 14. Representation of DNA organisation in the nucleus and the main mechanisms involving epigenetic modifications. 146 bp of DNA wraps around eight histones, two copies for each monomer H2A, H2B, H3 and H4, and this unit is called nucleosome. DNA and histones together form the chromatin, a high organised and compacted structure in which the genomic material is kept in the nucleus. Three mechanisms are able to modulate gene expression without modifying the DNA sequence: 1) non – coding RNA gene sequencing, 2) DNA methylation and 3) Histone modifications.

1.5.1. Non – coding RNA gene silencing

RNA was originally considered just an intermediary taking part to the translation process; the portion of the genome that did not codify for any proteins was considered “junk” (Ohno S, 1972) and, because of its apparent lack of function, it was not considered an interesting object of study.

However, with improved genomics techniques we now appreciate that less than 3% of the genome encodes for proteins (Li and Liu, 2019), with the remaining 80% having biological activities that are independent from protein – regulated processes (Dunham

et al., 2012). Within that 80%, sequences for non-coding RNAs were discovered and further studies uncovered their role as modulators of gene expression through epigenetic mechanisms (Hon *et al.*, 2017).

Several classes of RNAs have been discovered and classified depending on the length and the structure; in the case of liver disease, microRNAs are the most abundant type to play a role in gene regulation. Generally speaking, miRNAs have an average length of 22 nucleotides, and they are synthesised as longer precursors (primary miRNA); they are recognised by DiGeorge Syndrome Critical Region 8 (DGCR8) and the precursor is cleaved by the ribonuclease III Drosha. After being processed to pre miRNA, they are exported in the cytoplasm via the XPO5/RanGTP complex and are prone to the action of the RNase III endonuclease Dicer, which results in the maturation of the miRNAs. The mature miRNA is then loaded on the enzyme AGO, forming the miRNA-induced silencing complex (miRISC). They can interact with different regions in the target mRNAs, although they mainly bind to the 3'UTR. When the complementary miRNA interacts with its target transcript, the endonuclease activity of AGO is activated and the miRNA-mRNA complex is cleaved, weaking the interaction between the two species and inducing the degradation of the mRNA (Figure 15) (O'Brien *et al.*, 2018).

In the context of the liver, miRNAs are considered potential biomarkers for liver disease stages, as they are involved in HSCs transdifferentiation during the progression from fibrosis to CLDs. Some are thought to promote a profibrotic phenotype (miR-21, -221/222, -181b and -150) while others have the opposite effect (miR-29b, -101, -122 and -214,3p). The role of miR-29b in particular was confirmed in Bile Duct Ligation (BDL) and chronic CCl_4 mouse models, where three members of the miR-29 family were downregulated compared to the control mice; moreover, when the three members were overexpressed, the expression of the fibrotic gene *COL1A1* was suppressed in HSCs, proving the importance of the miRNA family in liver fibrosis (Page and Mann, 2015). Later studies also used comparative bioinformatics and Ago2 ChiP next generation sequencing to investigate new miRNA targets. Furthermore, the discovery of their circulating form, thanks to the protection given by Ago2 or exosomes, opened the possibility to use circulating miRNA as potential biomarkers in non-invasive analyses (Moran-Salvador and Mann, 2017).

Recent studies however suggested that miRNAs might be dispensable for HSCs differentiation (Caviglia *et al.*, 2017); in particular, Caviglia et al. showed that miR-21 antisense inhibition did not affect the activation of HSCs and that in general absence of the miRNAs machinery did not alter the HSCs phenotype and activation. Furthermore, another recent paper from 2020 used RNA sequencing analyses to investigate changes in microRNAs in human activated HSCs and also compared the results to the ones obtained in rat HSCs. The results suggested that even if some miRNAs were conserved between the two samples, caution needed to be applied when translating data obtained from rodents (Sabater *et al.*, 2020).

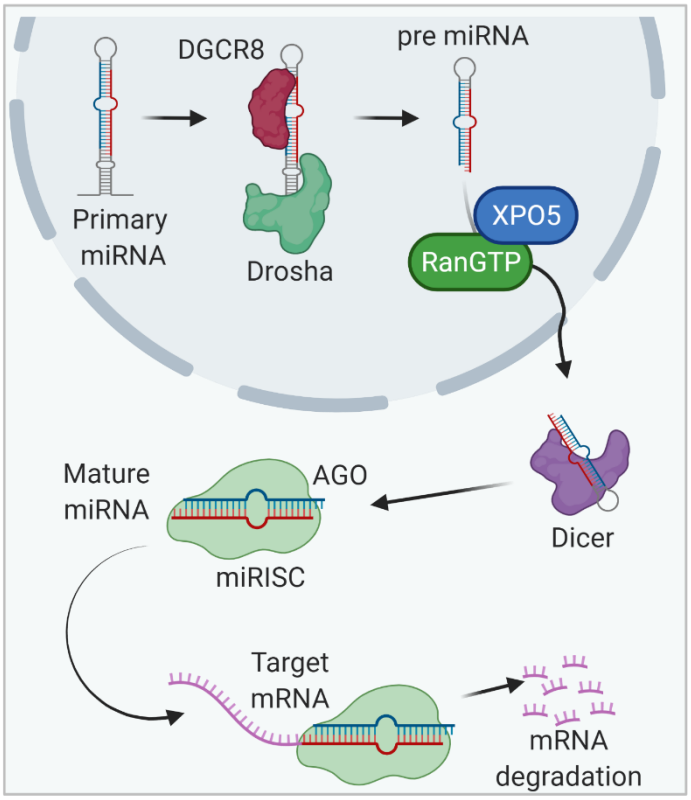

Figure 15. Processing mechanism to generate mature miRNAs. After being synthetised, the longer primary miRNA is recognised by DGCR8 and cleaved by the enzyme Drosha, generating a shorter pre miRNA; this form is recognised by the complex composed of XPO5 and RanGTP and translocated in the cytoplasm. Here the pre miRNA is recognised and processed by the endonuclease Dicer, resulting in the mature miRNA. The enzyme AGO loads the miRNA forming the miRISC complex, which is able to scan the mRNAs in the cytoplasm to find the target one. Once the mRNA is recognised, AGO uses its endonuclease activity to cut the miRNA – mRNA duplex, weaking their interaction and leading to the degradation of the mRNA.

1.5.2. DNA methylation

Another important mechanism that contributes to the epigenome landscape is DNA methylation. This modification occurs at the position 5' of cytosine nucleotides within cytosine-phospho-guanine dinucleotides (CpG), resulting in 5-methylcytosine (5–mC).

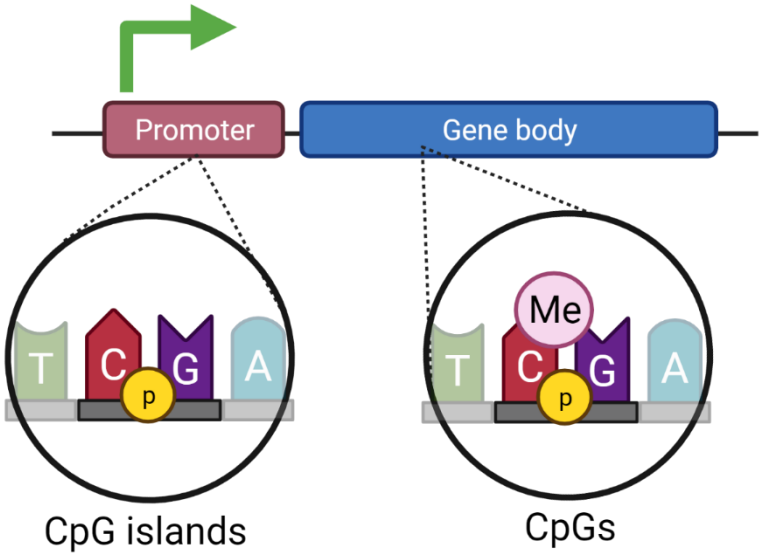

Figure 16. Distinction of different CpG groups based on their position and methylation. At the gene promoters the CpG islands are usually found unmethylated, as indication of active transcription. Whitin the gene body, they are simply called CpGs and they are found as 5 –mC.

Depending on the position within a gene sequence, different structures are identified. *CpG islands* are found at gene promoters, around 200 bp or longer in length; under basal conditions, they are unmethylated as indication of active state of the chromatin. Shorter stretches can also be found within the gene body, referred as *CpGs*, and they are normally methylated (Figure 16).

The methylation state of a cell is established at the early stages of embryo development; this mechanism is known to play an important role in X chromosome activation. Genomic methylation is a heritable feature that allows somatic cell differentiation and for this reason it was thought to be a highly stable pattern. 5–mC is created *de novo* by DNA methyltransferases (DNMTs) DNMT3A and 3B, while DNMT1 propagates the signal during DNA replication. 5–mC can be further modified to 5-hydroxymethylcytosine (5–hmC), which characterised actively transcribed genes; this reaction is catalysed by Ten Eleven Translocation enzymes (TETs), TET1, 2 and 3. TETs are able to reverse the action of DNMTs via a three chemical intermediates process, resulting in the demethylation of CpGs; the same target can then be ri –

methylated by DNMTs, as the process is reversible (Delatte, Deplus and Fuks, 2014). Together, these two families of enzymes are able to influence the methylation panorama of the cell and modulate gene expression.

In the liver, upon inflammatory stimulation or damage, quiescent HSCs transdifferentiate towards a fibrotic phenotype, becoming activated HSCs or myofibroblasts, whose role is to produce extracellular matrix for wound healing. This change in their expression profile is achieved by genome-wide changes in gene expression and in particular *via* global modifications to DNA methylation. A recent study has shown that TETs and DNMTs are essential in this process and their synergic activity modulates the progression of fibrosis (Page *et al.*, 2016). In particular, the results provided by this paper highlighted important changes in the expression levels of the enzymes involved in the control of methylation in the scenario of fibrogenesis. DNMT1, 3A and 3B were more expressed in fibrotic livers compared to control ones, while TETs followed the opposite trend. This resulted in a loss of 5-hmC, but no effect was detected on 5-mC levels. Similar results were obtained in two other fibrosis models, Bile Duct Ligation (BDL) and CCl_4 chronic treatment, confirming the importance of methylation changes in order to regulate the transition to the fibrotic phenotype. The *in vitro* model of HSCs confirmed the changes at the methylation level during activation seen in other models; loss of 5-hmC and higher expression of DNMT3A and 3B were found to be mandatory features for the activation towards myofibroblasts. Further evidence to this, RNA interference against DNMT3A was used to assert the effect of the loss of this gene in activated HSCs. This manipulation resulted in a significant reduction of DNMT3A expression and two pivotal fibrogenic genes, Collagen 1A1 and αSMA, were found downregulated at the mRNA level. Further analyses demonstrated that this regulation was achieved through DNA methylation, thus highlighting the importance of DNMTs and TETs in the development of fibrosis, as well as their potential role as drug targets.

1.5.3. Histone modifications

The third system that regulates the epigenome is histone modifications. As previously seen, DNA is complexed with proteins called histones and they can carry different modifications on the N terminal tails, influencing the surrounding structure of chromatin and the accessibility for transcription factors.

Several families of enzymes, known as writers, modify the histone code by catalysing methylation, acetylation, and phosphorylation; however, less known histone modifications, such as SUMOylation, ADP-ribosylation and ubiquitination are also important for the resulting effect on gene expression. Erasers contribute to the histone code by exerting the opposite effect of writers, as they are able to remove modifications present on the histone tails, providing a dynamic cycle in the regulation of chromatin structure. The same modification can be added to different residues with different effects. For example, methylation of Histone 3 Lysine 36 (H3K36) results in transcriptional activation, while the same modification on Histone 3 Arginine 8 (H3R8) is associated with repression of gene expression (Armstrong, 2011). Also, the overall effect can change depending on how many groups of the same type are added on a residue. As an example, monomethylated H4K20 induces transcriptional silencing, but if trimethylated it is a signal for heterochromatin formation. Lastly, all the modifications present on the surrounding residues can influence the final state of the chromatin (Jenuwein and David Allis, 2001). This complex language which results from the contribution of all these different modifications is known as histone code.

From a general point of view, acetylation is usually, but not always, associated with gene expression, due to the more accessible conformation of chromatin that is found in a more “relaxed” state. On the other hand, methylation is associated with transcription repression. According to this model, lysine residues present a positive charge under normal conditions and a salt bridge with the negatively charged DNA backbone is possible. When an acetyl group is added by Lysine Acetyltransferases (KATs, also known as Histone Acetyltransferases, HATs), the positive charge is lost and a bulkier side chain is introduced, resulting in a decreased binding affinity. Instead, when methyl group(s) are added by Lysine Methyltransferases (KMTs, also known as Histone Methyltransferases, HMTs), different degrees of bulkiness may be achieved and the charge is retained, maintaining a high affinity and impeding transcription factors binding (Tessarz and Kouzarides, 2014). Other enzymes involved in these mechanisms are the counterparts of the enzymes just described, respectively Histone Deacetylases (HDACs), usually associated to gene expression repression due to their removal of acetyl groups, and Lysine Demethylases (KDMs), via which the gene transcription is activated after the methyl group(s) have been removed (Figure 17).

However, exceptions to these general rules do exist; for example, when Lysine 42 on Histone 3 (H3R42) is asymmetrical dimethylated, the action results in increasing nucleosome instability and activation of the transcription pathway; this was proven in an *in vitro* stimulated transcription experiment, in which the RNA pol II was found to migrate more easily through the template presenting that precise modification, thus suggesting a loss of the nucleosome stability and an increased processivity of the polymerase (Casadio *et al.*, 2013).

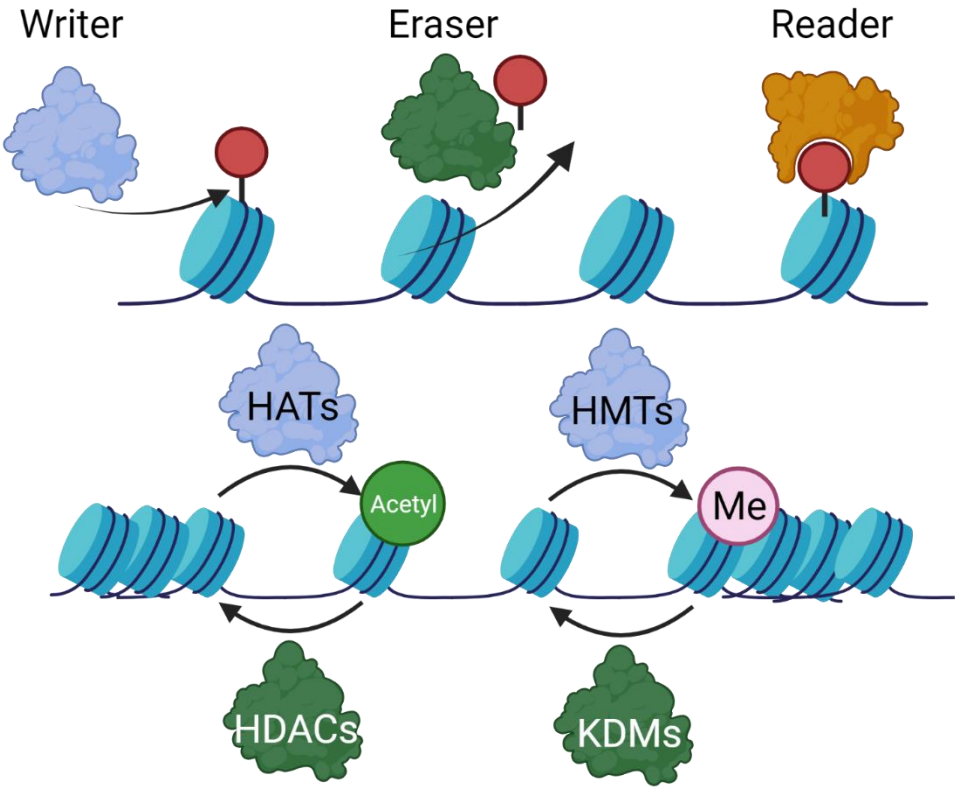

Figure 17. The three classes of proteins involved in the histone code. The writers are recognised as enzymes being able to add groups to the histone tails. The erasers can undo the work of the writers, removing the same groups. Lastly, the readers are enzymes able to read the modifications occurring at the histone tails and they do regulate the gene expression based on the overall structure of the surrounding chromatin. Histone Acetyltransferases (HATs) and Histone Methyltransferases (HMTs) are an example of writers, with commonly recognised opposite effects: by adding Acetyl groups, HATs induce gene expression by promoting a relaxed status of the chromatin, making it accessible for transcription. On the other hand, HMTs add methyl groups compacting the chromatin, which is not available for transcription. Histone Deacetylases (HDACs) and Lysine Demethylases (KDMs) are the erasers able to remove the same groups added by HATs and HMTs respectively.

In the context of liver inflammation and fibrosis, modifications in the histone code are important source of gene expression regulation in both directions. As previously presented, the complex p50:p50:HDAC1 is able to down-regulate pro-fibrotic genes in chronic inflammation and tumour models because of the action of the eraser HDAC1, which removes the acetyl groups from the gene promoters that need to be inhibited

(Jurk *et al.*, 2014; Wilson *et al.*, 2015a). Opposite effects to fibrosis are achieved in the same context by another epigenetic modifier, the pro-fibrotic master regulator methyl-CpG binding protein 2 (MeCP2). In a previously seen model of HSCs, MeCP2 was shown to suppress the transcription of the type I collagen suppressor PPARγ through the methylation of H3K9 within the same gene; furthermore, MeCP2 is able to stimulate the expression of the Lysine Methyltransferase EZH2 (KMT6) that methylases H3K27 in the same PPARγ gene, forming a repressive chromatin structure and inhibiting its transcription, resulting in the activation of HSCs towards the fibrotic phenotype (Mann *et al.*, 2010). MeCP2 is also able to positively regulate another epigenetic modifier, the Lysine Methyltransferase ASH1 (KMT2H) that through the methylation of the H3K4 is instead able to induce the expression of different pro-fibrotic genes, such as αSMA and Collagen I (Perugorria *et al.*, 2012).

1.6. Aims of the project

Inflammatory responses are triggered in the case of tissue damage or in presence of a potential harmful pathogen. For many years, the ability to initiate the process and recruit immune cells was associated to tissue-resident dendritic cells (DCs) and tissue resident macrophages, since both cell types are able to present antigens to educate immune cells on the task and to secrete chemoattractants directed at them.

Recent studies however hint at the possibility that epithelial cells capacity to stimulate immune responses has been largely undervalued and that the epithelial cells themselves are able to influence DCs and their action on immune responses (Schleimer *et al.*, 2007) ; growing evidence from mouse models also suggest that epithelial cells dysregulation in different tissues can cause unlimited inflammation with long-term consequences (Swamy *et al.*, 2010). Particular attention has been given to NF-κB and several experiments have established a central role for it in epithelial cells in regulating immune cell biology. Hepatocytes – specific deletion of IKKγ, which is an upstream regulator of NF-κB, resulted in steatohepatitis, TNF – mediated liver damage, fibrosis and HCC (Luedde *et al.*, 2007).

Based on these findings and on previous results from our lab, where *nfkb1*$^{-/-}$ mouse models showed an increased inflammatory and aged phenotype, we wanted to investigate the effect of knocking out nfκb1 in hepatocytes only. Therefore, the aims of this PhD are:

- Using primary murine hepatocytes, compare wt and *nfκb1*$^{-/-}$ hepatocytes in response to LPS treatment employing RNA sequencing.
- Working in a Precision Cut Liver Slices (PCLS) model, compare wt and nfκb1$^{\Delta heps}$ slices in response to LPS treatment.
- By ageing wt and nfκb1$^{\Delta heps}$ mice for 19 months, characterise the model and evaluate any difference in the phenotype.

Chapter 2. Materials and Methods

2.1. Cell cultures

2.1.1. Hepatocytes

Hepatocytes were isolated from mouse livers using a two-step perfusion method. Mice were anaesthetised using ketamine and xylazine. Once sufficient depth of anaesthesia was achieved, the abdomen was opened and the diaphragm cut to expose the superior vena cava which was then clamped with a microvascular clamp. The inferior vena cava was then cannulated with a 22G cannula, and the liver was perfused with 50 ml of Krebs-ringer bicarbonate buffer (Sigma) with EDTA. Immediately after starting the perfusion the portal vein was cut and used as an outlet. The liver was then perfused with 50 ml of Krebs-ringer bicarbonate buffer with $CaCl_2$ and 1mg/ml of collagenase (from *Clostridium histolyticum,* SIGMA). The liver was harvested and dissected, and the hepatocytes were collected in Krebs-ringer bicarbonate buffer and filtered through a 100μm cell strainer. The cells were centrifuged, and the pellet was washed in 10% William medium E (10% fetal bovine serum, 100 U/ml penicillin, 100 μg/ml streptomycin and 2mM L-glutamine). Living hepatocytes were separated from dead cells through a Percoll gradient; the pellet was washed and resuspended in the previously described William medium E media and hepatocytes were seeded in 6 wells plates coated with 50 mg/ml rat tail collagen (Gibco). After 3 hours, the media was replaced to remove non-viable cells and fresh media with/out treatment was added.

2.1.2. Treatments

Hepatocytes were treated with 100ng/mL of Lipopolysaccharide (LPS, from *Escherichia coli* O128:B12, SIGMA) for 2, 6 or 24 hours. After removing the rest culture media, fresh media with or without LPS was then added to the cells.

2.2. Animals

2.2.1. Ethics and husbandry

All animal work was approved by the Newcastle Animal Welfare and Ethical Review Board and carried out in accordance with the ARRIVE guidelines under a UK Home Office licence. Animals were housed in the Comparative Biology Centre (CBC) at Newcastle University and maintained in an air-conditioned environment on a 12-hour light/dark cycle with a humidity of 50% ± 10% and a temperature of 23°C ± 1°C. Food and water were provided ad-libitum and bedding was changed twice weekly.

2.2.2. Strains

All the mice used belonged to the C57BL/6J inbred strain. In particular, wild type, *Nfκb1* floxed (*Nfκb1*$^{flox/flox}$), hepatocyte specific *Nfκb1* knock out (*Nfκb1*$^{flox/flox}$ Alb Cre$^{+/-}$) and global *Nfκb1* knock out (*Nfκb1*$^{-/-}$) mice were used for the experiments.

2.2.2.1. Nfκb1$^{flox/flox}$ and Nfκb1$^{flox/flox}$ Alb Cre+/-

These colonies were generated previously in the research group. *Nfκb1*$^{flox/flox}$ mice present two LoxP sites flanking exon 4 of the *Nfκb1* gene. These mice are comparable to wild type mice, as the gene is normally expressed. The *Nfκb1*$^{flox/flox}$ Alb Cre+/- colony was obtained in a three steps mating. Firstly, homozygous *Nfκb1*$^{flox/flox}$ mice were matched with homozygous Alb cre mice (Alb Cre$^{+/+}$), in which the expression of the Cre recombinase enzyme is under the control of the albumin promoter. In this manner the presence of the enzyme was hepatocytes specific. 100% of the offspring was heterozygous for both the LoxP cassettes and the Cre enzyme (*Nfκb1*$^{flox/albcre}$). Secondly, this offspring was mated with homozygous *Nfκb1*$^{flox/flox}$ mice, in order to generate *Nfκb1*$^{flox/Albcre}$ *Nfκb1*$^{flox/flox}$, *Nfκb1*$^{flox/flox/Albcre}$ and *Nfκb1*$^{flox/-}$. Lastly, homozygous floxed heterozygous cre mice *Nfκb1*$^{flox/flox/Albcre}$ were crossed with homozygous floxed mice *Nfκb1*$^{flox/flox}$, to generate 50% *Nfκb1*$^{flox/flox}$ and 50% *Nfκb1*$^{flox/flox/Albcre}$. *Nfκb1*$^{flox/flox/Albcre}$ mice, due to the specific expression of the Cre enzyme in hepatocytes only, lack NFκB1 specifically in the liver and consist of a good model to study the effect of p50 in this organ. A schematic representation of the mating steps is found in figure 18. A similar model was obtained with the use of Adeno Associated Viruses (AAVs). In particular, AAV serotype 8 carrying the cre enzyme under the control of the Thyroxine Binding Globulin (TBG) promoter, was used to conditionally knock out *Nfκb1* in the liver in *Nfκb1*$^{flox/flox}$. An empty AAV8 was used as a negative control. The mice were injected with 1×10^{11} viral genomes (vg) and then harvested ten days after the tail injection.

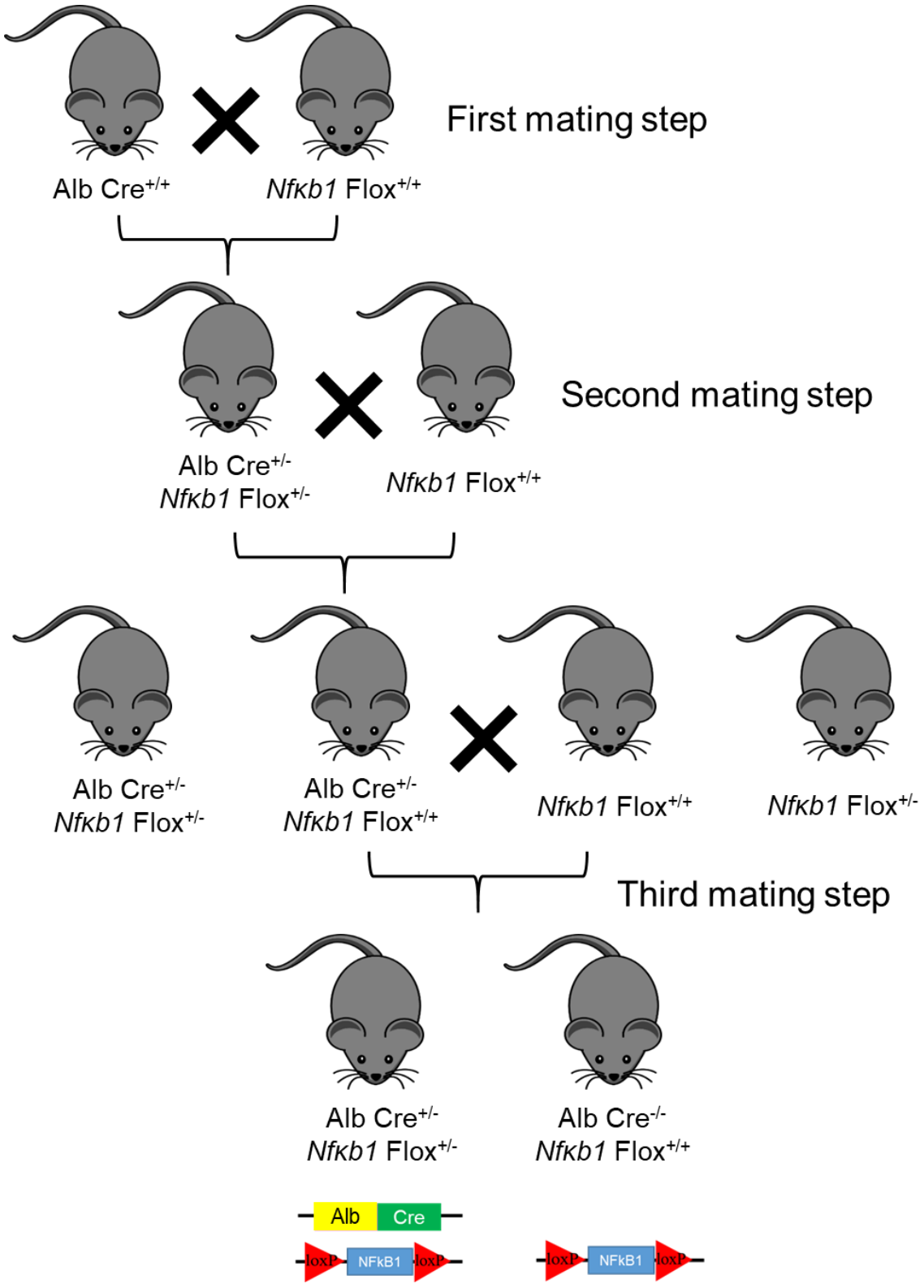

Figure 18. Graphic representation of the three mating steps required to obtain the *Nfκb1*$^{flox/flox}$ Alb Cre+/- strain.

2.2.3. Genotyping

The kit was purchased from Thermo Scientific. Mouse ear notches were digested according to the manufacturer's instructions. 20 µl of Dilution Buffer and 0.5 µl of DNARelease additive were added to the eat notches and digested for 2 minutes at 98°C. The PCR reaction mix consisted of 2X Phire Tissue Direct PCR Master Mix, Primers of interest 0.5 µM, 1 µl of the extracted genomic DNA and water up to 20 µl. The cycling protocol was the following: 98°C for 5 minutes, 25 cycles of 98°C for 5 seconds, 57°C for 5 seconds and 72°C for 20 seconds, 72°C for 1 minute and hold at 4°C. The products were visualised on an agarose gel, whose percentage depended on the gene of interest. The following primers were used for routine genotyping:

	Primers	Sequence
Alb Cre enzyme	Wild type Forward	TGCAAACATCACATGCACAC
	Common	TTGGCCCCTTACCATAACTG
	Mutant Forward	GAAGCAGAAGCTTAGGAAGATGG
NfκB1 flanking LoxP sites	Nfκb1-5arm-WTF	CTAAGACCTCCAGCCAGCAA
	Nfκb1-Crit-WTR	CATCTTCGGAGCCAAGAGAG
	5mut-R1	GAACTTCGGAATAGGAACTTCG

Table 2.1. List of primers for the genotyping of *Nfκb1*$^{flox/flox}$ Alb Cre+/- strain.

2.2.4. Nfκb1 hepatocytes specific knockout in Nfκb1$^{flox/flox}$ mice

Hepatocyte specific knockout of the *Nfκb1* gene in *Nfκb1*$^{flox/flox}$ mice was obtained by administering 1×10^{11} viral genomes (vg) of AAV8 TBG Cre and AAV8 empty (as control) to 6 weeks old mice via tail injection. 10 days after the injection the mice were overdosed using ketamine and xylazine and the livers perfused and processed to obtain hepatocytes; or the livers were harvested and then processed to obtain Precision Cut Liver Slices (PCLS).

2.3. Precision Cut Liver Slices (PCLS)

2.3.1. Slicing process

Mouse livers were harvest and kept in Krebs-ringer bicarbonate buffer on ice before being transferred to a Petri dish and cored using an 8mm skin biopsy punch. The cores were then placed in a metal mould and submerged with 3% low temperature melting

agarose. The agarose was allowed to cool on ice for 10 minutes. Once solidified, the edges were cut to facilitate the removal of the agarose block from the mould and was then superglued to the mounting stage. The vibratome was set up, with the mounting stage in the media chamber submerged in Krebs buffer and the razor blade into the desired cutting angle. The following settings were used: speed 0.3mm/sec, amplitude 2mm, thickness 250 µm. Slices were transferred to a 12 well plate, each well containing a transwell insert to which a single slice was added. 1 ml of Slice Media (William Medium E, 2% fetal bovine serum, 100 U/ml penicillin, 100 µg/ml streptomycin and 2mM L-glutamine, 0.5 µM Insulin/transferrin selenium mix, 0.1 µM dexamethasone) was added to the insert and 2 ml to the paired well. The plates were put on a rocker system inside the incubator and the slices were rested for 24 hours, before changing the media and treating them.

2.3.2. Treatments

PCLS were let to rest for 24 hours before the media was collected. Fresh media with or without treatment was then added to the slices and collected and substituted at different time points. The PCLS were treated with 1 µg/ml of LPS for 2 and 24 hours. Slices were then harvested for RNA, proteins and histology.

2.4. Enzyme linked immunosorbent assay (ELISA)

96-well ELISA plates were coated with 25 µl per well of the capture antibody (different dilutions depending on the kit used) in coating buffer, overnight at room temperature with agitation. The plate were then washed three times with 150 µl of 0.05% Tween 20 in PBS (PBS-T) per well. Each well was then blocked with 150 µl of blocking buffer (1% BSA in PBS) for 1h at room temperature on a rocker. The plate was then washed three times with 150 µl of PBS-T per well and then 25 µl of the standards and samples (prepared in blocking buffer) were added to the plate and incubated for 2h at room temperature on the rocker. The plate were then washed three times with 150 µl of PBS-T per well and then 25 µl of detection antibody were added to each well and plates were incubated for further 2h at room temperature with agitation. The plate was then washed as previously stated and 25 µl of Streptavidin-HRP were added to each well and incubated in the dark for 20 minutes at room temperature. The plate was then washed and 25 µl of the solution A+B or TMB was added to the wells and incubated in the dark. Once the reaction was close to saturation, 25 µl of stop solution were added and the absorbance was read within a range of 450-620 nm. The following kits were

used: Mouse Albumin Matched Antibody Pair Kit (Abcam, ab210890) and Mouse CXCL1/KC DuoSet ELISA (R&D Systems, DY453).

2.5. Lactate Dehydrogenase assay (LDH)

The kit was purchased from Invitrogen. The positive control was prepared lysing a liver slice in 1:10 Triton:PBS (200 µl) and then topped the volume up to 1.5 mL with liver media. For the negative control, fresh liver media was taken. The reaction mix was prepared following the manufacture instructions; one vial of substrate and 600 µl of assay buffer were added to a total volume of 15 mL of water and kept away from the light. 25 µl of samples and controls were added to the plate and 25 µl of the reaction mix were added on top. The plate was incubated in the dark for 30 minutes. The reaction was stopped with 25 µl of stop solution and the absorbance was measured at 490-680nm.

2.6. RNA

2.6.1. Extraction from cells

Cells were washed in cold PBS, scraped into cold PBS, then transferred to an Eppendorf and collected by centrifugation at 10,000 rpm for 2 minutes at 4°C. The pellets were resuspended in 350 µl of RLT buffer supplemented with 10 µl/mL of β-Mercaptoethanol. An equal volume of 70% EtOH was added to the lysate, and it was mix by inversion. Following steps included the use of the RNaesy Mini Kit from QIAGEN. After 1 minute incubation on ice, 700 µl of the lysate was transferred to a RNeasy spin column and span at 10,000 rpm for 1minute. The flow-through was discarded and 700 µl of Buffer RW1 were added to the column and span down at 10,000 rpm for 1 minute. The flow through was discarded and 500 µl of Buffer RPE were added to the column and span at 10,000 rpm for 1 minute. A second wash of the column was performed with the same buffer, but it was span for 2 minutes. The column was placed on a clean collection tube and span again at 10,000 rpm for 1 minute to eliminate any trace of phenol. The column was placed in a 1.5 mL collection tube and 50 µl of RNAse-free water was added and incubated for 1 minute at room temperature. The RNA was eluted by centrifugation at 10,000 rpm for 1 minute. The concentration was measure with the Nanophotometer.

2.6.2. Extraction from tissue

30 mg of frozen tissue were weighed and added to a 2 mL round-bottomed tube containing a metal bead and 600 µl of RLT buffer supplemented with 10 µl/mL of β-Mercaptoethanol. The tissue was disintegrated with the Tissue Lyser, twice, for 2' at 200 speed. The lysate was transferred to a QIAshredder and spin at maximum speed for 3'. The homogenate was transferred to a fresh tube and an equal volume of 70% EtOH was added to the lysate, and it was mix by inversion. Following steps included the use of the RNaesy Mini Kit from QIAGEN, as previously stated. The RNA was eluted in 50 µl of RNAse – free water and measured with the Nanophotometer.

2.6.3. Extraction from slices

Two slices were added to a 2 mL round-bottomed tube containing a metal bead and 500 µl of QIAzol (QIAGEN). The slices were disintegrated with the Tissue Lyser, twice, for 2 minutes at 200 speed. The lysate was transferred to a QIAshredder (QIAGEN) and spin at maximum speed for 1 minute. The homogenate was transferred to a fresh tube and 140 µl of Chloroform (SIGMA) were added and the mix was vortex for 15 seconds until homogeneous. After a 3-minute incubation at room temperature, the samples were span at 4°C for 15 minutes at 13,000 rpm. The aqueous phase was collected and transferred to another tube. An equal volume of 70% EtOH was added to the lysate, and it was mix by inversion.

Following steps included the use of the RNaesy Mini Kit from QIAGEN, as previously stated. The RNA was eluted in 30 µl of RNAse – free water and measured with the Nanophotometer.

2.6.4. cDNA

1 µg of RNA was prepared in 8 µl of RNAse-free water. 2 µl of RQ1 mix (1:1 enzyme:buffer) were added to the tubes and span for 5 seconds. The samples were incubated at 37°C for 30 minutes. 1 µl of stop solution was added to the mix and incubated for 2 minutes at room temperature. 0.5 µl of random primers were added to the samples and incubated at 70°C for 5 minutes. The tubes were immediately placed on ice for 5 more minutes. 8.5 µl of the RetroTranscriptase mix (2 µl of RNase-free water, 1 µl of MMLV RetroTranscriptase, 4 µl of RT buffer, 0.5 µl of RNAsin and 1 µl of dNTPs) were added and the reaction was carried on at 42°C for 1 hour. The reaction generated cDNA at 50 ng/µl that were diluted to 10 ng/µl as working concentration.

2.6.5. Polymerase Chain Reaction

Polymerase Chain Reaction (PCR) was used to assert the quality of the synthetized cDNA, to validate primers and to check the presence of genes of interest. The reaction was prepared in a final volume of 25 µl: 12.5 µl DreamTaq PCR Master Mix (2X), 9.5 µl of Nuclease free Water, 1 µl of 2.5nM mix of forward and reverse primers and 1 µl of 10 ng/µl cDNA. The reaction was carried on in a thermocycler as following: 94°C for 2 minutes, 25 cycles of 94°C for 10 seconds, primers specific annealing temperature for 30 seconds, 72°C for 30 seconds; then 72°C for 7 minutes and a final hold of 4°C. The PCR products were run on an agarose gel (different percentages depending on the aim) and visualised with a Gel Doc.

2.7. RNA sequencing and analysis

RNA was extracted from hepatocytes as previously described. The samples were sent to the Genomics Core Facility at Newcastle University for RNA Integrity Number (RIN) quantification and library preparation. The same company performed the sequencing of the samples (TruSeq Stranded mRNA-Seq at ~30M 100 bp single reads per sample) on NovaSeq 100 cycle SP followed by MiSeq Nano QC run. The raw FastQ files underwent quality control analysis using fastQC (available online at http://www.bioinformatics.babraham.ac.uk/projects/fastqc/) and all the samples passed the QC check. The sequences were trimmed using Trimmomatic software, in order to improve the quality of the reads and eliminate the adaptors used for the sequencing. The reads were checked once more time with fastQC to make sure that the quality stayed the same or improved, after the trimming. Before carrying on with any further analyses, the adaptors sequences were eliminated from the reads pool. Mapping and quantification steps were performed using Salmon software (version 0.12.0). The sequences were quasi aligned to the genome of reference (mouse) to quantify levels of expression of transcripts via reads abundancies. Salmon values were then loaded on R studio (version 1.2.1335) for differential expression (DE) analysis. A batch effect was included in the design model in order to overcome the differences between replicates from different mice. Different R packages were used depending on the required task: “tximport” was used to import the reads counts; “DESeq2” was used to create the counts matrix, to estimate the dispersion, to perform the normalization and to obtain the Principal Component Analysis (PCA) graph. The mRNAs were considered differentially expressed when $\log_2 fold\ change > 2$ and p-value (adjusted with Bonferroni’s correction) < 0.001. Heatmaps were obtained using “DESeq2” package (Yalamanchili, Wan and Liu, 2017).

2.8. qPCR

2.8.1. Primer design

The primers were designed using Primer 3, an online tool (https://primer3.ut.ee/). The sequence of the gene of interest was taken from the corresponding Ensembl page. In particular, the cDNA transcript was used in order to generate the pairs of primers. The following settings were used as input in order to generate the different possibilities of primers: length of 18-24 bases, optimal of 20; GC content of 40-60%, optimal 50%; melting temperature of 50-60°C, optimal 57°C, with less than 5°C of difference between the T_m of the two primers; product size ranges 100-250 bp. Two pairs for each gene interest were then taken, chosen based on the absence of estimated secondary structures or self-complementation. The primers were also checked on the Blast platform (https://blast.ncbi.nlm.nih.gov/Blast.cgi) The primers were then ordered through the Sigma Aldrich website. 0.025μmole and desalt purification were the chosen features. The primers were then reconstituted following the manufacturer's instructions in TE buffer (10 mM TrisHCl pH 8, 1mM EDTA).

2.8.2. Primer validation

Primers were validated with PCR and quantitative PCR (qPCR). For qPCR, the best pair of primers asserted with PCR was validated using a 7 point doubling dilution test, starting from neat cDNA at 10 ng/μl. The R^2 obtained from the graph of dilution/CT were used to decide whether the primers were suitable for qRT – PCR.

2.8.3. qRT – PCR

Quantitative PCR (qPCR) or Real Time PCR (RT-PCR) reactions were prepared in a final volume of 13 μl: 6.5 μl of Sybr Green JumpStart Taq ReadyMix (2x) (SIGMA), 4.5 μl of Nuclease free water, 1 μl of 2.5μM primers and 1 μl of 10 ng/μl cDNA. The reactions were loaded in 96 wells plate and span down at 1200 rpm for 1 minute. A QuantStudio3 machine by Applied BioSystems was used to run the following qPCR program: 95°C for 5 seconds, 40 cycles of 95°C for 5 seconds, primers specific annealing temperature for 30 seconds, 72°C for 30; then 95°C for 15 seconds, 60°C for 1 minute and 95°C for 1 second, to obtain the melting curve. The raw data were first analysed with QuantStudio software, and the fold changes were calculated with ΔΔCt and gene expression ratio with the Pfaffl method (Pfaffl, 2001). The primers used in this work are found in the table below.

Gene	Primers	Sequence	Annealing °C
ALB	Forward	GAAAACCAGGCGACTATCTCCA	57
	Reverse	TGCACACTTCCTGGTCCTCA	
CCL2	Forward	TTAAAAAACCTGGATCGGAACCAA	57
	Reverse	GCATTAGCTTCAGATTTACGGGT	
CXCL2	Forward	CCAACCACCAGGCTACAGG	57
	Reverse	GCGTCACACTCAAGCTCTG	
KC CXCL1	Forward	GCGAAAAGAAGTGCAGAGAG	57
	Reverse	GCCCTACCAACTAGACACAA	
IL6	Forward	GAGGATACCACTCCCAACAGA	60
	Reverse	AAGTGCATCATCGTTGTTCATA	
NFKBI exon 4	Forward	CTACGGAACTGGGCAAATGT	55
	Reverse	TCGAAATCCCCTCTGTTTTGGT	
CCL20	Forward	GTCTGCTCTTCCTTGCTTTG	57
	Reverse	AATGTCACAAGCTTCATCGC	
TNFAIP3	Forward	CATGTGGGGGTGTCAGGAT	57
	Reverse	ATTCGTCATTCCAGTTCCGA	
NFKBIZ	Forward	GACTCCTCCGATTTCTCCTG	57
	Reverse	CTCCTTCACCGAGTTCTTCA	
GAM	Forward	CAAGATCTGGAGTTGCTGGG	57
	Reverse	GCCTTTGATCACCTCCTTCT	
NGAL1	Forward	TTGACAACTGAATGGGTGGT	57
	Reverse	TGTTAAGACAGGTGGATGGG	
KIM1	Forward	GCGCTGTGGATTCTTATGTG	57
	Reverse	CCGACTGCTCTTCTGATAGG	
GAPDH	Forward	TGCACCACCAACTGCTTAG	57
	Reverse	GATGCAGGGATGATGTTC	
ACTB	Forward	TGTTACCAACTGGGACGACA	57
	Reverse	GGGGTGTTGAAGGTCTCAAA	

Table 2.2. Primers for mouse targets used in this work, with sequences and annealing temperature.

2.9. Western blot

Cells or tissues were disrupted in modified RadioImmunoPrecipitation Assay Buffer (RIPA, 50mM TrisHCl pH 8, 1% Triton X-100, 0.5% Sodium Deoxycholate [DOC], 0.1% Sodium Dodecyl Sulphate [SDS], 150mM NaCl, protease and phosphatase inhibitors freshly added), left for 30 minutes on ice and then centrifuged at maximum speed for 15 minutes at 4°C. The supernatant was kept, and the protein concentration was quantified using the detergent-compatible protein assay kit (Biorad Laboratories). 2 µl of supernatant were added to 18 µl of molecular grade water. 98 µl of Reagent A, 2 µl of Reagent S and 800 µl of Reagent B were added one after the other to the tube and incubated in the dark for 20 minutes. The samples were quantified at 750nm.

Protein extracts were diluted in 5x Loading buffer and the samples were then boiled at 100°C for 5 minutes. The samples were fractioned by 10% acrylamide gel run in Running Buffer (25mM Tris, 190mM Glycine, 0.1% SDS). The proteins were then transferred to a nitrocellulose membrane in Transfer Buffer (25mM Tris, 190mM Glycine, 20% Methanol). The efficiency of the transfer was checked by incubating the membrane with Ponceau S Staining Buffer. The membrane was washed and blocked in Blocking Buffer, made of 5% milk in TBS-T (20 mM Tris pH 7.5, 150mM NaCl, 0.1% Tween 20) for 1h at room temperature. The membrane was then incubated with the primary antibody overnight at 4°C or with the HRP-coupled for 1h at room temperature. The membrane was washed three times with TBS-T for 5 minutes each and then it was incubated with the secondary antibody conjugated to HRP. The membrane was washed again three times with TBS-T for 5 minutes each. Proteins were then detected with chemiluminescence.

The antibodies used in this work are found in the table below.

Protein	Primary antibody	Secondary antibody
p105/p50	HRP Rabbit anti – p105/p50 [E381], ab195854 1/1000 dilution	-
LTβ	Rabbit anti – LTβ polyclonal, abx101341 1/1000	Anti – rabbit HRP coupled 1/2000
p21	Rat anti – p21 [HUGO291], ab107099 1/1000	Anti – rat HRP coupled 1/2000
p16	Rabbit anti – p16 polyclonal, AHP1488 1/1000	Anti – rabbit HRP coupled 1/2000
βActin	Mouse anti – βActin [AC-15], A5441 1/2000	Anti – mouse HRP coupled 1/5000

Table 2.3. Antibodies used for the detection of targets of interest during Western Blot.

2.10. Histology

2.10.1. Haematoxylin and eosin stain

Formalin-fixed and paraffin embedded PCLS and tissue sections of 5 μM were dewaxed in clearene (Leica) twice for 3 minutes each and then dehydrated in 100% EtOH for 3 minutes and then placed into 70% EtOH for 3 minutes. The slides were then washed in running tap water and incubated in Mayers Haematoxylin for 3 minutes. The slides were washed again in running tap water and incubated in Scott's water for at least 40 seconds. Slides were washed once more in running tap water and incubated in Eosin for 1 minute. The slides were briefly washed in running tap water and then dehydrated through graded alcohols 50%, 70%, 100% and 100% for 2 minutes each. Slides were then transferred to clearene twice for 2 minutes and then coverslips were mounted with Pertex mountant.

2.10.2. Periodic Acid Schiff stain

Formal-fixed and paraffin embedded kidneys sections of 5 μm were used for staining and they were dewaxed in clearene twice for 3 minutes each and then dehydrated in 100%, 70% and 50% EtOH for 3 minutes each. The slides were then rehydrated in distilled water and then incubated in periodic acid solution 1g/dL for 5 minutes. The slides were then rinsed in distilled water and incubated in Schiff's reagent (parasoaniline HCl 6 g/dL and sodium metabisulfite 4% in HCl 0.25 mol/L) for 15 minutes. After being rinsed under running tap water, the slides were counterstained with Mayers Haematoxylin for 3 minutes. The slides were then washed in running tap water and incubated in Scott's water for at least 40 seconds. Slides were then washed once more in running tap water and incubated in Eosin for 1 minute. The slides were then washed in running tap water before undergoing dehydration through graded alcohols 50%, 70%, 100% and 100% for 2 minutes each. Slides were then transferred to clearene twice for 2 minutes and then coverslips were mounted with Pertex mountant.

2.11. Immunohistochemistry

Formal-fixed and paraffin embedded tissue sections of 5 μM were used for staining. The sections were dewaxed and dehydrated as previously described. Endogenous peroxidase activity was blocked by incubating the slides in Methanol/2% Hydrogen Peroxide (SIGMA) for 15 minutes. The slides were briefly washed in PBS. Antigen retrieval was performed differently depending on the antibody used (Table 2.3). The

slides were once again washed in PBS and mounted into a sequenza. Tissues were blocked first with Avidin (Vector) for 15 minutes, followed by 3 washes of PBS, and then with Biotin (Vector) for 15 minutes, followed by three washes with PBS. The slides were then incubated with Blocking Buffer (20% swine serum in PBS) for 1h at room temperature. After that, the slides were incubated with primary antibodies overnight at 4°C. After 3 washes of PBS, slides were incubated with secondary antibody for 45 minutes at room temperature and washed again and incubated with Vector ABC Tertiary (Vector) for 30 minutes. After 3 washes of PBS, the DAB peroxidase kit (Vector) was used to visualise the antigen. Lastly the slides were counterstained with Mayers Haematoxylin, washed in running tap water and then dehydrated and mounted as previously described. The details for each staining are found in the table below.

Antigen	Antigen Retrieval	Primary antibody	Secondary antibody
CD3	1mM EDTA pH 8	Rat anti – human CD3 [CD3-12], MCA1477 1/200 dilution	Goat anti – rat biotin conjugated 1/200
CD45R	Citric saline pH 6	Rat anti – mouse CD45R [RA3-6B2], ab64100 1/200	Goat anti – rat biotin conjugated 1/200
CD44v6	1mM EDTA pH 9	Rat anti – mouse CD44v6 [9A4], BMS145 1/200	Goat anti – rat biotin conjugated 1/200
αSMA	Citric saline pH 6	Mouse anti – αSMA FITC [1A4], F3777 1/1000	Anti – FITC biotin conjugated 1/300
p21	1mM EDTA pH 8	Rat anti – human, mouse p21 [HUGO291] ab107099 1/100	Goat anti – rat biotin conjugated 1/200

Table 2.3. Details for antigen retrieval and antibodies used for the staining of the target antigens.

2.12. Microscopy analysis

Sections were analysed at 100x (4x for H&E) using a Nikon Eclipse Upright microscope and NIS-Elements BR analysis software (NIS-Elements Br, Nikon, UK), to detect to positive cells and positive area expressed as a percentage of total tissue containing area. A minimum of twelve consecutive non-overlapping fields of were analysed per stain.

2.13. Statistical analysis

Data are mean ± standard error of the mean (SEM), where *, **, *** and **** denote P values of <0.05, <0.01, <0.001 and <0.0001 respectively and n/s indicates a non-significant difference. P values were calculated using GraphPad prism 8 using either a two-tailed unpaired Student t test, two-tailed paired Student t test or an ANOVA with Tukey Post-hoc test unless otherwise stated.

Chapter 3. RNA sequencing data suggest importance of NFκB1 to limit inflammation in primary hepatocytes

3.1. Introduction

Models for liver inflammation are important research tools because they allow the investigation of the mechanisms involved in organ specific inflammatory response, aiming to find new pathways and new targets for drug discovery and intervention. *In vivo* models are usually preferred since they represent a more physiological and comprehensive setting, which includes the contribution of different organs to the systemic response to inflammation. Mice are often chosen for *in vivo* modelling, because of the genomic similarity they share with humans (99%), their small size that facilitates large scale studies and the fast generation of litters, which allows shorter waiting for experiments. Despite the similarity, mouse models sometimes fail to recapitulate human diseases, rendering the results unreliable at predicting the outcome in human studies (Vandamme, 2014). Also, the genetic variability existing even between littermates of the same sex can make experiments more challenging and time consuming, as more mice might be needed to increase the pool of samples. Lastly, animal work is heavily affected by costs and ethical approval. For these reasons, new *in silico* and *in vitro* models are required as substitutes, especially for preliminary data. *In silico* models offer predictions based on bioinformatics and computational biology, but they are often quite limited in their application, because the results are based on algorithms and data from previous experiments available on databases. This approach is useful in drug discovery and development when a library of candidates needs to be initially screened for a well-known target and predictions are generated based on pre-existing data. *In vitro* models include purified enzymes, also known as acellular preparation of enzymes (Underhill and Khetani, 2018), and cell cultures; purified enzymes are mainly used in high – through put screenings of libraries of drug candidates at the early stages of drug discovery, so they offer fast results, but they still require follow – up validation. Cell cultures on the other hand provide a more similar environment to an *in vivo* model, with some limitations. There are two types of cell cultures.

Cell lines are the most used and they are created by pre-existing cells that have been passaged over a long period of time. They can be naturally immortalised, e.g., cell lines from tumours, or they can acquire this feature due to artificial modifications. Cell lines are easy to handle, treat and use in experiments; they do not always represent a good

model, because the prolonged culture can lead to the accumulation of mutations, which cause the cells to progressively lose the characteristics of the tissue they derive from. On the other hand, primary cells are directly isolated from the tissue, with either enzymatic or mechanic methods. The cells are then cultured in plastic, fed with media supplied with growth factors and nutrients that will help them adapt to the new environment. Despite a shorter life span compared to cell lines, primary cells provide a model that recalls the original tissue, representing a more biologically significant example. Moreover, with the advent of personalised medicine, the use of primary cells unlocks the possibility to study specific cells from a specific patient, which will respond differently to treatments when compared to another individual, based on age, gender, and clinical conditions.

In the case of the liver, hepatocytes are usually the primary cells of choice to address important questions regarding inflammation (Boess *et al.*, 2003). After liver perfusion with collagenase (from Clostridium histolyticum), hepatocytes are separated from other cell types with the use of a Percoll gradient and they are seeded on a layer of rat tail collagen. A 3h rest is needed to allow the attachment of the viable cells and the media is then discarded to get rid of dead cells and death factors released by the dying cells. Another layer of collagen can be added on top of the cells creating the sandwich culture. If not, the cells are cultured as a conventional monolayer and can either be used after seeding (monoas) or after overnight rest (mono).

The current practise in the Newcastle Fibrosis Research lab is to use hepatocytes as monoas. Some considerations have to be made regarding this *in vitro* model. Hepatocyte isolation is a stressful process that involves the perfusion of the liver with the enzyme collagenase, which destroys the extracellular matrix, facilitating the release of the cells from the liver. It has been reported that gene expression changes quite rapidly in freshly isolated hepatocytes, mediating a pro - inflammatory acute response before being cultured. Moreover, the disaggregation of hepatocytes and the consequent loss of cell – cell interactions result in progressive dedifferentiation, where the transcription of liver – specific genes is greatly downregulated, while the expression of more common genes remains stable (Elaut *et al.*, 2006). However, hepatocytes are able to survive for about a week and this system is frequently used as a liver model because it represents a well-accepted compromise with some key advantages. In fact, the liver is mainly composed of hepatocytes, which constitute 80% of the total mass of the organ. Hence, from a single mouse it is possible to isolate enough cells to cover different experimental conditions, limiting the use of large number of mice and

diminishing the chance of inaccurate results due to genetic variability existing between two different organisms, even if coming from the same background and the same genotype.

This *in vitro* system was used to characterise the gene expression in response to LPS treatment in primary murine hepatocytes, isolated from both wt (Nfκb1$^{flox/flox}$) and hepatocytes-specific p50 knockout (Nfκb1$^{flox/flox}$ AlbCre+) livers.

3.2. The genetics of Nfκb1$^{flox/flox}$ AlbCre+ hepatocytes and why to use them as a model to study *Nfκb1* contribution to inflammation in the liver

To generate a cell-specific knock out of our protein of interest, we use a Cre-LoxP system in a mouse model.

Figure 19 exemplifies the genetics of the strains employed in this experiment, Nfκb1$^{flox/flox}$ and Nfκb1$^{flox/flox}$ AlbCre+. Both Nfκb1$^{flox/flox}$ and Nfκb1$^{flox/flox}$ AlbCre+ strains carry the *Nfκb1* gene, with exon 4 flanked by loxP cassettes. In Nfκb1$^{flox/flox}$ AlbCre+ mice, the Cre recombinase is under the control of the Albumin promoter, which provides the hepatic specificity to the system. When the enzyme is expressed, it recognises the loxP cassettes, it excises the DNA in between these sites (Kim *et al.*, 2018), resulting in hepatic specific knock out of the nfκb1 gene. As Nfκb1$^{flox/flox}$ mice do not express the Cre enzyme, they remain phenotypically wild type and are used as a negative control for the system.

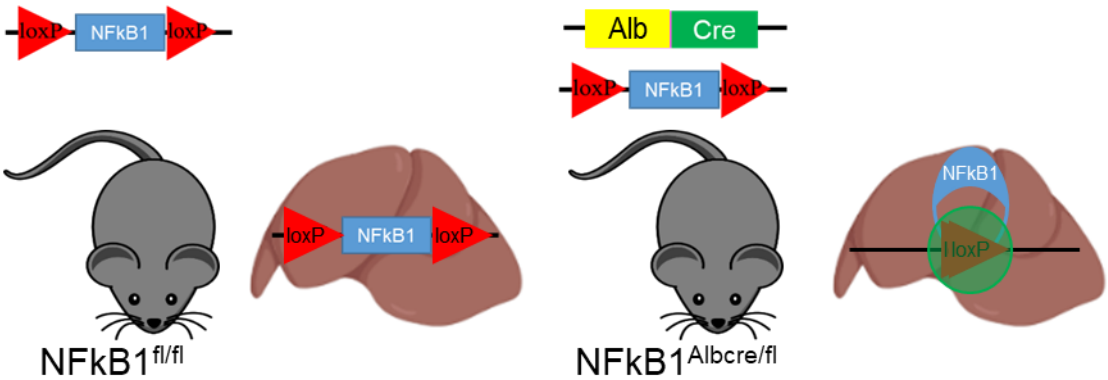

Figure 19. Graphical explanation of the Cre-lox system used to create a hepatocytes-specific nfkb1 knock out. Both strains present the nfkb1 gene flanked by loxP cassettes, but the AlbCre strain expresses the enzyme under the control of albumin promoter, obtaining the knockout of nfkb1 in hepatocytes only.

Despite the advantages of using this system for time and space - controlled knock out, several studies have been published to address questions about aspecific activity/effect of the Cre enzyme. The Cre enzyme itself can produce a phenotype, by

either altering cell physiology just by being expressed (Pomplun *et al.*, 2007) or by recognising criptic loxP sites in the genome and causing DNA damage at those locations (Huh, Mysorekar and Mills, 2010). It can also be active in different organs from the ones intended (Wicksteed *et al.*, 2010) and have a mosaic activity in the organ of interest, if not all the cells express the enzyme or if the Cre recombinase activity fails to recombine the flox allele (Schile, 2011). The use of a Cre transgenic strains would have been another control to test whether the Cre enzyme itself was having effects in our system. In regard to aspecific activity of the Cre enzyme in other organs, it would be discussed further in this work.

3.3. Validation and characterisation of primary murine hepatocytes *in vitro*

First, I set a pilot experiment with a small pool of mice to characterise primary murine hepatocytes *in vitro* and the different responses to LPS based on the presence/absence of Nfκb1.

Other stimuli could have been chosen to study inflammation in isolated hepatocytes, including TNFα (Yang and Seki, 2015), especially considering the low levels of Toll Like Receptor 4 that hepatocytes express (Vaure and Liu, 2014). However, LPS itself is a strong inducer of TNFα (Maeda *et al.*, 2003), and previous works have confirmed the ability of LPS to trigger inflammation in hepatocytes (Kheder, Hobkirk and Stover, 2016; Lee *et al.*, 2017).

Male mice from both Nfκb1$^{flox/flox}$ AlbCre+ and Nfκb1$^{flox/flox}$ strains were taken at 6-8 weeks of age and their livers perfused to obtain viable hepatocytes (Figure 20A). Freshly isolated hepatocytes were compared to hepatocytes cultured in plastic at different time point to examine their gene expression during the time course, for a total of 27h~ (Figure 20B). To answer the question, whether there were differences in response to inflammation when comparing wt hepatocytes and p50-/- hepatocytes, cells were treated with 100ng/mL of LPS for 24h and 2h (Figure 20C); the time points for the stimulation of an inflammatory response with its following resolution were taken from previous examples in literature (Hamesch *et al.*, 2015).

Untreated cells cultured for the same time as the treated ones were used as control.

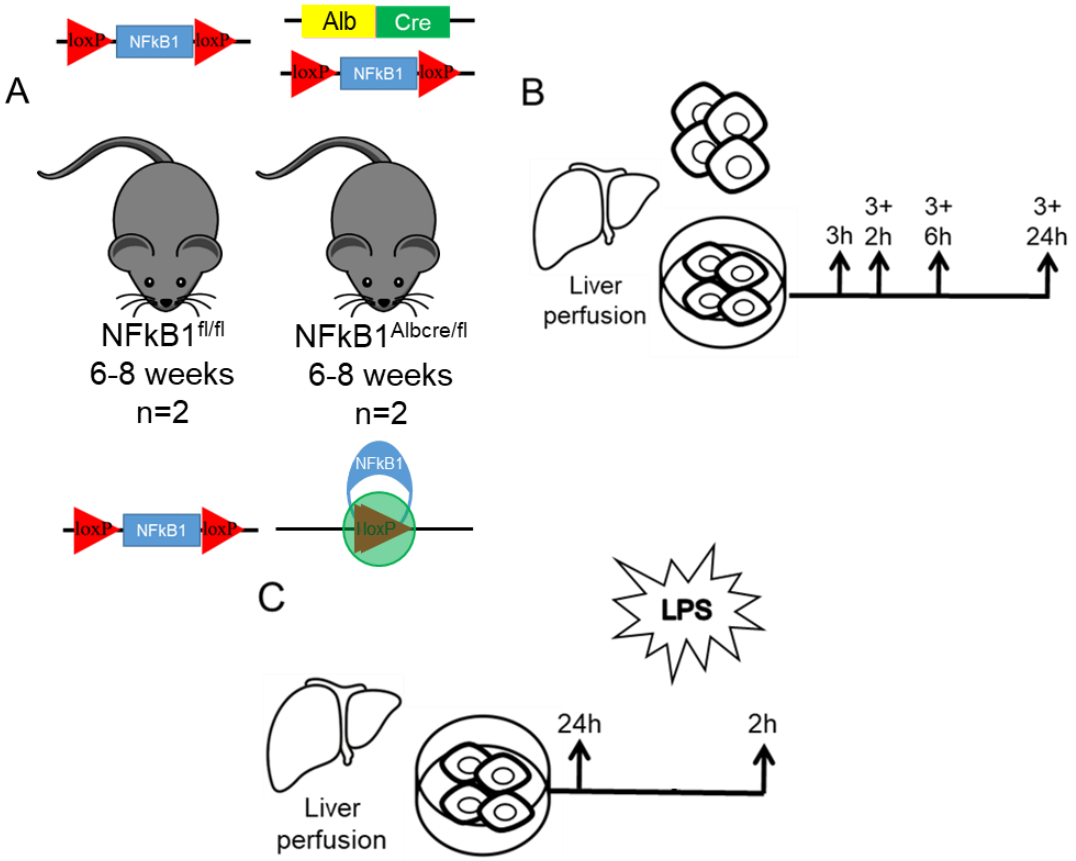

Figure 20. Graphical representation of the experiment. A, n=2 mice, between 6 and 8 weeks old, for both genotypes were taken for the experiment; B, the livers were perfused, and freshly isolated hepatocytes were compared with seeded hepatocytes harvested at different time points; C, seeded hepatocytes were treated for 24h and 2h with LPS 100ng/ml and untreated cells harvested at the same time (27h~) were used for the comparisons.

3.3.1. Time course experiment showed acute pro – inflammatory response due to the isolation

Different markers were used to characterise the hepatocytes along the time course and freshly isolated hepatocytes were used as control when comparing the different time points sampled. For this first part of the experiment Nfκb1$^{flox/flox}$ AlbCre+ hepatocytes were represented by n=1 only, due to problems with the isolation of a sufficient number of cells to perform the experiment.

Albumin was used to check the state of differentiation of hepatocytes, considering that albumin secretion is among the activities for which hepatocytes have specialised (Buyl *et al.,* 2015). As presented in figure 21, albumin levels dropped similarly in both genotypes after the 3h rest, indicating that it was not enough time for the hepatocytes to recover from the isolation. When looking at the inflammatory profile, Nfκb1$^{flox/flox}$ AlbCre+ and Nκfb1$^{flox/flox}$ hepatocytes showed an increased in levels expression of different inflammatory molecules, with similar fold changes when compared to the control (freshly isolated hepatocytes).

The only exception is KC, which presented comparable levels between freshly isolated and rested hepatocytes in Nfκb1$^{flox/flox}$ AlbCre+.

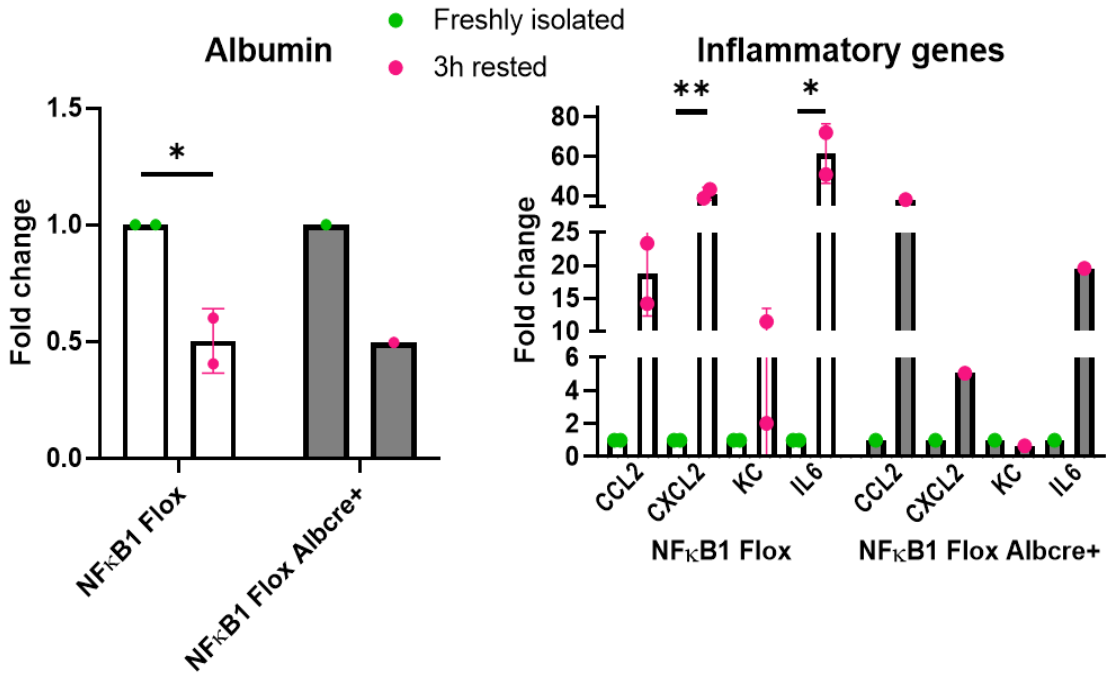

Figure 21. qPCR results for the comparison between freshly isolated and 3h rested hepatocytes. Albumin levels showed a drop in expression levels, indicating stressed hepatocytes. The inflammatory molecules panel showed comparable increased levels of cytokines and chemokines in both genotypes. No statistics analysis was performed for the Nfκb1$^{flox/flox}$ AlbCre+ as only n=1 was used for this portion of the experiment, while the analysis was possible for ctrl samples (n = 2)

Next, different time points were sampled and compared with the 3h rested hepatocytes to check the adaptation process of the cells. For albumin, the expression levels with both genotypes significantly dropped after the 3h rest time point, possibly indicating that a progressive de – differentiation process (Figure 22). The fold changes are comparable between the two primary cells, and they were both found to have the lowest expression level of Albumin at 27h~ culture.

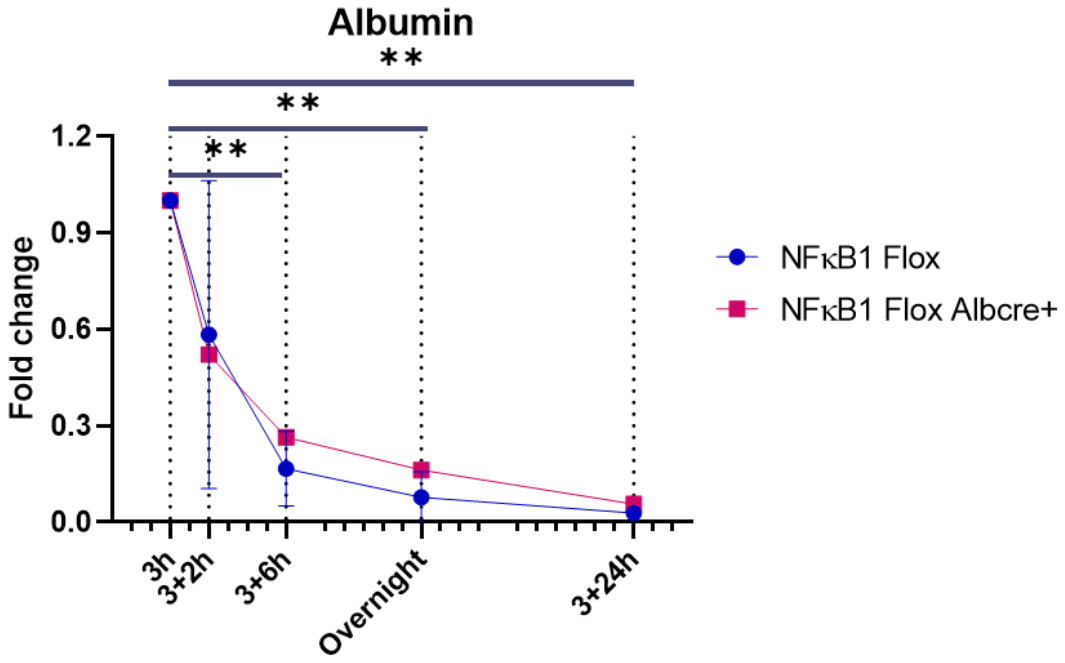

Figure 22. qPCR result for Albumin, marker of hepatic fitness. 3h rested hepatocytes were used as control for the comparison with the other time points in the time-course experiment. No statistics analysis was performed for the Nfκb1$^{flox/flox}$ AlbCre+ as only n=1 was used for this portion of the experiment, , while the analysis was possible for ctrl samples (n = 2).

CCL2, CXCL2, KC and IL6 were used again as inflammatory markers to check the status of the hepatocytes in culture.

CCL2 displayed a decreasing trend during the time course in Nfκb1$^{flox/flox}$ AlbCre+ cells, with consistent levels from 6h post rest to the endpoint (~27h). Nfκb1$^{flox/flox}$ cells initially increased the expression of CCL2 at 2h post rest, but then followed a similar decrease to what observed for Nκfb1$^{flox/flox}$ AlbCre+ hepatocytes. For CXCL2, levels increased at 2h post rest in both cell preps, with Nfκb1$^{flox/flox}$ displaying a fold change equal to 2, while the Nfκb1$^{flox/flox}$ AlbCre+ preps presented a fold change lower than in the control cell. The expression then decreased similarly in both genotypes, with consistent levels until the end of the time course.

Lastly, KC and IL6 presented the same trend for both cell preps along the whole-time course, with decreasing expression starting at 2h post rest (figure 23).

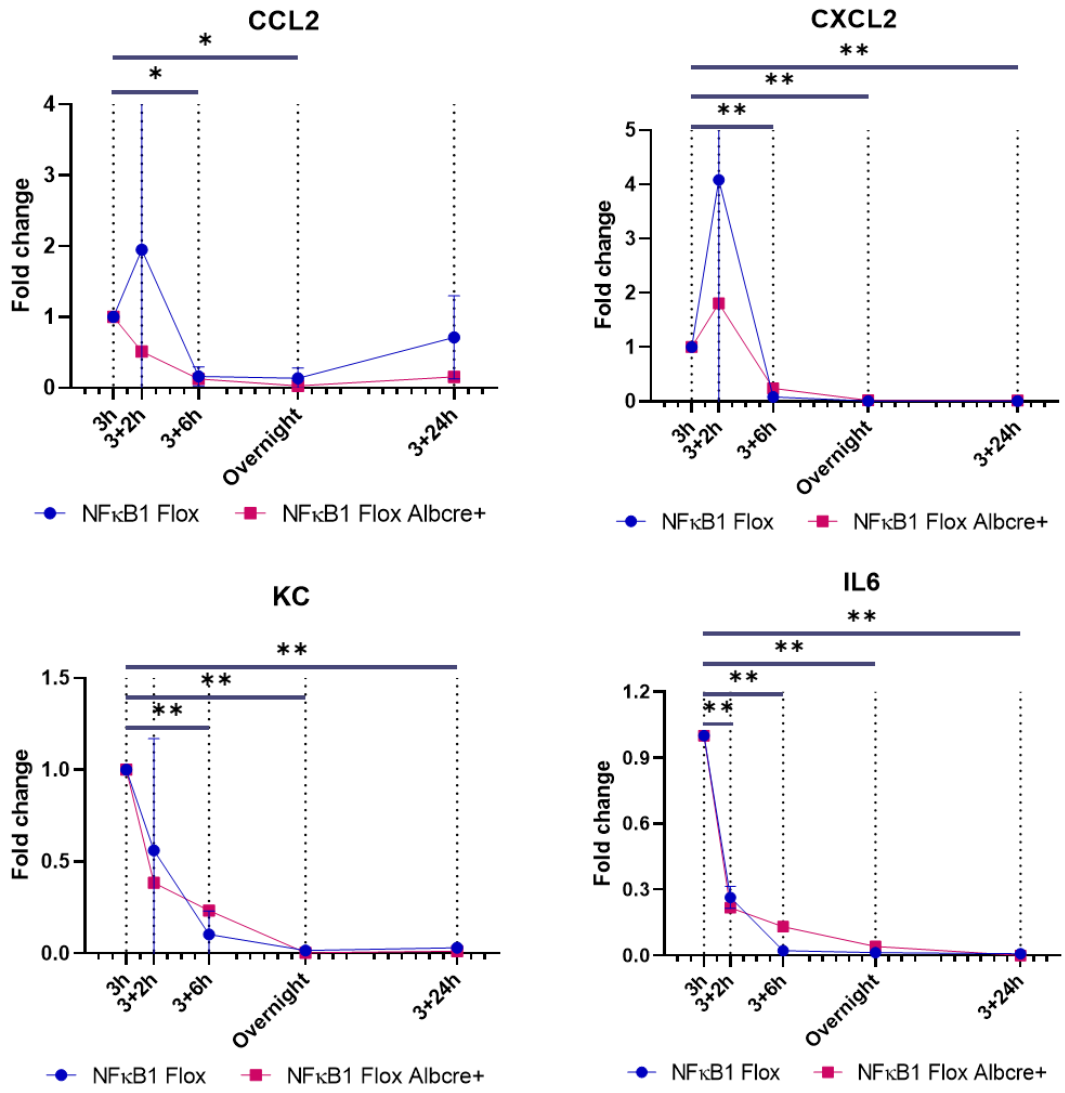

Figure 23. qPCR results for inflammatory markers. 3h rested cells were used as a control. No statistics analysis was performed for the Nfκb1$^{flox/flox}$ AlbCre+ as only n=1 was used for this portion of the experiment, , while the analysis was possible for ctrl samples (n = 2).

3.3.2. Two time points LPS experiment defined a paradigm for inflammation wave progression

For the last part of the experiment, hepatocytes were treated for 24h and 2h with LPS 100ng/ml to generate an acute inflammatory response. Untreated cells, but cultured for the same amount of time, were used as control in the comparisons.

The same markers analysed in the previous part of the experiment were used to assess the inflammatory response of Nfκb1$^{flox/flox}$ AlbCre+ and Nfκb1$^{flox/flox}$ hepatocytes to LPS stimulation (Figure 24).

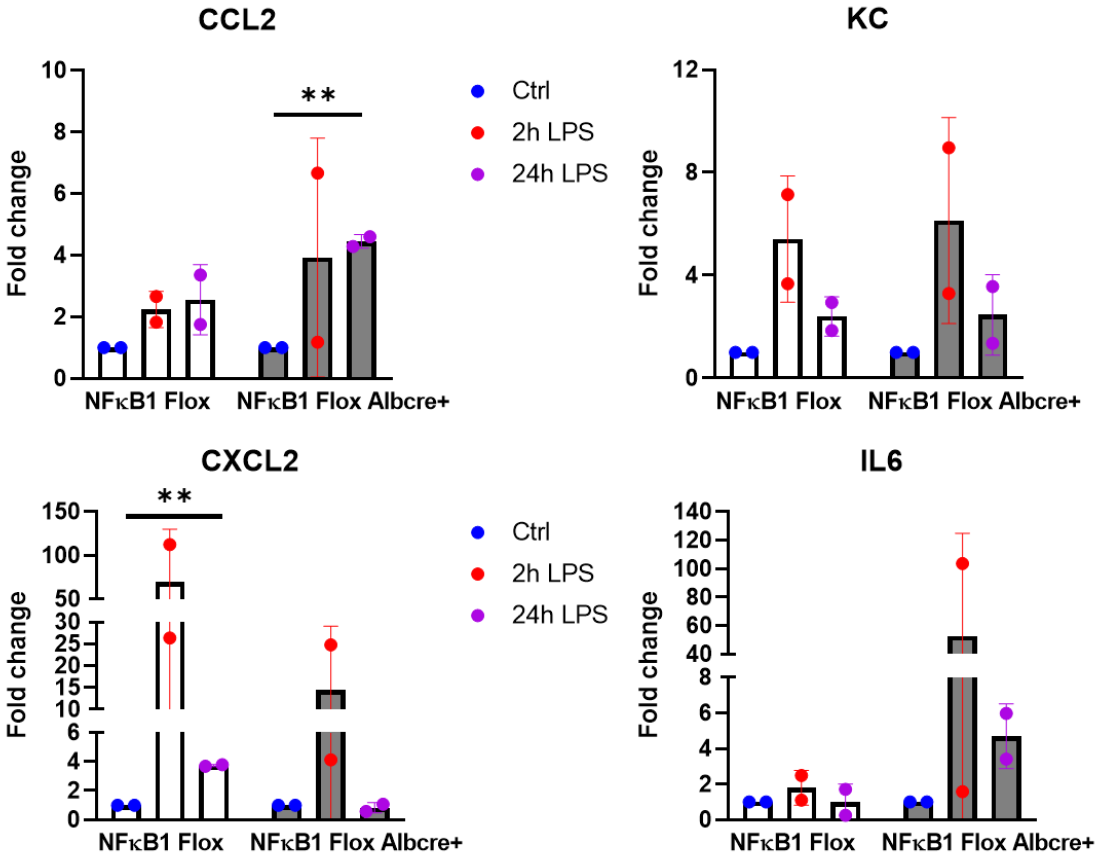

Figure 24. qPCR results for inflammatory markers. Untreated cells kept in culture as long as the treated ones were used as a control and all the samples were harvested at the same time. Statics analyses were performed for both genotypes (n=2)

As aforementioned, for the Nfκb1$^{flox/flox}$ AlbCre+ genotype only one cell prep was used in the first two parts of the experiment because one liver did not perfuse well, and the number of viable hepatocytes was limited and not enough to cover the whole experiment. The viable cells from the second liver were kept for this last part, which we considered to be the most important one, since it aimed to investigate whether any differences occurred between the two genotypes, in response to an inflammatory stimulus.

CCL2 levels increased upon LPS treatment after 2h in both genotypes. However, Nfκb1$^{flox/flox}$ AlbCre+ hepatocytes seemed to present a higher expression of the chemokine compared to Nfκb1$^{flox/flox}$, but the variability between the two samples in the p50 ko hepatocytes was high. Unexpectedly, the expression did not drop at 24h time point, but instead CCL2 was more expressed at 24h LPS than at 2h LPS, in both genotypes, with a significant difference in Nfκb1$^{flox/flox}$ AlbCre+. The LPS treatment had an effect on KC expression, as both genotypes have a 6~ fold increase at the 2h. As expected, the levels dropped at the 24h but for this particular chemokine it did not drop

to the baseline level, and the expression decreased to half of the fold change observed at 2h. No significant differences were found in the same genotype and between them. CXCL2 represents the expected result from an inflammation wave. In fact, the chemokine peaked at 2h LPS, with Nfκb1$^{flox/flox}$ hepatocytes producing more CXCL2 than Nfκb1$^{flox/flox}$ AlbCre+ hepatocytes. At 24h both genotypes showed a decreased in the expression levels, with Nfκb1$^{flox/flox}$ cells having a significant difference with the baseline, meaning that the expression levels did not go back to the control; Nκfb1$^{flox/flox}$ AlbCre+ hepatocytes did result in decreased expression of CXCL2, but comparable to the control.

Lastly, IL6 expression levels increased at 2h and Nfκb1$^{flox/flox}$ AlbCre+ cells seemed to have a higher expression of IL6, but the variability between the two samples does not allow to confirm that. The same cells showed a decrease at 24h LPS, as expected, but unlike Nfκb1$^{flox/flox}$, Nfκb1$^{flox/flox}$ AlbCre+ hepatocytes did not go back to the baseline, but instead the fold change was 4 higher than the baseline.

3.3.3. Preliminary data support the use of hepatocytes as in vitro model

A deep understanding of the mechanisms involved in the inflammatory response in the liver is pivotal to find interesting new candidates to further investigate and to target for drug discovery. New models for liver inflammation are therefore required and they need to be reliable but also feasible. Here we validated an *in vitro* model for liver inflammation, using primary hepatocytes isolated from mouse liver. The advantage of this method is that 80% of the liver consists of hepatocytes, so from the same liver it is possible to isolate enough cells to cover different experimental conditions. A disadvantage could be that the isolation process is quite harsh, and the gene expression and the fitness of the cells can be impacted.

I set a pilot experiment using primary murine hepatocytes isolated from both wt (Nfκb1$^{flox/flox}$) and hepatocytes – specific p50 knockout (Nfκb1$^{flox/flox}$ AlbCre+) in order to validate the model to study the acute inflammatory response (2h and 24h LPS) and to investigate whether differences in gene expression could be detected when comparing the two genotypes.

The results of the experiment confirmed that primary hepatocytes are a good working model to study inflammation in the liver, with some limitations. A rest is needed before starting any assays or treatments in order to allow the cells to acclimate to the new conditions, especially after the isolation process. According to some results obtained when looking at the inflammatory profile during a time course, the overnight rest could

be preferred over the 3h; however, this would extend the total time of culture for cells, and the experiment suggested that 27h~ is the limit, since the majority of the inflammatory genes showed a peak in expression at that last time point. This probably indicates that the cells are either dying or entering a de – differentiation stage.

Also, two time points for LPS treatment successfully mimicked an acute inflammatory response in hepatocytes and with particular attention to the comparison between wt and $p50^{\Delta hep}$, the results suggested that the latter might have a more inflamed phenotype upon LPS stimulation.

Because of the promising data, we decided to investigate further the changes in gene expression under different conditions in $Nfκb1^{flox/flox}$ and $Nfκb1^{flox/flox}$ AlbCre+ hepatocytes, using RNA sequencing.

3.4. RNA sequencing

For the RNA sequencing experiment, six male mice for each genotype were taken, $NfκB1^{fl/fl}$ as control and $NfκB1^{Albcre/fl}$ as hepatocyte-specific knock out of p105/p50. The livers were perfused following the collagenase protocol and viable hepatocytes were isolated and seeded. After 3h rest, the cells were either treated with 100ng/ml of LPS (2h and 24h) or left unstimulated. RNA and protein were extracted, and the RNA sent to sequencing (Figure 25).

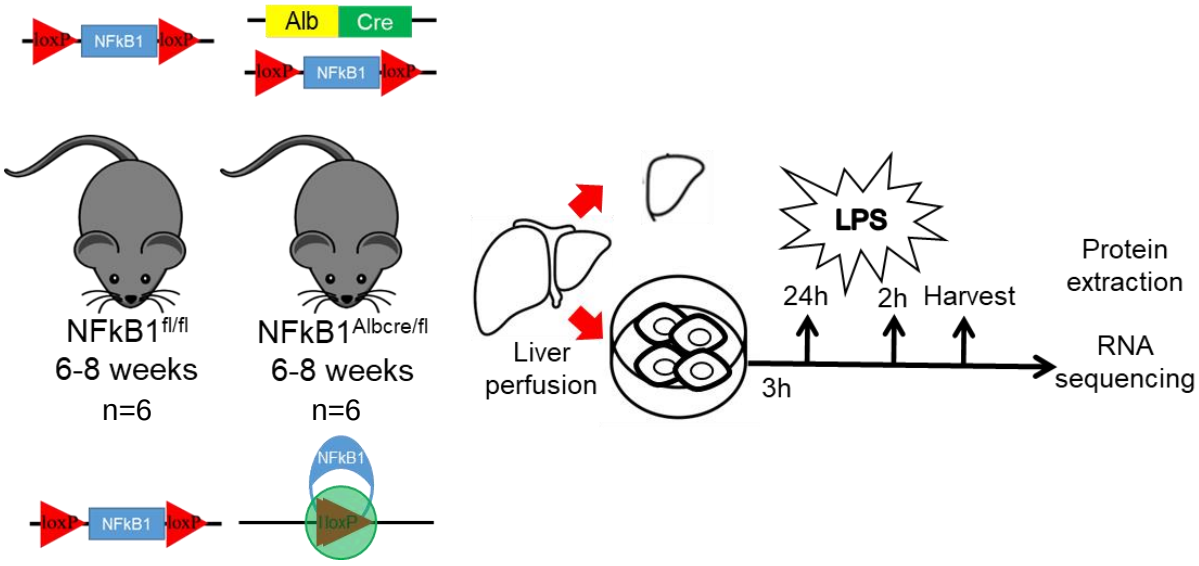

Figure 25. Set up of the experiment for the RNA sequencing. 6 mice for each genotype were used and their livers perfused with collagenase to obtain hepatocytes, which were seeded afterwards. The cells were treated with LPS for 2h and 24h or left untreated. RNA and proteins were isolated for following analyses.

3.4.1. Nfκb1 hepatocytes specific knockout is confirmed on different levels

Before sending the samples to sequencing, we checked Nfκb1 RNA and proteins levels in both genotypes, NfκB1$^{fl/fl}$ and NfκB1$^{Albcre/fl}$, to confirm the results obtained with the genotype assay and to make sure that the system was working. Before starting the perfusion, a small portion of the liver was clumped to prevent the action of the collagenase in that part of the tissue, and it was later harvested and used to isolate RNA and proteins, alongside the hepatocyte preparations.

The RNA was retrotranscribed and used to detect exon 4 belonging to nfκb1, as a control of efficient excision mediated by the Cre enzyme in hepatocytes. As presented in figure 26A, the first four lanes showed no specific amplification when using primers designed to recognise exon 4, as the signal detected at ~50bp is likely to correspond to primer dimers (yellow box). The specific amplicon, as visible in Cre – lanes, was detected at ~100bp, indicating correct amplification when targeting exon 4. This result confirmed that the genotype was correct and that the Cre enzyme recombined the DNA, as expected. On the other hand, the other four lanes on the right side did present an amplicon, meaning that the system was not leaky and the presence of the loxP cassettes flanking exon 4 did not affect the surrounding regions. The presence of p50 in NfκB1$^{Albcre/fl}$ hepatocytes was also checked at the protein level. Whole livers samples were run alongside hepatocytes preparations, from both genotypes; there was a remarkable difference in p50 expression in the two genotypes when looking at the whole liver (figure 26B), however the protein was still detectable at lower levels in livers from NfκB1$^{Albcre/fl}$ (Cre +) mice. This was expected, as the Cre-loxP system was designed to express the enzyme in hepatocytes only, but the liver is composed of other cell types, including hepatic stellate cells and immune cells, that will produce the protein. The confirmation of this result was given by the isolated primary hepatocytes (left side, figure 26B); NfκB1$^{Albcre/fl}$ hepatocytes did not express NfκB1, while the control group presented high levels of the protein, when no Cre enzyme was in the system (Cre -). Lastly, the efficiency in triggering an inflammatory response was assessed by qPCR. Higher levels of KC, IL6 and CCL2 were found at 2h and 24h LPS treatment, when compared to the untreated control (Figure 26C).

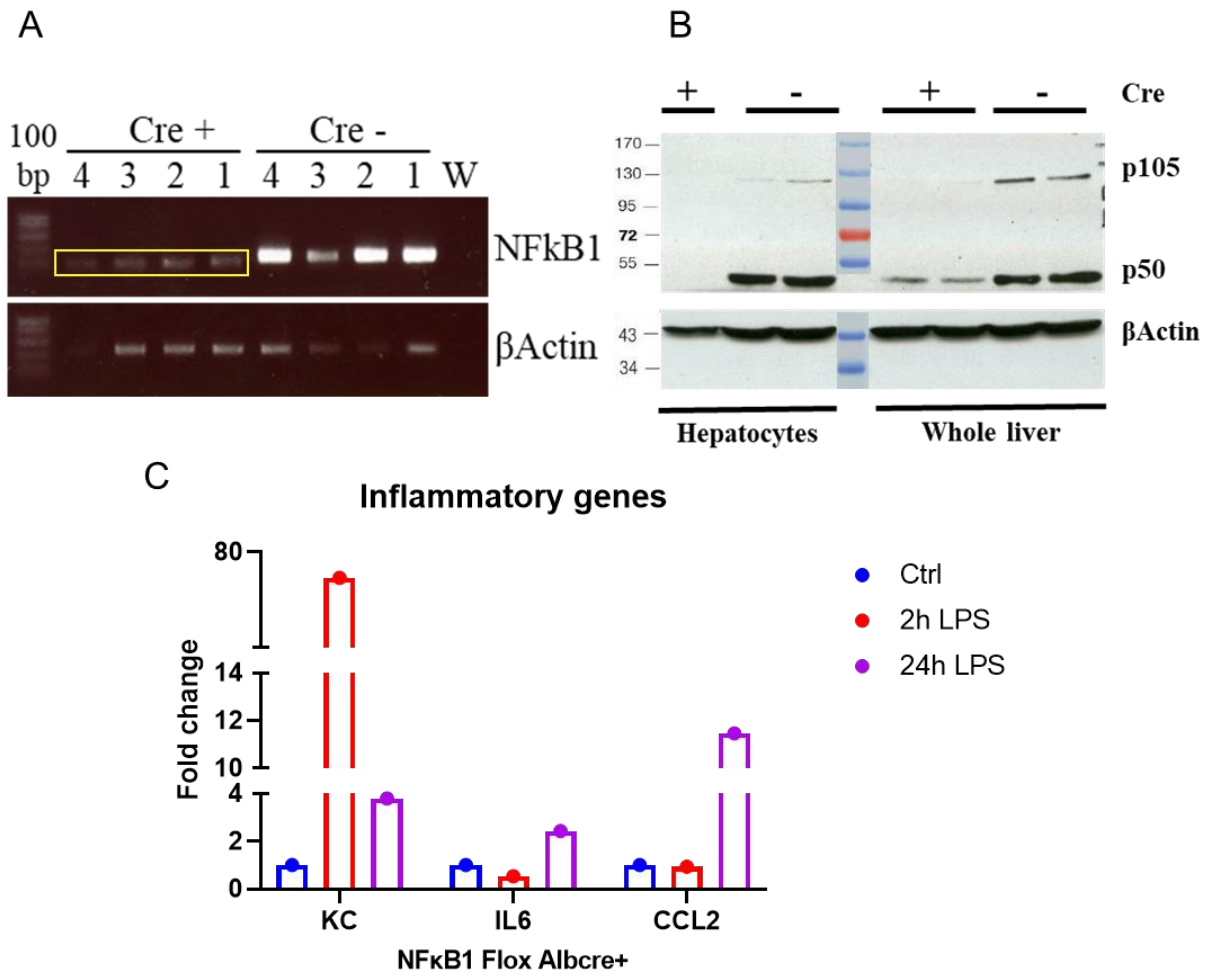

Figure 26. Confirmation results before sending the samples to sequencing. A, the RNA was extracted and retrotrascribed and the presence of exon 4 was checked by PCR. In NfκB1$^{Albcre/fl}$ samples, expressing the Cre enzyme (Cre +), there was no amplification of exon 4 and the visible fainted band at the bottom was likely to be primer dimers (yellow box). NfκB1$^{fl/fl}$ samples did not express the Cre enzyme (Cre -) and the amplification of exon 4 was visible in all four lines, indicating that the system worked. B, similar results were observed at protein levels: hepatocytes expressing the Cre enzyme did not present p50, while control hepatocytes did. In whole liver samples the differential expression of p50 in the two genotypes was observed, but livers expressing Cre + still presented p50 because the of the heterogeneous composition of the liver parenchyma that includes other cell types. C, qPCR results on one hepatocytes preparation to check the efficient trigger of an inflammatory response. The three inflammatory markers were found to be more expressed at 2h and 24h LPS treatment, when compared to untreated control hepatocytes.

3.4.2. RNA sequencing process

The RNA sequencing process was carried out by an external facility. We received the FastaQ files from the sequencing and the results were analysed in the lab as exemplified in figure 27. The FastaQ files were checked for the quality of the reads obtained for every sample. The reads were then trimmed in order to remove the adaptors added before the sequencing run. Also, trimming at this point could be beneficial to improve the quality of the reads, as the processivity of the polymerase decreases at the beginning and at the end of a strand. The reads could be checked

again for their quality after the trimming, to see whether other steps are needed or if the reads could be used for the alignment. At this step, R studio was used to align the reads to the genome of reference and the differential expression of genes was calculated.

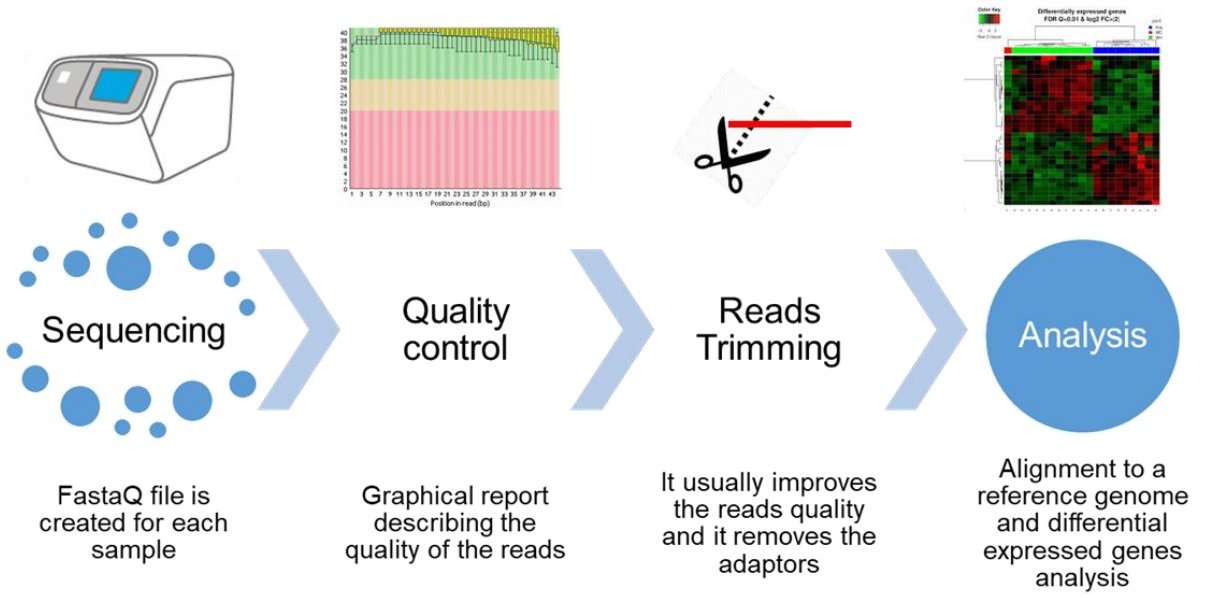

Figure 27. Schematic representation of the workflow for RNA sequencing analysis. The results of the sequencing were generated as FastaQ files. A quality control of the reads was necessary prior starting the analysis; the reads were then trimmed, primarily to eliminate the adaptors, but also to improve the quality. Once trimmed, the reads were aligned to the reference genome and the differential gene expression was investigated.

A Principal Component Analysis (PCA) was initially generated, and it summarised how different the samples were from each other; the greater the values of x and y axes, the more different were the samples (figure 28, top panel). It was firstly observed that the samples coming from the same hepatocytes preparation, independently on the treatment, clustered together, as indicated by orange and blue circles corresponding to NfκB1$^{Albcre/fl}$ (WT) and NfκB1$^{Albcre/fl}$ (KO), respectively. In the same figure another cluster was also noticed and highlighted by purple circles, showing samples from different genotyping clustering together, e.g., WT2 and KO3 (top right quadrant) and WT6, KO6 and KO5 (bottom right quadrant) which it was unexpected. Both observations could be explained by a greater variability between hepatocytes preparations compared to the similarities between cells with the same treatment. In light of this preliminary output, the samples in the purple circles were not included in the following analyses and another PCA was generated with 4 samples for each genotype (Figure 28, bottom panel).

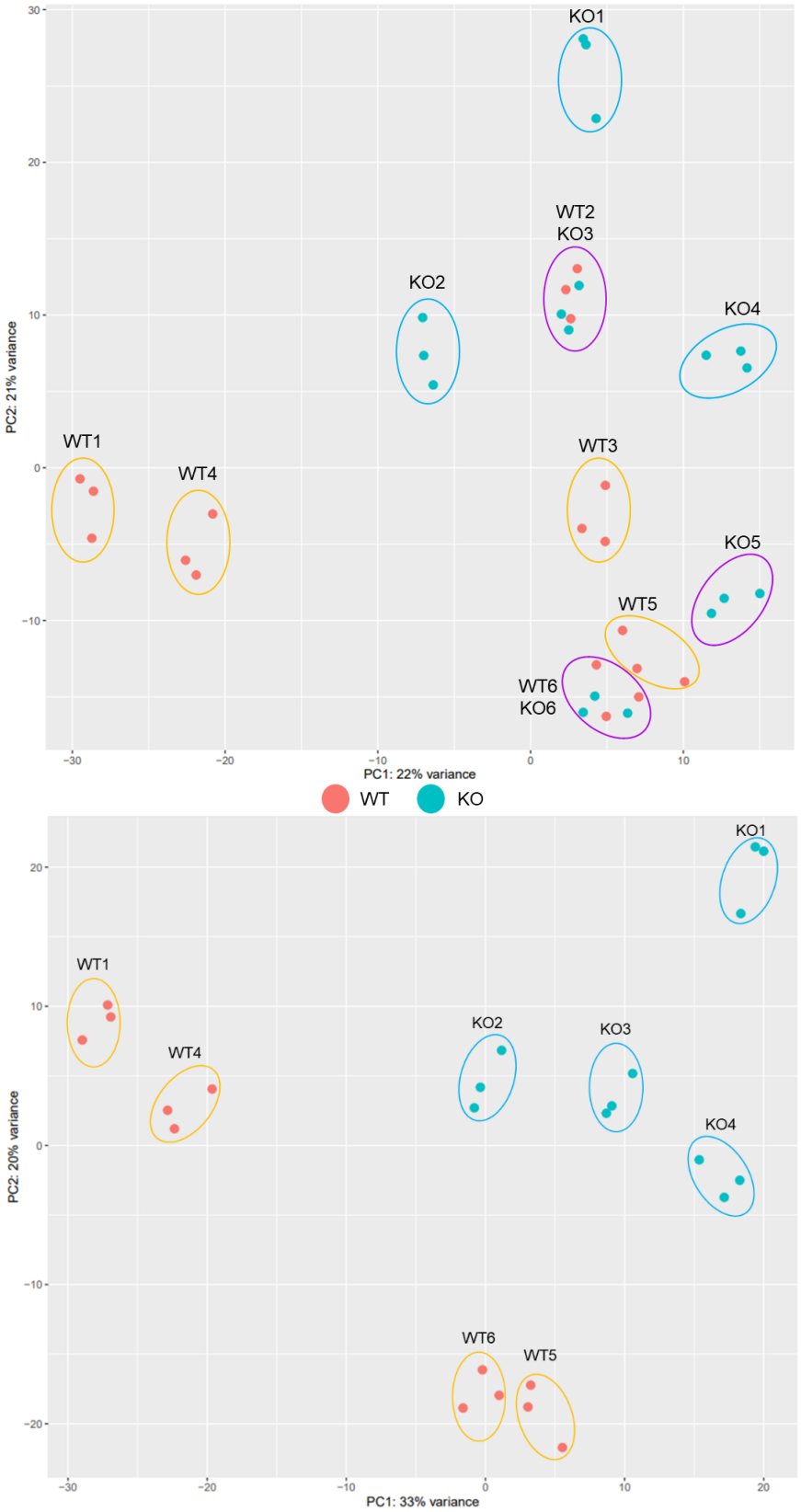

Figure 28. PCA graphs. NfκB1$^{Albcre/fl}$ samples are identified by KO1-6, while NfκB1$^{fl/fl}$ samples are WT1-6. Top panel, PCA shows how the clustering was predominantly affected by the origin of the samples, rather than the treatment. Orange and blue circles indicate expected clustering based on the genotype, while purple circles highlight those samples that clustered unexpectedly. Bottom panel, after removing the samples found in the purple circles, another PCA was generated and clustering seemed to have improved.

Despite the evident improvement of the clustering based on the different genotype, this PCA evidences the division into two subgroups within the WT group, as samples WT1 and 4 grouped in the left top quadrant while WT5 and 6 were found in the bottom right corner, indicating a great variability withing the same genotype. A correction to limit the batch effect was applied prior to any analysis because of these further observations.

3.4.3. Baseline comparison points at novel pathways under the control of NFκB1

Baseline comparison between untreated cells from both genotypes generated the volcano plot reported in figure 29A. This type of scatter plot is a representation of statistical significance (reported as adjusted p value on the y axis) versus magnitude of change (reported as log2 fold change on the x axis) when comparing two conditions, in this case WT cells ($NfκB1^{fl/fl}$) as control and NfκB1 KO hepatocytes ($NfκB1^{Albcre/fl}$) as experimental condition. The coloured points represent the genes having adjusted p-values < 0.05, chosen as threshold; blue dots represent genes with decreased expression compared to the control, while red dots represent genes more expressed in the experimental condition. Black dots are genes that are neither differentially expressed or statistically significant.

Differentially expressed genes (DEGs) in unstimulated conditions for both genotypes are represented in the heatmap in figure 29B, with fold change > 2 and adjusted p-values <0.05. 1767 hits were identified, and the results were loaded on the free online tool Protein Annotation THrough Evolutionary Relationship (Panther, http://www.pantherdb.org) in order to understand the functions and the pathways that the genes found with the sequencing belonged to (Mi *et al.*, 2013).

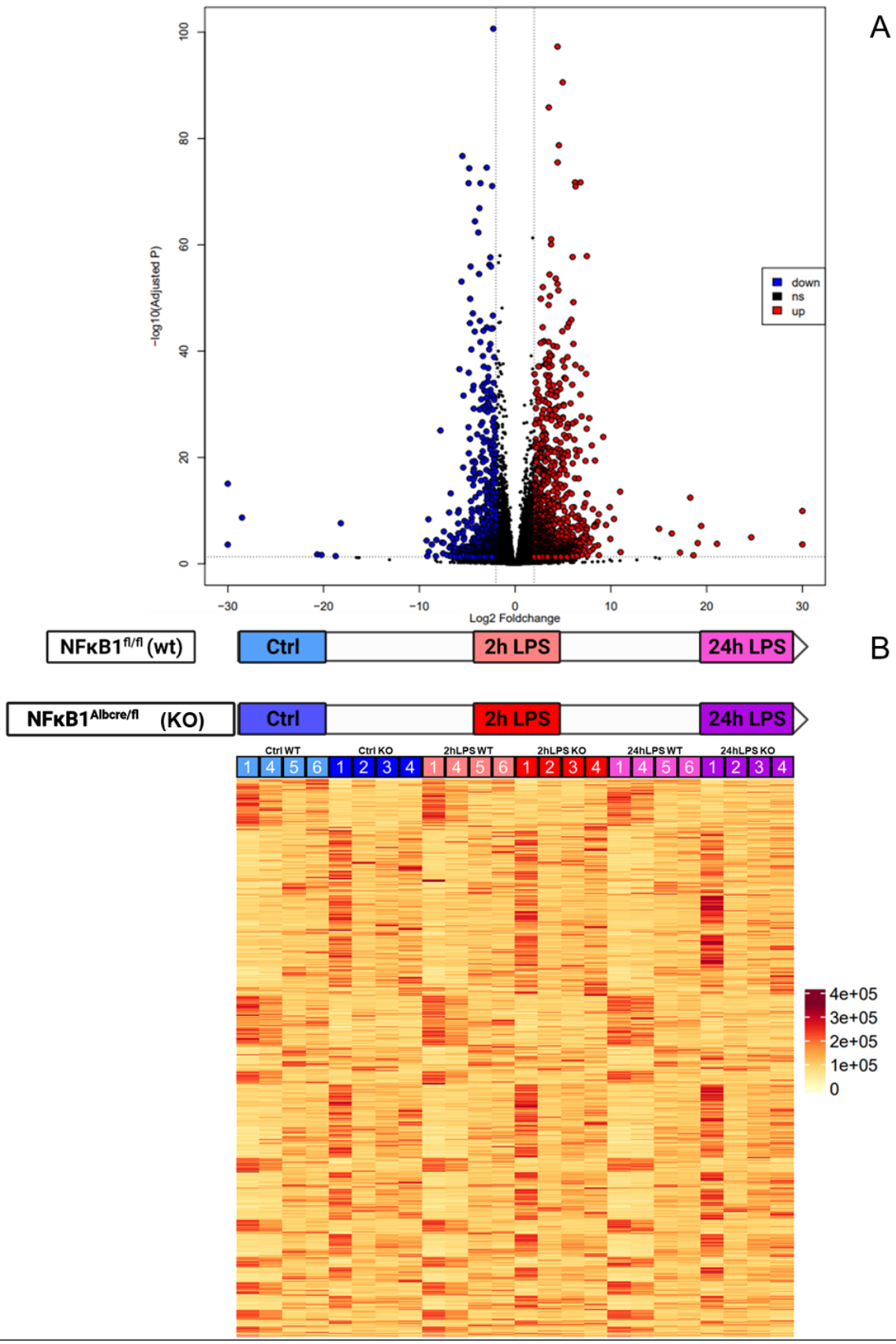

Figure 29. A, Volcano plot enabling a quick visualisation of which genes are differentially expressed and statically significant when comparing WT vs NfκB1 KO (n=4). B, heatmap displaying differentially expressed genes found from the RNA sequencing, when comparing untreated cells (ctrl)for both genotypes. The other columns correspond to the other conditions (the two LPS treatments in the two genotypes) and how the same genes behaved in those sample. Statically differentially expressed genes were considered those with fold change > 2 and adjusted pvalue < 0.05.

On the same online platform, it was possible to obtain a pie chart summarising the biological processes to which the genes belonged to. The results are shown in figure 30. The first two GO terms found were general and generic, such as cellular process leading the list and biological regulation in second position. Intriguingly, it appeared that there was a great portion (13,53%) that belonged to metabolic processes.

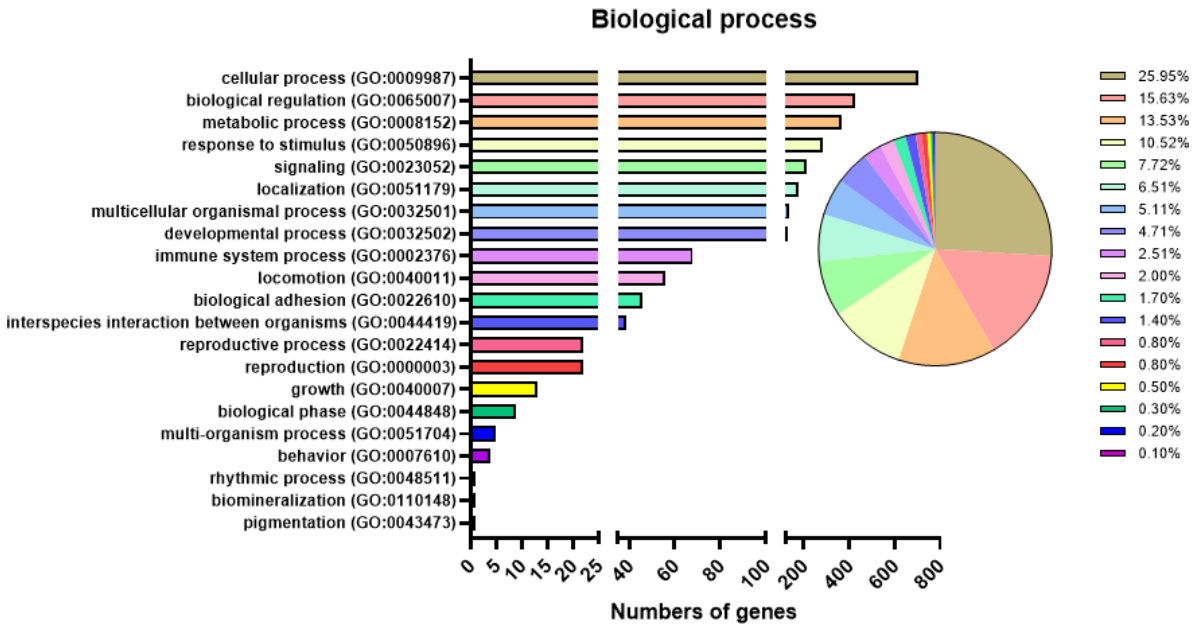

Figure 30. Graph showing the number of genes found for every GO term and the pie chart generated on Panther, indicating the percentage that each GO term represents compared to the whole set of genes uploaded on the platform. The last three GO terms did not correspond to a percentage as it was too little compared to the whole. Colours are matched between the graph and the pie chart.

The same list of genes was checked for Panther pathways, in order to investigate which pathways were mostly affected, in both directions, by the lack of p50 in hepatocytes. Some well-known pathways involving p50 were found, including signalling involved in inflammation and response to stimulus (figure 31). Intriguingly, pathways involved in p53 signalling, cell cycle and DNA replication were also found to be affected by the absence of p50. In particular, genes involved in these pathways were downregulated in $p50^{-/-}$ hepatocytes (Figure 32). Interestingly, some of these genes encode for epigenetic modifiers, like Dnmt3l and EZH2.

DNA methyltransferase 3 like, or Dnmt3l, is involved in *de novo* DNA methylation through the recruitment of Dnmt3a, as it does not possess enzymatic activity itself (Dé Ric Ché, Lieber and Hsieh, 2002). Dnmt3l can act as a transcriptional repressor in a HDAC1 – dependent fashion (Deplus *et al.*, 2002) and recent studies showed that Dnmt3l is also able to interact with transcription factors, including p65, to direct the active Dnmt3A/B to specific target sequences, modulating their methylation (Pacaud

et al., 2014). Interestingly, EZH2 is a lysine methyltransferase enzyme, and it interacts with the Dnmt family of proteins, in particular Dnmt3a (Rush *et al.*, 2009). EZH2 itself is also a direct target of NF-κB in the CD40L pathway and it has been linked to the repression of p53 action, linking the alternative NF-κB pathway to senescence and tumour progression (Iannetti *et al.*, 2014).

Other genes found from the sequencing are directly involved in the cell cycle and in particular in the regulation of checkpoints: different cyclins were listed, such Cyclin A2 and F, but also kinases and phosphatases involved in the same signalling pathway, like Cdk1 and Cdc25c, respectively.

Cyclin A2 is considered the mammalian S phase cyclin (Hochegger, Takeda and Hunt, 2008) and upon expression it induces the activation of its catalytic partners, Cdk2 and Cdk1 (Kalaszczynska *et al.*, 2009), the latter also present in the sequencing data. Together, Cyclin A and Cdk1 phosphorylate their targets and guarantee the correct progression of S phase, as inactivation of Cdk1 results in prolonged S phase (Katsuno *et al.*, 2009) and cyclin A2 is often overexpressed in cancer and it has been considered as a possible target to limit tumour progression (Gopinathan *et al.*, 2014). Cyclin F is a non – canonical cyclin, as it does not activate or bind Cyclin – Dependent Kinases (CDKs) (D'Angiolella, Esencay and Pagano, 2013); it is the founding member of a larger group of proteins containing a F-box domain (Jin *et al.*, 2004), which is essential for the interaction with Skp1, a component of the SCF ubiquitin ligase machinery (Bai, Sen and Hofmann, 1996). By directing the SCF complex to target genes, Cyclin F has been implicated in ubiquitination and degradation of several proteins involved in the cell cycle (Emanuele *et al.*, 2020), including the RB – family tumour suppressor p130 (Enrico *et al.*, 2021), highlighting an important link between ubiquitination regulation and cell cycle. Among other cell cycle – associated proteins, Cyclin – Dependent Kinase 1 (Cdk1) and Cell Division Cycle 25C (Cdc25c) both promote G2/M transition, with Cdc25c dephosphorylating Cdk1 in order to activate the complex cyclin B1/Cdk1 (Liu, Lu, *et al.*, 2020). Studies in mice suggested that Cdk1 is essential for mitosis and that Cdk1 alone is able to drive the progression of the mammalian cell cycle, compensating for the lack of interphase CDKs (Santamaría *et al.*, 2007). Its importance was also confirmed by mouse knockout models, showing that $Cdk1^{-/-}$ mice were not viable and therefore indicating that Cdk1 is also essential for early embryonic development (Diril *et al.*, 2012).

Cdc25c is one of the three isoforms found in the dual – specificity Cdc25 family of proteins, also comprising Cdc25a, controlling G1/S transition, and Cdc25b, a mitotic

starter (Cho *et al.*, 2015). Downregulation of Cdc25c causes the arrest of the cell cycle at G2/M in response to DNA damage (Liu, Zheng, *et al.*, 2020), mediated by the repressive effect of the phosphorylation of Cdc25c on Ser 216 (Bulavin *et al.*, 2003). Overexpression of Cdc25c correlates with tumour growth initiation, and abnormal levels of this protein are found in diverse human cancers, including liver (Kristjá and Rudolph, 2004).

NF-κB family of proteins have been associated with cell cycle regulation before, but this aspect is often shadowed by the role NF-κB plays in inflammation (Ledoux and Perkins, 2014). As a transcription factor, NF-κB controls the cell cycle by regulating the expression and activation of key regulators at specific stages, such as Cyclin D1 to promote the G1/S transition (Guttridge *et al.*, 1999) and Aurora A to regulate G2/M progression (Prajapati *et al.*, 2006).

Some oncogenes were also downregulated in $p50^{-/-}$ hepatocytes, such as BRCA1 and 2. Breast cancer susceptibility gene 1 and 2, respectively called BRCA1 and BRCA2, are important tumour suppressors involved in genomic stability and DNA Damage Repair (DDR) mechanisms (Gudmundsdottir and Ashworth, 2006). While BRCA1 is ubiquitously involved in homologous recombination and more broadly in other cellular processes in response to DNA damage, BRCA2 primarily takes part to homologous recombination, by regulating the function of RAD51 during DNA repair (Roy, Chun and Powell, 2012). In mouse models, heterozygous mutations at these two genes are compatible with life and do not present a dramatic phenotype, but most homozygous mutations are embryonically lethal (Evers and Jonkers, 2006). In humans, somatic mutations in BRCA1 and 2 predispose women to develop breast and/or ovarian cancer (Antoniou *et al.*, 2003). Mutations in the germline cause a more aggressive disease and poor prognosis, with cancer development at a very young age (Musolino *et al.*, 2007). Somatic mutations in the guardian of the genome, p53 (Bessette *et al.*, 1992), were also found to be common in BRCA1 and 2 breast (Smith *et al.*, 1999) and ovarian (Ramus *et al.*, 1999) tumours.

Previous studies showed that NF-κB is able to regulate the expression of BRCA2 by directly binding its promoter and further characterisation proved that BRCA2 expression was particularly enhanced when the promoter was bound by p65:p50, compared to p65 alone (Wu *et al.*, 2000). Similarly, BRCA1 has been identified as a novel activator of NF-κB in response to DNA damage, able to facilitate the p65 – dependent recruitment of p50 at the promoters of responsive genes, including Bcl2 (Harte *et al.*, 2014).

Pathway	Most represented category	Number of genes	% vs total genes in list	% vs total pathway hits
Inflammation mediated by cytokines and chemokines	Chemokine	35	2.6	6.5
Integrin signalling pathway	Collagen	25	1.9	4.7
Wnt signalling pathway	Cadherin	24	1.8	4.5
PDGF signalling	-	10	0.8	1.9
TGFβ signaling	TGFβ	9	0.7	1.7
p53 pathway	CDKN2A inhibitors	9	0.7	1.7
Cell cycle	CdkC, Cyclin D	5	0.4	0.9
DNA replication	DNA topoisomerase	5	0.4	0.9

Figure 31. Table representing the results from the pathways analysis on Panther. The top pathways found were well-known for p50 activity in their signalling, such as inflammation and pathways associated with immune responses. Although the smaller number of genes, non-canonical and novel pathways involving p53 signalling, cell cycle and DNA replication were found to have genes being differentially expressed when hepatocytes lack p50.

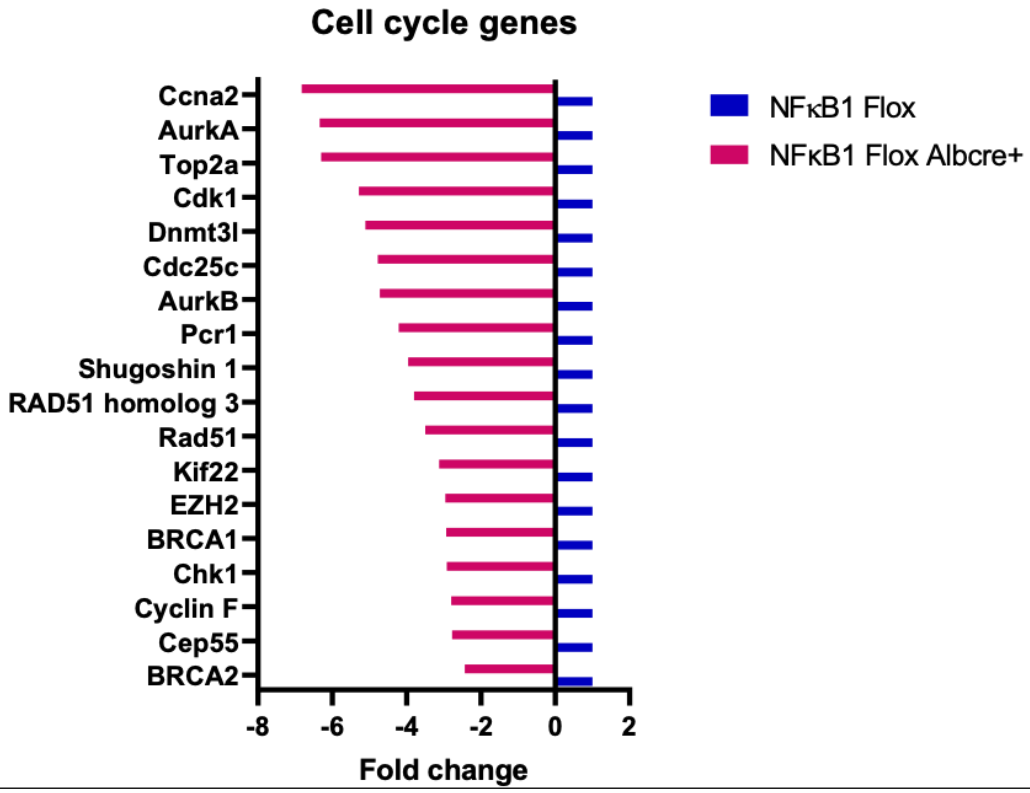

Figure 32. Fold changes of genes involved in p53 signalling, cell cycle and DNA replication that were found from the sequencing. In hepatocytes lacking p50, these genes were downregulated. Cyclins like Ccna2 and Cyclin F, and kinases involved in the cell cycle, as Cdk1 and Cdc25c, belonged to this subset of genes. Important oncogenes like BRCA1 and 2 were also found less expressed in $p50^{-/-}$ hepatocytes.

3.4.4. Repression of a set of inflammatory genes requires NFκB1 presence

Following the comparison between untreated cells from both genotypes, we then asked if they were any differences between untreated cells and the LPS treatments. The criteria for selecting DEGs were kept the same as for the previous comparison (fold change > 2 and adjusted p-value < 0.05). In figure 33, the differentially expressed genes with the highest fold change are listed for each condition. When comparing untreated cells with 2hLPS and 24hLPS in NfκB1$^{fl/fl}$ cells, 42 and 25 hits were found respectively; in 2h treated wt cells, the majority of the upregulated genes belonged to the family of cytokines and chemokines, confirming that the LPS induced an acute immune response. At 24h LPS those genes were no longer differentially expressed in wt cells, this a sign of negative regulation, an outcome expected at the resolution stage. A similar subset of genes were found to be upregulated when comparing untreated and 2h LPS treated NfκB1$^{Albcre/fl}$ cells. Interestingly, some of the same genes found upregulated in both 2hLPS samples (wt and p50$^{-/-}$) were also found in the list of genes upregulated at the 24hLPS treatment in p50$^{-/-}$ cells.

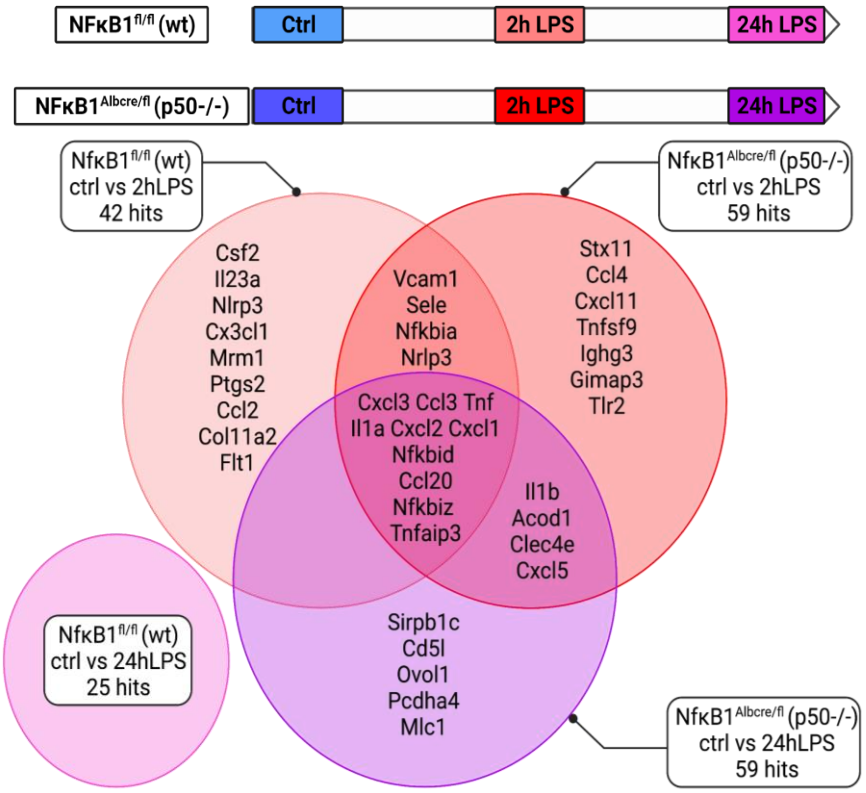

Figure 33. Venn diagram representation of the DEGs when comparing untreated and LPS treated cells withing the same genotype, either NfκB1$^{fl/fl}$ (wt) or NfκB1$^{Albcre/fl}$(p50$^{-/-}$). As expected, similar inflammatory genes were found upregulated in both genotypes at the 2h LPS treatment. No interesting genes were found at the 24h LPS In wt cells, however a smaller subset of inflammatory genes was shared among 2h LPS treatment in both genotypes and 24h LPS in p50$^{-/-}$ cells.

In particular, chemokines and cytokines involved in response to stimuli, including Cxcl3, Cxcl2, Ccl20 and Cxcl1, which demonstrated a fold change > 2 in all three samples. This could suggest that nfκb1 activity is not essential to induce the inflammatory response, but it is necessary in order to help with the resolution of it, by downregulating the expression of pro – inflammatory genes.

The results from sequencing analyses were confirmed by directly looking at both reads and raw fold changes for those genes shared by all three lists. In particular, five genes were further investigated, on the basis of their role in inflammation, which will be discussed later, and because of the pattern of expression that resulted from the experiment.

In figure 34, the reads from the sequencing are graphed for each gene analysed. In wt cells, the untreated sample showed baseline expression for all the genes, which then increased at 2h LPS, after the trigger of an acute response. At 24h LPS, the resolution of the inflammatory wave led to the downregulation of those same genes, bringing their levels back to the baseline.

On the other hand, nfκb1$^{-/-}$ cells displayed the same increased expression of the genes at 2h LPS, but surprisingly those levels were consistent at 24h LPS, indicating that the expression of those genes remained induced even at the resolution time point. By lacking p50, those cells appeared to be perturbed in their ability to inflammation.

Further confirmation of these results were found when checking the fold changes of those genes from the sequencing and the values are graphed in figure 35. Untreated cells for both genotypes were given an arbitrary fold change value of 1, as they were used as control for the comparisons. As observed in the previous graph, wt cells presented upregulation of this subset of genes at 2h treatment, with the highest fold change observed for Cxcl2 (6.45). At 24h treatment, wt cells went back to more physiological expression of those genes, resembling the values of the untreated cells. NfκB1$^{Albcre/fl}$ cells did show the same fold change at 2h LPS for the same genes, but the values were still high at 24h treatment, comparable to the 2h treatment in both genotypes.

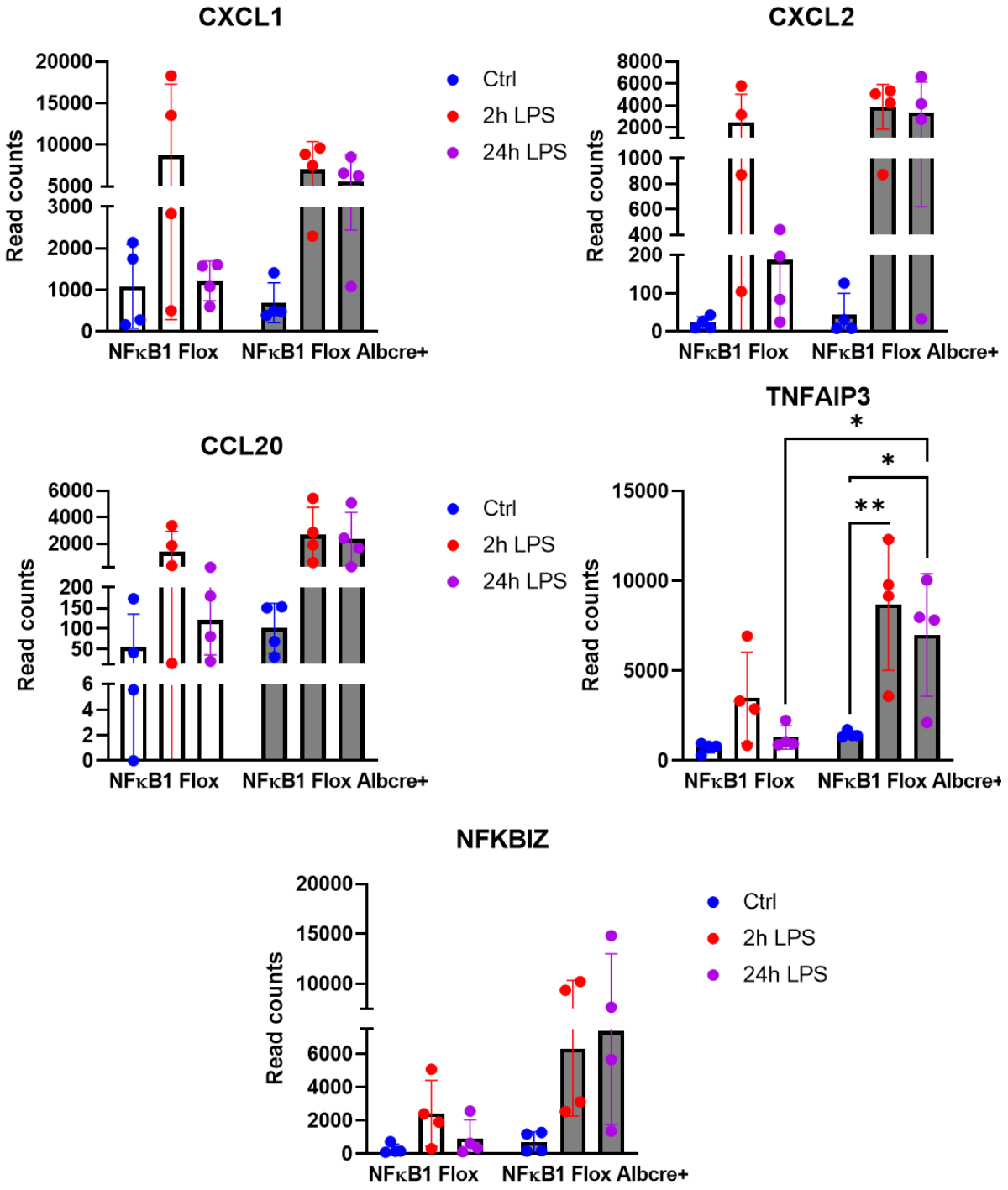

Figure 34. Raw reads from the RNA sequencing data (n=4 for each genotype). For all genes, both genotypes presented the smallest numbers of reads when the cells are untreated and there was also no significant differences between the two genotypes. At 2h LPS, cells from both genotypes presented greater expression of those genes, as the numbers of reads doubled from the previous condition. At 24h LPS, wt and $p50^{-/-}$ presented opposite patterns: wt cells decreased the expression of those genes at this time point, while ko cells presented levels of expression as high as the acute LPS treatment (2h). Statistical significance was calculated with two ways ANOVA.

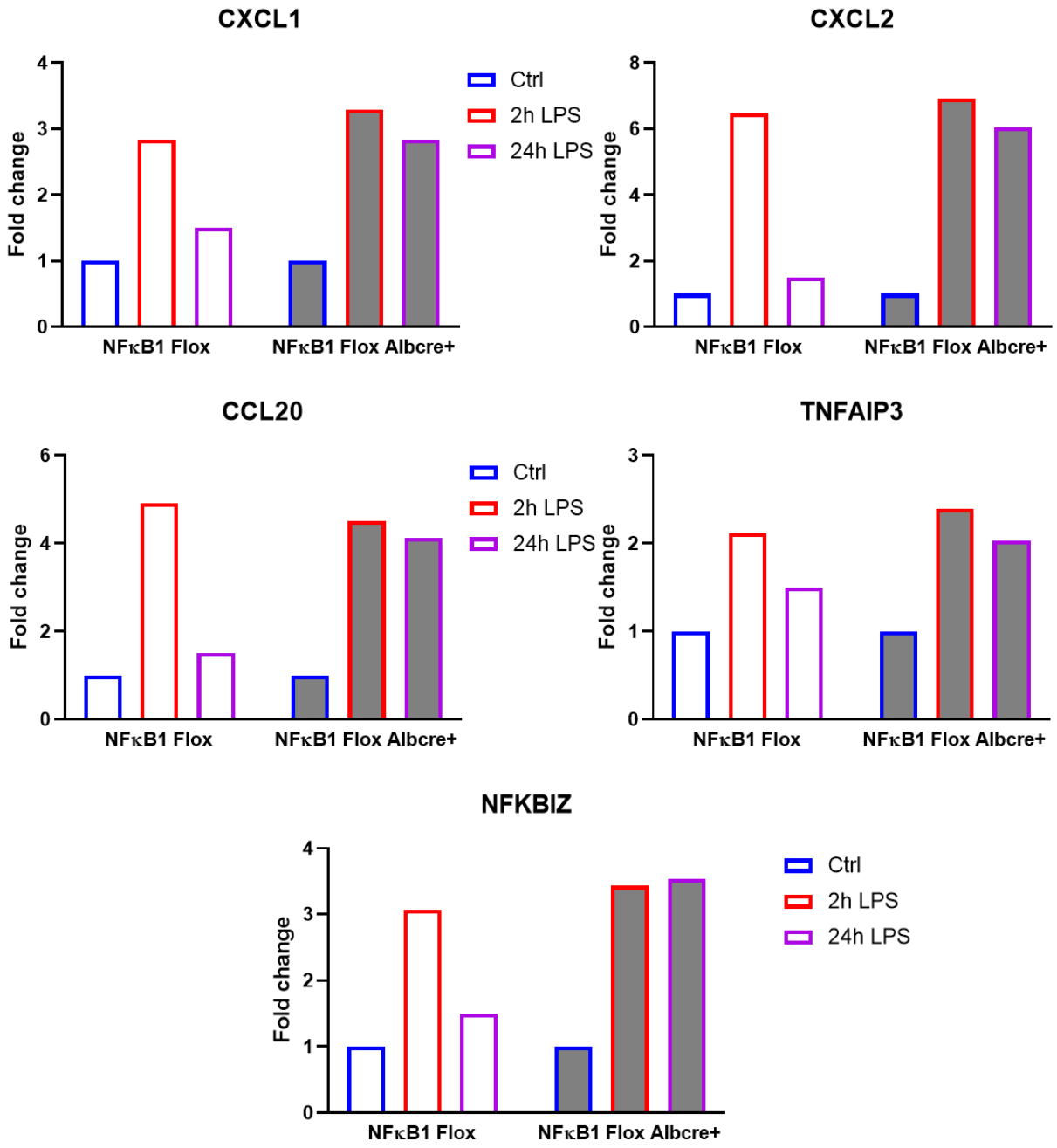

Figure 35. Fold changes from the RNA sequencing data. The results are an average of the 4 different samples used for each condition. NfκB1$^{fl/fl}$ cells increased the expression of the investigated genes at the 2h LPS, but then the expression decreased at 24h treatment. NfκB1$^{Albcre/fl}$ cells displayed the same increase at the 2h treatment, but no fold change decrease was observed at 24h LPS, as the expression of those genes did not seem to be reduced at that time point.

3.4.5. CXCL1

CXC motif chemokine ligand 1, CXCL1, is one of the four most studied CXC chemokines (Korbecki *et al.*, 2022) and its expression is elevated during inflammatory responses. In particular CXCL1 is a chemotactic for neutrophils (Bernhard Moser *et al.*, 1990) and it promotes their mobilization from the bone marrow (Martin *et al.*, 2003). CXCL1 expression is tightly controlled by the NF-κB family, and in particular the heterodimer RelA-p50 can induce the chemokine expression upon activation induced by TNFα and IL1β (Shatruck *et al.*, 1994). On the other hand, p50 homodimers are able to repress the expression of CXCL1 by recruiting the co – repressor HDAC1. Previous studies have shown that nfκb1$^{-/-}$ mice, by lacking the negative control that p50 homodimers exert on CXCL1, presented elevated expression of the chemokine compared to wt animals (Wilson *et al.*, 2015b), which in turn led to a greater number of infiltrated neutrophils, setting an ideal microenvironment for cancer development in the liver. CXCL1 has also been identified as a pro – inflammatory compound involved in the onset of the Senescence – Associated Secretory Phenotype (SASP), which entails the secretion of inflammatory molecules into the tissue environment, contributing to age related – conditions, including inflammageing (Jurk *et al.*, 2014).

3.4.6. CXCL2

CXC motif chemokine ligand 2, CXCL2, is another important inflammatory factor involved in inflammatory responses, and very similarly to CXCL1, it is responsible for the recruitment of neutrophils from the blood stream to the tissue of interest (Girbl *et al.*, 2018). Interestingly, recent studies highlighted that CXCL2 and CXCL1 together lead to the activation of NLR family pyrin domain containing 3 (NLRP3) inflammasome, a multiprotein complex that mediates innate immune responses to different stimuli (Zhou *et al.*, 2011). The activation is mediated by the interaction of the two chemokines with CXCR2 and uncovering this mechanism represented an important step towards therapeutics strategies to control inflammation, since dysregulation of inflammasomes activity can lead to chronic and deleterious inflammation (Boro and Balaji, 2017). Importantly, CXCL2 expression is also regulated by NF-κB, similarly to the control exerted on CXCL1, and CXCL2 is also upregulated in nfκb1$^{-/-}$ mice (Wilson *et al.*, 2015b). Lastly, CXCL2 is part of the group of inflammatory molecules generating the SASP and its expression increases with age.

3.4.7. CCL20

CCL20 is a CC chemokine that was originally found to be expressed only in lung and liver, working as a chemotactic for lymphocytes (Hieshima *et al.*, 1997). However subsequent studies found high levels of CCL20 mRNA in other inflamed tissues, such as tonsil and appendix (Harant, Eldershaw and Lindley, 2001). CCL20 can be expressed in response to different pro – inflammatory stimuli, including TNFα (Dieu-Nosjean *et al.*, 2000) and LPS (Tanaka *et al.*, 1999). Later studies linked CCL20 expression with TNFα – dependent activation of NF-κB, showing that both p65 and p50 were found at a site in the CCL20 promoter, in response to TNFα stimulation (Harant, Eldershaw and Lindley, 2001). Inhibition of CCL20 expression seems to be achieved through the repression of p50 homodimers, very similarly to other NF-κB targets. In support of this, Burke et al. showed p50 occupancy at the CCL20 promoter under basal conditions, inhibiting its expression; upon stimulation with IL1β, occupancy of p65 increased at the same site, while p50 was displaced. As confirmation of p50 repressive role on CCL20 gene, overexpression of p50 dramatically reduced the expression of CCL20, by blocking the recruitment of p65 to the promoter (Burke *et al.*, 2015). In the same study, they suggested that high levels of CCL20 correlate with pathologies associated with obesity and and/or diabetes.

3.4.8. TNFAIP3

As previously mentioned, TNFAIP3, or A20, is one of the most prominent and best studied deubiquitinating enzymes involved in the negative control of NF-κB activity (Shembade and Harhaj, 2012). By targeting an upstream regulator of NF-κB for proteasomal degradation, A20 prevents the downstream activation of NF-κB, limiting its activity (Kelliher *et al.*, 1998). Interestingly, A20 expression itself is regulated by NF-κB; in fact, two κB sites are found within TNFAIP3 promoter and it was postulated that NF-κB was able to bind to them in response to TNF, thus inducing the expression of A20, because of its role in the negative feedback of NF-κB activity (Krikoss, Lahertysg and Dixitlgt, 1992). Some later results supported this, by showing that A20 was co-regulated by NF-κB and p38 in response to LPS (Lai *et al.*, 2013). Mutations or knockout of TNFAIP3 lead to hypersensitivity to LPS and dysregulation of immune cells activity (Lee *et al.*, 2000).

3.4.9. NFKBIZ

NFKBIZ, or IκBζ, is part of the atypical IκB proteins, together with Bcl3 and IκBη; this class is particularly important for their emerging role as pleiotropic NF-κB cofactors, rather than only inhibitory proteins (Kamata, Tsuchiya and Asano, 2010). NFKBIZ in particular can exert a dual function on gene expression, depending on the target genes. As example of its pro – inflammatory action, IκBζ is very rapidly induced upon LPS and IL-1 stimulation, and it then associates with p50 homodimers found at IL6 gene promoter and the complex induces the expression of IL6 (Yamamoto *et al.*, 2003). However, IκBζ is indispensable for the expression of the potent anti – inflammatory cytokine IL10 in response to LPS, via recruitment of p50 subunit to the gene promoter and subsequent H3 histone modification, which leads to the expression of IL10 (Hörber *et al.*, 2016).

3.4.10. Validation of the RNA sequencing results

qRT-PCR was carried out to validate the five gene targets and using RNA left from sequencing library preparations; not all the samples had RNA left, so we restricted to n=2 for NfκB1$^{fl/fl}$ cells and n=3 for NfκB1$^{Albcre/fl}$ cells. The results are presented in figure 36. Regardless of considerable variability between the different samples of the same genotype, the trend observed from the qPCR results resembled that found in the sequencing. Wt cells showed the expected pattern, with increased fold changes at 2h LPS, which then went back to the baseline at 24h. Expression of the same genes in p50$^{-/-}$ cells on the other hand did not go back to baseline levels at 24h LPS, probably indicating that nfκb1 provides a negative regulation of those genes in the context of inflammation resolution.

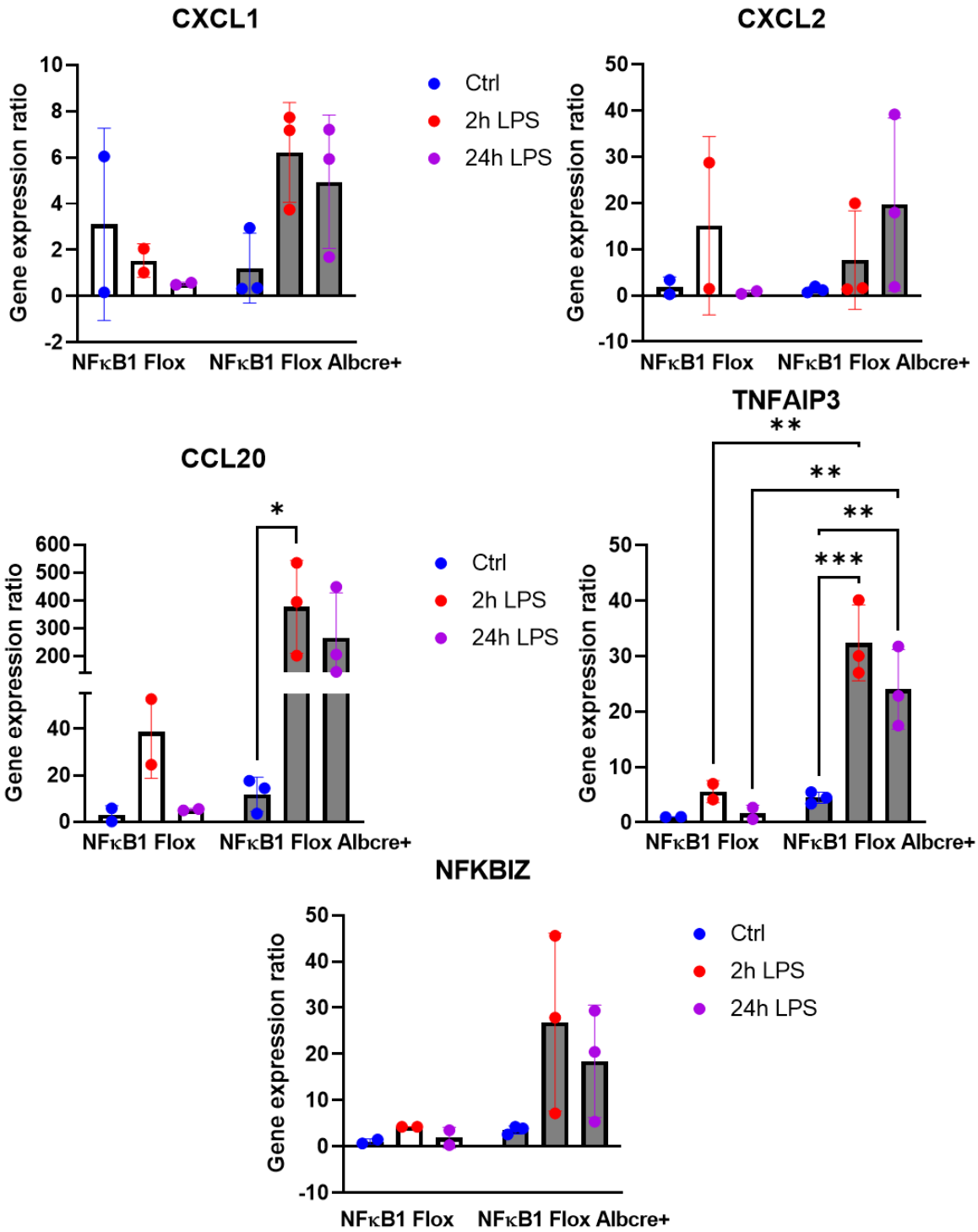

Figure 36.qPCR validation of the target genes from the RNA sequencing. These results were generated by using n = 2 for wt cells and n = 3 for $p50^{-/-}$ cells. As seen previously, wt cells presented the expected pattern, with genes being upregulated at 2h LPS and back to baseline at 24h LPS. Ko cells on the other hand showed the same increased fold change at 2h LPS, but not the decrease at 24h LPS, possibly indicating that by lacking p50, cells are missing a negative control on gene expression.

3.5. The effect of *nfkb1* on gene regulation is not gender dependent

Next, we wanted to ask whether this effect was gender dependent, as it has been demonstrated that females tend to be more protected from inflammation because of their high levels of oestrogen (Sabeh *et al.*, 2021).

To do this, we performed the experiment summarised in figure 37. Females from both NfκB1$^{fl/fl}$ and NfκB1$^{Albcre/fl}$ colonies were taken (n=5), their livers perfused, and viable hepatocytes obtained as previously described. After three hours rest, the cells were treated with LPS 100 ng/ml at two different time points. The cells were then harvested for RNA isolation.

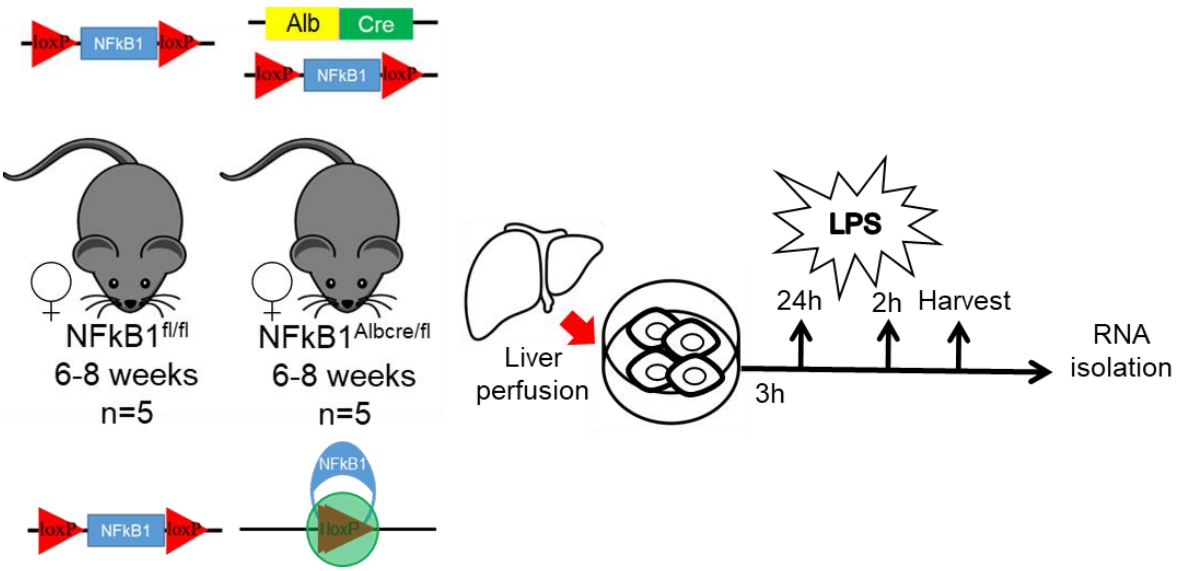

Figure 37. Graphic representation of the experiment using NfκB1$^{fl/fl}$ and NfκB1$^{Albcre/fl}$ female mice. Mice were taken when they were 6-8 weeks old, and their livers were perfused to isolate hepatocytes. After three hours rest, the cells were either treated or not with LPS at two different times points (2h and 24h). The cells were then harvested all at the same time and RNA was isolated to carry on the analysis.

The results are presented in figure 38. With the exception of Cxcl1 and Cxcl2, the other selected genes presented the same pattern, observed using cells from male mice. Nfκb1$^{fl/fl}$ cells showed increased fold change at 2h treatment and the 24h LPS coincided with the expression of the same genes being downregulated to normal baseline levels. However, Nfκb1$^{Albcre/fl}$ cells did not result in the same decrease observed at 24h treatment, as their values were still high and comparable to the 2h LPS time point. Cxcl1 represented an exception, as a decrease was observed at 24h LPS in KO but not in WT; Cxcl2 showed similar trends in both WT and KO cells, with decreasing levels of expression at 24h LPS.

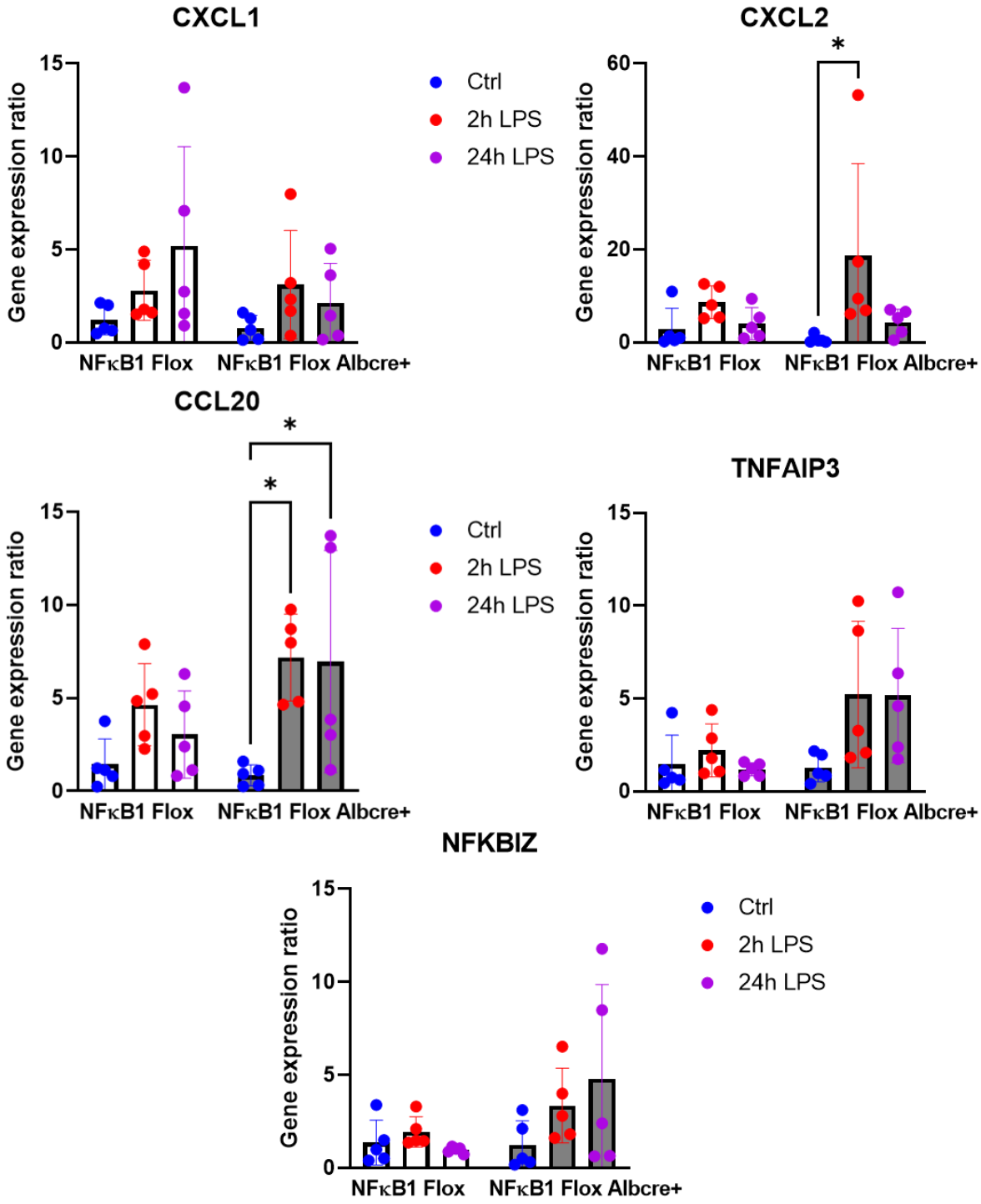

Figure 38. qPCR results for inflammatory genes in hepatocytes from females. Cxcl1 is the only gene among the five found from the sequencing that behaved differently compared to the others, which showed the same pattern observed in male hepatocytes. Statistical significance was calculated with two ways ANOVA.

3.6. Hepatocytes from *nfκb1*$^{-/-}$ mice show possible adaptation to the lack of p50

Lastly, we wanted to further investigate if the effect of nfkb1 on inflammation would have changed if the cells were isolated from p50 total knock out mice (Nfκb1$^{-/-}$). Similarly to what was previously done, 6-8 weeks old wt (C57BL/6J) and ko (Nfκb1$^{-/-}$) mouse livers were perfused, and isolated cells isolated were rested for 3h, prior to treatment with LPS. The experimental design is shown in figure 39.

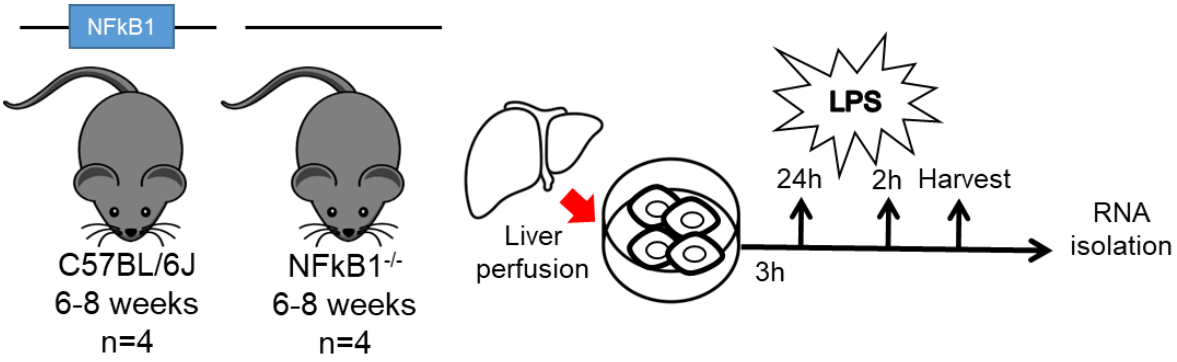

Figure 39. Graphic representation of the experiment in wt and total p50 knock out mice. N=4 mice were taken for each genotype and their liver perfused to obtained viable hepatocytes, which were then cultured and treated with LPS accordingly. RNA was isolated to perform qPCR.

Interestingly, the results showed a different pattern to the one observed in Nfκb1$^{Albcre/fl}$ cells. In particular, ko cells behaved more similarly to wt cells, as the expression of target genes at 24h LPS decreased to baseline levels. However, for CCL20 only Nfκb1$^{-/-}$ cells presented a greater increase of gene expression at 2h LPS, when compared to the wt (figure 40).

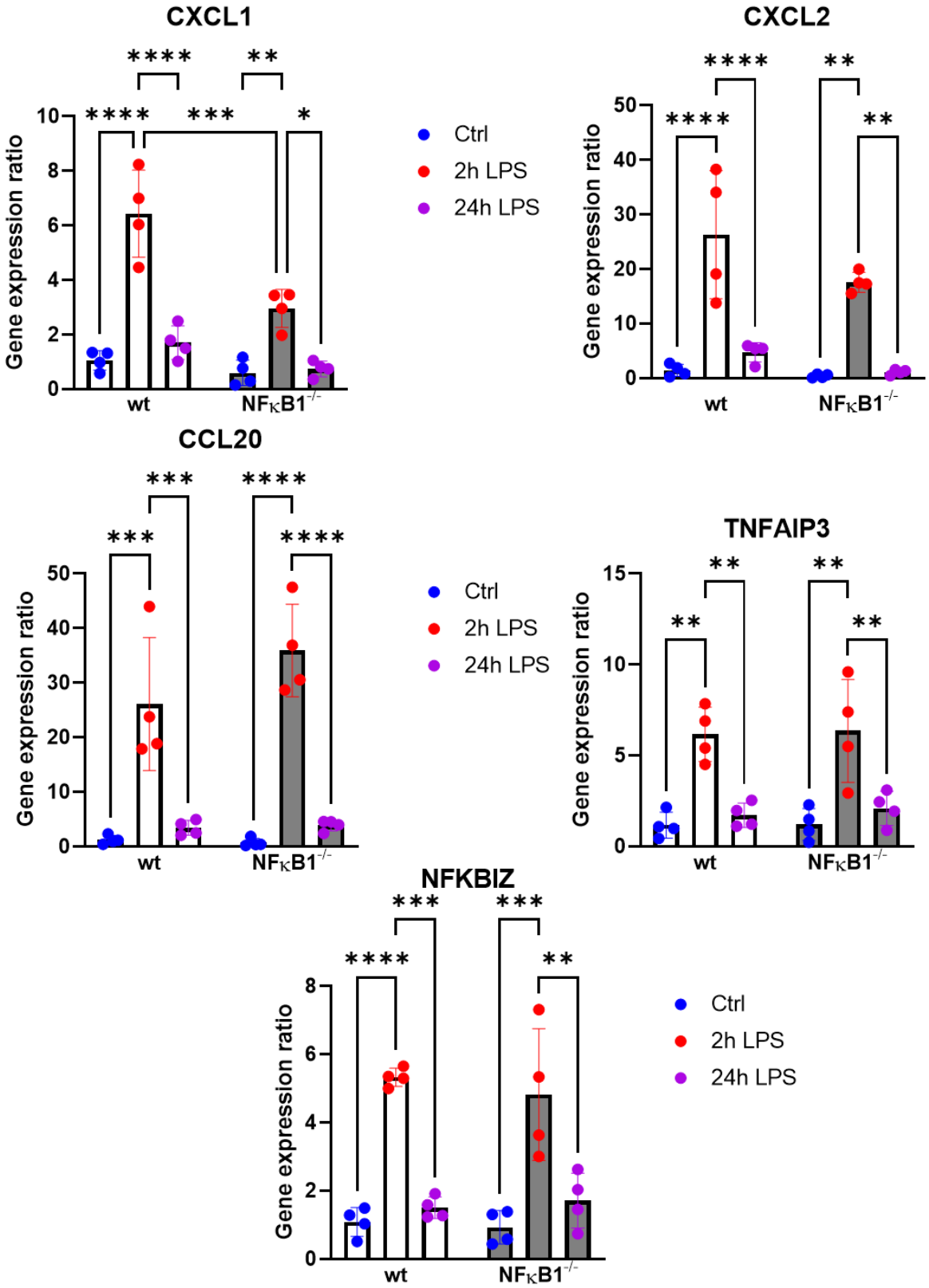

Figure 40. qPCR results for inflammatory genes in hepatocytes from wt and nfkb1$^{-/-}$ hepatocytes. N=4 for each genotype were used for the experiment. Ko cells presented a more similar pattern to wt cells; however, ko cells seemed to be more inflamed at 2h LPS when compared to wt. Statistical significance was calculated with two ways ANOVA.

3.7. Discussion

Previous studies in nfκb1$^{-/-}$ mice elucidated the importance of nfκb1 in controlling inflammation and tumour progression. In particular, nfκb1$^{-/-}$ mice were shown to be more prone to inflammation, when compared to wt mice, and to develop a microenvironment in which cancer development occurs. This phenotype is exacerbated during the aging process, as nκfb1$^{-/-}$ age faster and present a more inflamed condition than wt mice matching their age (Bianchi *et al.*, 2021).

The contribution of hepatic p50 in inflammation has not been yet investigated. To address this question, we isolated viable hepatocytes from control mice (Nfκb1$^{fl/fl}$) and p50$^{-/-}$ hepatocytes specific mice (Nfκb1$^{Albcre/fl}$) and we challenged them with LPS 100ng/ml at two different time points, 2h and 24h, in order to mimic an acute inflammatory response. The cells were used to isolate RNA and then it was sent to be sequenced.

Comparison between untreated cells from both genotypes resulted in 1767 genes been differentially expressed (fold change > 2 and adjusted p-value < 0.05) and the majority of them belonged to well-known pathways which involve p50, such as response to inflammatory stimulation and integrin signalling. Intriguingly, other pathways such as p53 signalling, cell cycle and DNA replication were also affected in both directions by the lack of p50, probably suggesting that nκfb1 might be able to play a role in those pathways, which is interesting for further investigations.

We then analysed the differences between untreated and LPS treated cells and the majority of the DEGs when comparing ctrl cells with 2h LPS in both genotypes were cytokines and chemokines, as expected. At 24h LPS those same genes were not found among the DEGs in wt cells, as the inflammatory signalling would be resolved by then and the expression of inflammatory genes repressed. However, when looking at 24h LPS in p50$^{-/-}$, we surprisingly found that some inflammatory genes were still expressed at that time point and moreover that a subset of those genes was present in both Nfκb1$^{fl/fl}$ and Nfκb1$^{Albcre/fl}$ cells at 2h LPS. We focused our attention on five of them (Cxcl1, Cxcl2, Ccl20, Tnfaip3 and Nfkbiz) because of their relevance in inflammation and because their levels of expression were consistent across the pool of samples for each condition and genotype, contrary to other genes from the RNA sequencing data. qPCR validation confirmed that unlikely wt cells, p50$^{-/-}$ hepatocytes were not able to repress the expression of those genes at 24h LPS. These results lead to the conclusion that hepatic p50 might not be necessary to trigger the inflammatory response, but it is

needed to repress the expression of a subset inflammatory genes, in order to limit the process.

The same experiment was repeated in hepatocytes from female mice to understand whether the effect was gender dependent. Very similarly to what was found in male mice, Nfκb1$^{Albcre/fl}$ hepatocytes failed to repress the expression of the five aforementioned genes.

Lastly, we asked if the output would have changed if the hepatocytes were isolated from total p50 knock out (nκfb1$^{-/-}$) mice. Surprisingly, wt and nfκb1$^{-/-}$ behaved similarly, as we did not detect upregulated expression of Cxcl1, Cxcl2, Ccl20, Tnfaip3 and Nfkbiz at 24h LPS, as expected during an acute response.

It is possible that by lacking p50 in their whole body, nfκb1$^{-/-}$ have developed a tolerance or alternative pathways that do not require nfkb1 in order to repress the expression of inflammatory genes at 24h LPS.

It will certainly be interesting to further investigate the contribution of hepatic nfkb1 in inflammation in a more complex setting, as primary hepatocytes represent a good *in vitro* model for preliminary data, but it does not take in consideration the intricated network of interactions that hepatocytes are able to establish with the other cells present in the liver parenchyma, namely hepatic stellate cells (HSCs) and immune cells (ICs).

Chapter 4. Precision Cut Liver Slices model clarifies the contribution of hepatic NFκB1 to inflammation at the organ level *in vitro*

4.1. Introduction

In vitro models like primary cells are considered a good compromise between the cell lines and *in vivo* models. In fact, primary cells like hepatocytes can be freshly isolated from the tissue *ex vivo* and then cultured in a 2D set that allows easy handling and treatments. However, primary cells rapidly change their phenotype because of the new environment, becoming something different from the organ *in vivo*. Also, since primary cells are not naturally immortalised, they can survive in culture only for a limited amount of time. The isolation method can also be a source of stress, as it usually involves enzymes aiming to digest the structure in which the organ is organised, aiming to the release of cells. Thus, the isolation process can result in the death or stress to hepatocytes, making the interpretation of data a challenge.

The data we generated with primary hepatocytes showed that it is possible to treat the cells with LPS at two different time points in order to mimic the natural progress of an inflammatory event. 27 hours (3 hours rest + 24 hours for treatments) is likely to be the longest the cells could be cultured for with our protocol, as proved by decreased expression of albumin and upregulation of inflammatory markers at the last time point. Because of the need to find new models to use to study liver diseases and drug discovery, progress has been made to improve the 2D monolayer of hepatocytes on a bed of collagen (Lauschke *et al.*, 2019). In order to provide more support to the cell growth and a more similar environment to the hepatic tissue, 3D models have been designed to resemble the liver parenchyma. Primary hepatocytes can be cultured as 3D aggregates, or spheroids, that support the maintenance of the hepatocytes phenotype for longer periods of time (Tostões *et al.*, 2012). Also, spheroids allow the co-culture with non-parenchymal liver cell types, namely Kupffer cells, endothelial cells and hepatic stellate cells, which facilitate the survival of the cells for several weeks (Bell *et al.*, 2016). Despite the better cell survival offered by this model, the generation of spheroids can often be challenging, as recent studies showed that the ability to form these structures relies on the quality and the characteristics of the cells, which vary from donor to donor (Lauschke *et al.*, 2019). Further studies tested the possibility to create organoids, 3D structures resembling the tissue of origin which promote the self-renewal and organisation of the cells to mimic the native environment. Although the

great progress achieved, these models have been mostly applied to therapeutic transplantation of hepatocytes in order to cure liver diseases, rather than research and drug discovery, especially for how expensive and time-consuming the process is (Peng, Kraaier and Kluiver, 2021).

A turning point in the development of new *in vitro* models to study the liver was achieved by the design of a bioreactor technology employing Precision Cut Liver Slices (PCLS). The principle is that 250µm – thick liver slices retain the structural organisation of the tissue, allowing the preservation of all the cell – cell interactions important to study an organ as a whole. Moreover, the rocking system on which they are cultured facilitate the efficient oxygenation and exchange of metabolites which increases the lifespan of the slices (Paish *et al.*, 2019).

I decided to use this model to investigate the contribution of hepatic p50 in inflammation, providing me with a system that would allow me to take in consideration the importance of cell – cell crosstalk during the inflammatory process.

4.2. Validation of the model

First, I decided to validate the model in wt animals. Before starting working with PCLS, I needed to take in consideration that the overall structure was different, and that the system was much more complex than a 2D cell culture. Therefore the concentration of LPS may be required at a higher dose; also, 2h could represent a too early time point for this 3D model, as it is more complex than a 2D.

To investigate these two aspects, I carried out an experiment with n = 3 wt mice; the livers were harvested and processed to obtain livers slices. Because of the stress caused by the cutting, the slices were left to rest for 24h, prior commencing any manipulations. The slices were treated at three different time points (2h, 6h and 24h)

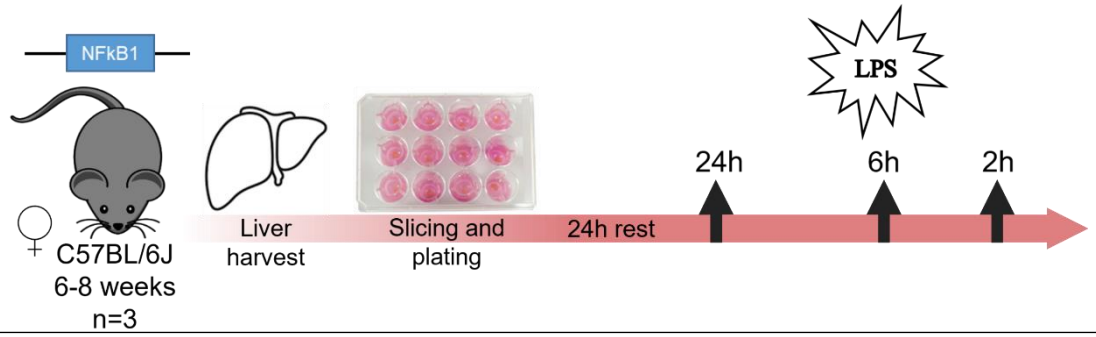

Figure 41. Set up of the experiment for the PCLS model validation. N = 3 wt mice were used and their livers processed to generate the slices. The slices were treated for 2h, 6h and 24h with 1µg/ml of LPS. The media was collected for soluble output and the slices were used to isolate RNA.

with 1µg/ml LPS. Media was collected to investigate soluble outputs while slices were harvested and used for RNA isolation (Figure 41).

The same five inflammatory genes investigated in the previous chapter (Cxcl1, Cxcl2, Ccl20, Tnfaip3 and Nfkbiz) were used as markers to assess the efficient trigger induced by LPS and to check the progress of the acute inflammatory event. The results are presented in figure 42. The pattern of expression of the genes analysed mirrored what was expected from an acute response. Inflammatory genes increased their expression at 2h LPS, with a significant upregulation (except for Cxcl2). At 6h LPS the expression of the genes was still high but decreased compared to the previous point. Lastly, 24h

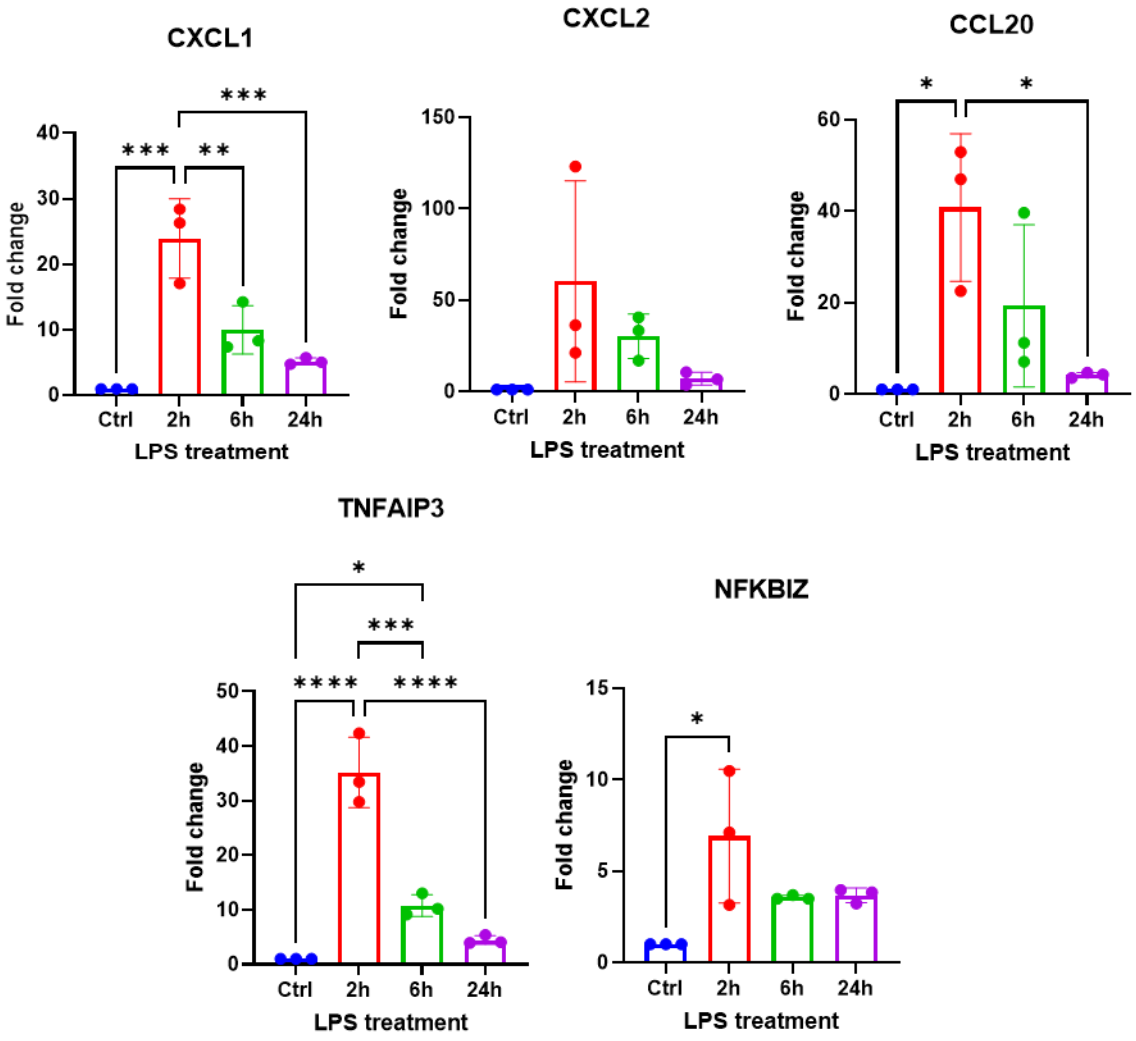

Figure 42. qPCR results for inflammatory genes in the time course (48h total). The treatments started 24h after the slicing process to allow the slices to recover. The slices were harvested at 48h, after been treated for 2h, 6h and 24h with 1µg/ml LPS or left untreated (Ctrl). The trend observed recalled what expected during the progress of acute inflammation. Expression of genes involved in the inflammatory processes is the highest at 2h LPS, with an evident reduction at 6h; at 24h LPS, the gene expression went back to levels comparable to the untreated cells, as the inflammatory event came to its resolution. Statistical significance was calculated with an ordinary one-way ANOVA with Tukey's post hoc test.

LPS represented the resolution step, with inflammatory genes levels reverting to a more baseline set.

Soluble outputs were also investigated to make sure that the slices did not die from the treatments and to check the secreted levels of pro – inflammatory cytokines, such as CXCL1. Lactate DeHydrogenase (LDH) assay was run to assess for toxicity. As evident in figure 43A, LDH levels were relatively high at the 24h timepoint, as expected after the slicing process. However as the slices were adapting to the new environment, levels decreased at 42h, with higher levels for 24h and 6h LPS samples as some cells were probably damaged by the LPS treatment. At the final timepoint (48h), the situation remained unchanged from the previous checkpoint, with consistent high levels of LDH for both 6h and 24h LPS. Soluble outputs for CXCL1 helped clarifying the inflammatory status of the slices based on the amount secreted in the media over time. The results in figure 43B showed that high levels were found at 24h, explainable by the stress of the slicing process that might have triggered an inflammatory response. CXCL1 levels then decreased at 42h, with the exception of 2h LPS, which registered the highest

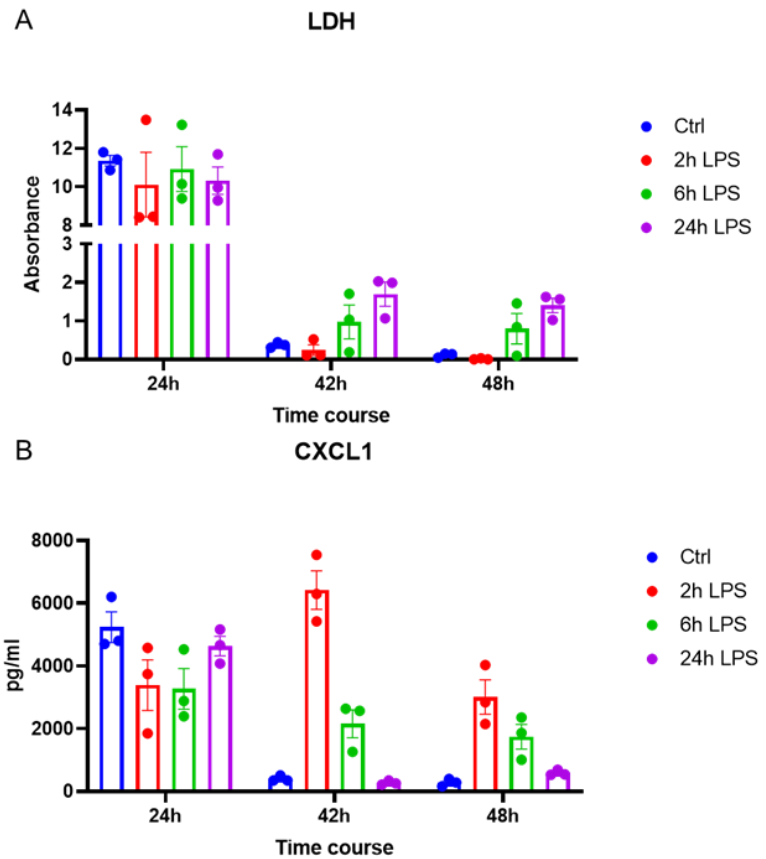

Figure 43. Soluble outputs from the media of the slices experiment. A, LDH was used to provide insights regarding the vitality of the slices. The lower value of LDH absorbance, the better, as LDH presence in the media indicates cells being lysed and releasing their content. B, CXCL1 output was used to assess the progression of the inflammatory event.

values in the whole time – course. Finally, at 48h levels were more similar to the baseline situation, but 2h and 6h LPS were still quite higher compared to both control and 24h LPS.

The results from this experiment allowed me to confirm 2h and 24h LPS as optimal timepoints to recreate a good model of acute inflammation in slices. Also, the concentration of LPS used was efficient in triggering a response in the slices, stimulating the expression of pro – inflammatory factors.

4.3. Contribution of other cell types minimizes the impact of *nfκb1*$^{-/-}$ hepatocytes in limiting inflammation

Following the validation of the model, I wanted to investigate the contribution of hepatic nfkb1 to an acute inflammation in the PCLS model.

Nfκb1$^{flox/flox}$ and Nfκb1$^{flox/flox}$ AlbCre+ livers were harvested and processed into slices. 24h after the slicing process the slices were treated for 2h and 24h with 1µg/ml LPS or left untreated. Media and slices were harvested for further analyses (Figure 44).

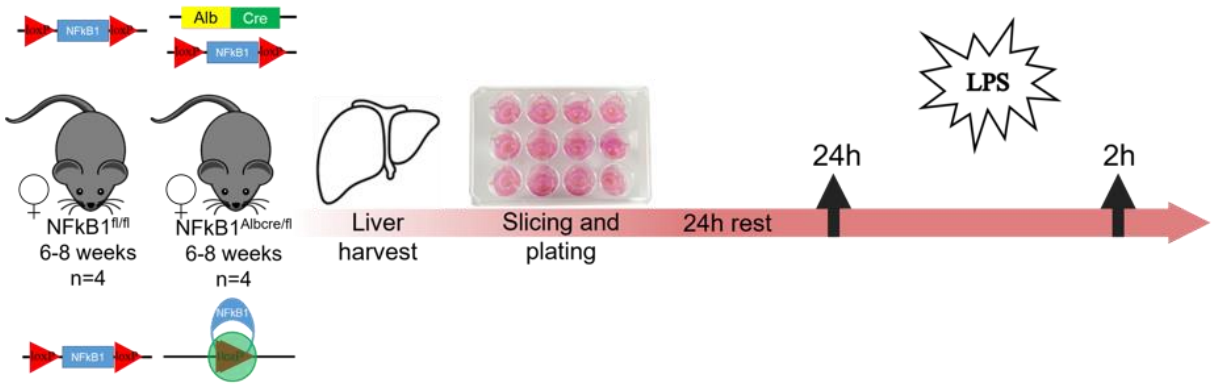

Figure 44. Nfκb1$^{flox/flox}$ and Nfκb1$^{flox/flox}$ AlbCre+ mice (n=4 for each genotype) were used and their livers harvested to be sliced. 24h after the slicing process the slices were either treated with 1µg/ml LPS for 24h and 2h or left untreated (ctrl). The slices were all harvested after 48h of culture and used for RNA and proteins extraction and immunohistochemistry.

The RNA was initially used to confirm the genotype of the mice by looking at the presence of p50 by PCR (Figure 45). Nfκb1$^{flox/flox}$ AlbCre+ liver slices displayed lower expression of p50 when compared to the control livers from NfκB1$^{fl/fl}$ mice, as expected. However p50 was still detectable in Nfκb1$^{flox/flox}$ AlbCre+ because of the contribution of other cell types present in the slices, as previously mentioned.

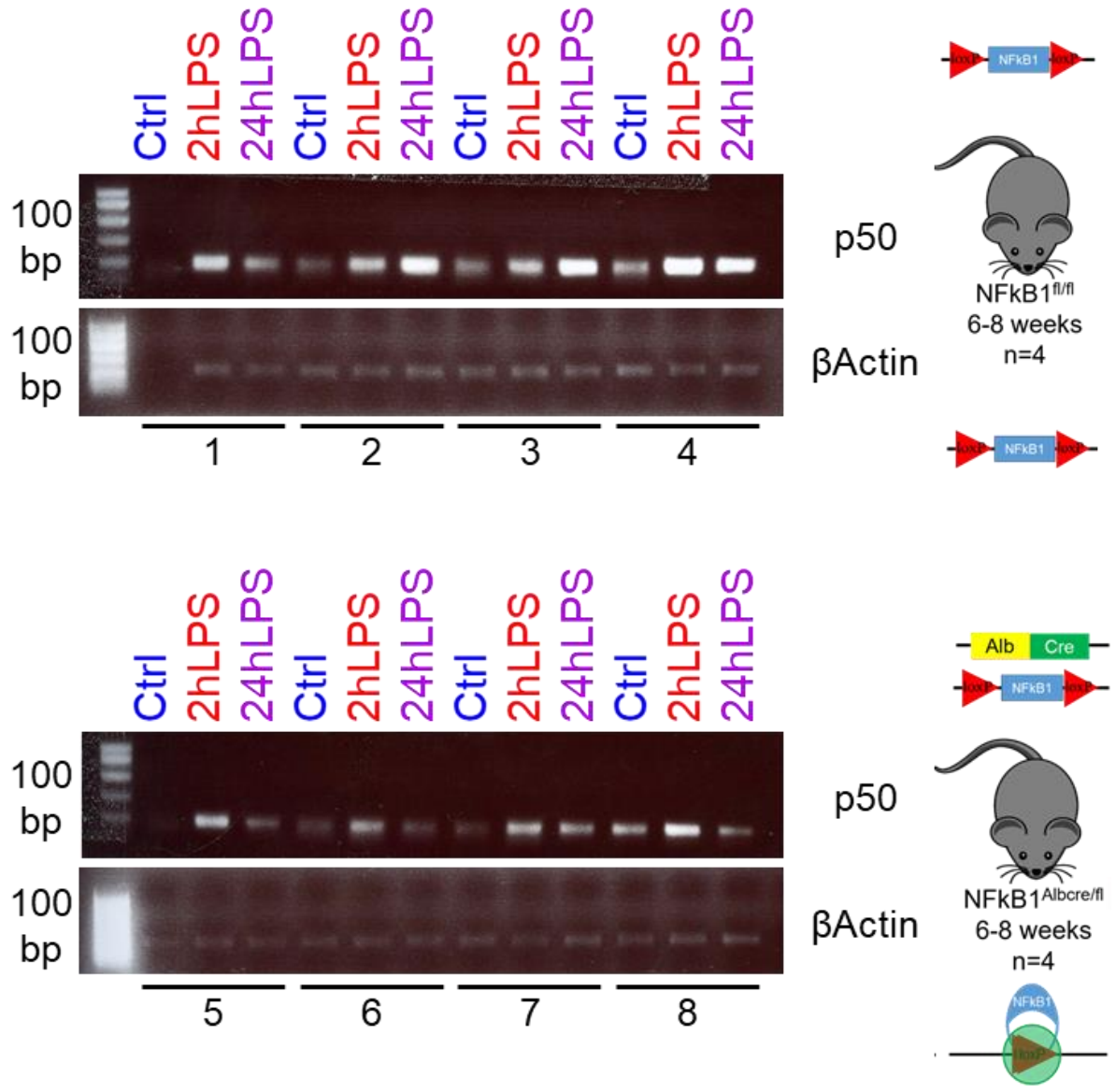

Figure 45. Nfκb1$^{flox/flox}$ and Nfκb1$^{flox/flox}$ AlbCre+ samples were assessed by PCR for the presence of p50 (expected size of the amplicon 145 bp) at the RNA level. A 100 bp ladder was used for comparison of the sizes. βActin was used as a control for the reaction. Each number at the bottom of the gels represents a different mouse liver, from which the slices were obtained and treated at the time points indicated at the top of the gels. p50 was found to be less expressed in Nfκb1$^{flox/flox}$ AlbCre+ when compared to the control, as expected. The target was still detectable in the knockout as the cre enzyme was expressed in hepatocytes only, therefore the other cells present in the liver would still express p50.

The presence of p50 was also investigated at the protein level in the same samples (Figure 46). Very similarly to what observed at the RNA level, a difference in p50 expression between the two genotypes was detected, under different conditions. However it must be noticed that there was some variability in the samples, and in

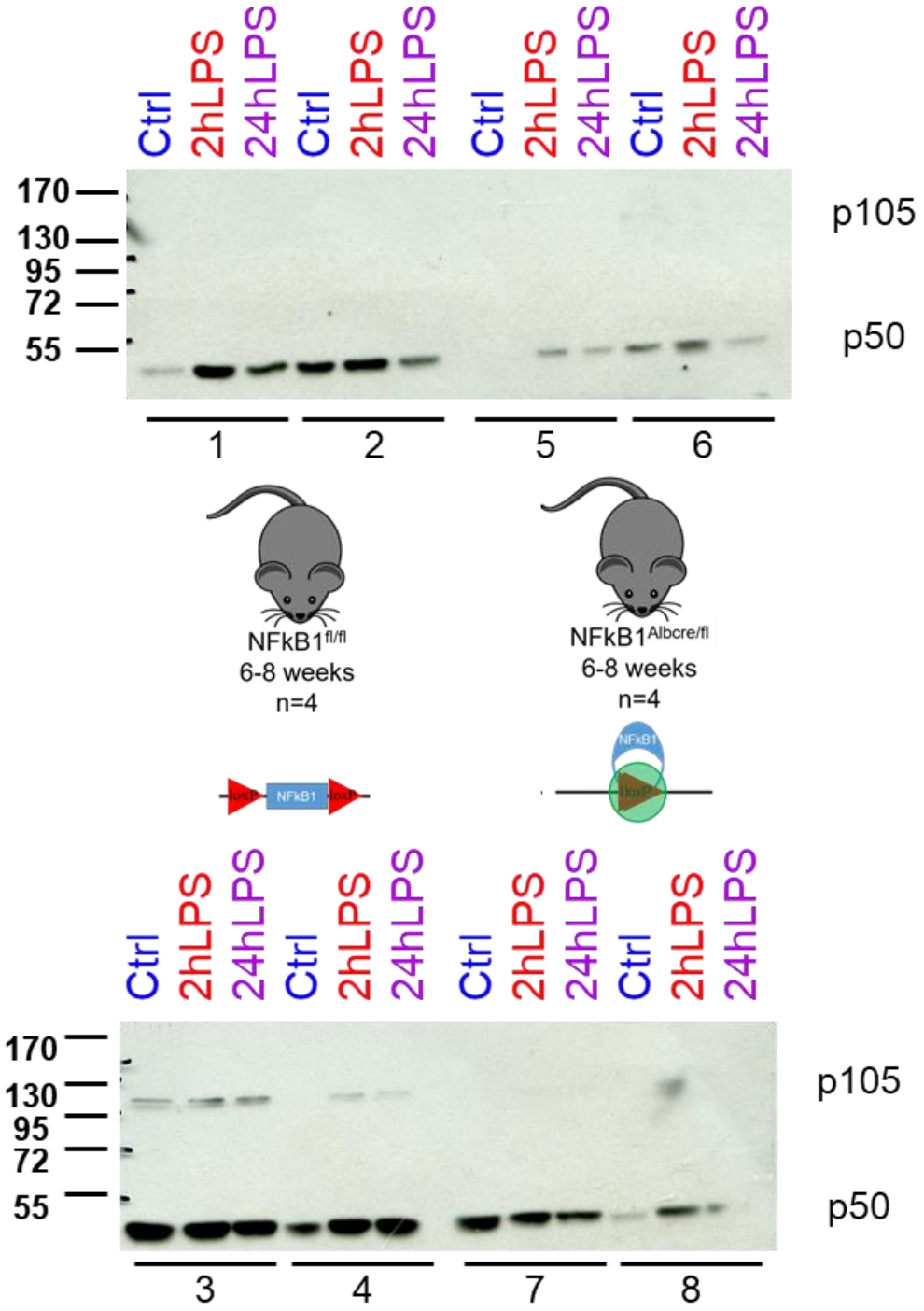

Figure 46. Nfκb1$^{flox/flox}$ and Nfκb1$^{flox/flox}$ AlbCre+ samples were assessed by Western Blot for the presence of p50 at the protein level. p50 was found to be less expressed in NfκB1$^{Albcre/fl}$ when compared to the control, as expected. The protein was still detectable in the knockout as the cre enzyme was expressed in hepatocytes only, therefore the other cells present in the liver would still express p50. Loading control on the gel did not work, despite trying different house keeping genes (data not shown).

particular all conditions from sample 7 showed levels of p50 comparable with a control mouse, even if the RNA levels showed less amplification for p50, when compared to control mice.

After confirming the genotype of the mice, the expression of previously investigated inflammatory genes was assessed by qPCR and ELISA (Figure 47). Nfκb1$^{flox/flox}$ slices displayed a similar trend to the one observed for control mice in previous experiments in both primary cells and PCLS. 2h LPS represented the time point with the highest expression for all the inflammatory genes analysed, while at 24h LPS the expression was dampened and went back to baseline levels, comparable to the untreated slices. Nfκb1$^{flox/flox}$ AlbCre+ slices also showed the same trend, contrary to the results obtained in primary cells. In fact, 2h LPS was still the time point with the greatest expression of the inflammatory genes, but in this model the expression went back to levels comparable to the untreated slices at 24h LPS, leading to the hypothesis that compensatory mechanisms provided by other cell types expressing p50 might be able to resolve the inflammatory event and repress the expression of inflammatory genes. The only exception to the trend was represented by CCL2, for which higher levels resulted at 24h LPS in Nfκb1$^{flox/flox}$ AlbCre+; however the results were very variable between the different samples, and it did not reach statistical significance.

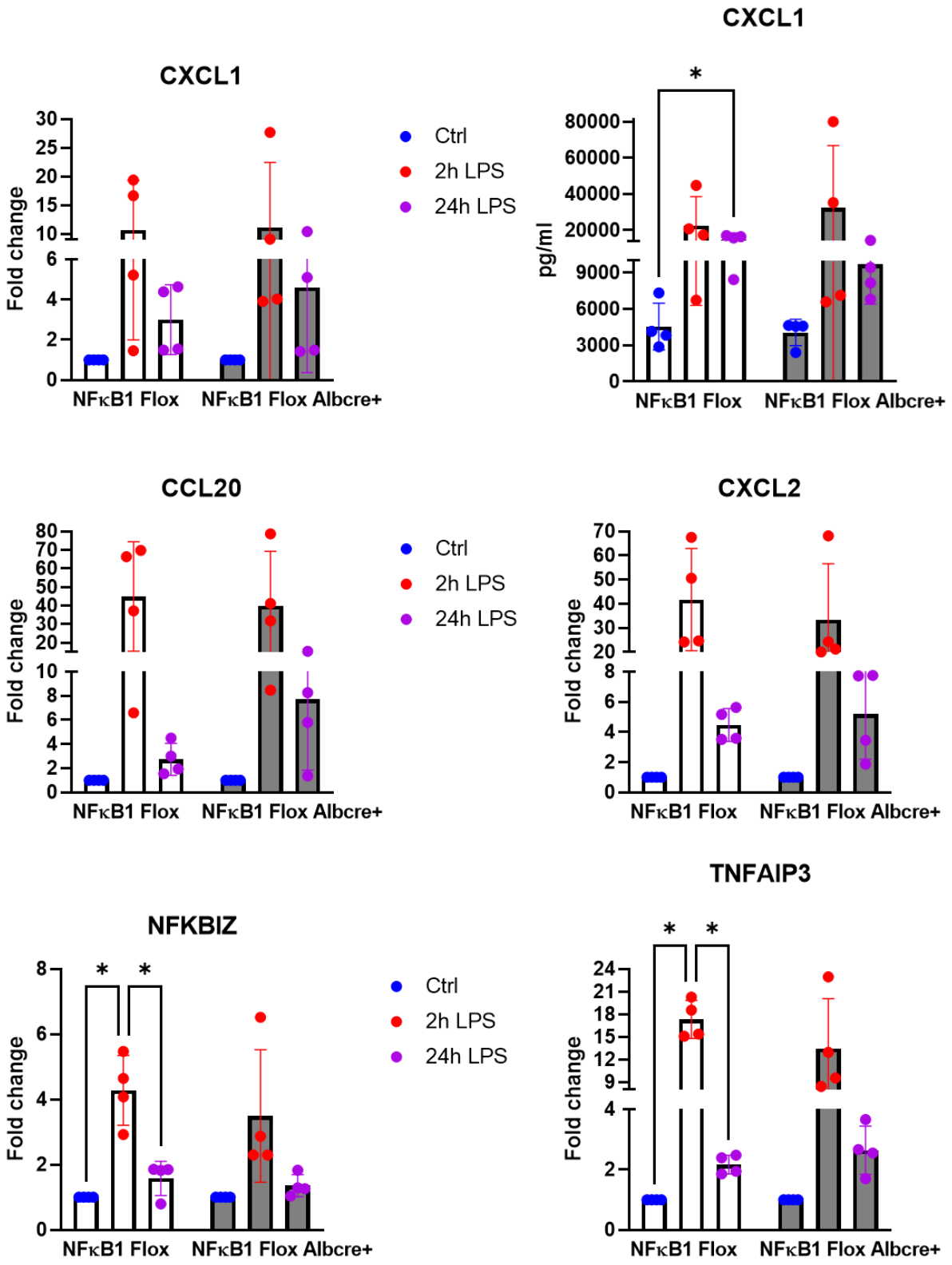

Figure 47. qPCR and ELISA results for previously investigated inflammatory genes. In this model, Nfκb1$^{flox/flox}$ and Nfκb1$^{flox/flox}$ AlbCre+ samples behaved similarly, presenting an increased expression at 2h LPS, which then decreased to baseline levels at 24h LPS. CXCL1 ELISA confirmed the results found at the RNA level. Statistical significance was calculated with an ordinary two-way ANOVA with Tukey's post hoc test.

I next wanted to investigate if they were any differences in the tissue architecture when comparing the two genotypes. Analyses of Haematoxylin & Eosin (H&E) displayed tissue damage after 2h LPS in both genotypes. The damage was consistent at 24h LPS in Nfκb1$^{flox/flox}$ AlbCre+ samples, but not in Nfκb1$^{flox/flox}$ (Figure 48).

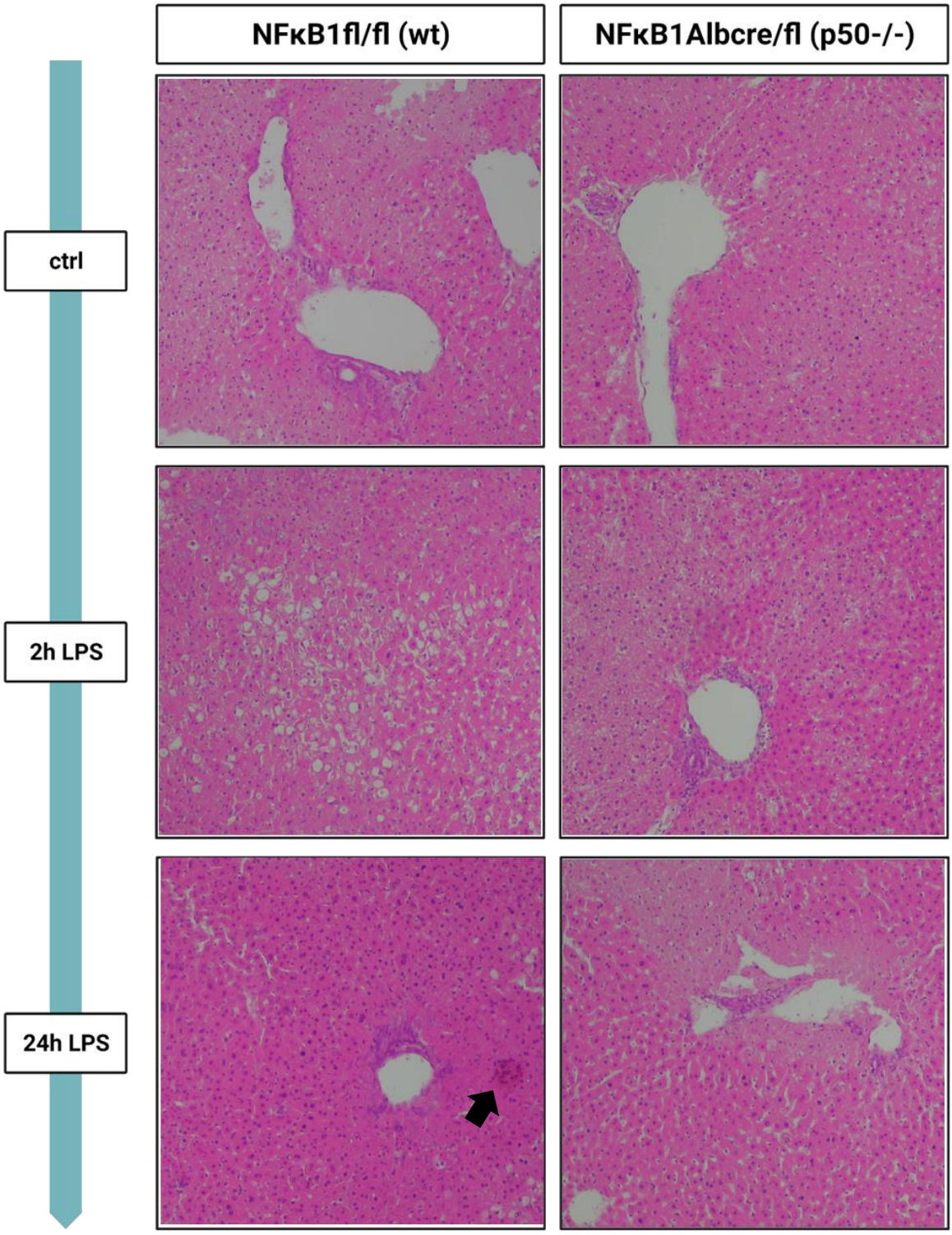

Figure 48. H&E slides for both genotypes. Nfκb1$^{flox/flox}$ and Nfκb1$^{flox/flox}$ AlbCre+ slices presented a certain degree of damage at 2h LPS, as expected. However, at 24h LPS there were some signs of residual inflammation in NfκB1$^{fl/fl}$ samples (arrow) but no damage was identified. On the other hand, NfκB1$^{Albcre/fl}$ showed tissue damage at 24h LPS, similarly to the degree observed at 2h LPS.

I then asked whether there was a difference in immune cell numbers in the tissue. The slices were stained for CD45R as marker of B cells. A greater number of CD45R +

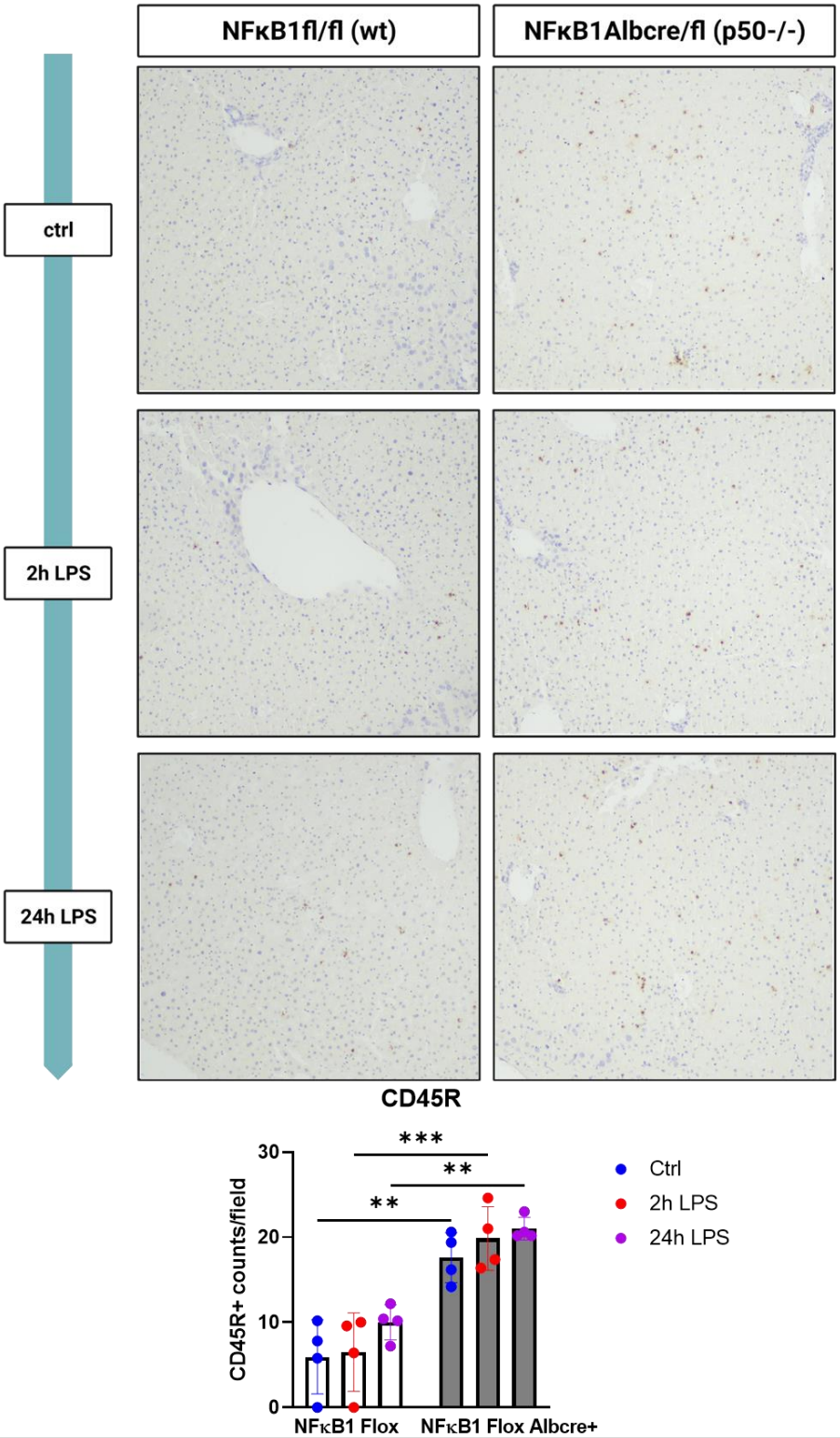

Figure 49. Immunohistochemistry for CD45R in Nfκb1$^{flox/flox}$ and Nfκb1$^{flox/flox}$ AlbCre+ slices. No significant differences were found between different conditions, but significant differences in positive cells numbers when found when comparing the same condition in the two genotypes. Statistical significance was calculated with an ordinary two-way ANOVA with Tukey's post hoc test.

cells was found in Nfκb1$^{flox/flox}$ AlbCre+ slides compared to the control samples, based on a specific condition (figure 49).

4.4. Time – specific knockout of nfkb1 does not alter the inflammatory response

I wondered whether the compensatory mechanisms hypothesised for Nfκb1$^{flox/flox}$ AlbCre+ slices could be justified by the adaptation to nfkb1 absence in hepatocytes. To test this hypothesis, I decided to employ time specific deletion of p50 from hepatocytes mediated by Adeno – Associated virus (AAV). Nfκb1$^{flox/flox}$ mice were injected with either AAV8 – TBG – Cre (AAV cre), to generate a hepatocyte specific knockout, or AAV8 – TBG – Null (AAV empty), as control. 10 days after injection, the livers were harvested to be processed into slices. 24h after the slicing process, the slices were either treated with 1µg/ml LPS for 2h and 24h or left untreated. Media and slices were harvested for further analyses (Figure 50).

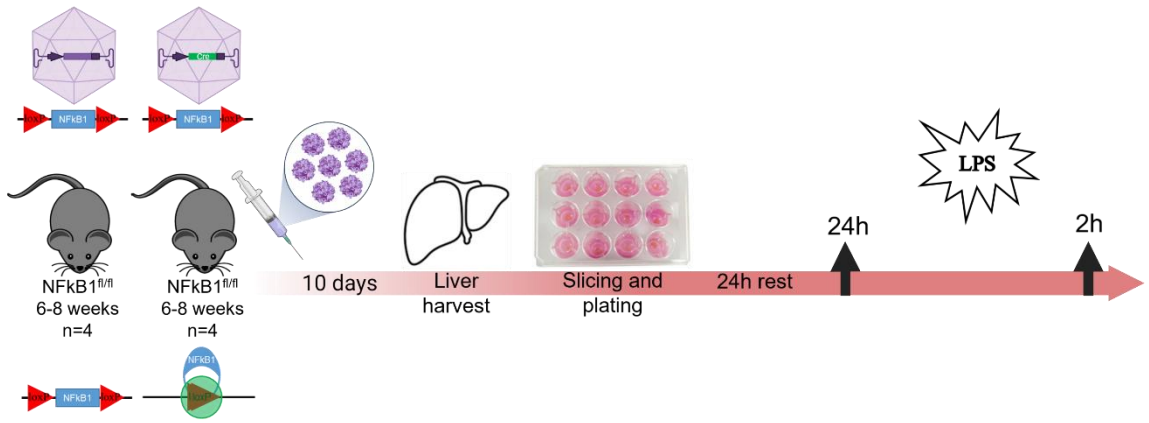

Figure 50. Experimental design for time – specific knockout of nfkb1 in hepatocytes driven by the infection with AAV8 – TBG – Cre. AAV8 – TBG – Null was used as a control. NfκB1$^{fl/fl}$ were injected with 1×10^{11} viral genomes (n=4 for each virus). 10 days post injection the livers were harvested and processed to slices. 24h after slicing, the slices were either treated with LPS for 2h and 24h or left untreated.

The efficiency of the AAV – driven p50 knockout was assessed at both RNA and proteins levels. Regarding the first, lower p50 expression resulted from the injection of AAV – TBG – Cre , but not as evident as in the Nfκb1$^{flox/flox}$ AlbCre+ model. In particular, both samples 15 and 16 exhibited comparable levels to the AAV – TBG – Null, especially after LPS stimulation (Figure 51).

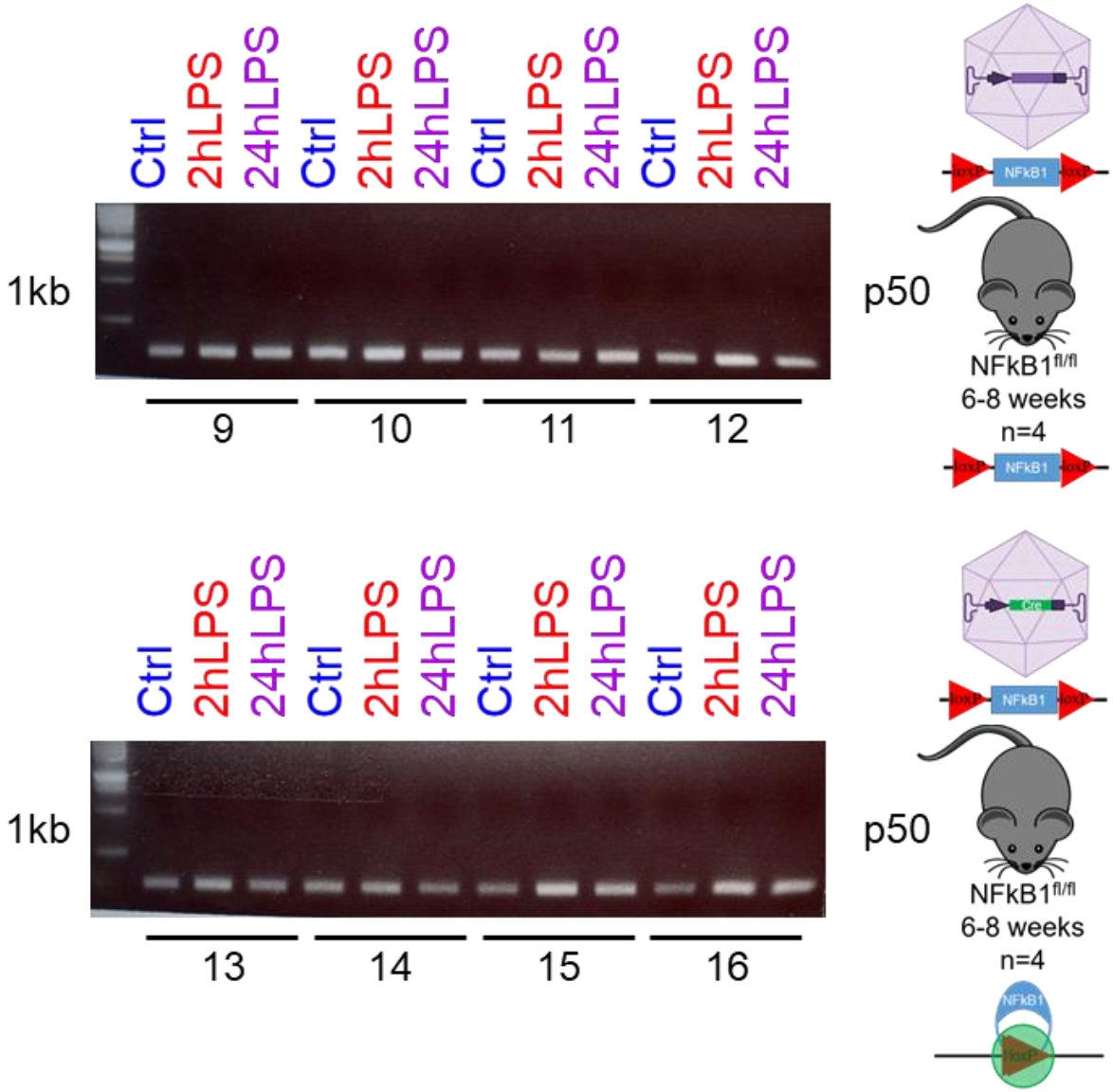

Figure 51. RNA expression levels of p50 in the two AAVs samples. The expected size for p50 amplicon was 145 bp. Each number at the bottom of the gels represents a mouse liver from which the slices were processed and treated as indicated by the time points above the gels. Overall, there was a difference in p50 expression in samples injected with AAV empty (top) and AVV cre (bottom), but not as well defined as in the Nfκb1$^{flox/flox}$ AlbCre+ model.

Similar results were found at the protein levels when checked for p50 expression via Western Blot (Figure 52). Some AAV cre samples displayed decreased p50 levels under both normal and unstimulated conditions (samples 13 and 14); however others (15 and 16) varied depending on the samples, as different levels of p50 were still detectable. No effect on p50 expression resulted from the use of AAV empty, as expected.

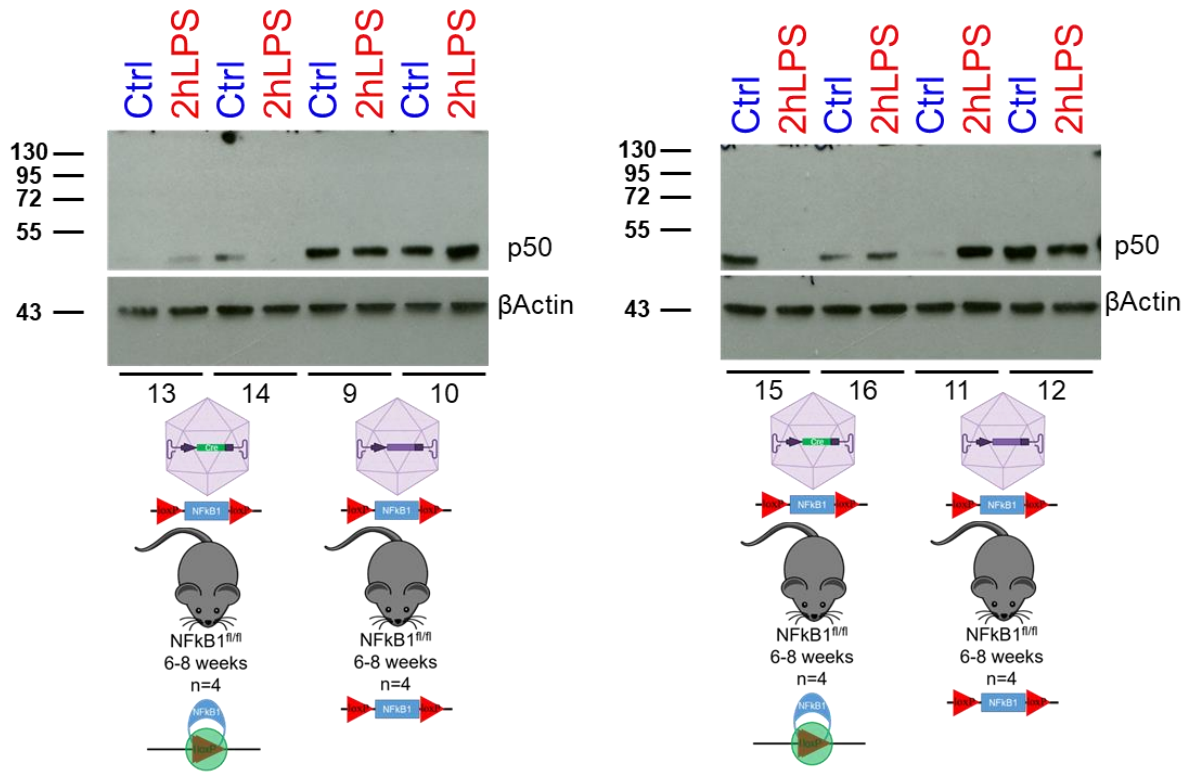

Figure 52. Protein expression of p50 assessed by Western blot. βActin was used as a loading control. The efficiency of the AAV – driven knockout varied from sample to sample, as the expression was reduced in half of the samples only, while the others showed p50 expression comparable to the control AAV.

Expression of inflammatory genes previously studied was assessed by qPCR and ELISA (Figure 53). Similarly to what I found in the previous PCLS experiment, no significant differences were found between the two AAV samples. In fact, both AAV empty and AAV cre showed a significant increase of pro – inflammatory genes at 2h LPS, with the only exception of CXCL1 ELISA results. The expression of the same genes significantly decreased at the 24h LPS, when compared to the 2h LPS treatment.

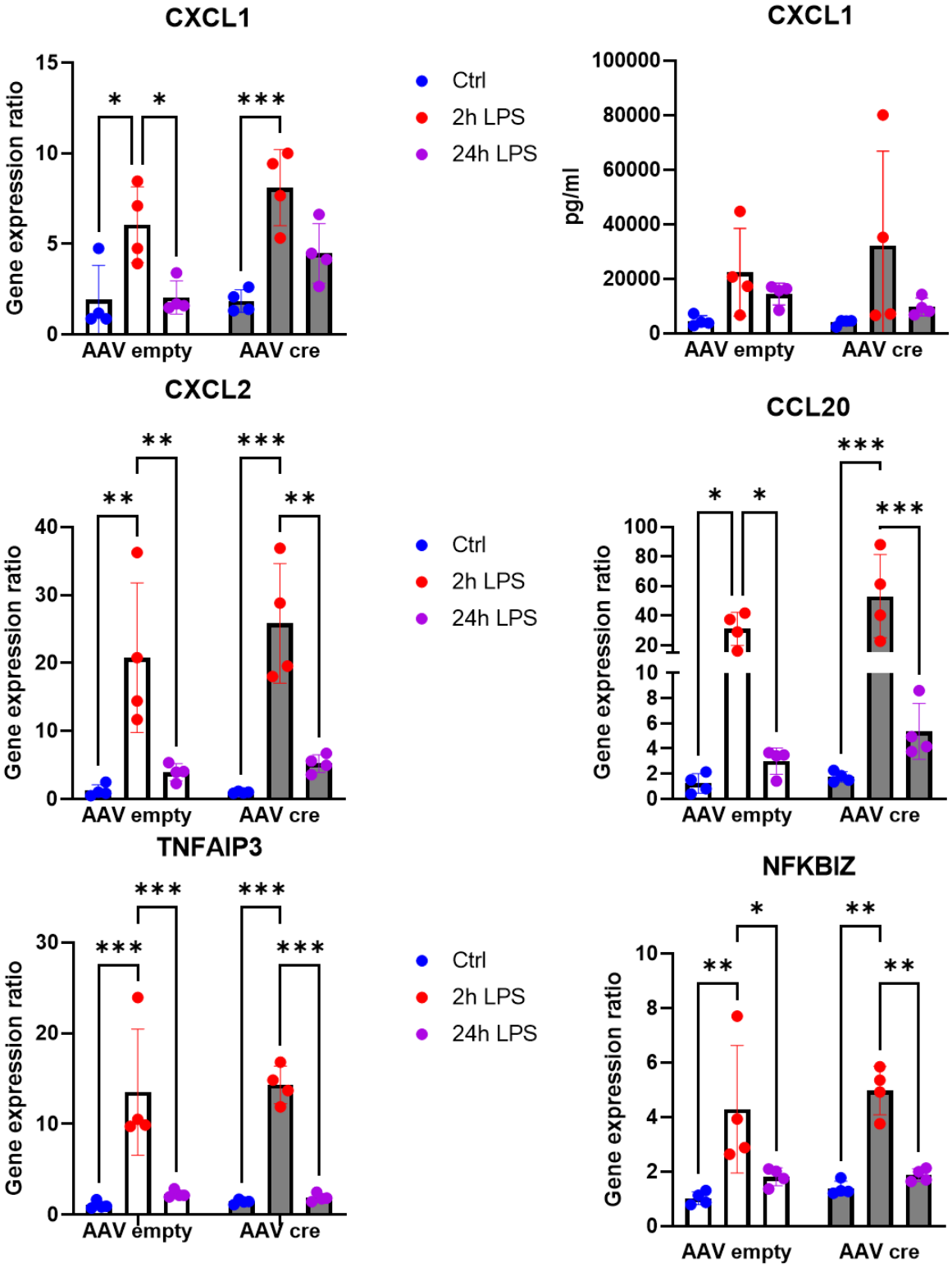

Figure 53. qPCR and ELISA results for pro – inflammatory genes of interest (n=4). No significant differences were found when comparing the two AVVs, however the increase at 2h LPS and the decreased at 24h LPS were found statistically significant within the same AAV. As seen in the previous PCLS, the inflammation event was limited even when p50 was deleted from hepatocytes. Statistical significance was calculated with an ordinary two-way ANOVA with Tukey's post hoc test.

Lastly, the slices were characterised from a macroscopic point of view, by analysis of H&E and CD45R IHC. Exception made for the control sample in the AAV cre, the overall tissue of the slices seemed damaged at all the time points in the experiment. This could be possibly justified by the slicing process that could sometimes damage the tissue (Figure 54).

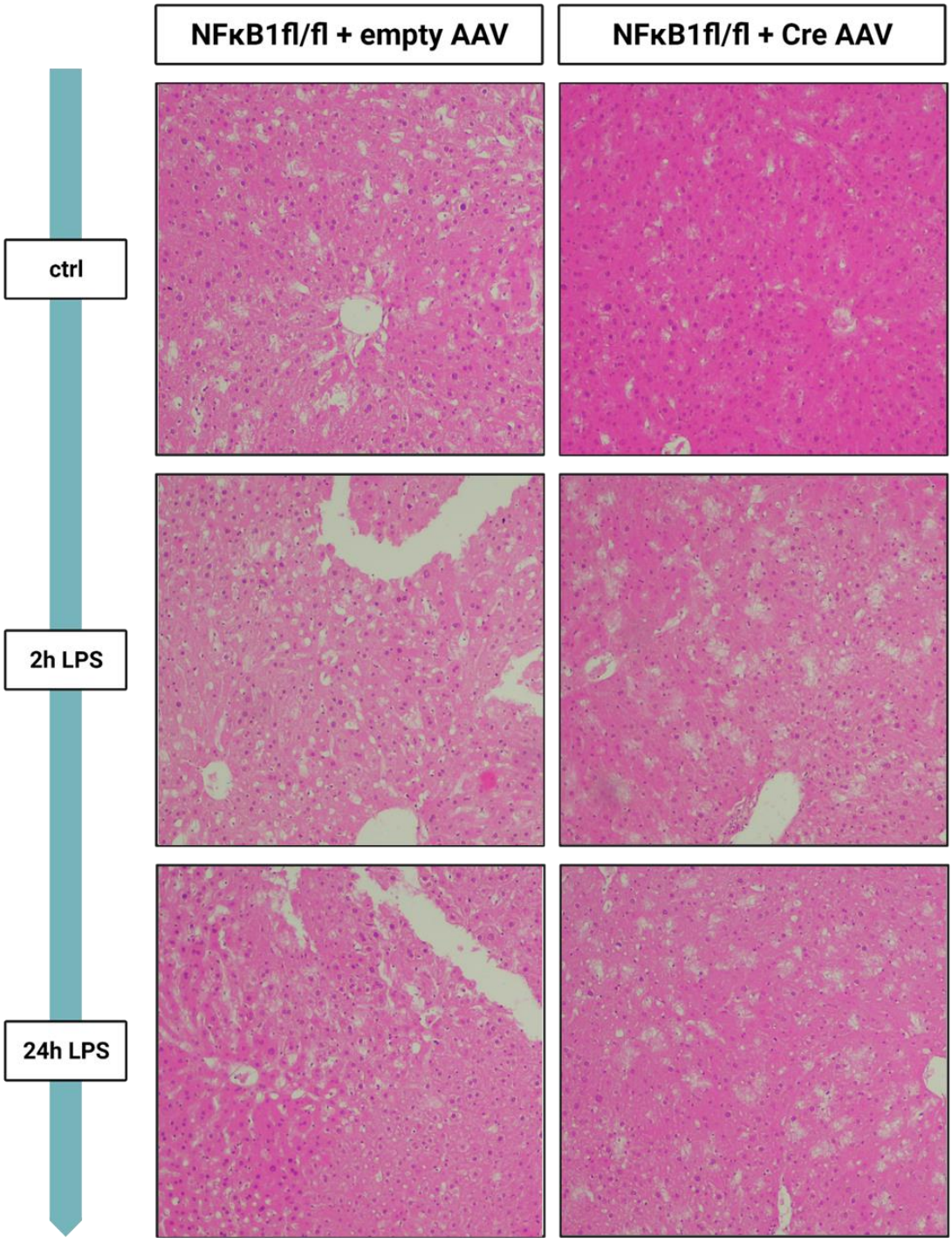

Figure 54. H&E in AAV empty and AAV cre slices. Overall, no differences seemed to occur between the two types of samples, at any condition. They all looked quite damaged, but that could be from the stress of the processing and then the LPS treatment (n=4)

The staining for CD45R revealed smaller number of B cells in both samples compared to the previous experiment without the AVVs. Also, no significant differences were

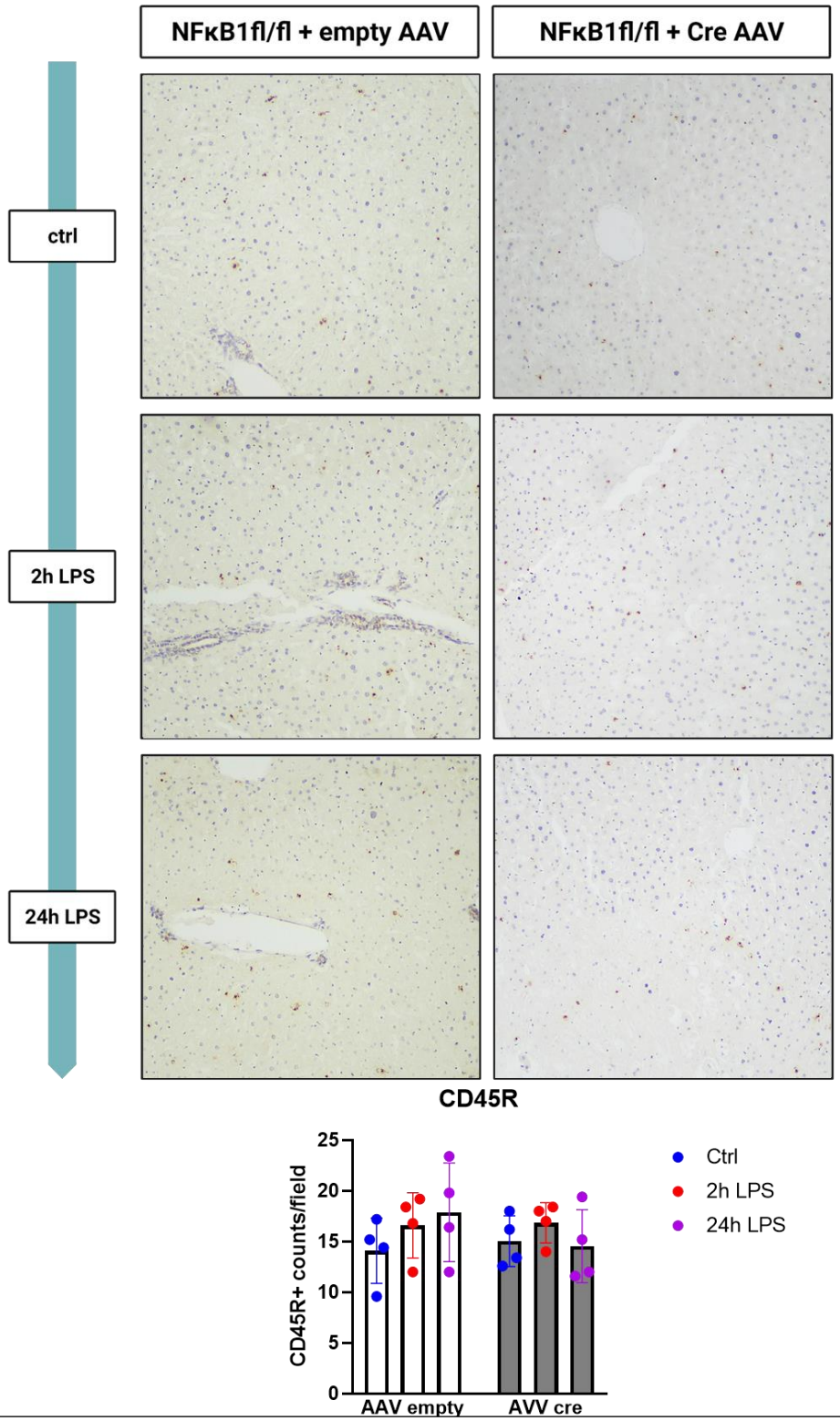

Figure 55. IHC staining for CD45R. No significant differences were identified in positive cell number, when comparing the two AAVs and when comparing the different conditions. No different pattern of positive cells was evident between the two samples (n=4).

detected between different conditions and between the two AVVs, as the number of positive cells was consistent in all the samples (Figure 55).

4.5. Nfκb1$^{-/-}$ PCLS exhibit a protective mechanism against LPS-induced inflammation

Lastly, I wanted to investigated the response of global nfκb1$^{-/-}$ PCLS after LPS treatment. Nfκb1$^{-/-}$ and wt mice were used for this experiment, n=3 for each genotype (Figure 56).

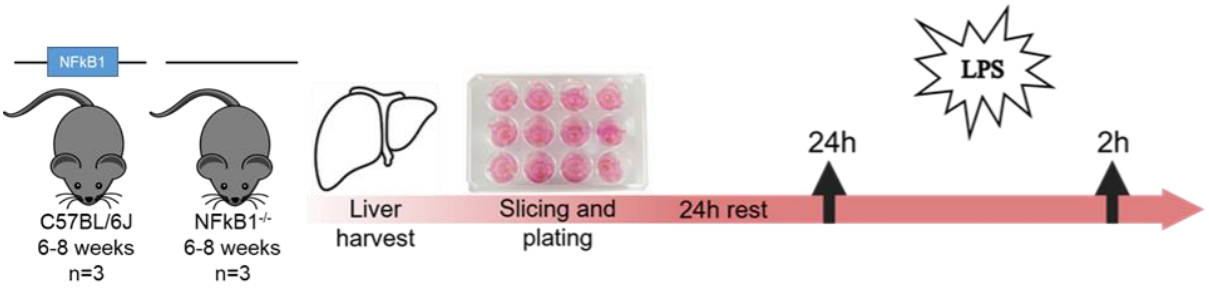

Figure 56. Experiment set up in wt and nfκb1$^{-/-}$ mice (n=3 for each genotype). Livers were harvested and processed to slices. 24h after the processing, the slices were either treated with 1µg/ml LPS for 2h and 24h or left untreated. 24h after, the slices and media were collected for future analyses.

Proteins were extracted in order to check for the presence of p50 in the samples. As shown in figure 57, wt mice presented a detectable signal for the protein of interest, while no signal was identified for the total knock out mice, as expected.

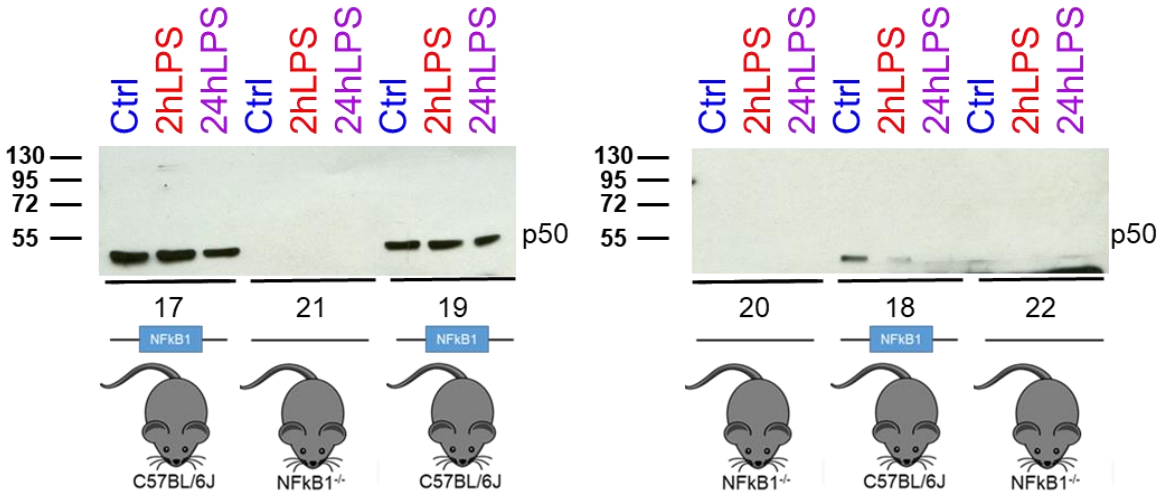

Figure 57. Western blot to check for the presence of p50 in the analysed samples. Wt mice did expressed p50 and this was evident under all the conditions. On the other hand nfκb1$^{-/-}$ mice did not express the protein, as expected.

As previously performed, RNA and media were used to assess the expression of inflammatory genes of interest to compare the response of the two genotypes to the LPS treatment (Figure 58).

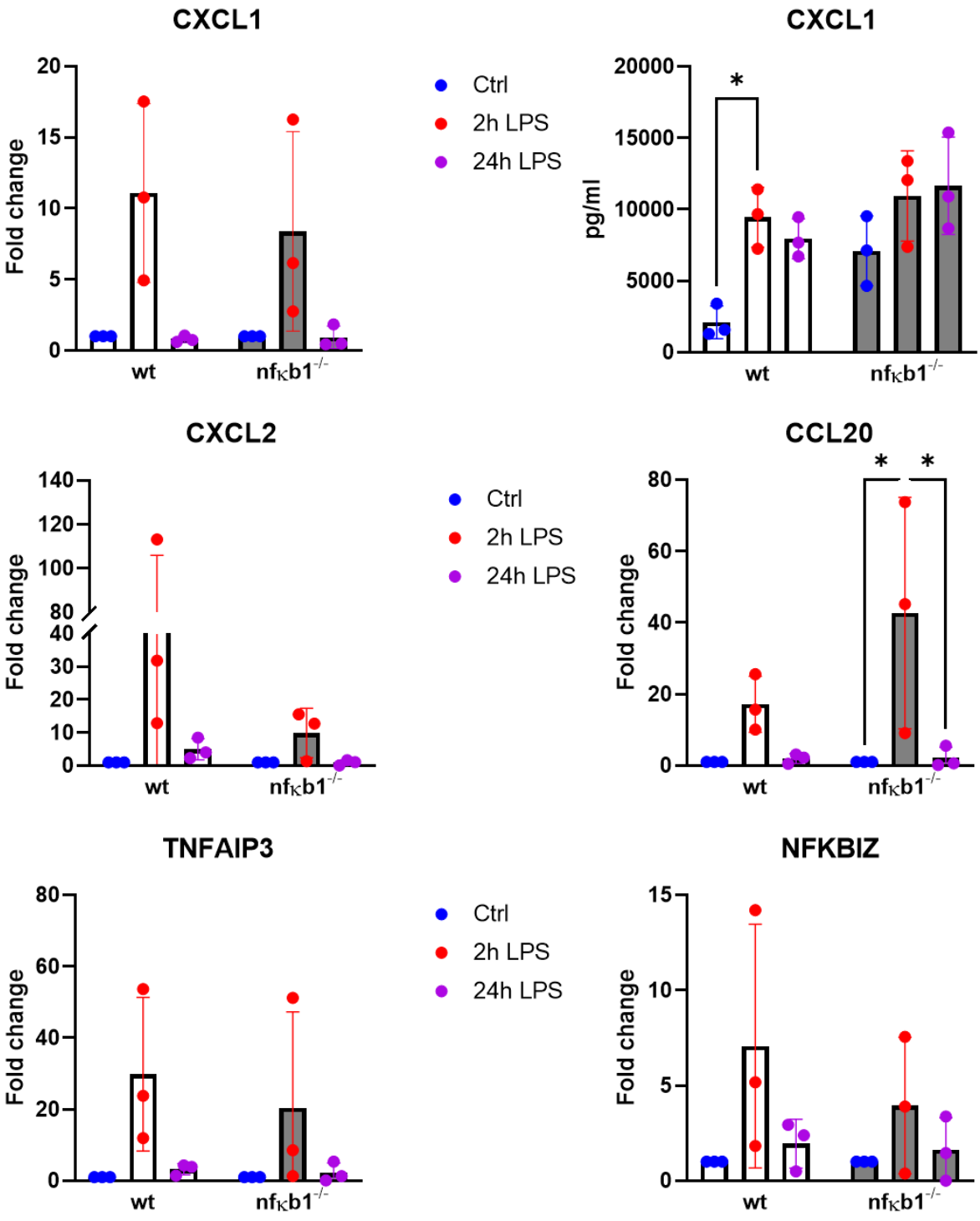

Figure 58. qPCR and ELISA results to characterise the inflammatory response in wt and nfκb1$^{-/-}$ mice. Statistical significance was calculated with an ordinary two-way ANOVA with Tukey's post hoc test (n=3).

Surprisingly, nfκb1$^{-/-}$ mice did not present a more inflamed phenotype as expected. With the exception of CCL20, the qPCR results for inflammatory genes showed higher expression at 2h LPS in wt mice than in ko mice. On the other hand, the ELISA results showed a greater expression of secreted CXCL1 in nfκb1$^{-/-}$ than in wt mice. The difference however was not significant. Overall, both genotypes displayed the canonical progression of the inflammatory event. The greatest expression of targets of interest was detected at 2h LPS, while a decrease was visible at 24h LPS, as indication of resolution.

Lastly, the slices were stained with H&E to check if any structural differences were evident between the two genotypes (Figure 59).

No evident structural differences were detected between the two genotypes. Some wt slices looked more damaged than others, but that might be due to the slicing process, rather that harm caused by the LPS.

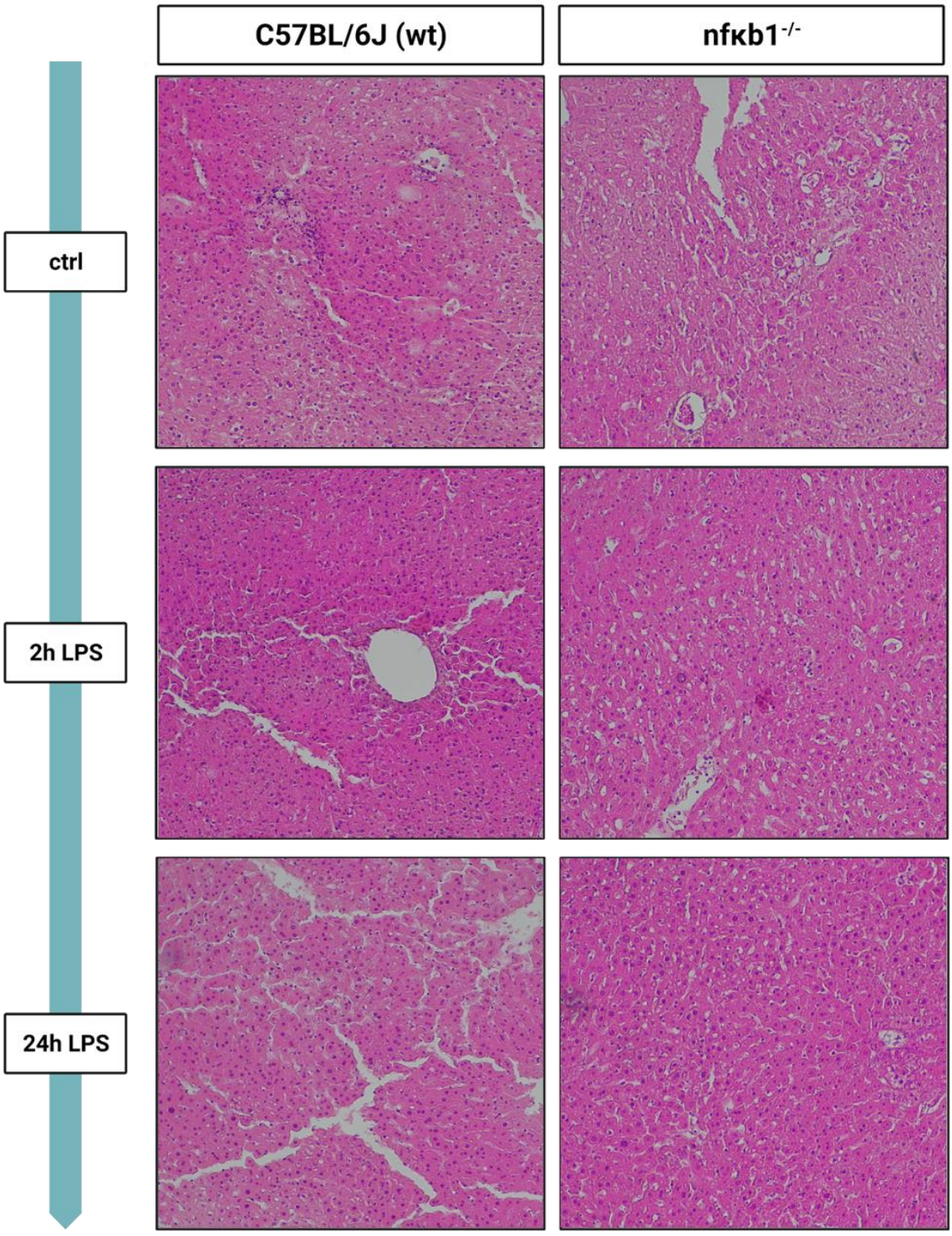

Figure 59. H&E slides for both wt and nfκb1$^{-/-}$ liver slices. Empty spaces present especially in the wt slices might be caused by the process, so it was not an indication of damage caused by the LPS treatment (n=3).

4.6. Discussion

In the field of liver diseases research, new *in vitro* models are needed in order to provide a good working system for drug discovery and for generating models of the disease of interest in a 3D set. In fact, it is important that the intricate network of cell – cell interactions is taken in consideration, as the majority of the conditions affecting the liver are generated by the contribution of the many cell types present in the organ. Precision Cut Liver Slices (PCLS) have provided a revolutionary and less complicated 3D model, when compared to spheroids or organoids. The organ is cut into 250 µm slices, allowing the conservation of the structural organisation of the liver and the generation of many samples from the same source, which can then be treated and tested after different condition.

I validated the model in order to define a good paradigm for an acute inflammatory event, making sure that chosen time points and LPS concentration generated the desired effect. 1µg/ml LPS was sufficient to generate a peak in the expression of previously investigated inflammatory genes, with a subsequent decreasing tendency at 6h LPS; at 24h LPS the levels of expression was back to normal, comparable to the untreated cells. 2h and 24h LPS were picked as time points for the generation of an inflammatory response and its resolution.

First, I wanted to investigate the contribution of hepatic nfκb1 to a more complicated system than the one seen for isolated primary hepatocytes. Surprisingly, $NfκB1^{Albcre/fl}$ slices behaved very similarly to $NfκB1^{fl/fl}$ slices, increasing the expression of pro – inflammatory genes at 2h LPS and decreasing it at 24h LPS, contrary to what found in isolated hepatocytes. This is possibly justified by compensatory mechanisms activated as adaptation to the consistent lack of p50 at the moment of the inflammatory event resolution. Interestingly, more immune cells were found $NfκB1^{Albcre/fl}$ when comparing the same condition in the two genotypes. This could explain why $NfκB1^{Albcre/fl}$ did not show the lack of inflammation limitation that it was detected in primary hepatocytes. The immune cells present in the parenchyma might be able to make up for p50 absence in hepatocytes, dampening the inflammation in the organ at 24h LPS.

To test this theory, we employed Adeno Associated Viruses (AVVs) with a specific tropism for hepatocytes, in order to knock out p50 from the specific cell type at a desired time, eliminating the development of adaptation to the absence of the protein of interest. $NfκB1^{fl/fl}$ mice were injected with either AAV8 – TBG – Cre, to generate the specific knockout, or AAV8 – TBG – Null, as control. The efficiency of the system was checked by RNA and proteins, and both results indicated that the AVV system did not

work equally in all samples, as some slices from the AAV cre injection did expressed p50 at levels comparable to the control virus. The inflammatory profile confirmed that, as no difference was detected in the trend of expression of the genes of interest and the number of T cells found in the two virus – injected samples was similar. It is possible that 10 days might have not been enough time to allow the virus activity in the liver. Also, possible future experiments could include a greater number of viral genomes used for the injection.

Lastly, the model was used to assess the response of nfκb1$^{-/-}$ to LPS treatment. Surprisingly, *NfκB1*-/- slices did not present a more inflamed phenotype compared to the wt cells. Also, no differences in structural organisation were found when checking the H&E staining. It is possible that the LPS concentration was too low and the nfκb1$^{-/-}$ might have evolved a protection, limiting the effect of the bacterial product.

Future experiments to elucidate the function of hepatic nfκb1 should be considered in *vivo*, in order to eliminate the effect of isolation and culture in plastic that could mask other events happening in the tissue.

Chapter 5. Hepatic NFκB1 might play a systemic role during the inflammageing process

5.1. Introduction

Ageing is a physiological process which implies the progressive decline of cell and tissue functionality (López-Otín *et al.*, 2013); concomitantly, the immune system does not efficiently fulfil its role anymore and the consistent triggers due to a sterile, chronic, low grade inflammation result in the onset of inflammageing, which contributes to the creation of a loop that exacerbates both inflammation itself and ageing (Fulop *et al.*, 2021).

By lacking the anti – inflammatory p50, nfκb1$^{-/-}$ mice aged faster compared to wt matching their age and they display a more inflamed phenotype and the onset of a variety of different age – related pathologies, including autoimmunity, fat accumulation in the liver and early mortality (Bianchi *et al.*, 2021).

We wanted to investigate whether hepatic p50 had any effect on the ageing process in the liver and whether it could exert a systemic role.

To investigate this, we aged both Nfκb1$^{flox/flox}$ AlbCre+ and Nfκb1$^{flox/flox}$ male mice for 19 months (Figure 60A), as it correlates nicely with an ageing phenotype in humans (Figure 60B)(Flurkey, Currer and Harrison, 2007).

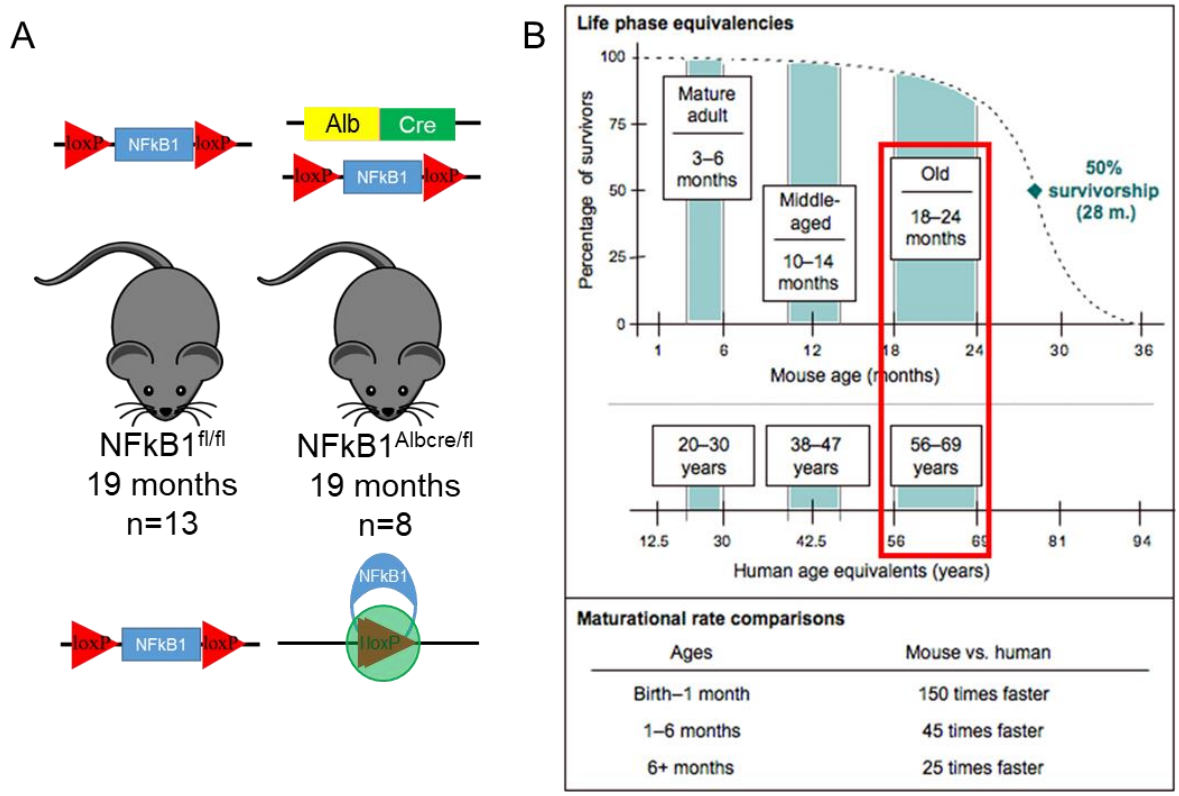

Figure 60. A, graphic representation of the experimental setup; mice from both Nfκb1$^{flox/flox}$ AlbCre+ and Nfκb1$^{flox/flox}$ strains were aged for 19 months in order to generate an ageing model. B, comparison between age ranges in mice vs human; figure adapted from (Flurkey, Currer and Harrison, 2007).

5.2. Nfκb1$^{flox/flox}$ AlbCre+ mice expressed p50 in other organs, but significantly less in the liver

Before commencing any characterisation of the aged phenotype, Nfκb1$^{flox/flox}$ AlbCre+ mice needed to be tested for the efficiency and organ – specificity of the knockout, to make sure that p50 was deleted only in hepatocytes in the liver, and not in other organs. The kidney was taken as control organ and liver and kidney from both genotypes were compared for the protein levels of p50. The results are presented in figure 61.

As previously mentioned in this work, the knockout in Nfκb1$^{flox/flox}$ AlbCre+ mice is specific to hepatocytes, while the remaining cells of the liver express p50; this explains the presence of a signal for the protein in some Nfκb1$^{flox/flox}$ AlbCre+ livers (Figure 61A). However, some samples presented unexpected results, including one Nfκb1$^{flox/flox}$ AlbCre+ liver sample expressing levels of p50 comparable to control livers

(top gel, first lane), one kidney sample without any p50 signal (middle gel, last lane) and a control liver sample expressing less p50 in the liver compared to other Nfκb1$^{flox/flox}$ mice (bottom gel, seventh lane). From a technical point of view, there did not seem to be any evident problem, with either the gel or the protein loading, as inferable from the consistent loading control (GAPDH) across the samples and the different gels; moreover, the proteins were prepared on the same day and the gels were also run at the same time in the same tank, to remove technical variability as much as possible. Even if it was not clear what happened for these samples, the overall result seemed to suggest that there was a difference in p50 levels when comparing Nfκb1$^{flox/flox}$ AlbCre+ and Nfκb1$^{flox/flox}$ livers, but not when comparing the kidney, thus indicating the desired effect of the knockout only in livers from Nfκb1$^{flox/flox}$ AlbCre+ mice.

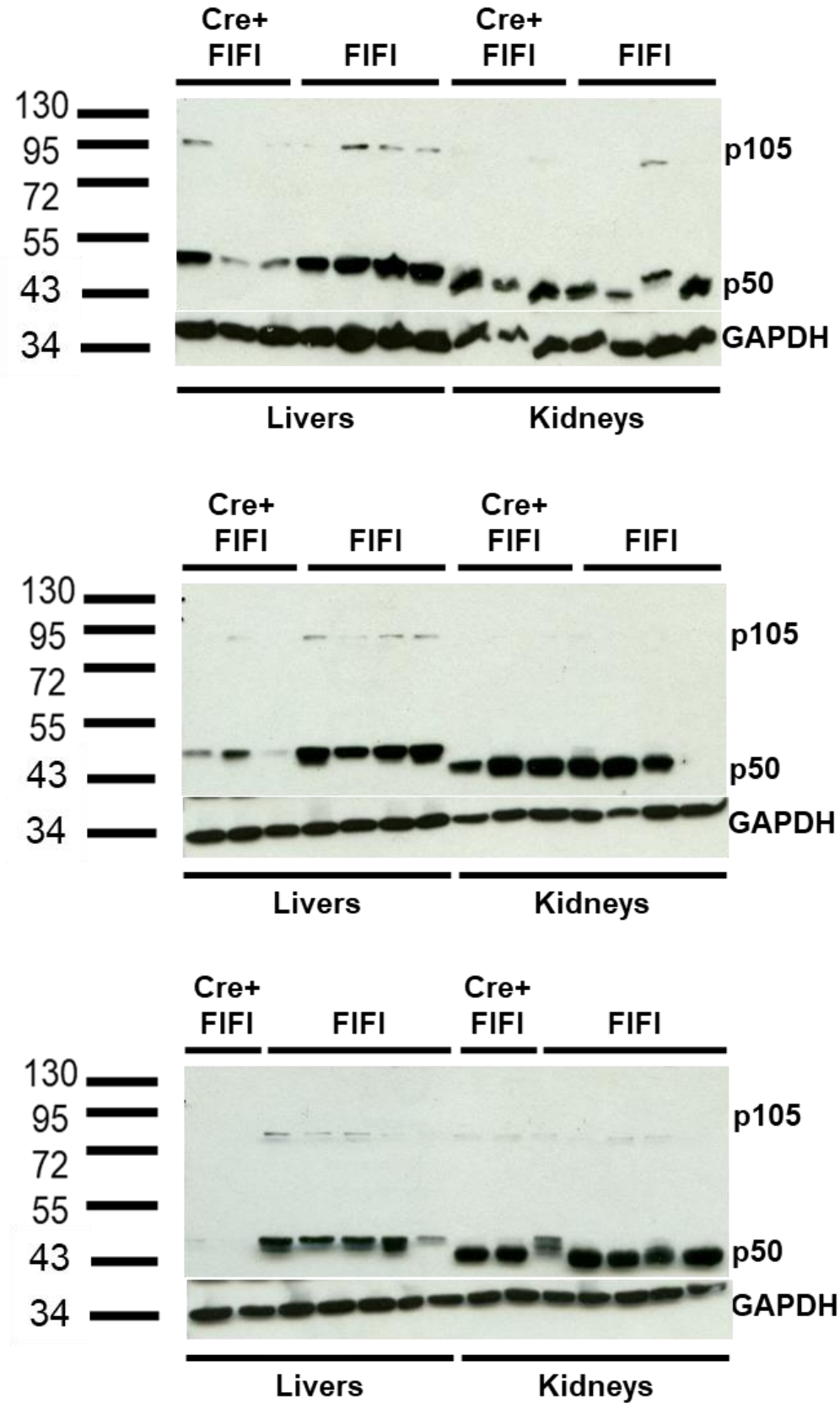

Figure 61. Protein levels of p50 in livers and kidneys from aged Nfκb1$^{flox/flox}$ AlbCre+ and Nfκb1$^{flox/flox}$. A, in each gel matching samples for liver and kidney and both Nfκb1$^{flox/flox}$ AlbCre+ and Nfκb1$^{flox/flox}$ samples were run, for comparison. GAPDH was used as a loading control.

5.3. Nfκb1$^{flox/flox}$ AlbCre+ mice developed more liver steatosis during the ageing process

Previous studies have shown that fat accumulation in the liver, namely steatosis, is an event associated with the ageing, in both rodents and humans (Nguyen *et al.*, 2018). The mechanism is not fully understood, but Jurk et al. proposed that it might be the result of the accumulation of senescent cells; this was supported by the outcome when treating with senolytic drugs, which reduced the overall fat accumulation (Ogrodnik *et al.*, 2017). Experiments from our lab showed that nfκb1$^{-/-}$ mice accumulate more liver fat compared to wt matching their age (Bianchi *et al.*, 2021). We wanted to investigate whether a similar phenotype was observed in the present model of aged mice with a hepatocyte – specific knockout of p50. No difference in liver/body weight ratio was found between the two genotypes (Figure 62A), but analyses of H&E sections of liver tissue revealed that 50% of Nfκb1$^{flox/flox}$ AlbCre+ mice significantly developed more steatosis, graded between 2 and 3 (Brunt *et al.*, 1999)(Figure 62B). Nfκb1$^{flox/flox}$ also showed fat accumulation, but significantly less compared to NfκB1$^{Albcre/fl}$ (Figure 63). 70% of Nfκb1$^{flox/flox}$ mice (9 out of 13) did not show any fat accumulation (grade 0), and the 30% left showed only grade 1-2 steatosis. The results observed in Nfκb1$^{flox/flox}$ AlbCre+ mice could be explained by a partial penetrance of the phenotype, which would likely cause the heterogeneous observed in this model.

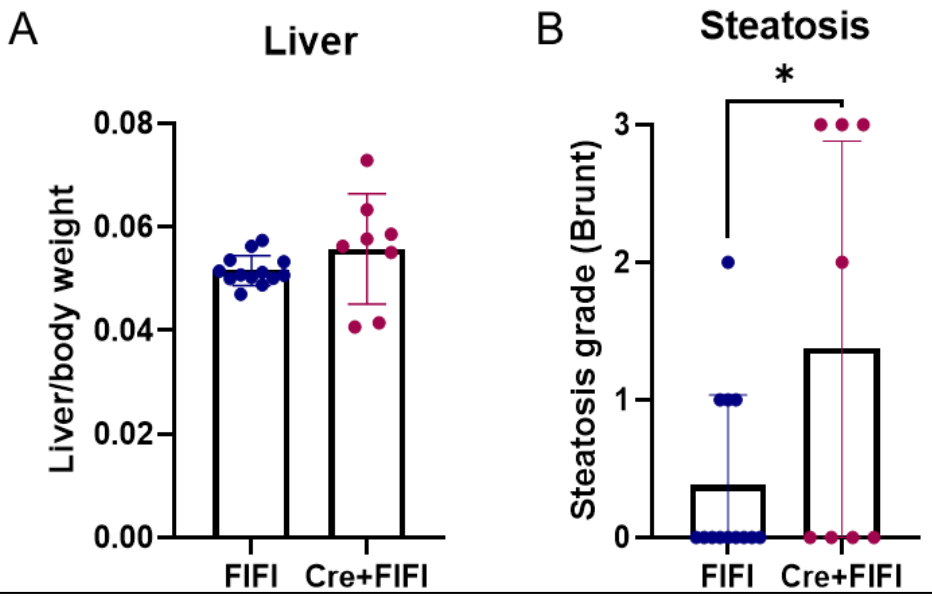

Figure 62. Initial analyses of the livers from aged Nfkb1$^{flox/flox}$ AlbCre+ and Nfkb1$^{flox/flox}$ mice. A, liver/body weight ratio was not found to be different when comparing the two genotypes. B, H&E sections of liver tissue resulted in significantly more fat accumulation in Nfkb1$^{flox/flox}$ AlbCre+ livers than in Nfkb1$^{flox/flox}$. Grading was performed following Brunt et al. (4). Statistical significance was calculated with an unpaired t test.

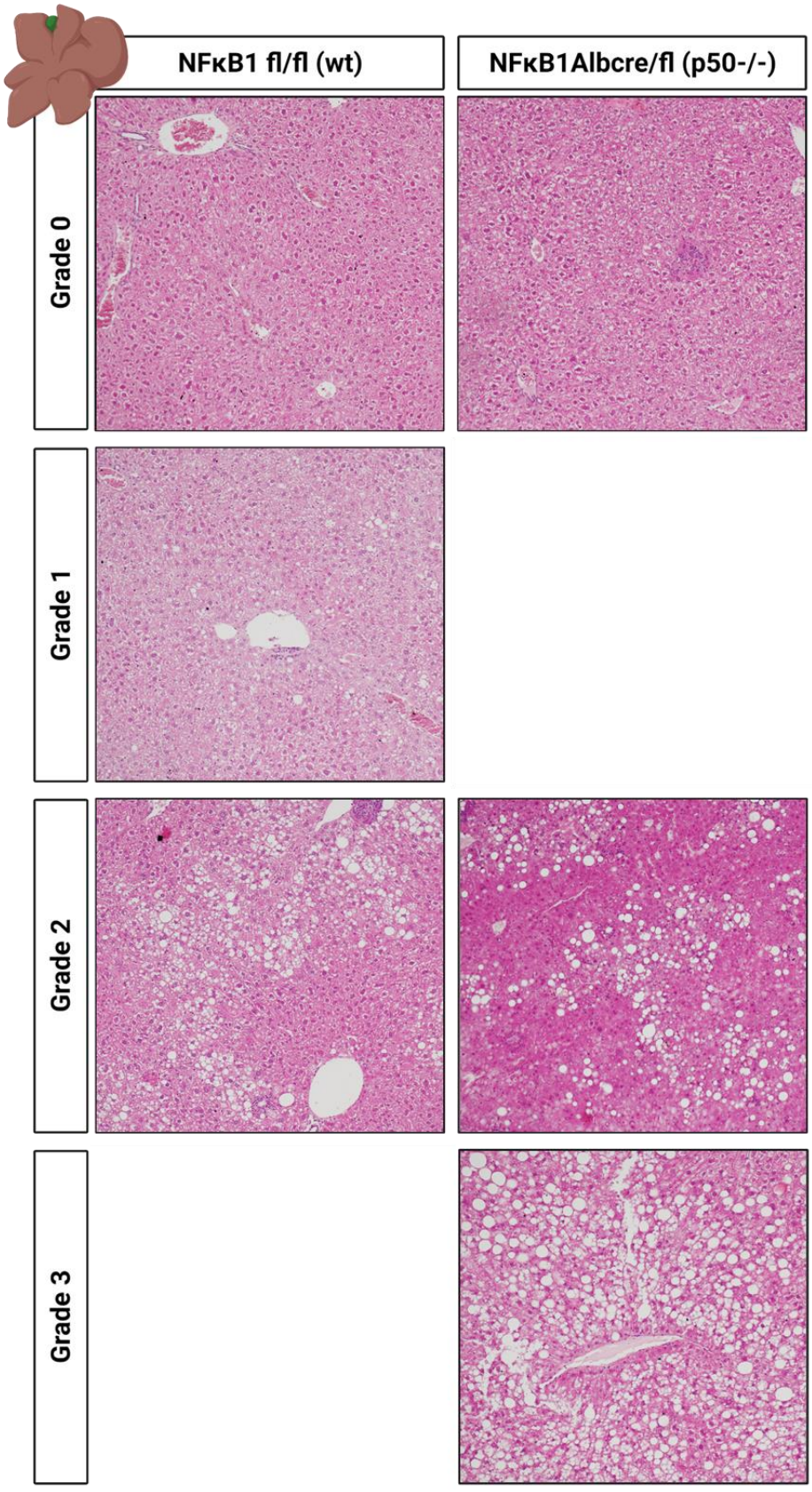

Figure 63. Different grades of steatosis were found in livers from aged mice of both genotypes. Not all the different grades of steatosis were present in the samples and an empty space was left to indicate that. While the majority of Nfκb1$^{flox/flox}$ mice did not display any steatosis (grade 0), 50% of Nfkb1$^{flox/flox}$ AlbCre+ mice showed fat accumulation spanning from grade 2 to 3.

5.4. Greater number of immune cell aggregates localised in Nfκb1$^{flox/flox}$ AlbCre+ livers

From the same H&E sections, the presence of immune cells aggregates across the liver tissue was observed in both genotypes, but with a significant greater number in Nfκb1$^{flox/flox}$ AlbCre+ mice (figure 64). For their organisation and position within close proximity to blood supplies, these aggregates resembled ectopic lymphoid structures (ELSs) (Carragher, Rangel-Moreno and Randall, 2008). Staining for T and B cells markers confirmed that the composition of the observed clusters recalled the composition found in ELSs, but not the organisation (Figure 65) (Pitzalis *et al.*, 2014).

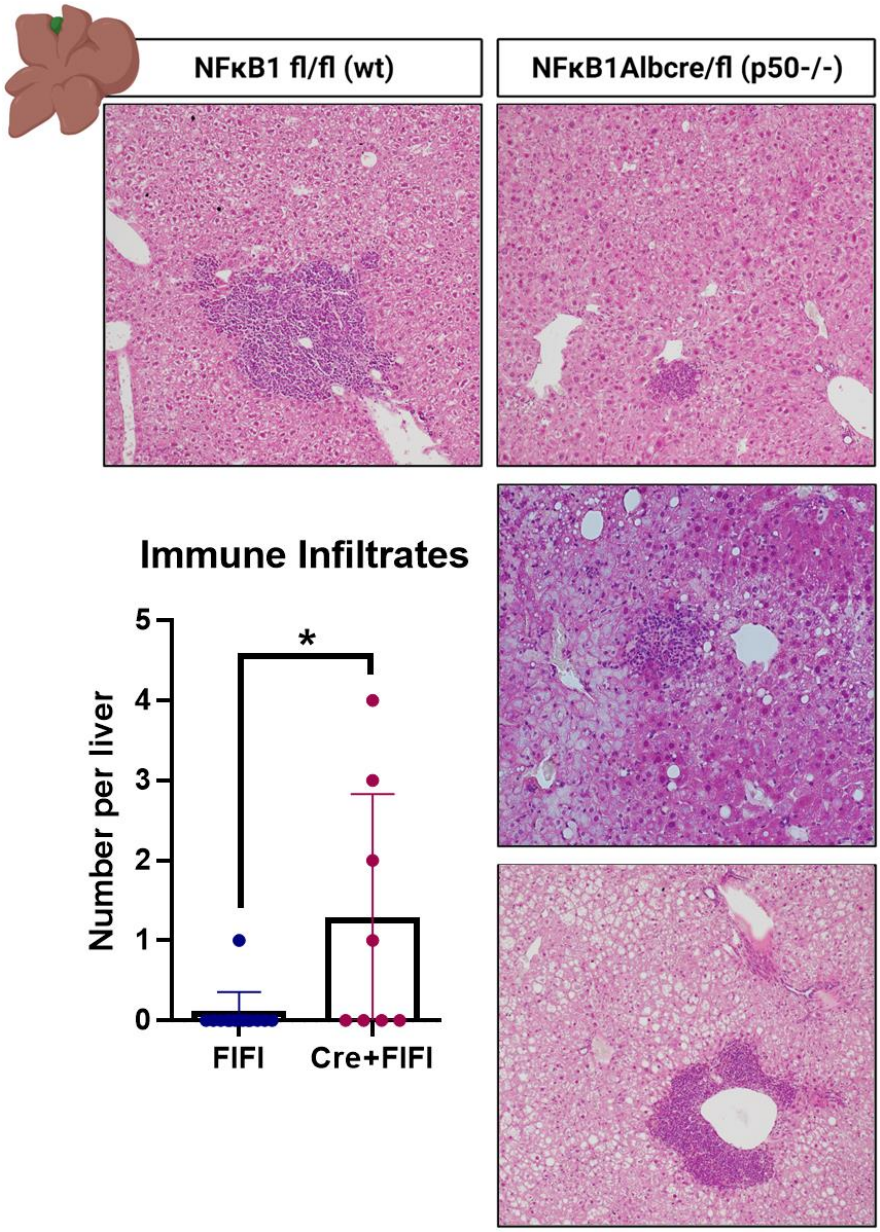

Figure 64. Immune cells aggregates found in livers from aged Nfkb1$^{flox/flox}$ AlbCre+ and Nfkb1$^{flox/flox}$ mice. 50% of aged Nfκb1$^{flox/flox}$ AlbCre+ samples presented infiltrates, with a significant greater number than in Nfkb1$^{flox/flox}$ AlbCre+. Statistical significance was calculated with unpaired t test.

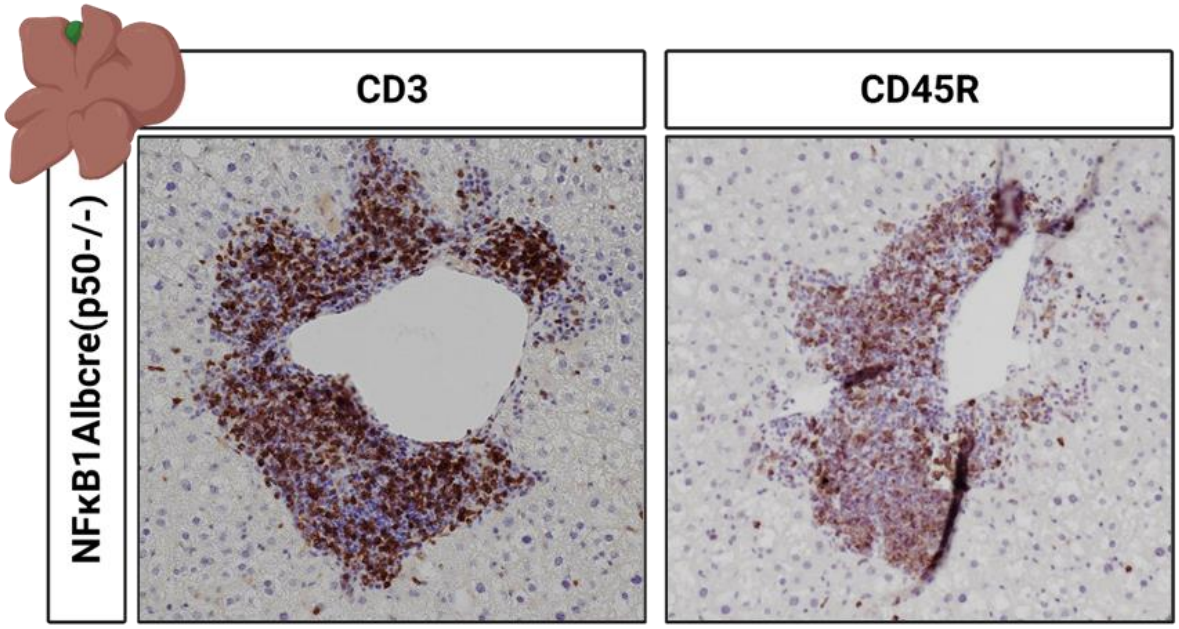

Figure 65. Representative figures of staining against CD3 and CD45R to assess the composition of the immune aggregates found in Nfκb1$^{flox/flox}$ AlbCre+ liver samples.

However, no significant differences were found in positive cells numbers between the two genotypes, and this might be justified by the penetrance of the phenotype in Nfκb1$^{flox/flox}$ AlbCre+ samples; in fact, as presented in the graphs in figure 66, if Nfκb1$^{flox/flox}$ AlbCre+ livers were divided based on the presence of infiltrates, the number of immune cells found in Nfκb1$^{flox/flox}$ AlbCre+ livers without infiltrates were comparable to the control mice, for both genotype. also, no differences in spleen/body weight ratios between gentoypes seemed to confirm this hypothesis (Figure 66).

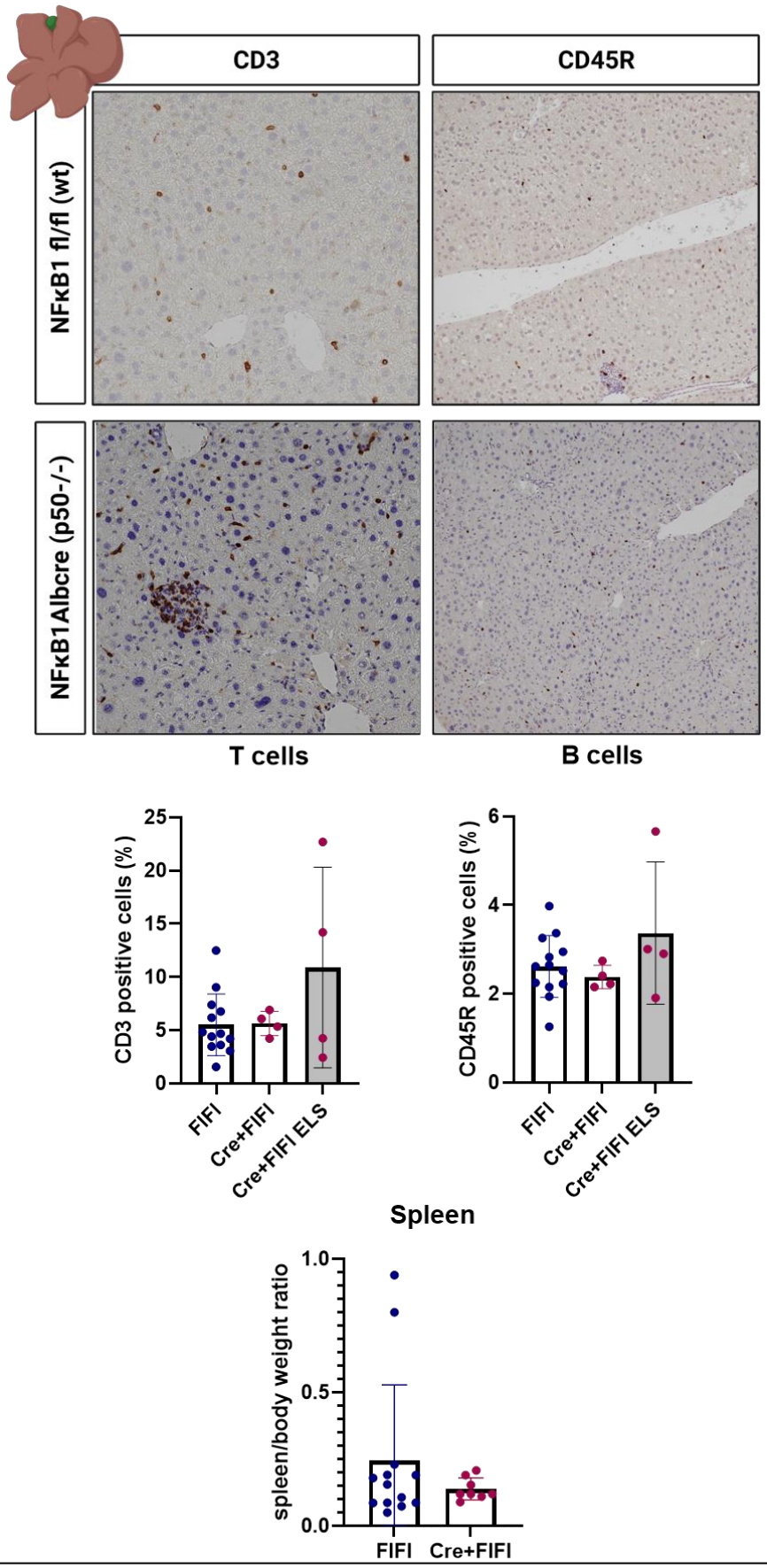

Figure 66. Quantification of positive cells for both populations of immune cells did not suggest a difference in numbers between the two genotypes and in particular it seemed like there was a different penetrance of the phenotype; this was possibly confirmed by no differences in spleen/body weight ratios.

Similar results were obtained in aged nfκb1$^{-/-}$ mice, but they also spontaneously developed more tumours in the liver compared to their wt littermates (Wilson *et al.*, 2015b); moreover, another paper showed that ELSs acted as microniche for tumour progenitors cells, because of constitutive activation of NF-κB in hepatocytes (Finkin *et al.*, 2015). Interestingly, we did not observe any tumour growth in aged Nfκb1$^{flox/flox}$ AlbCre+. Further characterisation for HCC progenitor cells in the immune cells aggregates confirmed that in our model the ELSs did not host cancer progenitors cells, and that in general there was no indication of predisposition to tumour growth in aged Nfκb1$^{flox/flox}$ AlbCre+ mice (figure 67).

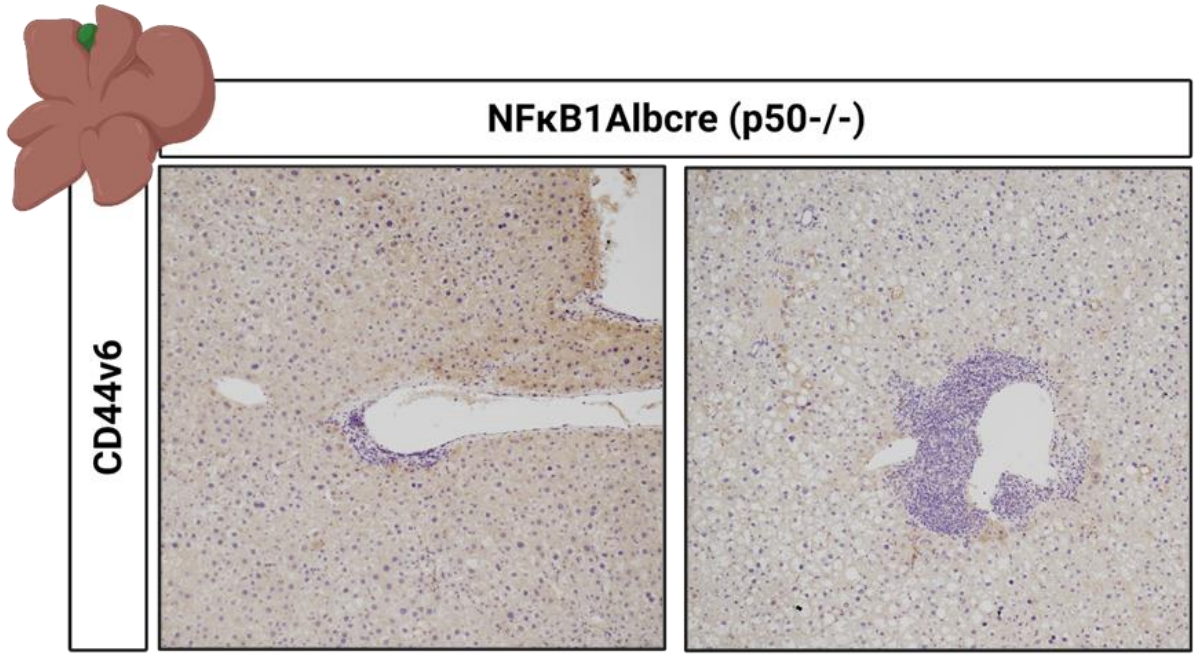

Figure 67. CD44v6 staining to investigate if immune cell aggregates in Nfκb1$^{flox/flox}$ AlbCre+ in the liver hosted cancer progenitors cells. No indication of their presence was found in this model.

Another indication of the different phenotype obtained in this model was the result when observing Lymphotoxin β (LTβ) expression in the two genotypes. In fact, previous works have shown that in the case of ELSs promoting HCC, increased levels of LTβ were observed on hepatocytes, promoting the generation of ELS with subsequent onset of tumour growth (Finkin *et al.*, 2015). Western blot analysis in Nfκb1$^{flox/flox}$ AlbCre+ and Nfκb1$^{flox/flox}$ did not allow to draw any conclusion, because of the variability in signal intensity in both Nfκb1$^{flox/flox}$ AlbCre+ and Nfκb1$^{flox/flox}$ samples (Figure 68, red rectangles). More specifically, one samples from Nfκb1$^{flox/flox}$ AlbCre+ seemed to overexpress LTβ (top gel, first lane), while of two Nfκb1$^{flox/flox}$ samples, one lacked any signal (bottom gel, seventh lane), while the other presented a fainter band compared to other samples belonging to the same group (bottom gel, tenth lane);

further confirmations would definitely be needed, by repeating the western blot again or by increasing the number of samples, in order to define the trend for LTβ expression and whether a LTβ – dependent mechanism was responsible for the ELS formation in Nfκb1$^{flox/flox}$ AlbCre+ livers (Figure 68).

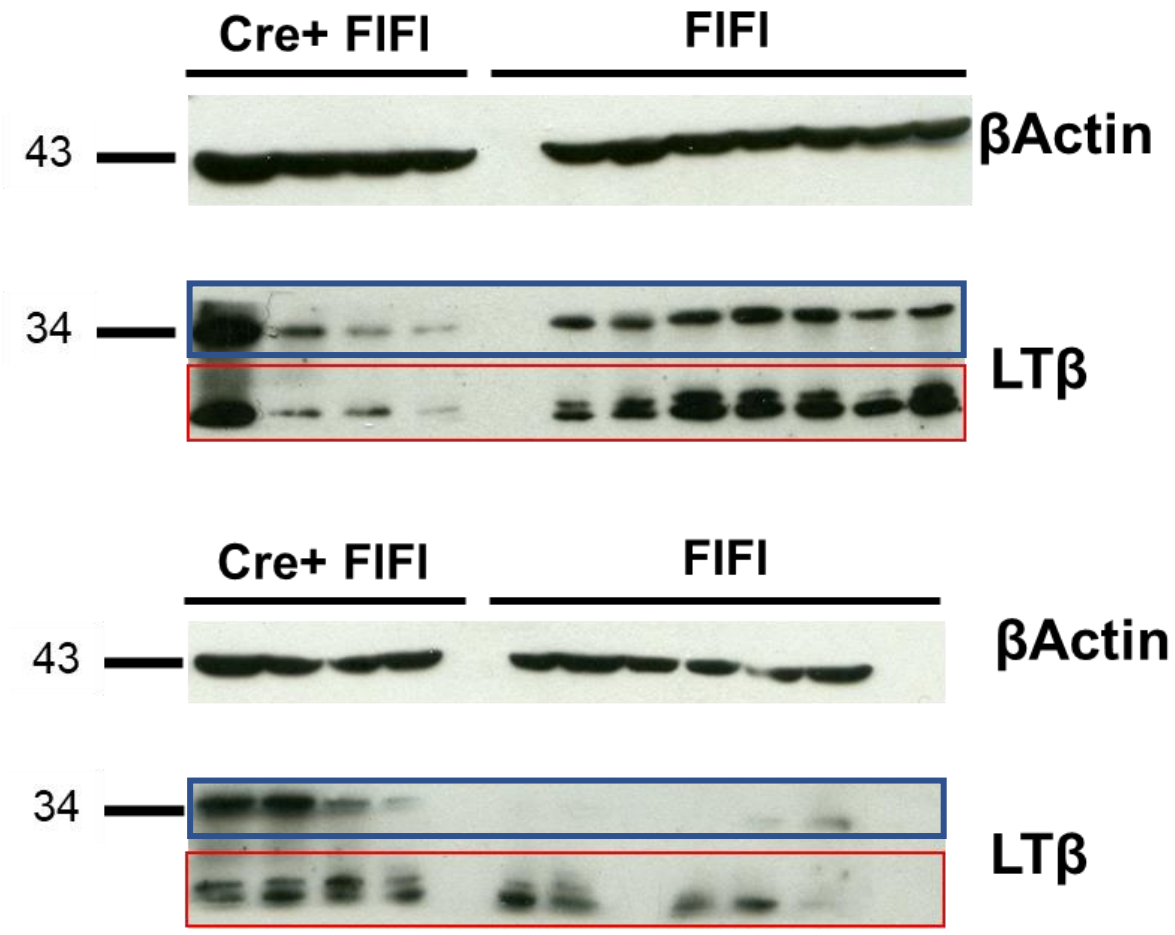

Figure 68. Western blot analyses for LTβ in livers from both genotypes of aged mice. Even if a certain degree of variability was detected for samples in both genotypes, the signal in the red rectangles seemed to point at no overall difference in LTβ expression between Nfκb1$^{flox/flox}$ AlbCre+ and Nfκb1$^{flox/flox}$ samples. Nonspecific bands were also detected for the majority of the samples (blue rectangles).

Lastly, we wanted to check whether the increased presence of immune cells aggregates implied more damage and therefore fibroblast activation in aged Nfκb1$^{flox/flox}$ AlbCre+ livers, leading to more deposition of α – smooth muscle actin (αSMA) (Page *et al.*, 2016). Interestingly, positive staining was found in only 50% of Nfκb1$^{flox/flox}$ AlbCre+ livers, possibly indicating heterogenous penetrance; only 38% of

Nfκb1$^{flox/flox}$ mice showed presence of αSMA (Figure 69), with no significant differences in area of deposition.

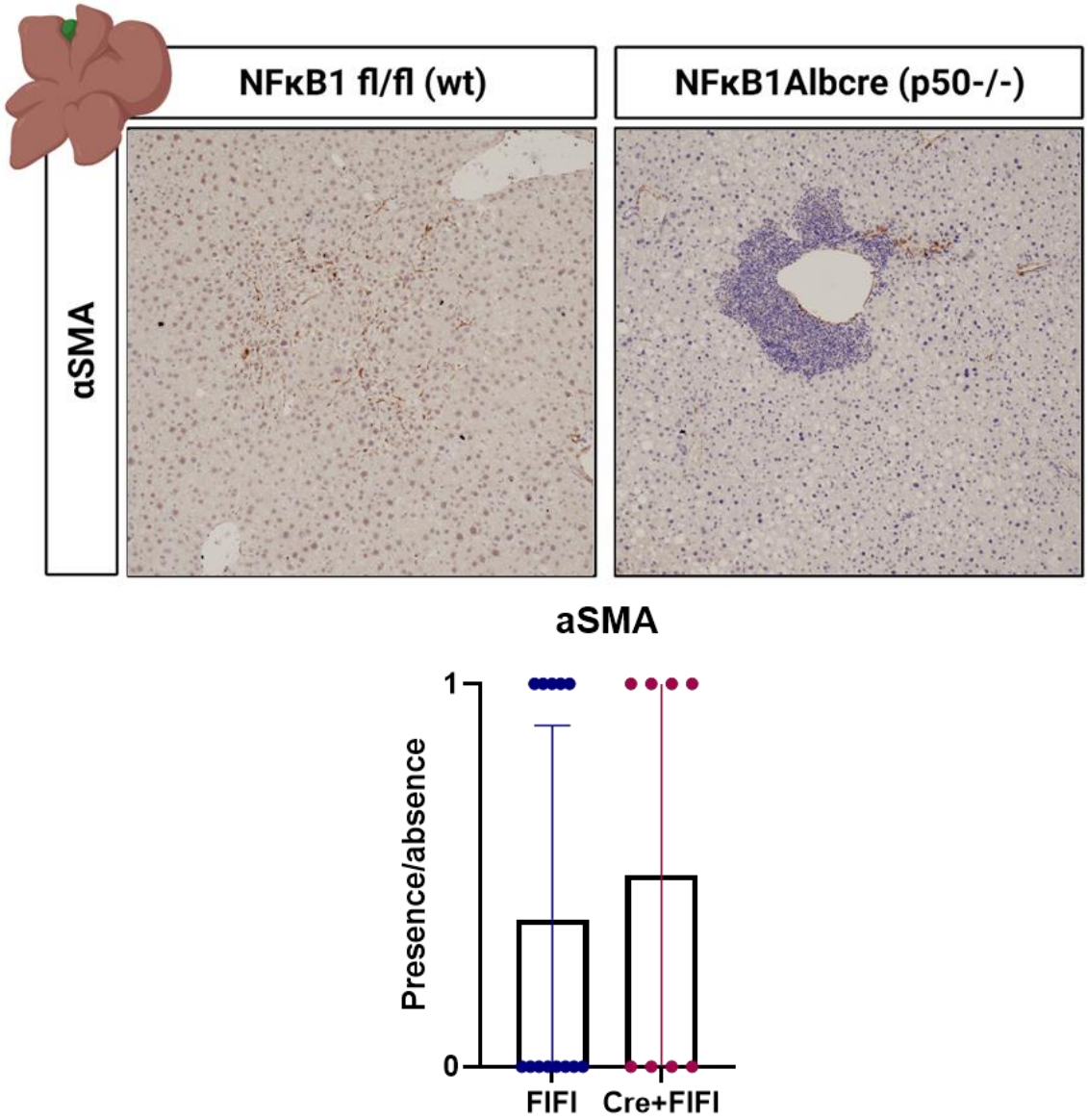

Figure 69. Staining for αSMA did not reveal any differences in the livers of the two genotypes, express in presence (=1) and absence (=0) in the graph; in particular the majority of Nfκb1$^{flox/flox}$ samples (62%) did not show any positivity for this marker, and only 50% of Nfκb1$^{flox/flox}$ AlbCre+ liver samples presented αSMA positivity, possibly indicating a partial penetrance of the phenotype.

5.5. Characterisation of other organs in aged Nfκb1$^{flox/flox}$ AlbCre+: Lungs

We wanted to investigate whether the deletion of p50 in hepatocytes could cause any systemic consequences in other organs, despite expressing the protein of interest.

We started with the lungs and organ/body weight ratios were consistent between the two genotypes (Figure 70). H&E sections of the tissue showed no macroscopic differences between the two genotypes and no immune cells aggregate was observed (Figure 70). However, following the results from Bianchi et al. (Bianchi *et al.*, 2021), we asked whether they were variations in number of specific immune cells in the two genotypes when looking at the lung. Staining for T and B cells did not reveal any difference in numbers of cells, nor in the pattern of aggregation in the tissue (Figure 70).

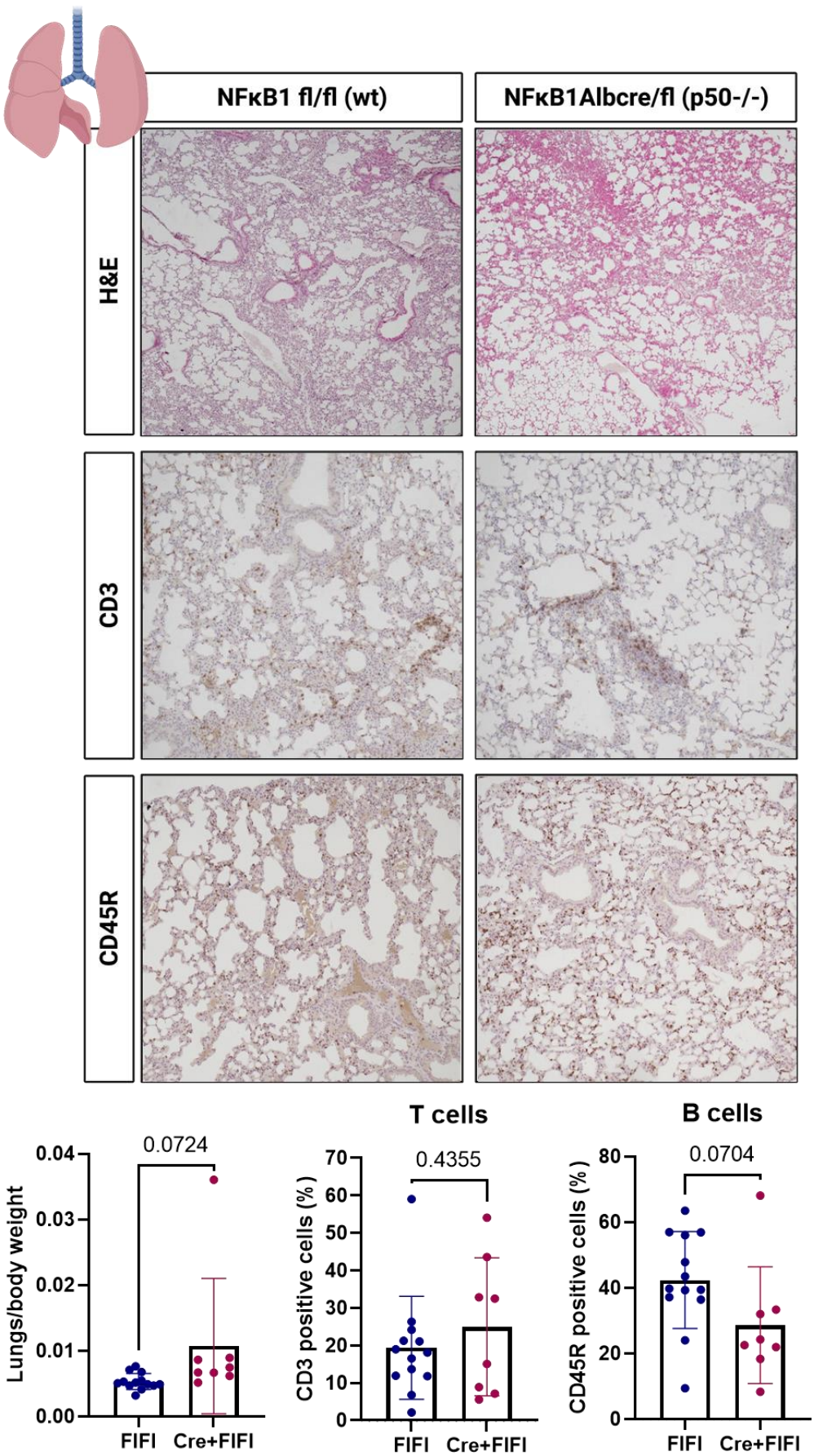

Figure 70. Characterisation of lungs in aged Nfκb1$^{flox/flox}$ and Nfκb1$^{flox/flox}$ AlbCre+ in mice. No macroscopic differences were found from H&E sections and staining for immune cells did not detect any difference in number or pattern of aggregation.

5.6. Characterisation of other organs in aged Nfκb1$^{flox/flox}$ AlbCre+: Kidney

Next, we focused our attention on the kidneys, and H&E sections of tissue revealed that 62.5% of Nfκb1$^{flox/flox}$ AlbCre+ samples presented severe kidney damage with loss of organisation and glomeruli architecture, confirmed by Periodic acid – Schiff (PAS) staining. Kidney tissue from Nfκb1$^{flox/flox}$ mice did not present any visible damage and the structure of the glomeruli resembled the physiological organisation seen in healthy, young tissue (Figure 71A-C). Kidney/body ratios were consistent between the two genotypes (Figure 71D). To understand whether the kidney functionality was affected by the ageing process and differentially impacted because of the absence of p50 in hepatocytes, we checked some important kidney stress markers by qRT-PCR. These markers would normally be investigated at the serum level, as secretion of these molecules have been correlated with kidney damage and injury, as explained in the following paragraph. However, the serum from these mice was not available, so I tried to investigate the expression of these molecules with the samples that were available, in this case cDNA.

Glutaminase Kidney Isoform, mitochondrial, GAM, is an important enzyme for the catabolism of glutamine in the kidneys, which is acutely activated in response to the onset of metabolic acidosis; increased ammoniagenesis and gluconeogenesis from plasma glutamine is the mechanism taking place in order to re – establish the blood acid – base balance (Curthoys, 2001). Neutrophil Gelatinase – Associated Lipocalin, NGAL, is a protein produced by the nephron epithelia in response to damage and it has become a well – accepted marker for acute kidney injury (AKI) (Singer *et al.*, 2013). Lastly, Kidney Injury Molecule 1, KIM1, is a molecule that is upregulated in proximal tubular cells following a kidney injury (Sabbisetti *et al.*, 2014). As inferable from the graph in Figure 71, panel E, qRT-PCR results did not reveal any significant differences in expression for these stress markers when comparing the two genotypes.

However, as previously mentioned, these results were obtained at the RNA level, so this outcome should be confirmed by checking for the same markers in the serum.

Interestingly, four of the Nfκb1$^{flox/flox}$ AlbCre+ mice presenting damage in the kidneys were also the samples with immune infiltrates in the liver, indicated by red arrows in figure 72, suggesting a possible correlation between liver and kidney damage because of the absence of *nfkb1* in hepatocytes.

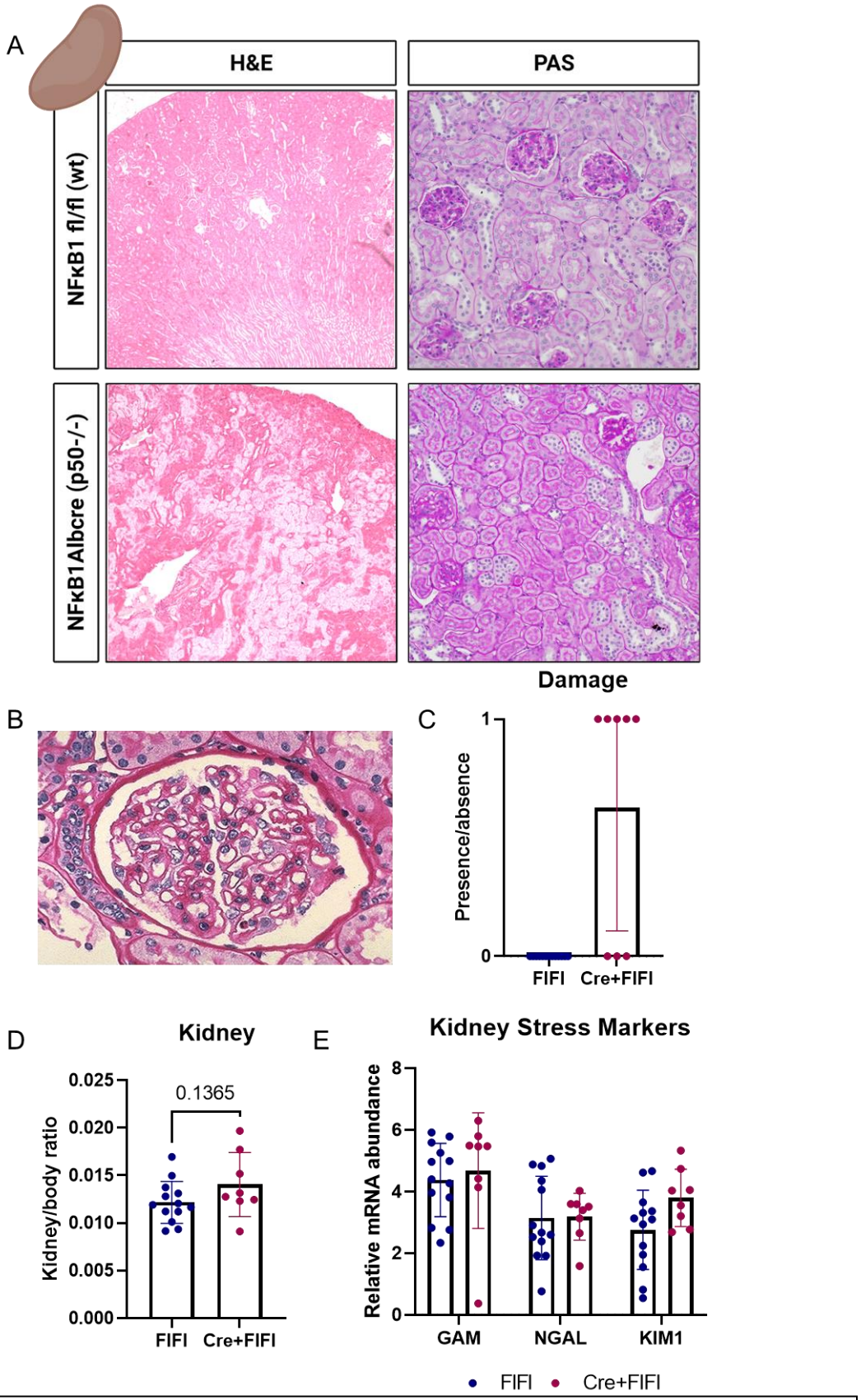

Figure 71. Characterisation of kidneys in aged Nfκb1$^{flox/flox}$ and Nfκb1$^{flox/flox}$ AlbCre+ in mice. A, H&E sections and PAS staining highlighted differences in structure and tissue architecture, as 50% of Nfκb1$^{flox/flox}$ AlbCre+ kidneys presented extensive damage and loss of glomeruli organisation. B, example of a glomeruli from healthy and young tissue. C, graph representing the presence of kidney damage in the two genotypes. D, kidney/body ratios were consistent between the two genotypes. E, kidney stress markers analysed by qRT-PCR, with no differences found in their expression.

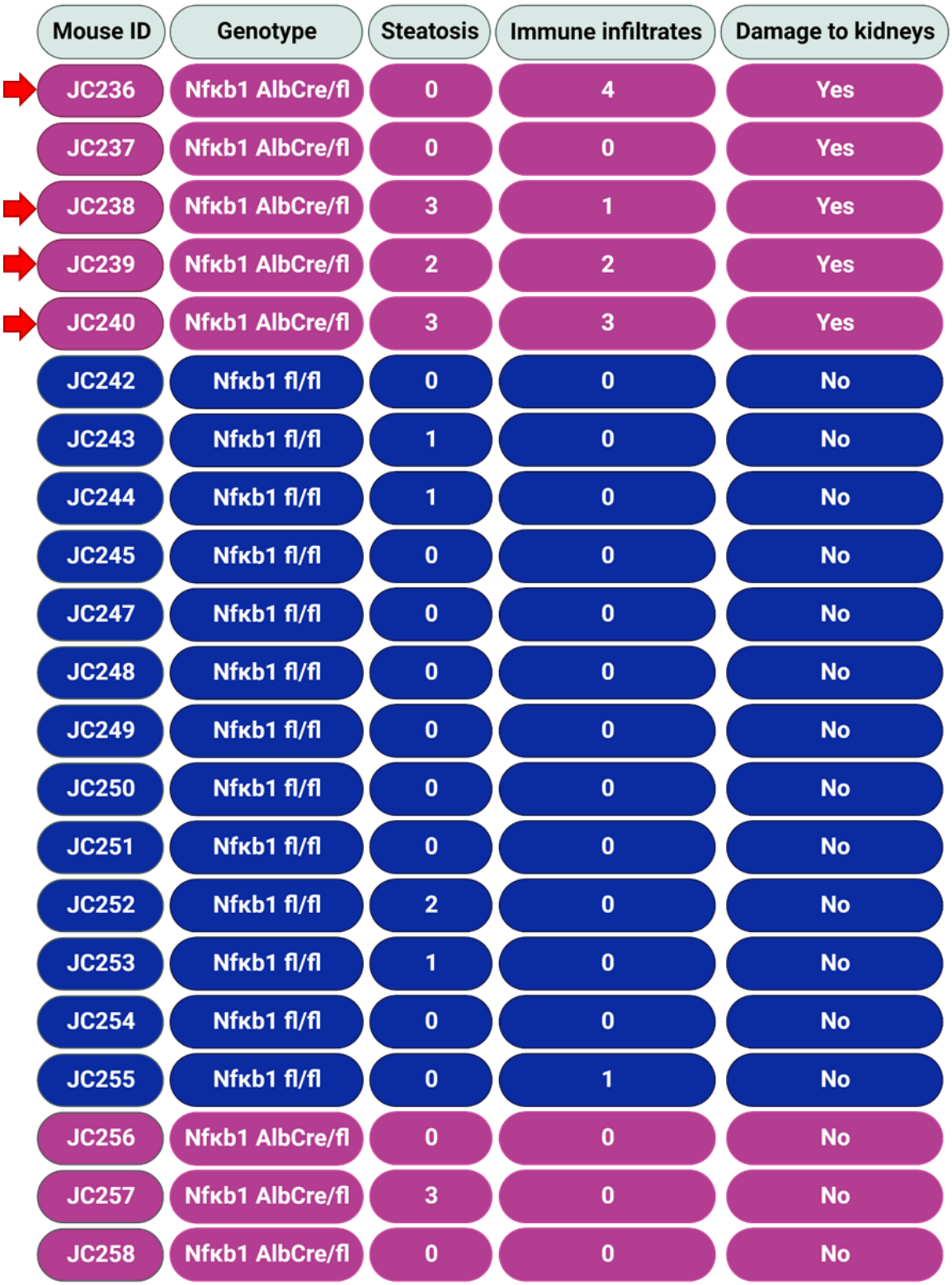

Mouse ID	Genotype	Steatosis	Immune infiltrates	Damage to kidneys
JC236	Nfκb1 AlbCre/fl	0	4	Yes
JC237	Nfκb1 AlbCre/fl	0	0	Yes
JC238	Nfκb1 AlbCre/fl	3	1	Yes
JC239	Nfκb1 AlbCre/fl	2	2	Yes
JC240	Nfκb1 AlbCre/fl	3	3	Yes
JC242	Nfκb1 fl/fl	0	0	No
JC243	Nfκb1 fl/fl	1	0	No
JC244	Nfκb1 fl/fl	1	0	No
JC245	Nfκb1 fl/fl	0	0	No
JC247	Nfκb1 fl/fl	0	0	No
JC248	Nfκb1 fl/fl	0	0	No
JC249	Nfκb1 fl/fl	0	0	No
JC250	Nfκb1 fl/fl	0	0	No
JC251	Nfκb1 fl/fl	0	0	No
JC252	Nfκb1 fl/fl	2	0	No
JC253	Nfκb1 fl/fl	1	0	No
JC254	Nfκb1 fl/fl	0	0	No
JC255	Nfκb1 fl/fl	0	1	No
JC256	Nfκb1 AlbCre/fl	0	0	No
JC257	Nfκb1 AlbCre/fl	3	0	No
JC258	Nfκb1 AlbCre/fl	0	0	No

Figure 72. Table to summarise the results from the analyses which highlighted a possible correlation between immune infiltrates in the liver and damage in the kidneys in Nfκb1$^{flox/flox}$ AlbCre+ mice. Indicated by the red arrow, four samples from the Nfκb1$^{flox/flox}$ AlbCre+ cohort presented both high number of T and B cells infiltrates in the liver parenchyma and severe kidney damage. Three of the samples also presented severe steatosis in the liver (grade 2 and 3).

As previously performed for liver and lungs, immune cells and fibroblast activation markers were investigated in the kidneys of both aged Nfκb1$^{flox/flox}$ and Nfκb1$^{flox/flox}$ AlbCre+ mice.

No differences were found in number of immune cells foci when comparing the two genotypes (Figure 73); surprisingly more αSMA deposition seemed to be present in

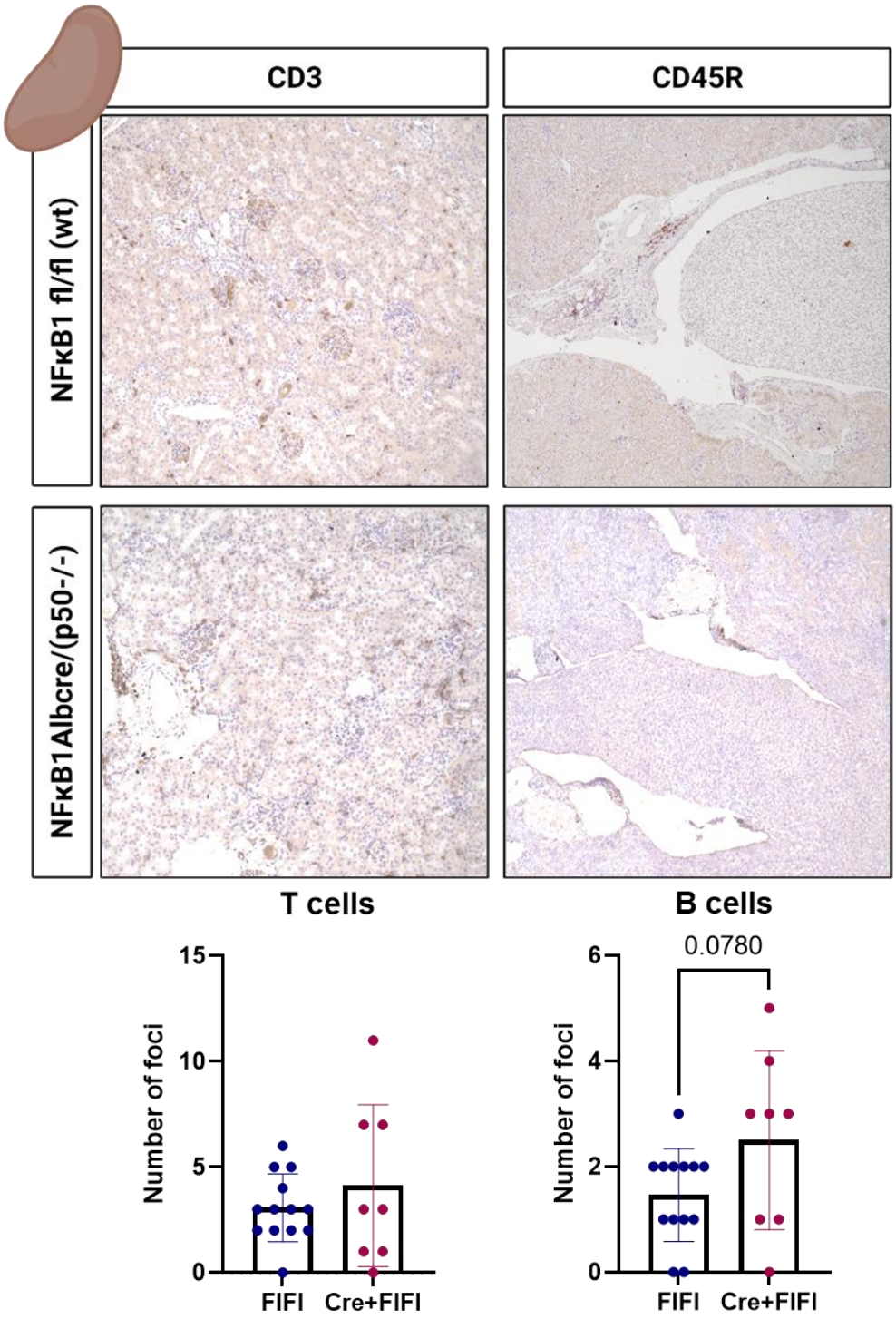

Figure 73. Characterisation of kidneys in aged Nfκb1$^{flox/flox}$ and Nfκb1$^{flox/flox}$ AlbCre+ for immune cells markers. No differences were found in number of immune cells foci for both T and B cells population. Statistical significance was calculated with an unpaired t test.

Nfκb1$^{flox/flox}$ kidneys when compared with Nfκb1$^{flox/flox}$ AlbCre+ samples, but the quantification was proved to be quite challenging because of the background signal obtained for some samples, including Nfκb1$^{flox/flox}$ AlbCre+(Figure 74).

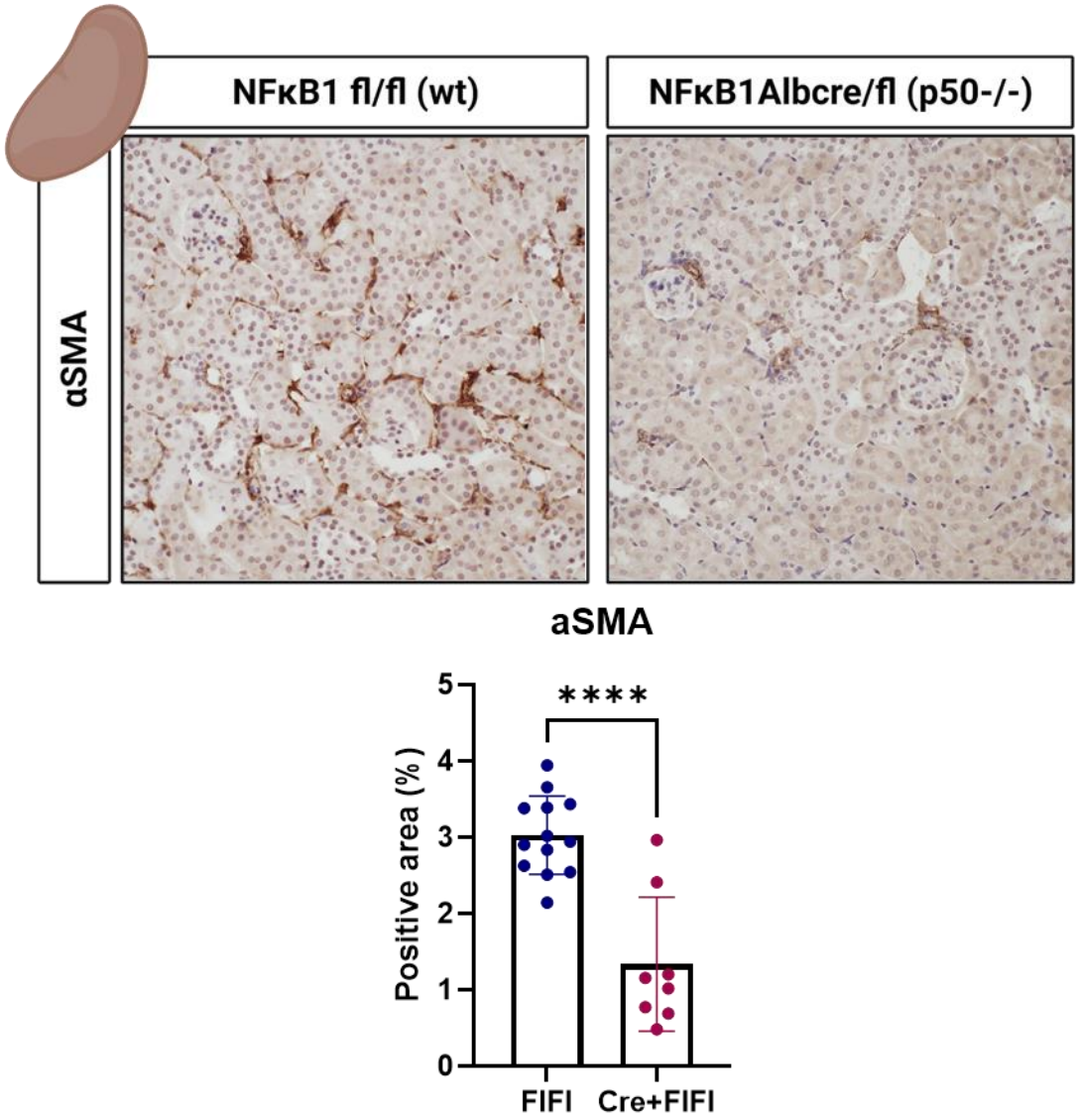

Figure 74. Characterisation of kidneys in aged Nfκb1$^{flox/flox}$ and Nfκb1$^{flox/flox}$ AlbCre+ for αSMA deposition and possible fibroblast activation. According to the results, Nfκb1$^{flox/flox}$ mice seemed to significantly accumulate more αSMA in the kidneys compared to Nfκb1$^{flox/flox}$ AlbCre+. Statistical significance was calculated with an unpaired t test.

5.7. Senescent markers in livers and kidneys

Accumulation of senescent cells is a well – documented phenomenon during the ageing process; by secreting a specific group of factors globally known as senescence – associated secretory phenotype (SASP), senescent cells induce tissue dysfunction in a paracrine manner (Ogrodnik *et al.*, 2017). After noticing a correlation between liver and kidney damage in 50% of Nfκb1$^{flox/flox}$ AlbCre+ mice, we decided to investigate whether the phenotype could have been caused by a greater presence of senescent cells in the tissues of both liver and kidney.

p21 and p16 are considered two markers of senescence, since they are both cyclin – dependent kinase inhibitors that can induce cell cycle arrest and if expressed ectopically they can induce a senescent phenotype (Mcconnell *et al.*, 1998). Staining for p21 in liver tissue did not reveal any differences in number of senescent cells between the two genotypes (Figure 75). Intriguingly, as observed in previous analyses, 50% of Nfκb1$^{flox/flox}$ AlbCre+ samples showed high levels of p21 cells, compared to the other half of the samples.

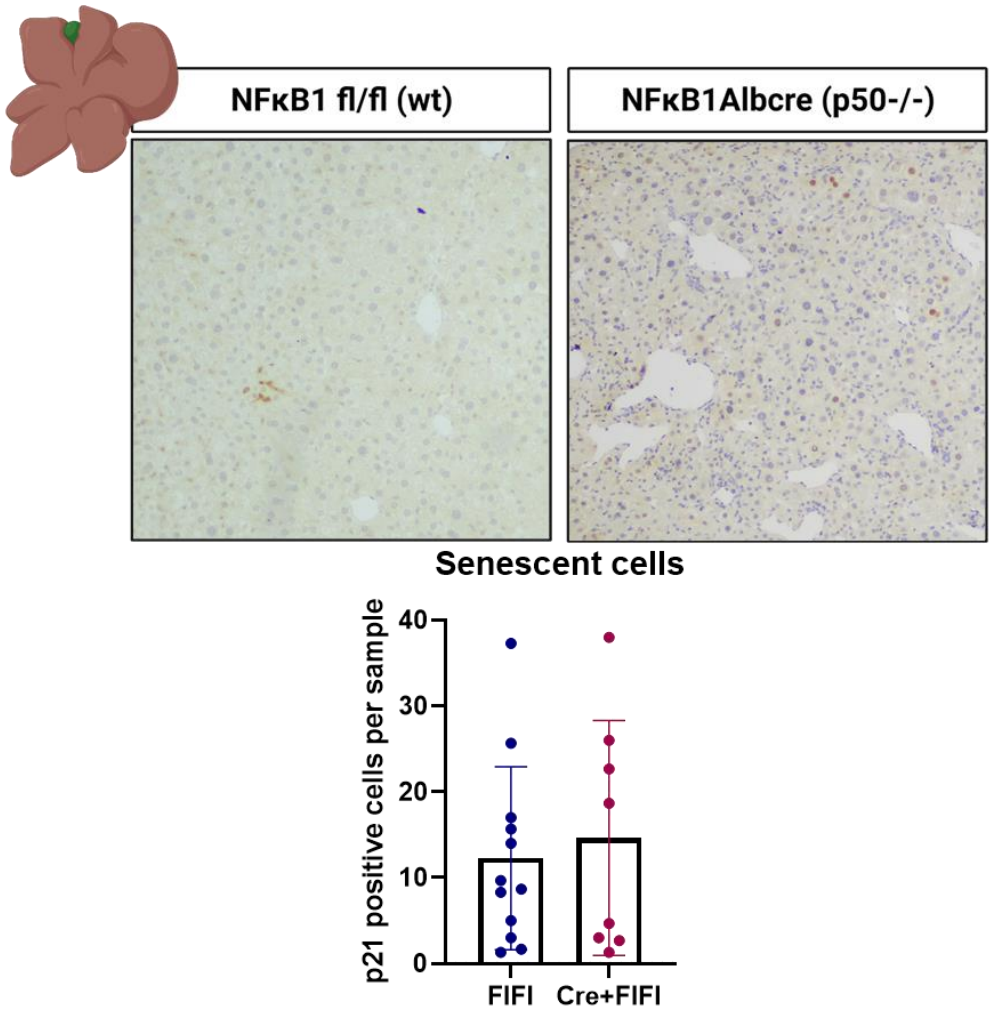

Figure 75. p21 staining in liver samples revealed that there was no difference in accumulation of senescent cells when comparing aged Nfκb1$^{flox/flox}$ and Nfκb1$^{flox/flox}$ AlbCre+ mice.

The staining against p21 was not successful in the kidneys, so I decided to use the same antibody to detect p21 in kidney protein samples in a western blot.

Very interestingly, western blot analyses in the kidneys showed an overall greater accumulation of p21 in Nfκb1$^{flox/flox}$ AlbCre+ samples when compared to the wt (Figure 76), but also great variability in samples from Nfκb1$^{flox/flox}$ mice. In particular three samples presented p21 levels comparable to Nfκb1$^{flox/flox}$ AlbCre+ samples (bottom gel, sixth, ninth and tenth lane), and one resulted in a fainter band compared to other

samples of the same genotype (bottom gel, fifth lane). p16 showed a similar variability, as there was a considerable difference in signal between samples from Nfκb1$^{flox/flox}$ kidneys (Figure 76). It would be interesting to characterise this further, and in particular it would be useful to either run the western blot again to confirm the results, or new samples should be added in order to increase the samples pool and the chance to obtain conclusive and clear results.

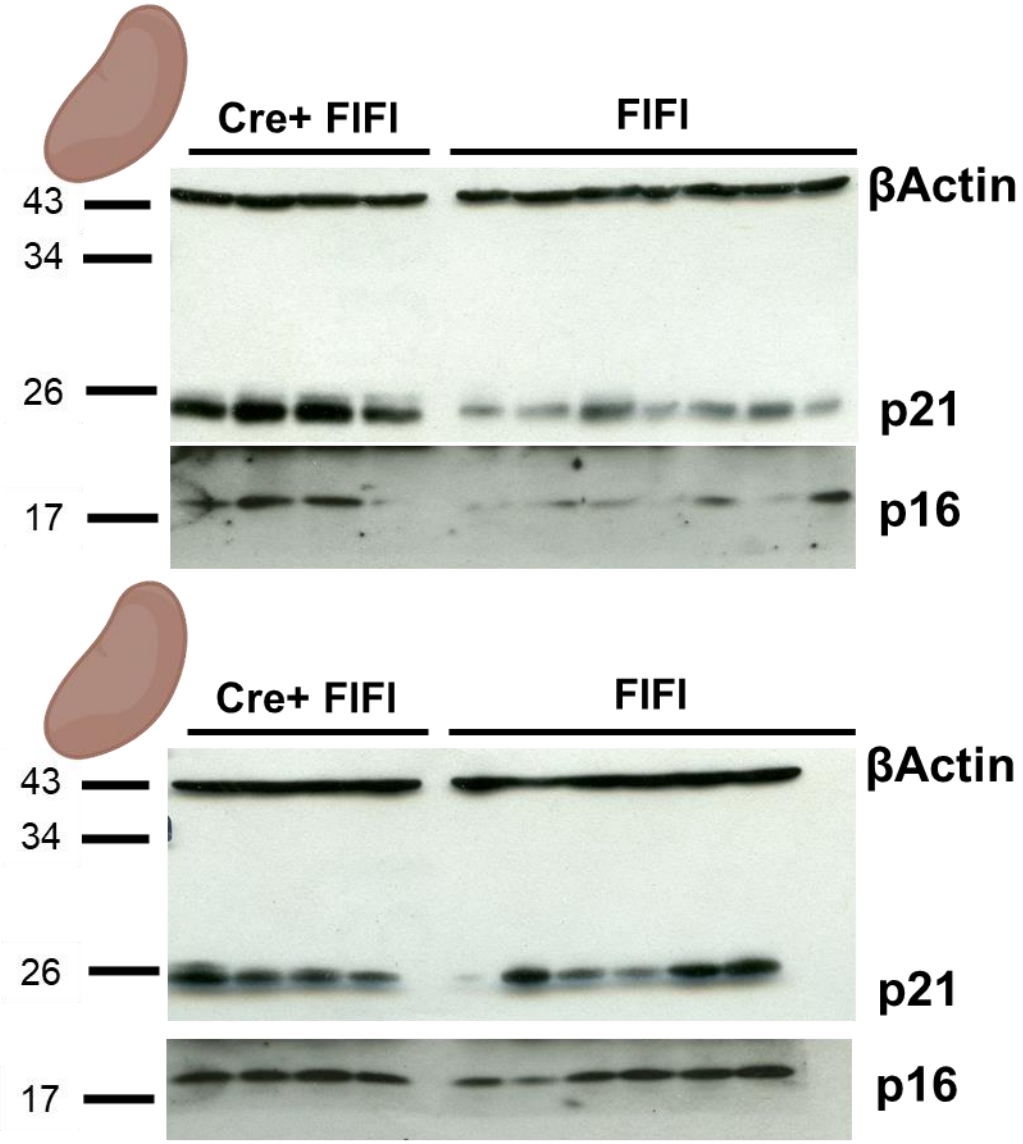

Figure 76. Western blot analyses for p21 and p16 in kidney samples from aged Nfκb1$^{flox/flox}$ and Nfκb1$^{flox/flox}$ AlbCre+ mice. The results seemed to suggest a greater expression of p21 in Nfκb1$^{flox/flox}$ AlbCre+ kidney samples, however some variability in the detected signal was observed in Nfκb1$^{flox/flox}$ samples. A similar output has been observed in p16 levels, making it hard to draw any conclusion. Overall, no difference seemed to result at p16 protein levels when comparing the two genotypes.

5.8. 3 month old mice did not present any differences between genotypes

Lastly, we wanted to determine the temporal development of the phenotype observed in Nfκb1$^{flox/flox}$ AlbCre+ mice, and in particular the time point when the livers and the kidneys start displaying damage. Based on the development of mice, we decided to investigate the phenotype at 3 months of age, since it is considered the point at which mice become mature adult (Flurkey, Currer and Harrison, 2007).

As presented in figure 77, a cohort of 6 Nfκb1$^{flox/flox}$ and 4 Nfκb1$^{flox/flox}$ AlbCre+ mice were aged until 3 months of age.

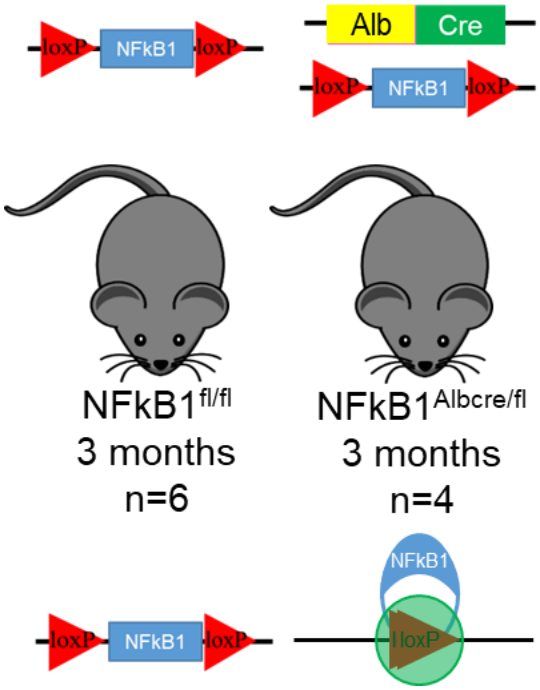

Figure 77. Graphic representation of the experiment involving 3 months old mice from both Nfκb1$^{flox/flox}$ and Nfκb1$^{flox/flox}$ AlbCre+ strains.

First, we looked at livers and kidneys, considering the results obtained in the 19 months old, aged model. No macroscopic differences could be observed in H&E sections of liver and kidney samples at this stage; also, similarly to what was found in 19 months old mice, the organ/body weight ratios were consistent between the genotypes for both liver and kidney (Figure 78).

Next, we investigated whether there were differences in immune cells present in both livers and kidneys at this stage.

In the livers, staining for T and B cells did not highlight any differences in numbers or pattern of aggregations between the two genotypes (Figure 79). Similar results were also obtained in kidney samples, where similar number of immune cells foci were found in both genotypes (Figure 80).

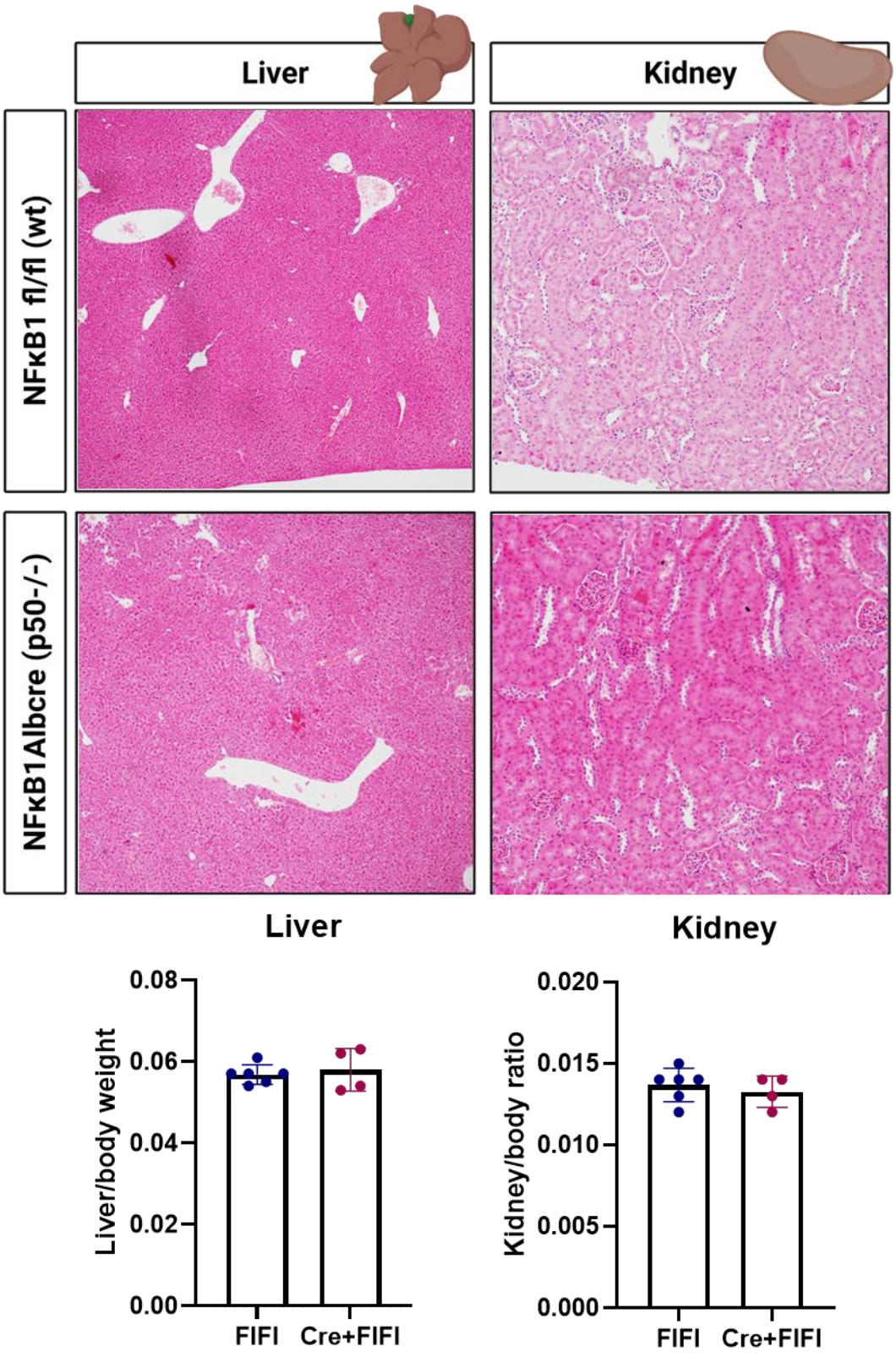

Figure 78. H&E sections from 3 months old Nfκb1$^{flox/flox}$ and Nfκb1$^{flox/flox}$ AlbCre+ mice. At a macroscopical level, no difference in structure or architecture was found when comparing livers and kidneys from the two genotypes. Also, organ/body weight ratios were consistent between Nfκb1$^{flox/flox}$ and Nfκb1$^{flox/flox}$ AlbCre+ mice.

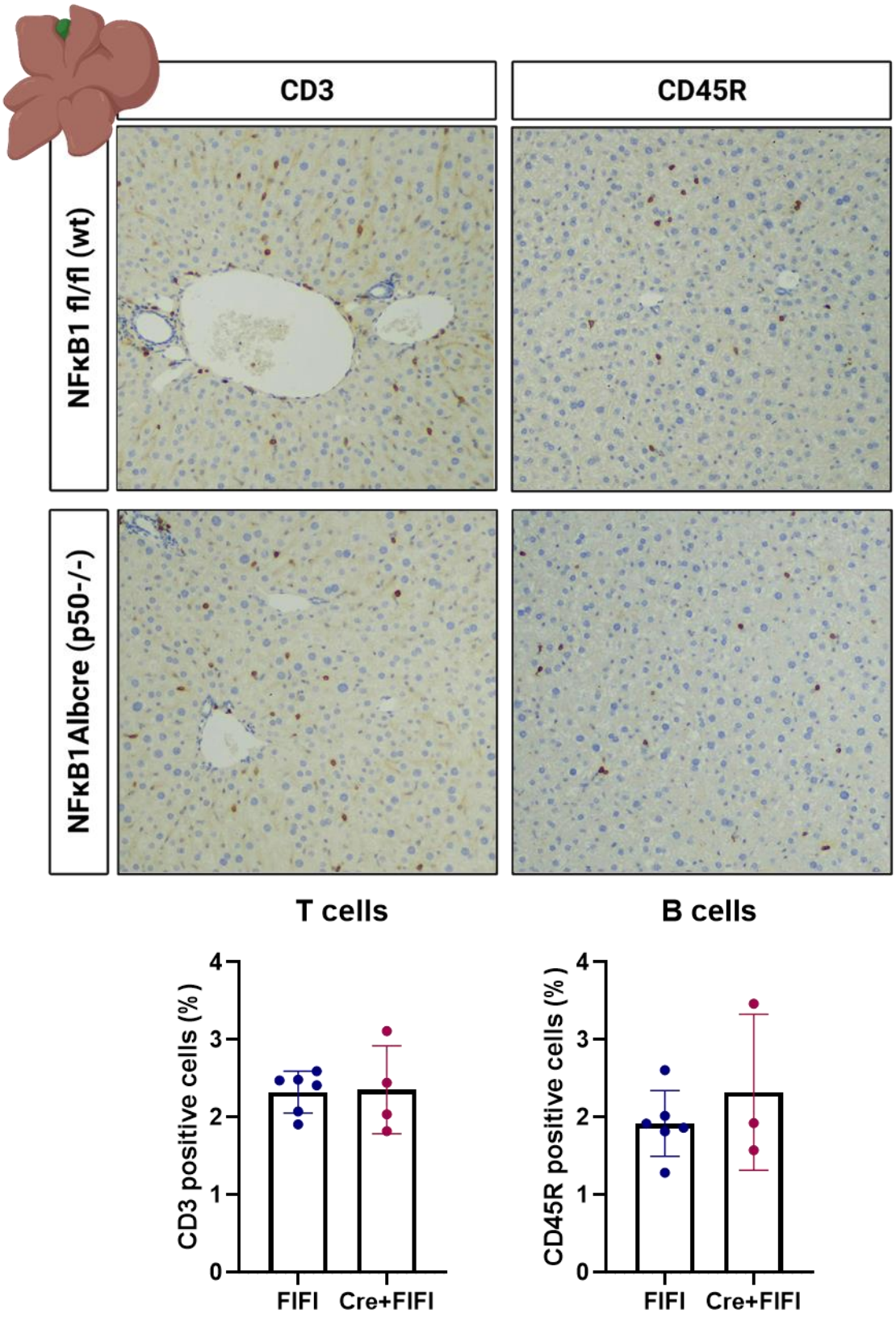

Figure 79. Staining for immune cells markers in livers from 3 months old Nfκb1$^{flox/flox}$ and Nfκb1$^{flox/flox}$ AlbCre+ mice. No differences were found in either number of immune cells in the tissue or pattern of aggregation, for both cell populations.

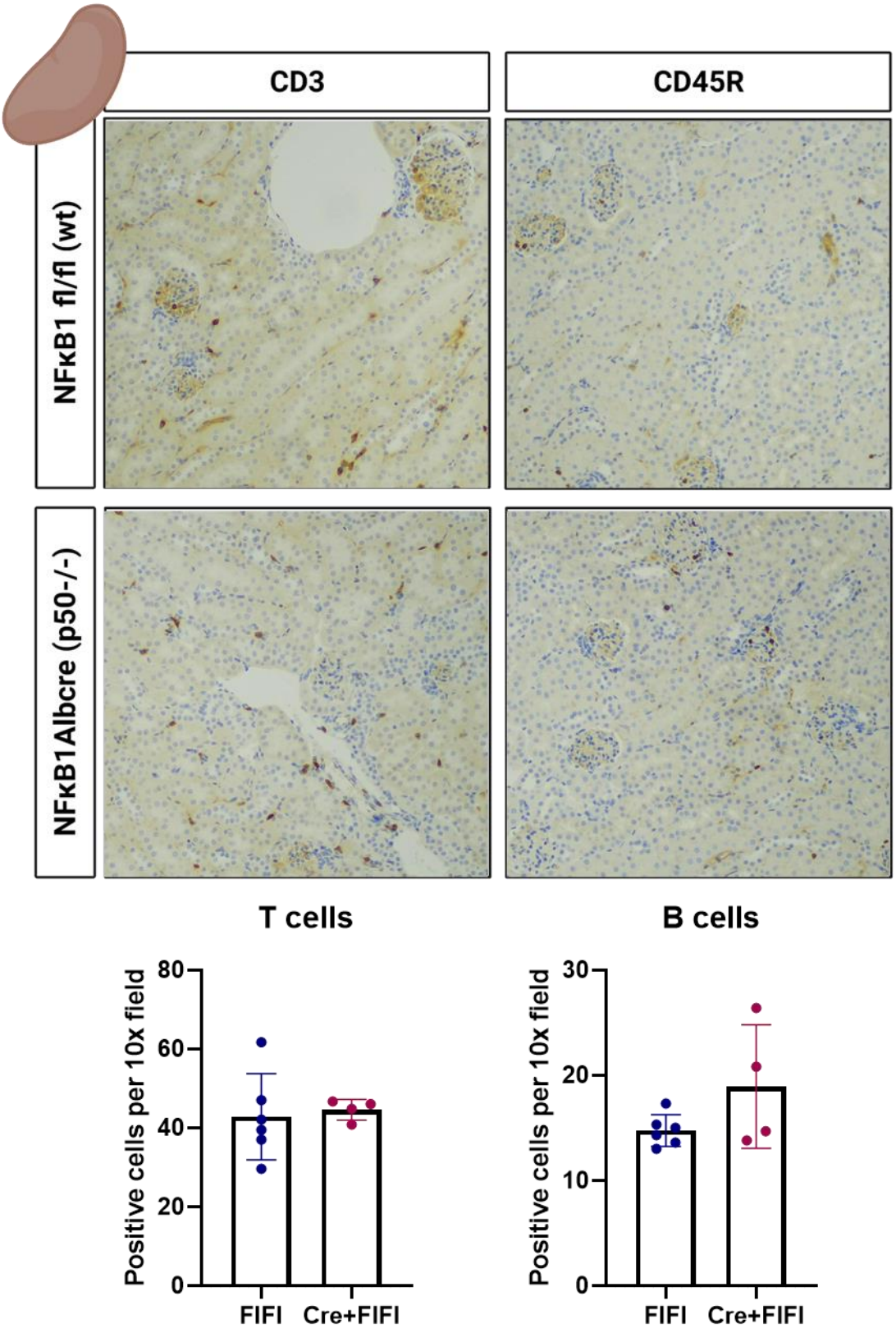

Figure 80. Staining for immune cells markers in kidneys from 3 months old Nfκb1$^{flox/flox}$ and Nfκb1$^{flox/flox}$ AlbCre+ mice. No differences were found in either number of immune cells in the tissue or pattern of aggregation, for both cell populations.

5.9. Discussion

Previous ageing models using nfκb1$^{-/-}$ mice showed that by lacking the anti – inflammatory NFκB subunit p50 mice aged faster and presented a more inflamed phenotype compared to their wt littermates (Jurk *et al.*, 2014).

Here we used Nfκb1$^{flox/flox}$ AlbCre+ mice in order to dissect the contribution of hepatic p50 to the ageing and inflammageing process.

50% of Nfκb1$^{flox/flox}$ AlbCre+ accumulated more fat in the livers and they displayed a greater presence of immune cells aggregates. For their position in the tissue and for the cell populations found in those cluster, they resembled ectopic lymphoid structures, that in the case of the liver correlates with HCC (Finkin *et al.*, 2015). Surprisingly, aged Nfκb1$^{flox/flox}$ AlbCre+ did not develop tumours. Also, no sign of predisposition to tumour growth was found but further experiments would be required in order to exclude LTβ – dependent mechanisms for infiltrates generation in the liver tissues.

Interestingly, the same Nfκb1$^{flox/flox}$ AlbCre+ mice that developed the phenotype in the liver, also presented damage in the kidneys, despite expressing p50; no damage was found in the kidneys from the control mice. No differences in immune cells number or pattern of aggregation were found in kidneys from Nfκb1$^{flox/flox}$ AlbCre+.

However, when investigating for senescence markers in livers and kidneys, 50% of Nfκb1$^{flox/flox}$ AlbCre+ presented an increased number of p21 positive cells. Also, Nfκb1$^{flox/flox}$ AlbCre+ kidneys were investigated for p21 and p16, as markers of senescence, but future experiments would be required to confirm the results.

However, the working theory hypothesised so far is represented in figure 81. By lacking p50, hepatocytes secrete more inflammatory cues and SASPs as the mouse ages, spreading senescence in a paracrine fashion and damaging the tissue and themselves. Through the blood stream, these factors are probably delivered to the

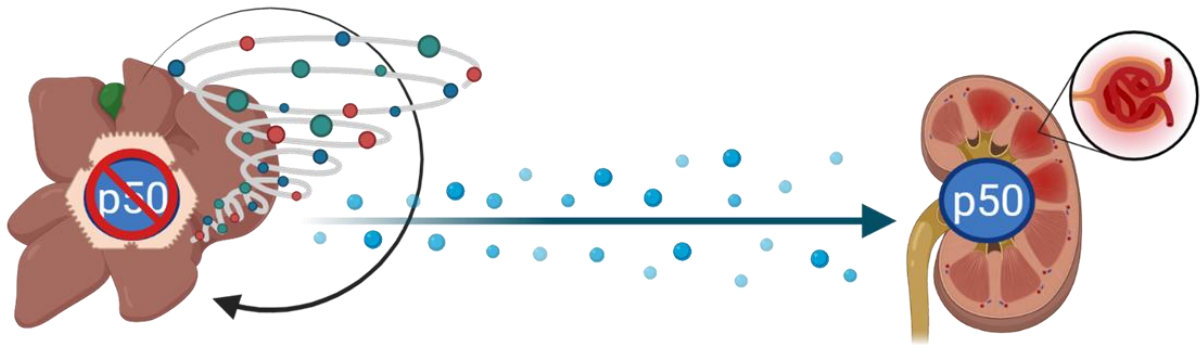

Figure 81. Working hypothesis based on the results obtained so far. By lacking p50, hepatocytes are more inflamed and as the mouse ages, they promote the onset of inflammageing and senescence, which is systemically spread to the kidneys, resulting in damage and senescence.

kidneys, that are damaged and make more senescence compared to control mice, despite expressing nfκb1.

Future experiments should revolve around the investigation of the soluble factors responsible and the definition of the timeline of the progression to this phenotype. It would be useful to take blood and urine at specific time points, as the mouse ages, in order to study the kidney functionality and the soluble factors present in the bloodstream as the phenotype progresses (Figure 82).

This should help elucidating the mechanism by which hepatic p50 is likely to exert a systemic role in inflammation and inflammageing.

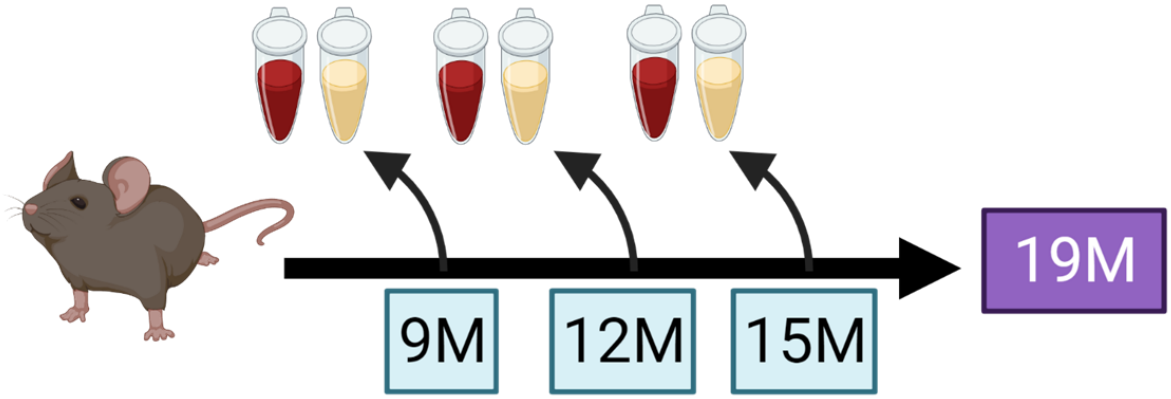

Figure 82. Proposed follow – up experiment in order to characterise the kidney functionality with soluble markers and to define the timeline of the progression of the phenotype observed in aged Nfκb1$^{flox/flox}$ AlbCre+ mice.

Chapter 6. General discussion and conclusions

This work has provided insights into the role hepatic p50 plays in inflammation and ageing. By using a Cre – LoxP system to selectively knock out the *nfκb1* gene from hepatocytes, I obtained a mouse model to conditional remove p50 from a specific cell type to dissect its functions in isolated cells, within the tissue the cells belong to and systemically.

6.1. Hepatic p50 regulation on gene expression in acute inflammation

Discussed in chapter 3, I validated primary hepatocytes as *in vitro* model to study inflammation in the liver and in particular, I isolated primary cells from Nfκb1$^{flox/flox}$ AlbCre+/- mice to investigate how gene regulation was affected by the absence of p50 during an acute inflammatory response triggered by LPS. RNA seq data showed that under basal conditions, hepatocytes lacking p50 presented differential expression of genes involved in inflammation, metabolism and cell cycle, when compared to wt cells. After stimulation with LPS, p50-/- cells failed to repress the expression of a subset of inflammatory genes at the moment of resolution. This might indicate that p50, despite being part of the pro – inflammatory P65:p50 (Hayden and Ghosh, 2008), is dispensable for the onset of an acute inflammatory response, but it is necessary to dampen it after the initial trigger.

This phenotype was not found to be gender – dependent and interestingly, p50-/- cells isolated from *nfκb1*$^{-/-}$ mice showed a different trend from p50-/- hepatocytes isolated from Nfκb1$^{flox/flox}$ AlbCre+ mice, probably indicating that other cells present in the tissue might have educated and affected the gene expression in hepatocytes in a different fashion.

6.2. Acute inflammatory response in the tissue is not affected by the absence of hepatic p50

In addition to *in vitro* systems, research in the liver inflammation field has been focused on *ex vivo* models that could offer a more complex setting and open the way to personalised medicine and transplants. Here I validated Precision Cut Liver Slices (PCLS) as a model to study acute liver inflammation *ex vivo*; in particular I employed liver tissue from Nfκb1$^{flox/flox}$ AlbCre+/- mice to study how the absence of hepatic p50 affected the inflammatory response within the tissue, taking in consideration the presence of other cell types and a tissue – like organisation. I did not observe differences in targets gene expression between control and Nfκb1$^{flox/flox}$ AlbCre+ slices. However, greater number of immune cells was found in the slices of Nfκb1$^{flox/flox}$ AlbCre+ mice, including under basal conditions. This seemed to suggest that during

the acute response in the tissue, there must be some other mechanisms aiming to compensate for the lack of *nfκb1* in hepatocytes. In the attempt to conditionally eliminate p50 in hepatocytes at a desired time to investigate the resulting phenotype, infection of flox mice with AAV carrying the Cre enzyme proved to be an inconsistent tool, as gene expression of p50 in some samples was not abolish by the use of the adeno – associated virus. Also, the results obtained recapitulated what I have seen in Nfκb1$^{flox/flox}$ AlbCre+ slices, as no differences were found in trends upon LPS stimulation.

Lastly, slices isolated from total *nfκb1*$^{-/-}$ mice did not present differences in gene expression with wt cells during the acute event induced by LPS, very similarly to what observed in isolated primary liver cells.

6.3. Lack of hepatic p50 exacerbates the inflammageing process

Ageing is a physiological process which entails the decreasing functionality of cells and tissues (López-Otín *et al.*, 2013). As the individual ages, the immune system does not work efficiently anymore and the dysregulation of inflammatory process leads to the phenomenon of inflammageing, characterised by a low grade sterile chronic inflammation which exacerbates both inflammation and ageing, generating positive feedback (Fulop *et al.*, 2021). We wanted to investigate the role of hepatic nfκb1 in the ageing process. 50% of mice lacking hepatic p50 showed greater fat accumulation in the liver and presence of immune cells aggregates, resembling ectopic lymphoid structures. Interestingly, the kidneys from the same mice presented damage and loss of glomeruli architecture, despite expressing p50. Following results suggested increased levels of p21, a marker of senescence, in the damaged kidneys, leading to the hypothesis that the absence of hepatic p50 might be the cause of this systemic effect. I hypothesised that hepatocytes lacking p50 have an increased inflamed phenotype, but at the acute stage it did not seem to arise significant differences at the organ level and systemically. However, as the mouse ages, it is likely that the consistent and chronic secretion of inflammatory factors damage the tissue and the cells themselves, also spreading senescence. These factors are likely to be able to travel the blood stream and reach organs expressing p50 which are damaged regardless the presence of the protein.

6.4. Conclusions

Taken altogether, the results presented in this work provided new insights into the gene expression regulation that p50 exerts in a specific cell type, namely hepatocytes, in inflammation and ageing.

From previous work in *nfκb1-/-* mice, we learnt that global absence of p50 not only affects the overall health along the ageing process, but with specific attention to the liver, lack of p50 triggers spontaneous tumours growth and premature ageing and death (Jurk *et al.*, 2014). The interest in characterising nfκb1 role in hepatocytes arose from the idea that epithelial cells can educate and influence the activity of the resident immune cells in a specific tissue (Swamy *et al.*, 2010).

First, I wanted to test whether by lacking p50, hepatocytes would differ from control hepatocytes, because of the direct effects of p50 absence on gene expression. Primary hepatocytes without p50 displayed a more inflamed phenotype in a model of acute inflammation triggered by LPS and this led to the hypothesis that p50 is dispensable to initiate the response, but its presence in hepatocytes is necessary to limit inflammation. Next I carried on the characterisation of p50-/- hepatocytes response within the tissue of origin, allowing the interaction with other cells during acute inflammation. Interestingly, a different trend was observed when characterising this model, probably indicating that other anti – inflammatory mechanisms might be at play in order to compensate for the reduced ability of Nfκb1$^{flox/flox}$ AlbCre+ hepatocytes to limit inflammation in an acute event. An ageing model using Nfκb1$^{flox/flox}$ AlbCre+/- mice might have clarified the role of hepatic p50 in chronic events and in particular that p50 absence has effect in the longer term, rather than at the acute stage. In fact, chronic inflammation during the ageing process might be the source of the remarkable differences between Nfκb1$^{flox/flox}$ and Nfκb1$^{flox/flox}$ AlbCre+ mice, in the liver and systemically. Hepatocytes lacking *nfκb1* might assume a more inflamed and senescent phenotype along the aging process, and these two events exacerbate each other. The damage could then be transferred through the bloodstream to other organs expressing p50, but still displaying damage and possibly loss of function. This phenotype was observed in 50% of the total Nfκb1$^{flox/flox}$ AlbCre+ mice, possibly explained by a different penetrance of the phenotype which arose these heterogenous results.

6.5. Future work

Despite having elucidated a possible systemic role for hepatic *nfκb1* in inflammation and ageing, the mechanisms underlying the phenotype have to be elucidated yet.

In particular, future experiments should aim to combine epigenome profiles with RNA seq analyses from primary hepatocytes isolated from Nfκb1$^{flox/flox}$ AlbCre+ mice, to infer whether the differential gene expression upon both unstimulated and stimulated conditions could be explained by direct effect of p50 on epigenetic modifications at the gene promoters, or by affecting other downstream effectors. Also, the samples pool

should be increased, especially for the RNA sequencing, since the data analysis pointed out at a great variability between samples, despite being from the same genotype. This could be explained by the stress hepatocytes face during the isolation process and how they response to it, and by increasing the number of samples this effect could be limited or decreased.

Within the same model, future directions should also revolve around exploring other epigenetic modifiers or co - factors in general that p50 homodimers are able to recruit. Preliminary *in vitro* data showed that by tagging two p50 proteins with two different tags (FLAG and STREP), it was possible to proceed to a two steps co – immunoprecipitation (TIP) (Sciuto *et al.*, 2018) to selectively pull down only p50 homodimers (Figure 83). Following steps should include scaling up to get enough material to be sent to Mass Spectrometry analyses, with the aim to find novel interactors of p50 homodimers. The same system could then be used in Chromatin

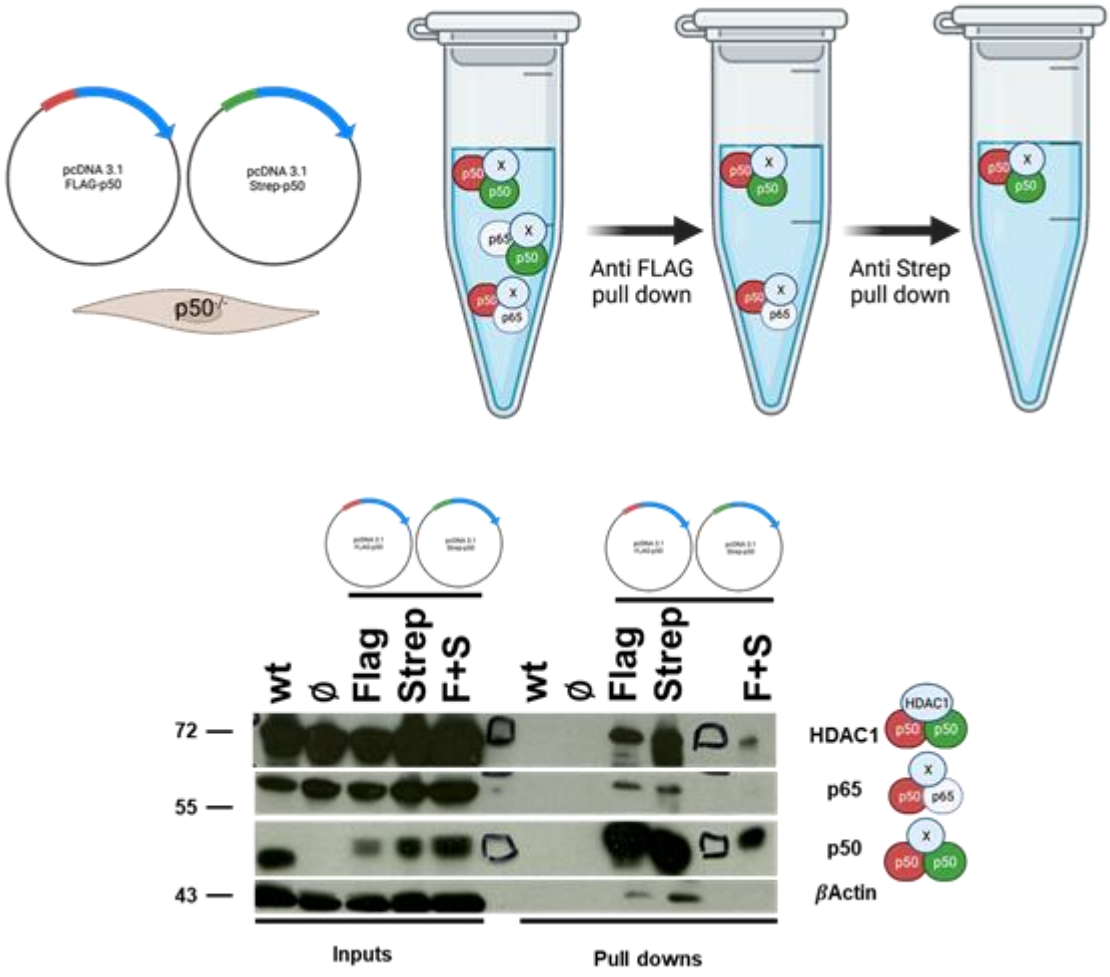

Figure 83. Graphic representation of the experimental setup for TIP and preliminary data. p50-/- murine embryonic fibroblast (MEFs) were transfected with two plasmids, carrying p50 – FLAG and p50 – STREP in a pcDNA3.1 vector. Two consecutive pull downs allowed to isolate p50 homodimers only, as presented in the western blot panel.

Immunoprecipitation (ChIP) assays and sent to sequencing to get a genome view of p50 homodimers targets, under different conditions.

Moreover, in this work I focused my attention on the acute inflammatory response, but the results from the ageing model highlighted that severe effects might be taking place further down the timeline. The PCLS model could offer a longer time span, up to 7 days (Paish *et al.*, 2019), which could open up the chance to treat slices from Nfκb1$^{flox/flox}$ AlbCre+ mice for longer and see whether the phenotype differs from the one previously observed in the acute inflammation model.

Lastly, the ageing model would require further characterisation; in particular, it would be interesting to investigate whether the gene expression of Nfκb1$^{flox/flox}$ AlbCre+ hepatocytes could be influenced by the immune cell aggregates that were found within

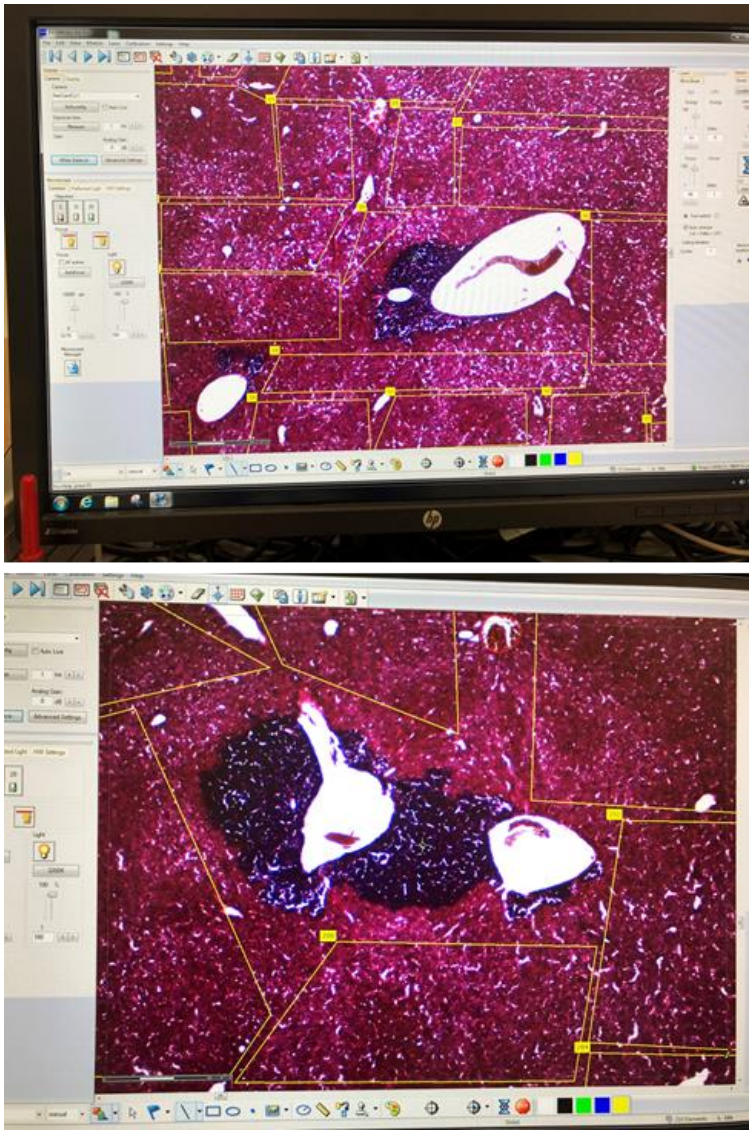

Figure 84. Screenshots representing the laser capture procedure on H&E livers slides. After selection and collection of the regions of interest, RNA isolation is obtained and could be either used for qRT – PCR validation or for RNA sequencing.

the tissue. To study this, I initially isolated RNA from specific tissue regions close to the immune infiltrates after laser capture technique, in order to send them to sequencing (Figure 84).

Moreover, I would be interest in quantifying soluble outputs in the serum to determine kidney functionality and senescence – associated phenotype, and their expression along the ageing process. Certainly, more mice should be also added to the samples pool, in order to confirm the phenotype observed and clarified some unconclusive results, including quantification of LTβ and senescence markers. Treatments with senolytic could also clarify whether the phenotype is caused by accumulation of senescent cells in the tissues or whether other possible mechanisms need to be explored.

These findings would contribute to gain a deeper knowledge of the processes involved in chronic inflammation and ageing, opening up to new therapeutical approaches to the inflammageing phenomenon.

Chapter 7. Appendices

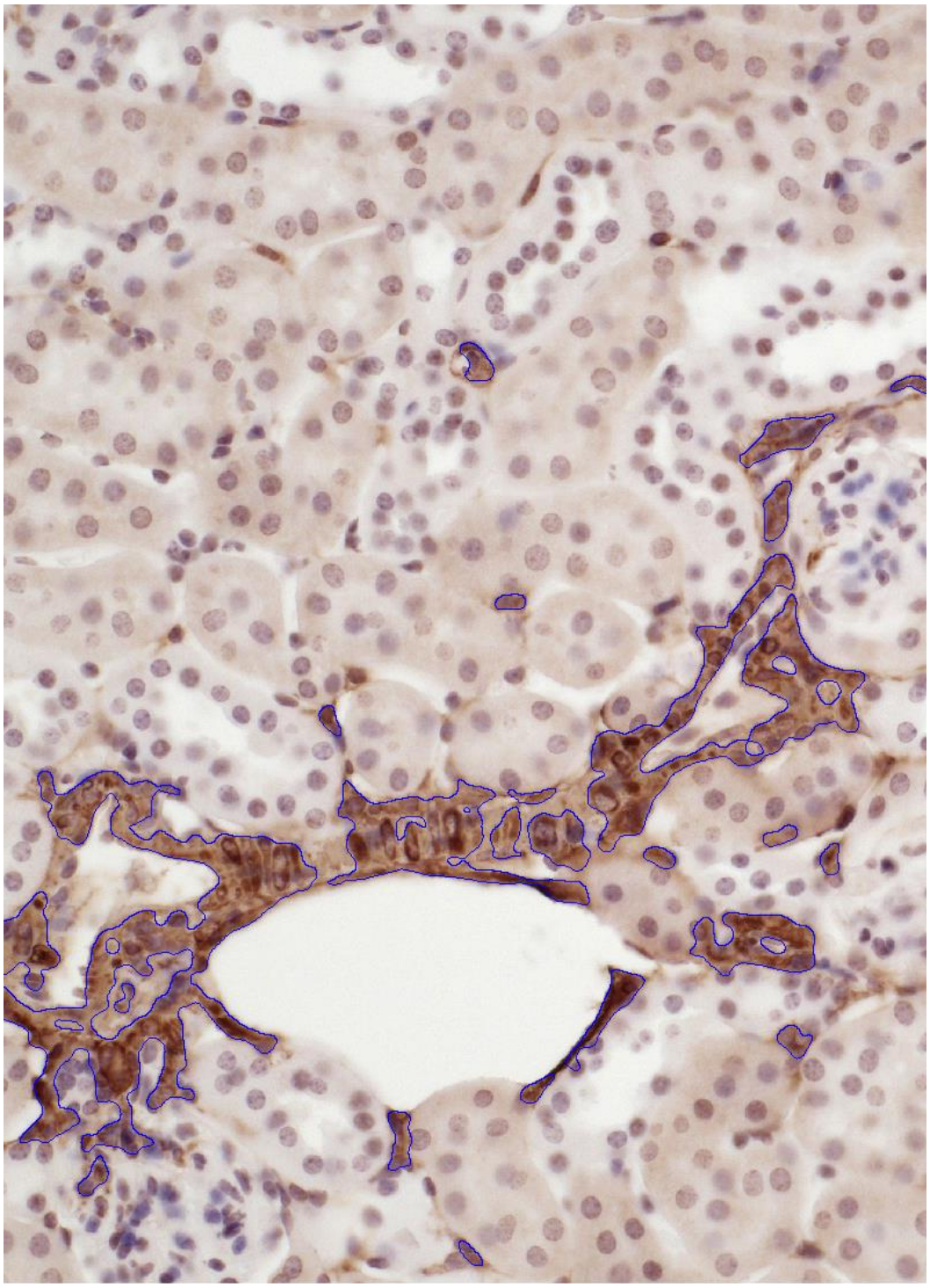

Figure 85. Screenshot of αSMA quantification in aged kidneys using a threshold on NIS-Elements BR analysis software (NIS-Elements Br, Nikon, UK). The area quantified as positive is marked by a blue line.

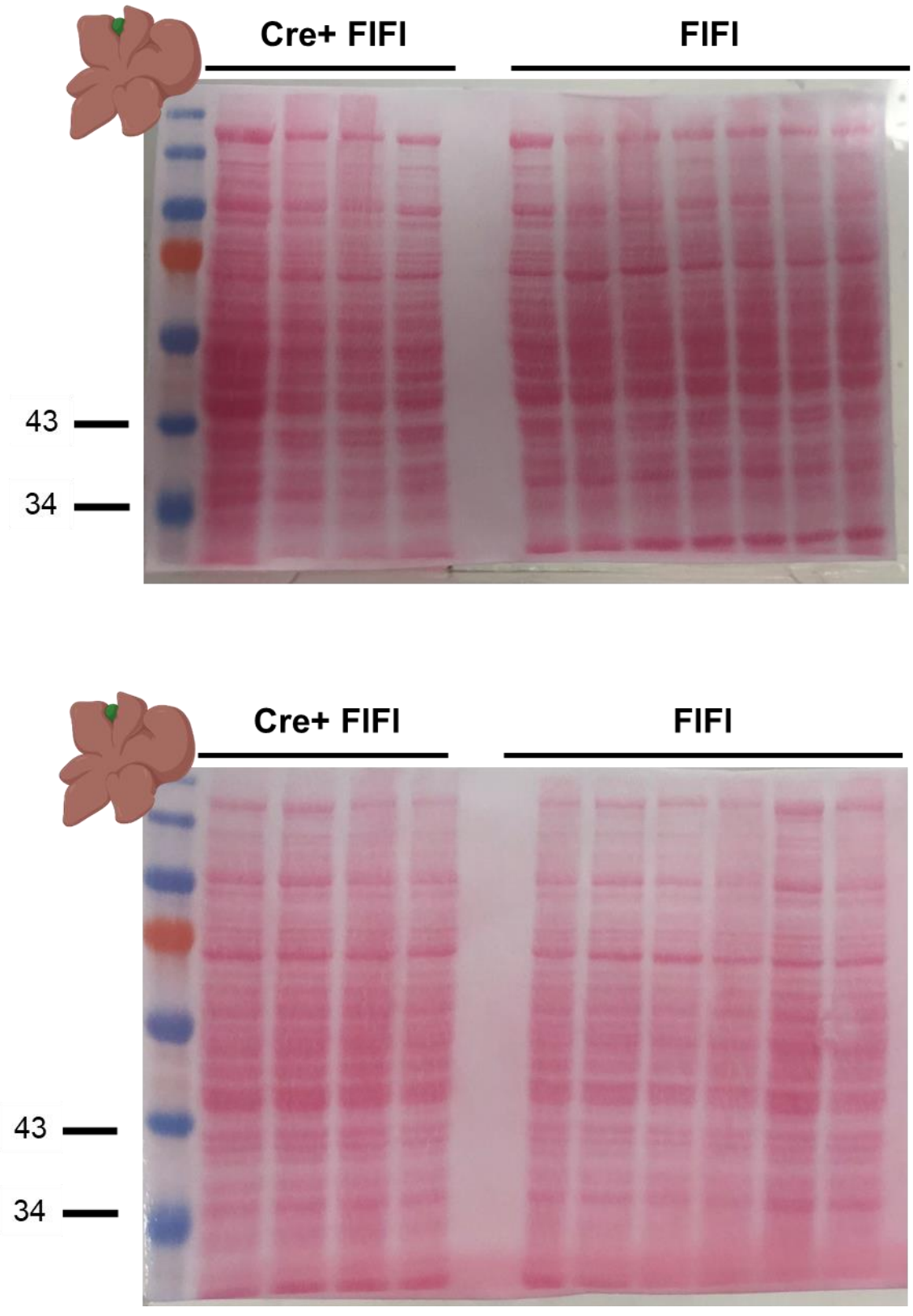

Figure 86. Ponceau staining after wet transfer for western blot in aged livers, looking at LTβ.

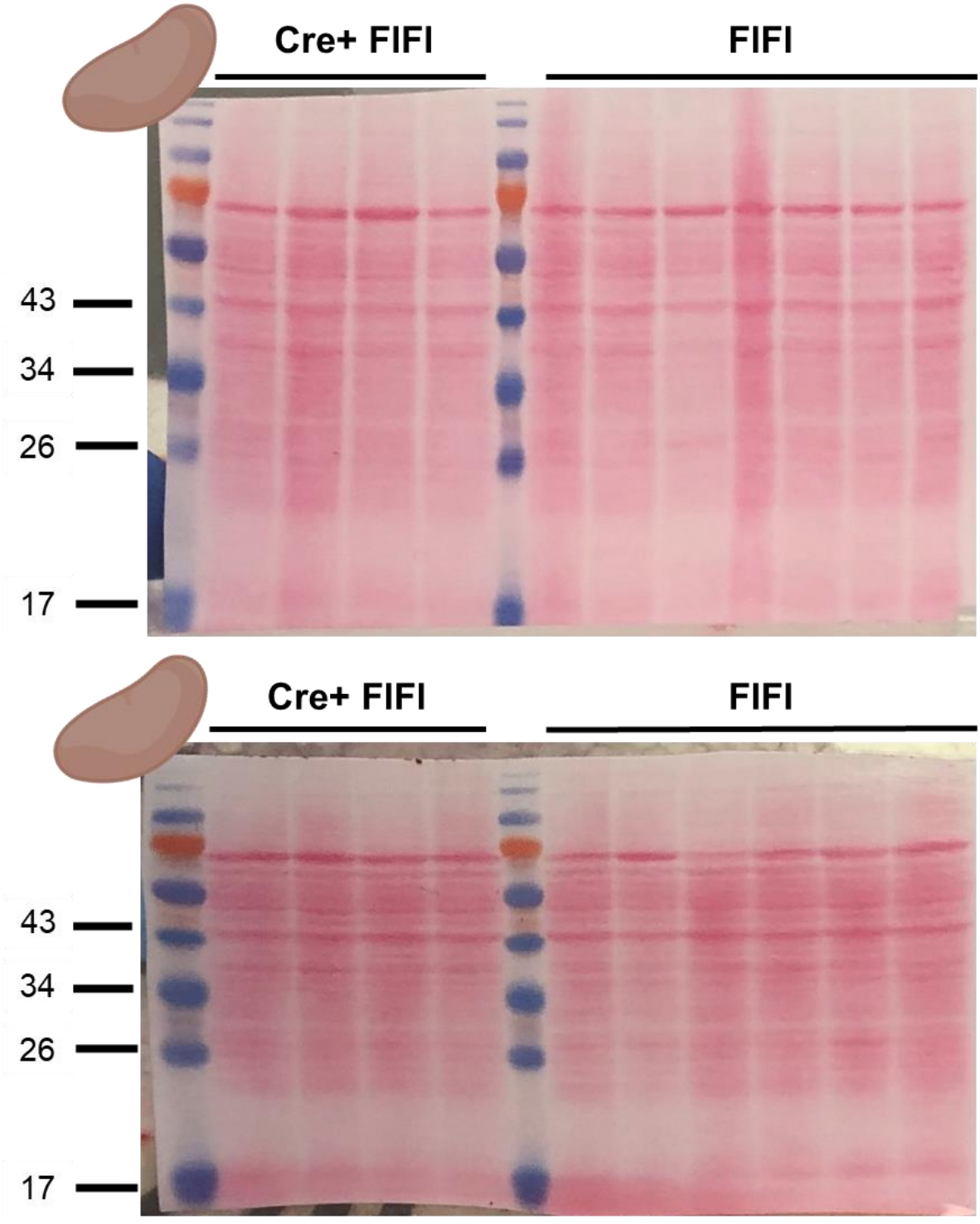

Figure 87. Ponceau staining after wet transfer for western blot in aged kidneys, looking at senescence markers.

References

Abramson, J. and Anderson, G. (2017) ‘Thymic Epithelial Cells’. Available at: https://doi.org/10.1146/annurev-immunol.

Aloisi, F. and Pujol-Borrell, R. (2006) ‘Lymphoid neogenesis in chronic inflammatory diseases’, Nature Reviews Immunology, pp. 205–217. Available at: https://doi.org/10.1038/nri1786.

Antoniou, A. et al. (2003) ‘Average risks of breast and ovarian cancer associated with BRCA1 or BRCA2 mutations detected in case Series unselected for family history: a combined analysis of 22 studies’, Am. J. Hum. Genet, 72, pp. 1117–1130.

Arisawa, T. et al. (2013) ‘Functional promoter polymorphisms of NFKB1 influence susceptibility to the diffuse type of gastric cancer’, Oncology Reports, 30(6), pp. 3013–3019. Available at: https://doi.org/10.3892/or.2013.2768.

Armstrong, L. (2011) ‘Post-Translation modification of histones’, in Epigenetics. Taylor and Francis.

Bai, C., Sen, P. and Hofmann, K. (1996) SKP1 Connects Cell Cycle Regulators to the Ubiquitin Proteolysis Machinery through a Novel Motif, the F-Box, Cell.

Baldwin, A.S. (1996) THE NF-κB AND IκB PROTEINS: New Discoveries and Insights, Annu. Rev. Immunol. Available at: www.annualreviews.org.

Bataller, R. and Brenner, D.A. (2005) ‘Liver fibrosis’, Journal of Clinical Investigation, 115(2), pp. 209–218. Available at: https://doi.org/10.1172/JCI200524282.

Beg, A.A. et al. (1995) ‘Embryonic lethality and liver degeneration in mice lacking the RelA component of NF-KB’, Nature, 376(6536), pp. 167–170.

Beinke, S. et al. (2003) ‘NF-κB1 p105 Negatively Regulates TPL-2 MEK Kinase Activity’, Molecular and Cellular Biology, 23(14), pp. 4739–4752. Available at: https://doi.org/10.1128/mcb.23.14.4739-4752.2003.

Belich, M.P. et al. (1999) ‘TPL-2 kinase regulates the proteolysis of the NF-kBinhibitory protein NF-kB1 p105’, Nature, pp. 363–368.

Bell, C.C. et al. (2016) ‘Characterization of primary human hepatocyte spheroids as a model system for drug-induced liver injury, liver function and disease’, Scientific Reports, 6. Available at: https://doi.org/10.1038/srep25187.

Benitez, P.C.A. et al. (2020) ‘Hepatic stellate cells and hepatocytes as liver antigen-presenting cells during B. Abortus infection’, Pathogens, 9(7), pp. 1–14. Available at: https://doi.org/10.3390/pathogens9070527.

Ben-Neriah, Y. (2002) Regulatory functions of ubiquitination in the immune system Ubiquitin-mediated protein modification. Available at: http://immunol.nature.com.

Bernal, G.M. et al. (2014) ‘Loss of Nfkb1 leads to early onset aging’, Aging, 6(11), pp. 931–942. Available at: https://doi.org/https://doi.org/10.18632/aging.100702.

Bernhard Moser, B. et al. (1990) Materials and Methods Brief Definitive Report NEUTROPHIL-ACTIVATING PROPERTIES OF THE MELANOMA GROWTH-

STIMULATORY ACTIVITY. Available at: http://rupress.org/jem/article-pdf/171/5/1797/1100497/1797.pdf.

Bessette, H. et al. (1992) ‘p53, guardian of the genome’, Nature, 358, pp. 15–16.

Bianchi, A. et al. (2021) ‘Moderate Exercise Inhibits Age-Related Inflammation, Liver Steatosis, Senescence, and Tumorigenesis’, The Journal of Immunology, 206(4), pp. 904–916. Available at: https://doi.org/10.4049/jimmunol.2001022.

Boess, F. et al. (2003) ‘Gene expression in two hepatic cell lines, cultured primary hepatocytes, and liver slices compared to the in vivo liver gene expression in rats: Possible implications for toxicogenomics use of in vitro systems’, Toxicological Sciences, 73(2), pp. 386–402. Available at: https://doi.org/10.1093/toxsci/kfg064.

Bomble, M. et al. (2010) ‘Analysis of antigen-presenting functionality of cultured rat hepatic stellate cells and transdifferentiated myofibroblasts’, Biochemical and Biophysical Research Communications, 396(2), pp. 342–347. Available at: https://doi.org/10.1016/j.bbrc.2010.04.094.

Bonizzi, G. and Karin, M. (2004) ‘The two NF-κB activation pathways and their role in innate and adaptive immunity’, Trends in Immunology, pp. 280–288. Available at: https://doi.org/10.1016/j.it.2004.03.008.

Boro, M. and Balaji, K.N. (2017) ‘CXCL1 and CXCL2 Regulate NLRP3 Inflammasome Activation via G-Protein–Coupled Receptor CXCR2’, The Journal of Immunology, 199(5), pp. 1660–1671. Available at: https://doi.org/10.4049/jimmunol.1700129.

Brunt, E.M. et al. (1999) Nonalcoholic Steatohepatitis: A Proposal for Grading and Staging the Histological Lesions.

Bulavin, D. v et al. (2003) Dual phosphorylation controls Cdc25 phosphatases and mitotic entry, NATURE CELL BIOLOGY.

Burke, S.J. et al. (2015) ‘CCL20 is elevated during obesity and differentially regulated by NF-κB subunits in pancreatic β-cells’, Biochimica et Biophysica Acta - Gene Regulatory Mechanisms, 1849(6), pp. 637–652. Available at: https://doi.org/10.1016/j.bbagrm.2015.03.007.

Burkly, L. et al. (1995) ‘Expression of relB is required for the development of thymic medulla and dendritic cells’, Nature, 373, pp. 531–536.

Buyl, K. et al. (2015) ‘Measurement of albumin secretion as functionality test in primary hepatocyte cultures’, Methods in Molecular Biology, 1250, pp. 303–308. Available at: https://doi.org/10.1007/978-1-4939-2074-7_22.

Carmody, R.J. et al. (2007) Negative Regulation of Toll-Like Receptor Signaling by NF-kB p50 Ubiquitination Blockade. Available at: https://doi.org/DOI: 10.1126/science.1142953.

Carragher, D.M., Rangel-Moreno, J. and Randall, T.D. (2008) ‘Ectopic lymphoid tissues and local immunity’, Seminars in Immunology, pp. 26–42. Available at: https://doi.org/10.1016/j.smim.2007.12.004.

Cartwright, T., Perkins, N.D. and L Wilson, C. (2016) 'NFKB1: a suppressor of inflammation, ageing and cancer', The FEBS journal, pp. 1812–1822. Available at: https://doi.org/10.1111/febs.13627.

Cartwright, T.N. et al. (2018) 'HDAC1 interacts with the p50 NF-κB subunit via its nuclear localization sequence to constrain inflammatory gene expression', Biochimica et Biophysica Acta - Gene Regulatory Mechanisms, 1861(10), pp. 962–970. Available at: https://doi.org/10.1016/j.bbagrm.2018.09.001.

Casadio, F. et al. (2013) 'H3R42me2a is a histone modification with positive transcriptional effects', Proceedings of the National Academy of Sciences of the United States of America, 110(37), pp. 14894–14899. Available at: https://doi.org/10.1073/pnas.1312925110.

Caviglia, J.M. et al. (2017) 'MicroRNA-21 and Dicer Are Dispensable for Hepatic Stellate Cell Activation and the Development of Liver Fibrosis'. Available at: https://doi.org/10.1002/hep.29627/suppinfo.

Chen, Y. et al. (2015) 'The NFKB1 polymorphism (rs4648068) is associated with the cell proliferation and motility in gastric cancer', BMC Gastroenterology, 15(1). Available at: https://doi.org/10.1186/s12876-015-0243-0.

Cheng, C.W. et al. (2013) 'Effects of NFKB1 and NFKBIA Gene Polymorphisms on Hepatocellular Carcinoma Susceptibility and Clinicopathological Features', PLoS ONE, 8(2). Available at: https://doi.org/10.1371/journal.pone.0056130.

Cho, Y.C. et al. (2015) 'Cell cycle-dependent Cdc25C phosphatase determines cell survival by regulating apoptosis signal-regulating kinase 1', Cell Death and Differentiation, 22(10), pp. 1605–1617. Available at: https://doi.org/10.1038/cdd.2015.2.

Collins, P.E. et al. (2015) 'Mapping the interaction of B Cell Leukemia 3 (BCL-3) and Nuclear Factor κB (NF-κB) p50 identifies a BCL-3-mimetic anti-inflammatory peptide', Journal of Biological Chemistry, 290(25), pp. 15687–15696. Available at: https://doi.org/10.1074/jbc.M115.643700.

Collins, P.E. et al. (2019) 'The IκB-protein BCL-3 controls Toll-like receptor-induced MAPK activity by promoting TPL-2 degradation in the nucleus', PNAS [Preprint]. Available at: https://doi.org/10.1073/pnas.1900408116/-/DCSupplemental.

Corsiero, E. et al. (2016) 'Ectopic lymphoid structures: Powerhouse of autoimmunity', Frontiers in Immunology. Frontiers Media S.A. Available at: https://doi.org/10.3389/fimmu.2016.00430.

Cunningham-Rundles, C. (2012) 'The many faces of common variable immunodeficiency', Hematology [Preprint]. Available at: http://ashpublications.org/hematology/article-pdf/2012/1/301/1501831/bep00112000301.pdf.

Curthoys, N.P. (2001) Glutamine Metabolism: Nutritional and Clinical Significance Role of Mitochondrial Glutaminase in Rat Renal Glutamine Metabolism 1,2. Available at: https://academic.oup.com/jn/article/131/9/2491S/4687534.

D’Angiolella, V., Esencay, M. and Pagano, M. (2013) ‘A cyclin without cyclin-dependent kinases: Cyclin F controls genome stability through ubiquitin-mediated proteolysis’, Trends in Cell Biology, pp. 135–140. Available at: https://doi.org/10.1016/j.tcb.2012.10.011.

Dé Ric Ché, F., Lieber, M.R. and Hsieh, C.-L. (2002) ‘The DNA methyltransferase-like protein DNMT3L stimulates de novo methylation by Dnmt3a’, PNAS [Preprint]. Available at: https://www.pnas.org.

Delatte, B., Deplus, R. and Fuks, F. (2014) ‘ Playing TET ris with DNA modifications ’, The EMBO Journal, 33(11), pp. 1198–1211. Available at: https://doi.org/10.15252/embj.201488290.

Deplus, R. et al. (2002) ‘Dnmt3L is a transcriptional repressor that recruits histone deacetylase’, Nucleic Acid Research [Preprint].

Dhanasekaran, R., Bandoh, S. and Roberts, L.R. (2016) ‘Molecular pathogenesis of hepatocellular carcinoma and impact of therapeutic advances [version 1; referees: 4 approved]’, F1000Research. Faculty of 1000 Ltd. Available at: https://doi.org/10.12688/F1000RESEARCH.6946.1.

Dieu-Nosjean, M.-C. et al. (2000) Macrophage Inflammatory Protein 3 Is Expressed at Inflamed Epithelial Surfaces and Is the Most Potent Chemokine Known in Attracting Langerhans Cell Precursors, J. Exp. Med. Available at: http://www.jem.org/cgi/content/full/192/5/705.

Diril, M.K. et al. (2012) ‘Cyclin-dependent kinase 1 (Cdk1) is essential for cell division and suppression of DNA re-replication but not for liver regeneration’, Proceedings of the National Academy of Sciences of the United States of America, 109(10), pp. 3826–3831. Available at: https://doi.org/10.1073/pnas.1115201109.

Dunham, I. et al. (2012) ‘An integrated encyclopedia of DNA elements in the human genome’, Nature, 489(7414), pp. 57–74. Available at: https://doi.org/10.1038/nature11247.

Ea, C.K. et al. (2012) ‘EHMT1 protein binds to nuclear factor-κB p50 and represses gene expression’, Journal of Biological Chemistry, 287(37), pp. 31207–31217. Available at: https://doi.org/10.1074/jbc.M112.365601.

Elaut, G. et al. (2006) Molecular Mechanisms Underlying the Dedifferentiation Process of Isolated Hepatocytes and Their Cultures, Current Drug Metabolism.

Elsharkawy, A.M. et al. (2010) ‘The NF-κB p50:p50:HDAC-1 repressor complex orchestrates transcriptional inhibition of multiple pro-inflammatory genes’, Journal of Hepatology, 53(3), pp. 519–527. Available at: https://doi.org/10.1016/j.jhep.2010.03.025.

Emanuele, M.J. et al. (2020) ‘Complex Cartography: Regulation of E2F Transcription Factors by Cyclin F and Ubiquitin’, Trends in Cell Biology. Elsevier Ltd, pp. 640–652. Available at: https://doi.org/10.1016/j.tcb.2020.05.002.

Enrico, T.P. et al. (2021) ‘Cyclin F drives proliferation through SCF-dependent degradation of the retinoblastoma-like tumor suppressor p130/RBL2’, eLife [Preprint]. Available at: https://doi.org/10.7554/eLife.

Evers, B. and Jonkers, J. (2006) ‘Mouse models of BRCA1 and BRCA2 deficiency: Past lessons, current understanding and future prospects’, Oncogene, pp. 5885–5897. Available at: https://doi.org/10.1038/sj.onc.1209871.

Fagerlund, R. et al. (2005) ‘NF-κB is transported into the nucleus by importin α3 and importin α4’, Journal of Biological Chemistry, 280(16), pp. 15942–15951. Available at: https://doi.org/10.1074/jbc.M500814200.

Finkin, S. et al. (2015) ‘Ectopic lymphoid structures function as microniches for tumor progenitor cells in hepatocellular carcinoma’, Nature Immunology, 16(12), pp. 1235–1244. Available at: https://doi.org/10.1038/ni.3290.

Fliegauf, M. et al. (2015) ‘Haploinsufficiency of the NF-κB1 Subunit p50 in Common Variable Immunodeficiency’, American Journal of Human Genetics, 97(3), pp. 389–403. Available at: https://doi.org/10.1016/j.ajhg.2015.07.008.

Florio, T.J. et al. (2022) ‘Differential recognition of canonical NF-κB dimers by Importin α3’, Nature Communications, 13(1). Available at: https://doi.org/10.1038/s41467-022-28846-z.

Flurkey, K., Currer, J.M. and Harrison, D.E. (2007) ‘Mouse models in aging research’, in J.G. Fox et al. (eds) The Mouse in Biomedical Research. 2nd edn. Elsevier, pp. 367–72.

Franzoso, G. et al. (1998) Mice Deficient in Nuclear Factor (NF)-B/p52 Present with Defects in Humoral Responses, Germinal Center Reactions, and Splenic Microarchitecture, The Journal of Experimental Medicine •. Available at: http://www.jem.org.

Fulop, T. et al. (2021) ‘Immunology of Aging: the Birth of Inflammaging’, Clinical Reviews in Allergy and Immunology [Preprint]. Springer. Available at: https://doi.org/10.1007/s12016-021-08899-6.

Gao, J. et al. (2014) ‘Genetic polymorphism of NFKB1 and NFKBIA genes and liver cancer risk: A nested case-control study in Shanghai, China’, BMJ Open, 4(2). Available at: https://doi.org/10.1136/bmjopen-2013-004427.

García-García, V.A. et al. (2021) ‘Role of nf-κb in ageing and age-related diseases: Lessons from genetically modified mouse models’, Cells. MDPI. Available at: https://doi.org/10.3390/cells10081906.

Gardam, S. et al. (2008) ‘TRAF2 and TRAF3 Signal Adapters Act Cooperatively to Control the Maturation and Survival Signals Delivered to B Cells by the BAFF Receptor’, Immunity, 28(3), pp. 391–401. Available at: https://doi.org/10.1016/j.immuni.2008.01.009.

Girbl, T. et al. (2018) ‘Distinct Compartmentalization of the Chemokines CXCL1 and CXCL2 and the Atypical Receptor ACKR1 Determine Discrete Stages of Neutrophil Diapedesis’, Immunity, 49(6), pp. 1062-1076.e6. Available at: https://doi.org/10.1016/j.immuni.2018.09.018.

Gopinathan, L. et al. (2014) ‘Loss of Cdk2 and cyclin A2 impairs cell proliferation and tumorigenesis’, Cancer Research, 74(14), pp. 3870–3879. Available at: https://doi.org/10.1158/0008-5472.CAN-13-3440.

Gudmundsdottir, K. and Ashworth, A. (2006) 'The roles of BRCA1 and BRCA2 and associated proteins in the maintenance of genomic stability', Oncogene, pp. 5864–5874. Available at: https://doi.org/10.1038/sj.onc.1209874.

Guma, M. et al. (2011) 'Constitutive intestinal NF-κB does not trigger destructive inflammation unless accompanied by MAPK activation', Journal of Experimental Medicine, 208(9), pp. 1889–1900. Available at: https://doi.org/10.1084/jem.20110242.

Guttridge, D.C. et al. (1999) NF-B Controls Cell Growth and Differentiation through Transcriptional Regulation of Cyclin D1, MOLECULAR AND CELLULAR BIOLOGY. Available at: https://journals.asm.org/journal/mcb.

Hamesch, k. et al. (2015) 'Lipopolysaccharide-induced inflammatory liver injury in mice', Laboratory Animals, 49, pp. 37–46. Available at: https://doi.org/10.1177/0023677215570087.

Harant, H., Eldershaw, S.A. and Lindley, I.J.D. (2001) 'Human macrophage inflammatory protein-3K/CCL20/LARC/Exodus/ SCYA20 is transcriptionally upregulated by tumor necrosis factor-K via a non-standard NF-UB site', FEBS letters, 509, pp. 439–445.

Harte, M.T. et al. (2014) 'NF-κB is a critical mediator of BRCA1-induced chemoresistance', Oncogene, 33(6), pp. 713–723. Available at: https://doi.org/10.1038/onc.2013.10.

Hayden, M.S. and Ghosh, S. (2008) 'Shared Principles in NF-κB Signaling', Cell, pp. 344–362. Available at: https://doi.org/10.1016/j.cell.2008.01.020.

Heissmeyer, V. et al. (2001) ' Shared Pathways of IκB Kinase-Induced SCF βTrCP -Mediated Ubiquitination and Degradation for the NF-κB Precursor p105 and IκBα ', Molecular and Cellular Biology, 21(4), pp. 1024–1035. Available at: https://doi.org/10.1128/mcb.21.4.1024-1035.2001.

Hieshima, K. et al. (1997) Molecular Cloning of a Novel Human CC Chemokine Liver and Activation-regulated Chemokine (LARC) Expressed in Liver CHEMOTACTIC ACTIVITY FOR LYMPHOCYTES AND GENE LOCALIZATION ON CHROMOSOME 2*. Available at: http://www-jbc.stanford.edu/jbc/.

Hochegger, H., Takeda, S. and Hunt, T. (2008) 'Cyclin-dependent kinases and cell-cycle transitions: does one fit all?', Nature review Molecular Cell Biology [Preprint]. Available at: www.nature.com/reviews/molcellbio.

Hoffmann, A., Leung, T.H. and Baltimore, D. (2003) 'Genetic analysis of NF-κB/Rel transcription factors defines functional specificities', EMBO Journal, 22(20), pp. 5530–5539. Available at: https://doi.org/10.1093/emboj/cdg534.

Hon, C.C. et al. (2017) 'An atlas of human long non-coding RNAs with accurate 5′ ends', Nature, 543(7644), pp. 199–204. Available at: https://doi.org/10.1038/nature21374.

Hörber, S. et al. (2016) 'The atypical inhibitor of NF-κB, IκBζ, controls macrophage interleukin-10 expression', Journal of Biological Chemistry, 291(24), pp. 12851–12961. Available at: https://doi.org/10.1074/jbc.M116.718825.

Huang, T.T. et al. (2000) A nuclear export signal in the N-terminal regulatory domain of IB controls cytoplasmic localization of inactive NF-BIB complexes, PNAS February 1. Available at: www.pnas.org.

Huh, J., Mysorekar, I.U. and Mills, J.C. (2010) 'Inducible activation of Cre recombinase in adult mice causes gastric epithelial atrophy, metaplasia, and regenerative changes in the absence of "floxed" alleles', Am J Physiol Gastrointest Liver Physiol, 299, pp. 368–380. Available at: https://doi.org/10.1152/ajpgi.00021.2010.-The.

Hunter, P. (2012) 'The inflammation theory of disease', Embo Reports, 13(11), pp. 968–970.

Iannetti, A. et al. (2014) 'Regulation of p53 and Rb Links the Alternative NF-κB Pathway to EZH2 Expression and Cell Senescence', PLoS Genetics, 10(9). Available at: https://doi.org/10.1371/journal.pgen.1004642.

Janssens, S. and Tschopp, J. (2006) 'Signals from within: The DNA-damage-induced NF-κB response', Cell Death and Differentiation, pp. 773–784. Available at: https://doi.org/10.1038/sj.cdd.4401843.

Jenuwein, T. and David Allis, C. (2001) Translating the histone code, Proc. Natl. Acad. Sci. U.S.A. Available at: https://www.science.org.

Jia, W. et al. (2022) 'Tertiary Lymphatic Structures in Primary Hepatic Carcinoma: Controversy Cannot Overshadow Hope', Frontiers in Immunology. Frontiers Media S.A. Available at: https://doi.org/10.3389/fimmu.2022.870458.

Jin, J. et al. (2004) 'Systematic analysis and nomenclature of mammalian F-box proteins', Genes and Development, pp. 2573–2580. Available at: https://doi.org/10.1101/gad.1255304.

Jurk, D. et al. (2014) 'Chronic inflammation induces telomere dysfunction and accelerates ageing in mice', Nature Communications, 2. Available at: https://doi.org/10.1038/ncomms5172.

Kalaszczynska, I. et al. (2009) 'Cyclin A Is Redundant in Fibroblasts but Essential in Hematopoietic and Embryonic Stem Cells', Cell, 138(2), pp. 352–365. Available at: https://doi.org/10.1016/j.cell.2009.04.062.

Kamata, H., Tsuchiya, Y. and Asano, T. (2010) 'IκBβ is a positive and negative regulator of NF-B activity during inflammation', Cell Research, 20(11), pp. 1178–1180. Available at: https://doi.org/10.1038/cr.2010.147.

Karin, M., Ben-Neriah, Y. and Ben-Neriah, K. (2000) PHOSPHORYLATION MEETS UBIQUITINATION: The Control of NF-kB Activity, Annual Review of Immunology. Available at: www.annualreviews.org.

Kato, T. et al. (2003) CK2 Is a C-Terminal IB Kinase Responsible for NF-B Activation during the UV Response tion in response to UV irradiation has remained enig-matic. Normally, NF-B transcription factors are regulated, Molecular Cell.

Katsuno, Y. et al. (2009) 'Cyclin A-Cdk1 regulates the origin firing program in mammalian cells', PNAS [Preprint]. Available at: www.pnas.org/cgi/content/full/.

Kelliher, M.A. et al. (1998) The Death Domain Kinase RIP Mediates the TNF-Induced NF-B Signal The RIP death domain also binds RAIDD (RIP-associ-ated ICH1/CED3-homologous protein with a death do-main) (Duan and Dixit, 1997). Hence, RIP may directly, Immunity.

Kheder, R.K., Hobkirk, J. and Stover, C.M. (2016) 'In vitro modulation of the LPS-induced proinflammatory profile of hepatocytes and macrophages-approaches for intervention in obesity?', Frontiers in Cell and Developmental Biology, 4(JUN). Available at: https://doi.org/10.3389/fcell.2016.00061.

Kim, H. et al. (2018) 'Mouse Cre-LoxP system: general principles to determine tissue-specific roles of target genes', Laboratory Animal Research, 34(4), p. 147. Available at: https://doi.org/10.5625/lar.2018.34.4.147.

Kontgen, F. et al. (1995) Mice lacking the c-rel proto-oncogene exhibit defects in lymphocyte proliferation, humoral immunity, and interleukin-2 expression.

Korbecki, J. et al. (2022) 'CXCL1: Gene, Promoter, Regulation of Expression, mRNA Stability, Regulation of Activity in the Intercellular Space', International Journal of Molecular Sciences. MDPI. Available at: https://doi.org/10.3390/ijms23020792.

Kravtsova-Ivantsiv, Y. et al. (2015) 'KPC1-mediated ubiquitination and proteasomal processing of nf-κb1 p105 to p50 restricts tumor growth', Cell, 161(2), pp. 333–347. Available at: https://doi.org/10.1016/j.cell.2015.03.001.

Krikoss, A., Lahertysg, C.D. and Dixitlgt, V.M. (1992) Transcriptional Activation of the Tumor Necrosis Factor a-Inducible Zinc Finger Protein, A20, Is Mediated by KB Elements*, OF BIOLOGICAL CHEMISTRY.

Kristjá, K. and Rudolph, J. (2004) 'Cdc25 Phosphatases and Cancer', Chemistry & Biology, 11, pp. 1043–1051. Available at: https://doi.org/10.1016/j.

Lai, T.Y. et al. (2013) 'Transcription of Tnfaip3 is regulated by NF-κB and p38 via C/EBPβ in activated macrophages.', PloS one, 8(9). Available at: https://doi.org/10.1371/journal.pone.0073153.

Lauschke, V.M. et al. (2019) '3D Primary Hepatocyte Culture Systems for Analyses of Liver Diseases, Drug Metabolism, and Toxicity: Emerging Culture Paradigms and Applications', Biotechnology Journal. Wiley-VCH Verlag. Available at: https://doi.org/10.1002/biot.201800347.

Lawrence, T. and Fong, C. (2010) 'The resolution of inflammation: Anti-inflammatory roles for NF-κB', International Journal of Biochemistry and Cell Biology, pp. 519–523. Available at: https://doi.org/10.1016/j.biocel.2009.12.016.

Ledoux, A.C. and Perkins, N.D. (2014) 'NF-κB and the cell cycle', Biochemical Society Transactions, 42(1), pp. 76–81. Available at: https://doi.org/10.1042/BST20130156.

Lee, E.G. et al. (2000) 'Failure to Regulate TNF-Induced NF-κB and Cell Death Responses in A20-Deficient Mice', Science, 289(5488), pp. 2350–2354.

Lee, Y.S. et al. (2017) 'Hepatocyte toll-like receptor 4 mediates lipopolysaccharide-induced hepcidin expression', Experimental and Molecular Medicine, 49(12). Available at: https://doi.org/10.1038/emm.2017.207.

Li, C.-W., Chang, P.-Y. and Chen, B.-S. (2016) 'Investigating the mechanism of hepatocellular carcinoma progression by constructing genetic and epigenetic networks using NGS data identification and big database mining method', Oncotarget, 7(48), pp. 79453–79473. Available at: www.impactjournals.com/oncotarget/.

Li, J. and Liu, C. (2019) 'Coding or noncoding, the converging concepts of RNAs', Frontiers in Genetics. Frontiers Media S.A. Available at: https://doi.org/10.3389/fgene.2019.00496.

Li, L. and Ghosh, S. (1996) A Glycine-Rich Region in NF-B p105 Functions as a Processing Signal for the Generation of the p50 Subunit, MOLECULAR AND CELLULAR BIOLOGY. Available at: https://journals.asm.org/journal/mcb.

Li, P. et al. (2013) 'Functional Promoter -94 ins/del ATTG Polymorphism in NFKB1 Gene Is Associated with Bladder Cancer Risk in a Chinese Population', PLoS ONE, 8(8). Available at: https://doi.org/10.1371/journal.pone.0071604.

Lin, L. and Kobayashi, M. (2003) 'Stability of the Rel homology domain is critical for generation of NF-κB p50 subunit', Journal of Biological Chemistry, 278(34), pp. 31479–31485. Available at: https://doi.org/10.1074/jbc.M304140200.

Liu, K., Lu, R., et al. (2020) 'Association and clinicopathologic significance of p38MAPK-ERK-JNK-CDC25C with polyploid giant cancer cell formation', Medical Oncology, 37(1). Available at: https://doi.org/10.1007/s12032-019-1330-9.

Liu, K., Zheng, M., et al. (2020) 'The role of CDC25C in cell cycle regulation and clinical cancer therapy: A systematic review', Cancer Cell International. BioMed Central Ltd. Available at: https://doi.org/10.1186/s12935-020-01304-w.

Liu, T. et al. (2017a) 'NF-κB signaling in inflammation', Signal Transduction and Targeted Therapy. Springer Nature. Available at: https://doi.org/10.1038/sigtrans.2017.23.

Liu, T. et al. (2017b) 'NF-κB signaling in inflammation', Signal Transduction and Targeted Therapy. Springer Nature. Available at: https://doi.org/10.1038/sigtrans.2017.23.

Llovet, J.M. et al. (2021) 'Hepatocellular carcinoma', Nature Reviews Disease Primers. Nature Research. Available at: https://doi.org/10.1038/s41572-020-00240-3.

López-Otín, C. et al. (2013) 'The hallmarks of aging', Cell. Elsevier B.V., p. 1194. Available at: https://doi.org/10.1016/j.cell.2013.05.039.

Lu, Z.Y. et al. (2006) 'Age-related neural degeneration in nuclear-factor κB p50 knockout mice', Neuroscience, 139(3), pp. 965–978. Available at: https://doi.org/10.1016/j.neuroscience.2005.12.062.

Luedde, T. et al. (2007) 'Deletion of NEMO/IKKγ in Liver Parenchymal Cells Causes Steatohepatitis and Hepatocellular Carcinoma', Cancer Cell, 11(2), pp. 119–132. Available at: https://doi.org/10.1016/j.ccr.2006.12.016.

Maeda, S. et al. (2003) IKK Is Required for Prevention of Apoptosis Mediated by Cell-Bound but Not by Circulating TNFα, Immunity. Available at: http://www.immunity.

Malek, S. et al. (2001) 'IκBβ, but Not IκBα, Functions as a Classical Cytoplasmic Inhibitor of NF-κB Dimers by Masking Both NF-κB Nuclear Localization Sequences in Resting Cells', Journal of Biological Chemistry, 276(48), pp. 45225–45235. Available at: https://doi.org/10.1074/jbc.M105865200.

Mann, J. et al. (2007) 'Regulation of myofibroblast transdifferentiation by DNA methylation and MeCP2: Implications for wound healing and fibrogenesis', Cell Death and Differentiation, 14(2), pp. 275–285. Available at: https://doi.org/10.1038/sj.cdd.4401979.

Mann, J. et al. (2010) 'MeCP2 Controls an Epigenetic Pathway That Promotes Myofibroblast Transdifferentiation and Fibrosis', Gastroenterology, 138(2). Available at: https://doi.org/10.1053/j.gastro.2009.10.002.

Martin, C. et al. (2003) Chemokines Acting via CXCR2 and CXCR4 Control the Release of Neutrophils from the Bone Marrow and Their Return following Senescence.

Mazzucchelli, L. et al. (1999) 'BCA-1 is highly expressed in Helicobacter pylori-induced mucosa- associated lymphoid tissue and gastric lymphoma', Journal of Clinical Investigation, 104(10). Available at: https://doi.org/10.1172/JCI7830.

Mcconnell, B.B. et al. (1998) 'Inhibitors of cyclin-dependent kinases induce features of replicative senescence in early passage human diploid fibroblasts', Current Biology, 8, pp. 351–354. Available at: http://biomednet.com/elecref/0960982200800351.

Medzhitov, R. (2008) 'Origin and physiological roles of inflammation', Nature. Nature Publishing Group, pp. 428–435. Available at: https://doi.org/10.1038/nature07201.

Mi, H. et al. (2013) 'Large-scale gene function analysis with the panther classification system', Nature Protocols, 8(8), pp. 1551–1566. Available at: https://doi.org/10.1038/nprot.2013.092.

Moles, A. et al. (2013) A TLR2/S100A9/CXCL-2 signaling network is necessary for neutrophil recruitment in acute and chronic liver injury in the mouse.

Moorthy, A.K. et al. (2006) 'The 20S proteasome processes NF-κB1 p105 into p50 in a translation-independent manner', EMBO Journal, 25(9), pp. 1945–1956. Available at: https://doi.org/10.1038/sj.emboj.7601081.

Moran-Salvador, E. and Mann, J. (2017) 'Epigenetics and Liver Fibrosis', CMGH. Elsevier Inc, pp. 125–134. Available at: https://doi.org/10.1016/j.jcmgh.2017.04.007.

Musolino, A. et al. (2007) 'BRCA mutations, molecular markers, and clinical variables in early-onset breast cancer: A population-based study', Breast, 16(3), pp. 280–292. Available at: https://doi.org/10.1016/j.breast.2006.12.003.

Neyt, K. et al. (2012) 'Tertiary lymphoid organs in infection and autoimmunity', Trends in Immunology, pp. 297–305. Available at: https://doi.org/10.1016/j.it.2012.04.006.

Nguyen, P. et al. (2018) 'Elimination of Age-Associated Hepatic Steatosis and Correction of Aging Phenotype by Inhibition of cdk4-C/EBPα-p300 Axis', Cell Reports, 24(6), pp. 1597–1609. Available at: https://doi.org/10.1016/j.celrep.2018.07.014.

O'Brien, J. et al. (2018) 'Overview of microRNA biogenesis, mechanisms of actions, and circulation', Frontiers in Endocrinology. Frontiers Media S.A. Available at: https://doi.org/10.3389/fendo.2018.00402.

Oeckinghaus, A. and Ghosh, S. (2009) 'The NF-kappaB family of transcription factors and its regulation.', Cold Spring Harbor perspectives in biology. Available at: https://doi.org/10.1101/cshperspect.a000034.

Ogrodnik, M. et al. (2017) 'Cellular senescence drives age-dependent hepatic steatosis', Nature Communications, 8. Available at: https://doi.org/10.1038/ncomms15691.

Ohno S (1972) 'So much "junk" DNA in our genome', Brookhaven Symp Biol, 23, pp. 366–70.

Pacaud, R. et al. (2014) 'DNMT3L interacts with transcription factors to target DNMT3L/DNMT3B to specific DNA sequences: Role of the DNMT3L/DNMT3B/p65-NFκB complex in the (de-)methylation of TRAF1', Biochimie, 104(1), pp. 36–49. Available at: https://doi.org/10.1016/j.biochi.2014.05.005.

Page, A. et al. (2016) 'Hepatic stellate cell transdifferentiation involves genome-wide remodeling of the DNA methylation landscape', Journal of Hepatology, 64(3), pp. 661–673. Available at: https://doi.org/10.1016/J.JHEP.2015.11.024.

Page, A. and Mann, D.A. (2015) 'Epigenetic regulation of liver fibrosis', Clinics and Research in Hepatology and Gastroenterology. Elsevier Masson s.r.l., pp. S64–S68. Available at: https://doi.org/10.1016/j.clinre.2015.05.013.

Paish, H.L. et al. (2019) 'A Bioreactor Technology for Modeling Fibrosis in Human and Rodent Precision-Cut Liver Slices', Hepatology, 70(4), pp. 1377–1391. Available at: https://doi.org/10.1002/hep.30651/suppinfo.

Paz-Priel, I. et al. (2011) 'C/EBPA and C/EBPA oncoproteins regulate nfkb1 and displace histone deacetylases from NF-κB p50 homodimers to induce NF-κB target genes', Blood, 117(15), pp. 4085–4094. Available at: https://doi.org/10.1182/blood-2010-07-294470.

Peng, W.C., Kraaier, L.J. and Kluiver, T.A. (2021) 'Hepatocyte organoids and cell transplantation: What the future holds', Experimental and Molecular Medicine. Springer Nature, pp. 1512–1528. Available at: https://doi.org/10.1038/s12276-021-00579-x.

Perkins, N.D. (2012) 'The diverse and complex roles of NF-κB subunits in cancer', Nature Reviews Cancer, pp. 121–132. Available at: https://doi.org/10.1038/nrc3204.

Perkins, N.D. and Gilmore, T.D. (2006) 'Good cop, bad cop: The different faces of NF-κB', Cell Death and Differentiation, pp. 759–772. Available at: https://doi.org/10.1038/sj.cdd.4401838.

Perugorria, M.J. et al. (2012) 'Histone methyltransferase ASH1 orchestrates fibrogenic gene transcription during myofibroblast transdifferentiation', Hepatology, 56(3), pp. 1129–1139. Available at: https://doi.org/10.1002/hep.25754.

Pfaffl, M.W. (2001) A new mathematical model for relative quantification in real-time RT-PCR, Nucleic Acids Research.

Pitzalis, C. et al. (2014) ‘Ectopic lymphoid-like structures in infection, cancer and autoimmunity’, Nature Reviews Immunology. Nature Publishing Group, pp. 447–462. Available at: https://doi.org/10.1038/nri3700.

Pomplun, D. et al. (2007) ‘Alterations of pancreatic beta-cell mass and islet number due to Ins2-controlled expression of Cre recombinase: RIP-Cre revisited; part 2’, Hormone and Metabolic Research, 39(5), pp. 336–340. Available at: https://doi.org/10.1055/s-2007-976538.

Prajapati, S. et al. (2006) ‘IKKα regulates the mitotic phase of the cell cycle by modulating Aurora A phosphorylation’, Cell Cycle, 5(20), pp. 2371–2380. Available at: https://doi.org/10.4161/cc.5.20.3359.

Ramus, S.J. et al. (1999) ‘Increased frequency of TP53 mutations in BRCAI and BRCA2 ovarian tumours’, Genes Chromosomes and Cancer, 25(2), pp. 91–96. Available at: https://doi.org/10.1002/(SICI)1098-2264(199906)25:2<91::AID-GCC3>3.0.CO;2-5.

Rodier, F. et al. (2009) ‘Persistent DNA damage signalling triggers senescence-associated inflammatory cytokine secretion’, Nature Cell Biology, 11(8), pp. 973–979. Available at: https://doi.org/10.1038/ncb1909.

Roy, R., Chun, J. and Powell, S.N. (2012) ‘BRCA1 and BRCA2: Different roles in a common pathway of genome protection’, Nature Reviews Cancer, pp. 68–78. Available at: https://doi.org/10.1038/nrc3181.

Rush, M. et al. (2009) ‘Targeting of EZH2 to a defined genomic site is sufficient for recruitment of Dnmt3a but not de novo DNA methylation’, Epigenetics, 4(6), pp. 404–414. Available at: https://doi.org/10.4161/epi.4.6.9392.

Sabater, L. et al. (2020) ‘RNA sequencing reveals changes in the microRNAome of transdifferentiating hepatic stellate cells that are conserved between human and rat’, Scientific Reports, 10(1). Available at: https://doi.org/10.1038/s41598-020-78776-3.

Sabbisetti, V.S. et al. (2014) ‘Blood kidney injury molecule-1 is a biomarker of acute and chronic kidney injury and predicts progression to ESRD in type I diabetes’, Journal of the American Society of Nephrology, 25(10), pp. 2177–2186. Available at: https://doi.org/10.1681/ASN.2013070758.

Sabeh, R. el et al. (2021) ‘A gender-dependent molecular switch of inflammation via myd88/estrogen receptor-alpha interaction’, Journal of Inflammation Research, 14, pp. 2149–2156. Available at: https://doi.org/10.2147/JIR.S306805.

Salmien, A., Kaarniranta, K. and Kauppinen, A. (2012) ‘Inflammaging: disturbed interplay between autophagy and inflammasomes’, Aging, 4(3), pp. 166–175.

Santamaría, D. et al. (2007) ‘Cdk1 is sufficient to drive the mammalian cell cycle’, Nature, 448(7155), pp. 811–815. Available at: https://doi.org/10.1038/nature06046.

Savinova, O. v., Hoffmann, A. and Ghosh, G. (2009) ‘The Nfkb1 and Nfkb2 Proteins p105 and p100 Function as the Core of High-Molecular-Weight Heterogeneous Complexes’, Molecular Cell, 34(5), pp. 591–602. Available at: https://doi.org/10.1016/j.molcel.2009.04.033.

Schile, A. (2011) Slicing and dicing Cre/lox: part 1, https://www.jax.org/news-and-insights/jax-blog/2011/May/slicing-and-dicing-cre-lox-part-1.

Schleimer, R.P. et al. (2007) 'Epithelium: At the interface of innate and adaptive immune responses', Journal of Allergy and Clinical Immunology, pp. 1279–1284. Available at: https://doi.org/10.1016/j.jaci.2007.08.046.

Schrama, D. et al. (2001) Targeting of Lymphotoxin-to the Tumor Elicits an Efficient Immune Response Associated with Induction of Peripheral Lymphoid-like Tissue, Immunity.

Sciuto, M.R. et al. (2018) 'Two-Step Coimmunoprecipitation (TIP) enables efficient and highly selective isolation of native protein complexes', Molecular and Cellular Proteomics, 17(5), pp. 993–1009. Available at: https://doi.org/10.1074/mcp.O116.065920.

Sen, R. and Baltimore, D. (1966) Inducibility of K Immunoglobulin Enhancer-Binding Protein NFKB by a Posttranslational Mechanism, Cell.

Sen, R. and Baltimore, D. (1986) Multiple Nuclear Factors Interact with the Immunoglobulin Enhancer Sequences, Cell.

Sha, W.C. et al. (1995a) Targeted Disruption of the p50 Subunit of NF-KB Leads to Multifocal Defects in Immune Responses, Cell.

Sha, W.C. et al. (1995b) Targeted Disruption of the p50 Subunit of NF-KB Leads to Multifocal Defects in Immune Responses, Cell.

Shatruck, R.L. et al. (1994) MGSA/GRO Transcription Is Differentially Regulated in Normal Retinal Pigment Epithelial and Melanoma Cells, MOLECULAR AND CELLULAR BIOLOGY. Available at: https://journals.asm.org/journal/mcb.

Shembade, N. and Harhaj, E.W. (2012) 'Regulation of NF-κB signaling by the A20 deubiquitinase', Cellular and Molecular Immunology, pp. 123–130. Available at: https://doi.org/10.1038/cmi.2011.59.

Singer, E. et al. (2013) 'Neutrophil gelatinase-associated lipocalin: Pathophysiology and clinical applications', Acta Physiologica, pp. 663–672. Available at: https://doi.org/10.1111/apha.12054.

Smale, S.T. (2012) Dimer-specific regulatory mechanisms within the NF-jB family of transcription factors, John Wiley & Sons A/S Immunological Reviews. Available at: www.immunologicalreviews.com.

Smith, P.D. et al. (1999) 'Novel p53 mutants selected in BRCA-associated tumours which dissociate transformation suppression from other wild-type p53 functions', Oncogene, 18. Available at: http://www.stockton-press.co.uk/onc.

Steinbrecher, K.A. et al. (2008) 'Loss of Epithelial RelA Results in Deregulated Intestinal Proliferative/Apoptotic Homeostasis and Susceptibility to Inflammation', The Journal of Immunology, 180(4), pp. 2588–2599. Available at: https://doi.org/10.4049/jimmunol.180.4.2588.

Sun, S.-C. (2012) The noncanonical NF-κB pathway, John Wiley & Sons A/S Immunological Reviews. Available at: www.immunologicalreviews.com.

Sun, S.C. (2017) ‘The non-canonical NF-κB pathway in immunity and inflammation’, Nature Reviews Immunology. Nature Publishing Group, pp. 545–558. Available at: https://doi.org/10.1038/nri.2017.52.

Swamy, M. et al. (2010) ‘Epithelial decision makers: In search of the “epimmunome”’, Nature Immunology, pp. 656–665. Available at: https://doi.org/10.1038/ni.1905.

Takada, Y. et al. (2003) ‘Hydrogen peroxide activates NF-κB through tyrosine phosphorylation of IκBα and serine phosphorylation of p65. Evidence for the involvement of IκBα kinase and Syk protein-tyrosine kinase’, Journal of Biological Chemistry, 278(26), pp. 24233–24241. Available at: https://doi.org/10.1074/jbc.M212389200.

Tanaka, Y. et al. (1999) Selective expression of liver and activation-regulated chemokine (LARC) in intestinal epithelium in mice and humans.

Tergaonkar, V. et al. (2005) ‘Distinct roles of IκB proteins in regulating constitutive NF-κB activity’, Nature Cell Biology, 7(9), pp. 921–923.

Tessarz, P. and Kouzarides, T. (2014) ‘Histone core modifications regulating nucleosome structure and dynamics’, Nature Reviews Molecular Cell Biology, 15(11), pp. 703–708. Available at: https://doi.org/10.1038/nrm3890.

Tostões, R.M. et al. (2012) ‘Human liver cell spheroids in extended perfusion bioreactor culture for repeated-dose drug testing’, Hepatology, 55(4), pp. 1227–1236. Available at: https://doi.org/10.1002/hep.24760.

Underhill, G.H. and Khetani, S.R. (2018) ‘Advances in engineered human liver platforms for drug metabolism studies’, Drug Metabolism and Disposition, 46(11), pp. 1626–1637. Available at: https://doi.org/10.1124/dmd.118.083295.

Vandamme, T. (2014) ‘Use of rodents as models of human diseases’, Journal of Pharmacy and Bioallied Sciences. Medknow Publications, pp. 2–9. Available at: https://doi.org/10.4103/0975-7406.124301.

Vaure, C. and Liu, Y. (2014) ‘A comparative review of toll-like receptor 4 expression and functionality in different animal species’, Frontiers in Immunology. Frontiers Research Foundation. Available at: https://doi.org/10.3389/fimmu.2014.00316.

Vicioso, Y. et al. (2021) ‘NF-κB c-Rel Is Dispensable for the Development but Is Required for the Cytotoxic Function of NK Cells’, Frontiers in Immunology, 12. Available at: https://doi.org/10.3389/fimmu.2021.652786.

Viñas, O. et al. (2003) ‘Human hepatic stellate cells show features of antigen-presenting cells and stimulate lymphocyte proliferation’, Hepatology, 38(4), pp. 919–929. Available at: https://doi.org/10.1002/hep.1840380418.

Weih, F. et al. (2003) Regulation of secondary lymphoid organ development by the nuclear factor-kB signal transduction pathway.

Wertz, I.E. et al. (2004) ‘De-ubiquitination and ubiquitin ligase domains of A20 downregulate NF-kB signalling’, Nature [Preprint]. Available at: www.nature.com/nature.

Wessells, J. et al. (2004) ‘BCL-3 and NF-κB p50 attenuate lipopolysaccharide-induced inflammatory responses in macrophages’, Journal of Biological Chemistry, 279(48), pp. 49995–50003. Available at: https://doi.org/10.1074/jbc.M404246200.

Wicksteed, B. et al. (2010) ‘Conditional gene targeting in mouse pancreatic β-cells: Analysis of ectopic cre transgene expression in the brain’, Diabetes, 59(12), pp. 3090–3098. Available at: https://doi.org/10.2337/db10-0624.

Wilson, C.L. et al. (2015a) ‘NFκ B1 is a suppressor of neutrophil-driven hepatocellular carcinoma’, Nature Communications, 6. Available at: https://doi.org/10.1038/ncomms7818.

Wilson, C.L. et al. (2015b) ‘NFκ B1 is a suppressor of neutrophil-driven hepatocellular carcinoma’, Nature Communications, 6. Available at: https://doi.org/10.1038/ncomms7818.

Wu, K. et al. (2000) ‘Induction of the BRCA2 promoter by nuclear factor-κB’, Journal of Biological Chemistry, 275(45), pp. 35548–35556. Available at: https://doi.org/10.1074/jbc.M004390200.

Xiao, G., Harhaj, E.W. and Sun, S.-C. (2001) NF-κB-Inducing Kinase Regulates the Processing of NF-κB2 p100, Molecular Cell.

Yalamanchili, H.K., Wan, Y.W. and Liu, Z. (2017) ‘Data analysis pipeline for RNA-seq experiments: From differential expression to cryptic splicing’, Current Protocols in Bioinformatics, 2017, pp. 11.15.1-11.15.21. Available at: https://doi.org/10.1002/cpbi.33.

Yamamoto, M. et al. (2003) Regulation of Toll/IL-1-receptor-mediated gene expression by theinducible nuclear protein IkBz, Nature Rev. Immunol. Available at: www.nature.com/nature.

Yang, Y.M. and Seki, E. (2015) ‘TNFα in Liver Fibrosis’, Current Pathobiology Reports. Springer, pp. 253–261. Available at: https://doi.org/10.1007/s40139-015-0093-z.

Yu, H. et al. (2020) ‘Targeting NF-κB pathway for the therapy of diseases: mechanism and clinical study’, Signal Transduction and Targeted Therapy. Springer Nature. Available at: https://doi.org/10.1038/s41392-020-00312-6.

Zhang, H. and Sun, S.C. (2015) ‘NF-KB in inflammation and renal diseases’, Cell and Bioscience. BioMed Central Ltd. Available at: https://doi.org/10.1186/s13578-015-0056-4.

Zhang, Q., Lenardo, M.J. and Baltimore, D. (2017) ‘30 Years of NF-κB: A Blossoming of Relevance to Human Pathobiology’, Cell. Cell Press, pp. 37–57. Available at: https://doi.org/10.1016/j.cell.2016.12.012.

Zhao, D. et al. (2016) ‘H3K4me3 Demethylase Kdm5a Is Required for NK Cell Activation by Associating with p50 to Suppress SOCS1’, Cell Reports, 15(2), pp. 288–299. Available at: https://doi.org/10.1016/j.celrep.2016.03.035.

Zhou, R. et al. (2011) ‘A role for mitochondria in NLRP3 inflammasome activation’, Nature, 469(7329), pp. 221–226. Available at: https://doi.org/10.1038/nature09663.